UNIVERSITY OF NATAL

BOWEN RATIO AND SURFACE TEMPERATURE TECHNIQUES FOR MEASURING EVAPORATION FROM CABBAGES

by

GASTAO LUKANGU

B.Sc. (Agric) A. Neto

Submitted in partial
fulfilment of the requirement
for the degree of

MASTER OF SCIENCE IN AGRICULTURE

in the
Department of Agronomy
University of Natal
Pietermaritzburg
Natal
1997

ABSTRACT

Good irrigation water management requires accurate, automated, non-destructive and simple techniques to measure crop water consumption. The actual evaporation from a cabbage crop was measured using the Bowen ratio energy balance technique (BREB), the surface temperature technique and the Penman-monteith method. All models used the shortened energy balance equation to estimate latent heat in which the advected energy is assumed to be negligible. Four irrigations were applied and 17 rainfall events were recorded during the experiment. The soil at the experimental field was a clay loam. An attempt to detect and reduce measurement error that could result from using inaccurate sensors was performed by calibrating the sensors. Data from inaccurate sensors were not used to compute the latent heat. Error and sensitivity analyse were performed, and the integrity of the weather data using the estimates of weather data from an appropriate model were checked. In addition, a comparative study showed that, for daily totals, there was a very small error in the latent heat calculations when fixed "constants" (density of air, specific heat capacity of air, psychrometric constant, slope of the saturation water vapour pressure vs temperature relationship and specific heat capacity of soil) were used instead of calculated ones.

The Bowen ratio (β), a fundamental input of the BREB technique, was estimated accepting the Similarity Principle and excluding nighttime data. However, an error in β was also observed during the daytime measurement of the profiles entities because the sensors were wet and the stability condition was different from neutral conditions under which the Similarity Principle could not be observed. Negative values of β were observed when there were strong winds advecting sensible heat into the field under study. Data were rejected during mornings, and during strong advection periods. Data were also rejected when the sensors were wet because of rain or irrigation. In this experiment, only 35 % of data were valid for determining latent and sensible heat estimated using the BREB technique. Comparative analysis showed that the BREB technique overestimated the latent heat by 17 % compared to the Penman-Monteith method. However, both the Penman-Monteith method and BREB technique could not be trusted because of the presence of advection, a component of the energy balance equation normally assumed to be negligible.

Either the surface to air temperature differential or the aerodynamic resistance, or both, were the source of overestimation of latent heat using the surface temperature technique. The surface to air

temperature differential was large in magnitude when there were high wind speeds and drier conditions in the upwind field. It was small with lighter wind speeds and wetter surface conditions. An error of less than 5 % was attributed to the use of fixed air density and specific heat capacity and acceptance of 2 % and 20 % error in measuring the net irradiance and soil heat flux density, respectively. A comparative study showed that the surface temperature latent heat was overestimated in relation to the Penman-Monteith and BREB latent heat. Generally, the technique has been reported to overestimate evaporation, although to a lesser extent than the 57 % error reported in this experiment when compared to the BREB technique. An analysis of the energy balance closure, taking the Penman-Monteith and BREB as standards, suggested that the surface temperature technique overestimated the consumption of sensible heat from the air. This observation was also confirmed when the eddy correlation technique was used to compare sensible heat estimated using the surface temperature technique. The effect of placement height of air temperature sensors suggested that the consumption of sensible heat would be overestimated if the sensor was placed far from the crop surface. This overestimation in consumption of sensible heat resulted in an overestimation of latent heat.

Irrigation water management was analysed using the crop water stress index (CWSI). The CWSI was calculated using the actual to potential evaporation ratio estimated using the Penman-Monteith method and the surface temperature techniques. The estimated and measured actual surface to air temperature differential, and the estimated potential and non-transpiring surface to air temperature differential were also used to estimate the CWSI using the Penman-Monteith method, the surface temperature technique and empirical method. The estimates of the CWSI using these techniques were inaccurate because of the poor correlation between the surface to air temperature differential and the water vapour pressure deficit (or water vapour pressure deficit and net irradiance). However, use of the CWSI estimated using the actual to potential evaporation ratio ($CWSI = 1 - \lambda E_a/\lambda E_p$) compared well to the standard CWSI determined using the Penman-Monteith approach. The actual canopy resistance was estimated using an empirical equation based on the potential canopy resistance, solar irradiance, soil water content and the shelter factor. A value of 50 s m^{-1} was estimated for potential (minimum) canopy resistance of the cabbage crop. The soil water content was poorly correlated to CWSI, while the canopy resistance was well correlated.

Comparative analysis showed that the estimated soil water content using the soil water balance equation was underestimated in relation to the soil water content measured using the ThetaProbe

(frequency domain reflectometry technique) when the evaporation component was overestimated, and *vice versa*. Soil water content was underestimated throughout the experiment when evaporation from the surface temperature technique was used. There was an underestimation of soil water content in the early stages and overestimation in later stages of the experiment when the BREB and Penman-Monteith evaporation were used. Use of the estimated soil water content using the soil water balance with the overestimated evaporation would result in an early date of irrigation application, an unnecessarily large irrigation amount and frequent irrigations.

More research is needed to find the cause of overestimation of evaporation using the surface temperature technique. The robustness of the equipment allowed a long period of measurement without frequent maintenance, as was required when using the BREB technique. The technique can monitor evaporation and irrigation management aspects at a regional scale. A combination of the Penman-Monteith, surface temperature and empirical method can assist the estimation of the crop water requirement by determining the CWSI. Future research would focus on quantification of sensible and latent heat advection, and analysis of additional resistances to water vapour flow from the surface to the atmosphere. The equipment for the BREB should be refined so that it measures actual latent heat under adverse weather conditions for a protracted period. A precise use of the soil water balance equation for water management should take into consideration runoff, vertical flow of soil water through a profile, intercepted water on plant surfaces and an accurately determined evaporation.

Declaration

I hereby certify that the research work reported in this thesis is the result of my on original investigation except where acknowledged.

Signed 

Gastao Lukangu

ACKNOWLEDGEMENTS

I would like to express my thank to:

Professor M. J. Savage of the Agrometeorological Section of the Department of Agronomy for his wise supervision and encouragement throughout the MSc Agric. and for the use of equipment. Thanks are also due to his patience and availability during the project;

Dr M.A. Johnston of the Soil Science Section of the Department of Agronomy, my co-supervisor, for his contribution in the write-up and laboratory analysis of soil physics related aspect of this thesis;

Dr C.S. Everson of the CSIR for his input in the conceptual phase of the project and for his advice on servicing of the equipment. Thanks are also due to advice and field checking of the sensors;

Professor R. G. Allen and Associate Professor I. Lopes for their valuable suggestions during data processing; Associate Prof. Timothy Fasheun for diversified scientific help provide during field work.

Mrs M. A. Savage for encouragement and editorial assistance in the write-up. Thanks are also due to Mr Barry Noel for editorial assistance;

Ms Jothi Moodley, Ms Amanda Klar, Mr Peter Dovey and Mr Tad Dorasamy for diversified help during field and laboratory work, and write-up. Professor P. L. Greenfield of the Department of Agronomy for encouragement. Thanks are also due to all members of the Department of Agronomy and Life Sciences Library whose contribution facilitated a good working environment;

All friends in Christ whose prayer was an inspiration for the completion of this project. Thanks are also due to Mr R. Bernardo and Ms Veronica Sebastiao due to their moral support and help during field work;

The Deutscher Akademischer Austauschdient (DAAD), the Foundation for Research and Development, Water Research Commission, the University of Natal and the Department of Agronomy for their financial support for living and study expenses, and acquisition of the equipment utilized in the project.Mr Wild and his son Alex of the Vita Farm (Tala Valley) for providing facilities for the performance of the experiment.

Prof. Otto Berg for helping to reach DAAD scholarship through German Embassy in Angola.

I would like to express my special thanks to my wife Antonieta and daughter Alexia, and parents for their patience and support overs my years of study, to my friends Mr J.P Vicente and Mrs M. A. Savage for their greater contribution to my life and in particular to this work.

I thank GOD for inspiring my skill in the measurement of evaporation, soil water content and the management of irrigation using these measurement. Thanks are also due to a wonderful family, supervisors, examiners, scientists, friends and financial institutions that HE put to my availability for the performance of this research.

TABLE OF CONTENTS

LIST OF SYMBOLS

a_o	ThetaProbe calibration constant	
a_1	ThetaProbe calibration constant	
BREB	Bowen ration energy balance	
Cp_{air}	specific heat capacity of dry air	J kg^{-1} K^{-1}
Cp_s	specific heat capacity of soil	J kg^{-1} K^{-1}
Cp_w	specific heat capacity of water	J kg^{-1} K^{-1}
CWSI	crop water stress index	
d	zero-plane displacement height (d = 0.67 h where h = crop height)	m
$d\theta$	true profile equivalent temperature difference (dθ)	K
E	water vapour flux density	kg s^{-1} m^{-2}
E_i	irrigation efficiency	
E(e)	error in water vapour pressure	kPa
$E(\theta)$	error in equivalent temperature $E(\theta)$	K
e_{air}	atmospheric water vapour pressure	kPa
e_{airc}	vapour pressure in the myriad of the intercellular space	kPa
$e_s(T_{can})$	saturation water vapour pressure at intercellular temperature	kPa
e_s	saturation water vapour pressure at air temperature	kPa
FC	field capacity	m^3 m^{-3}
$F_1(R_s)$	$R_{smax}/(1 + R_s)$ is the unitless solar radiation function	
$F_2(\theta)$	$1.2\ \theta_{wilting}/(0.9\theta_{rootZ} + 0.1\theta_{surfL})$ is the soil water function	
F3	shelter function	
G	soil heat energy flux density	W m^{-2}
g	gravitational acceleration	9.7922 m s^{-2}
H	sensible heat energy flux density	W m^{-2}
h	crop height	m
h	height of the soil core	m
h_l	altitude of the location	m
IR	surface temperature (infrared) technique	
I	gross irrigation	mm
I_o	effective irrigation	mm
J	energy stored in the crop volume	W m^{-2}
K_v	exchange coefficients for latent heat transfer	m^2 s^{-1}
K_h	exchange coefficients for sensible heat transfer	m^2 s^{-1}
K_T	clearness factor	
LAI	leaf area index	
M_c	mass of the soil core container	kg
M_d	molar mass of dry air	0.028964 kg mol^{-1}
M_{ds}	mass of the oven dried soil	kg
M_w	molar mass of water	0.018 kg mol^{-1}
P	carbon dioxide flux density	kg s^{-1} m^{-2}
P	$P_0 - \rho_{air} g\ h_l$ is the atmospheric pressure of the site	kPa
PM	Penman-Monteith technique	
P_o	atmospheric pressure at sea level	kPa
P_o	effective precipitation	mm
R	Universal gas constant	8.314 J K^{-1} mol^{-1}
RD	rooting depth	mm
RH	relative humidity	%
R_a	extraterrestrial solar irradiance	W m^{-2}

R_{sc}	solar constant	1353.7 W m^{-2}
R_n	net irradiance	W m^{-2}
RSC	relative sensitivity coefficient	
RP	refill point or the critical soil water content for the day in question	m^3 m^{-3}
R_s	observed solar irradiance	W m^{-2}
R_{so}	estimated solar irradiance of clear sky	W m^{-2}
r	radius of the soil core	m
r_a	aerodynamic resistance	s m^{-1}
r_{ah}	aerodynamic resistance for heat	s m^{-1}
r_{am}	aerodynamic resistance for momentum	s m^{-1}
r_{ap}	aerodynamic resistance for a well watered crop	s m^{-1}
$r_{astress}$	aerodynamic resistance for a water stressed crop	s m^{-1}
r_{av}	aerodynamic resistance for water vapour	s m^{-1}
r_c	canopy resistance	s m^{-1}
r_{cp}	canopy resistance for a well watered crop	s m^{-1}
r_i	quasi-resistance	s m^{-1}
r_l	stomatal resistance for leaves well exposed to solar radiation	s m^{-1}
t	local time	h
T'	temperature fluctuation of the air	°C
T_{an}	surface temperature	°C
T_{air}	air temperature	°C
T_{soil}	soil temperature	°C
$(T_{can} - T_{air})_{pe1}$	potential surface to air temperature differential using VPD as independent variable	°C
$(T_{can} - T_{air})_{Pe2}$	potential of surface to air temperature differential using VPD and net irradiance as independent variables	°C
$(T_{can} - T_{air})_p$	potential surface to air temperature differential calculated using the Penman-Monteith approach	°C
$(T_{can} - T_{air})_{ue1}$	non-transpiring surface to air temperature differential estimated from VPG and wind speed.	°C
$(T_{can} - T_{air})_{ue2}$	non-transpiring surface to air temperature differential estimated from net irradiance	°C
$(T_{can} - T_{air})_u$	non-transpiring surface to air temperature differential calculated using the Penman- Monteith approach.	°C
$(T_{can} - T_{air})_a$	the actual surface to air temperature differential calculated using the Penamn-Monteith approach.	°C
U_z	wind speed at height z_m above the surface	m s^{-1}
V	ThetaProbe output voltage	V
V	volume of the soil core	m^3
w'	vertical wind speed fluctuation	m s^{-1}
x	fetch (distance from the leading edge to the station)	m
z_h	heights for water vapour pressure and air temperature measurements	m
z_m	heights for wind measurements	m
z_o	surface roughness length	m
z_{oh}	surface roughness length for water vapour and heat transfer (z_{oh} = 0.0123h)	m
z_{om}	surface roughness lengths for momentum (z_{om} = 0.123h)	m
VPD	water vapour pressure deficit	kPa

β	Bowen ratio	
Δ	slope of the saturation water vapour pressure *vs* temperature relationship	kPa K^{-1}
ε	apparent dielectric constant	
ξ	relative error in any magnitude	
δ	solar declination	rad
δ_m	thickness of the equilibrium boundary sublayer	m
$\delta\theta$	measured profile equivalent temperature differential	K
γ	psychrometric constant	kPa K^{-1}
$\underline{\theta}$	zenith angle	rad
θ_V	volumetric soil water content	m^3 m^{-3}
θ_m	gravimetric soil water content	g g^{-1}
θ_{surfL}	soil water content at the soil surface	m^3 m^{-3}
θ_{va}	actual soil water content	m^3 m^{-3}
θ_{vi-1}	soil water content of the previous day	m^3 m^{-3}
$\theta_{wilting}$	soil water content at wilting point	m^3 m^{-3}
λE_a	actual latent heat energy flux density	W m^{-2}
$\lambda E_{(EC)}$	eddy correlation latent heat energy flux density	W m^{-2}
λE_p	potential latent heat energy flux density	W m^{-2}
$\lambda E_{a(IR)}$	surface temperature latent heat energy flux density	W m^{-2}
$\lambda E_{a(PM)}$	Penman-Monteith latent heat energy flux density	W m^{-2}
λ	latent heat of vaporization	J kg^{-1}
μ	quantum yield	J kg^{-1}
μP	energy flux density used in photosynthesis	W m^{-2}
ρ_{air}	density of air	kg m^{-3}
ρ_{soil}	particle density	kg m^{-3}
ρ_{bsoil}	soil bulk density	kg m^{-3}
ρ_w	density of water	998 kg m^{-3}
ω	sunset hour angle	rad
φ	latitude	rad
a	index symbolizing actual conditions	
c	index symbolizing canopy resistance	
e	index symbolizing empirical equation	
m	index symbolizing measured parameters	
p	index symbolizing potential conditions	
u	index symbolizing non-transpiring conditions	
1	index symbolizing regression equation between surface to air temperature differential and water vapour pressure deficit.	
2	index symbolizing the regression equation between surface to air temperature differential, and water vapour pressure deficit and net irradiance.	

LIST OF FIGURES

LIST OF TABLES

LIST OF APPENDICES

CHAPTER 1

INTRODUCTION

Water is rapidly becoming a critically limited resource because of increases in world population. The lack of efficient methods for water conservation is a major reason for water shortages. There is a need to solve these water-related problems if social, political, military and health catastrophes are to be avoided. There are many people, organizations and institutions involved in the management of water in the context of urban and rural environments, as well as agriculture, forestry and hydrology. However, solutions for water-related problems will depend on our understanding of water phenomena and on our capacity to measure water use. For example, use of the water in irrigation would involve measurement of soil water content and potentials, and the vertical flow of water in and out of soil water reservoir. This also involves the measurement of the amount of water added by irrigation and rain, the amount of runoff and the amount of water evaporated.

Evaporation is a major component of the soil water balance. It can be determined from measurements made on the soil, crop and microclimate. However, microclimatic methods are gaining popularity because of easy automation and sound theoretical basis. The Bowen ratio energy balance (BREB) and the surface temperature technique are examples. However, their performance under certain conditions is a cause for concern. The main reasons for the poor performance of microclimatic methods are the fulfilment of the assumptions adopted to derive the equations, sensor limitations and use of fixed "constants".

Understanding of the sensitivity of the technique used to estimate evaporation can be obtained by applying sensitivity analysis (Saxton, 1975; Beven, 1979; Alves, 1995). It is then possible to estimate the relative or absolute sensitivity of an output parameter (evaporation) to the changes in input parameters (e.g. air temperature, surface temperature, water vapour pressure, net irradiance, soil heat flux density, etc). Poor performance of evaporation measurement is obtained when inaccurate sensors are used. The calibration process can be used to detect and correct biassed sensors. Numerical

analysis, based on physical and empirical equations can also be used to assess the integrity and quality of the weather data by computing the extreme outliers for weather data measurement (Allen, 1996).

Most evaporation methods involve assumptions to avoid measurement of difficult components. For example, advection is usually excluded from the energy balance equation. Advection can contribute large amounts of energy to evaporation (Rosenberg, 1969a and 1969b; Rosenberg, Blad and Verma, 1983; Blad and Rosenberg, 1974). In the case of the BREB technique, only 53 % of daily data were reported to be reliable for estimating evaporation because of sensor and theoretical limitations (Tattari, Ikonen and Sucjsdorff, 1995). However, adaptations to the equipment have allowed some workers to measure evaporation throughout the day (Iritz and Lindroth, 1994; Cellier and Olioso 1993; Malek, 1992). It is common to use other alternatives to reduce errors caused by unreliable data for determining evaporation using the BREB technique (Malek, 1992; Savage, Everson and Metelerkamp, 1997). The surface temperature technique is the simplest technique and uses robust equipment to estimate evaporation. Nevertheless, a general overestimation of evaporation has been reported (Verma, Rosenberg, Blad and Baradas, 1976; Hatfield, 1983; Hatfield, 1984). However, on a smooth surface and under clear skies without advection Savage *et al.* (1997) found good agreement between sensible heat estimated using the surface temperature and eddy correlation techniques.

There are major problems in estimating evaporation for irrigation management purposes. For example, the crop water stress index (CWSI) which relates actual to potential evaporation (Jackson, Idso, Reginato and Pinter, 1981; Campbell and Norman, 1990), requires an estimate of the potential canopy resistance and "potential aerodynamic resistance" (O'Toole and Real, 1986; Jalali *et al.*, 1994). Estimates or measurements of actual canopy and aerodynamic resistances are also required to estimate the CWSI (Allen, Jensen, Wright and Burman, 1989; Malek *et al.*, 1991; Mascart *et al.*, 1991; Lindroth, 1993; Alves *et al.*, 1995). In addition, estimation of the CWSI using the surface temperature technique requires measurements and estimation of the actual, potential and non-transpiring surface to air temperature differential (Ids, Jackson, Pinter, Reginato and Hatfield,

transpiring surface to air temperature differential (Ids, Jackson, Pinter, Reginato and Hatfield, 1981a). The empirical method for estimating the CWSI has been related to the regression of the surface to air temperature differential (Y) and the water vapour pressure deficit (X), or water vapour pressure deficit (X_1) and net irradiance (X_2) (Idso *et al.*, 1981a; Jalali *et al.*, 1994). The CWSI can be estimated accurately if the correlation is high. A high correlation can be obtained when the various assumptions adopted to derive the energy balance equation are fulfilled. For example, a strong correlation of the regression may not be observed during strong sensible or latent heat advection.

Evaporation measurements are also used in irrigation management using the soil water balance equation. In its simplest form, the water balance states that, in a given volume of soil, the difference between the amount of water added and the amount of water withdrawn during a certain period is equal to the change in water content during the same period (Hillel, 1982). Soil water content is then estimated using the soil water balance and the estimated evaporation (Stegman, 1983; Cohen, Lopes, Slaks and Gogel, 1997). The irrigation requirement is estimated using the actual soil water content and the predetermined values of soil water content for the field capacity and the refill point (Campbell and Campbell, 1982). However, the performance of each evaporation technique may affect the performance of the estimated soil water content and subsequent irrigation requirements using the soil water balance method.

In this study, two techniques were used to measure evaporation: the BREB and the surface temperature technique. The performance of these two techniques under field conditions was investigated. The Penman-Monteith method and eddy correlation technique were used as standards for estimated latent and sensible heat, CWSI and the irrigation water requirement. The soil water content and irrigation requirement estimated using the ThetaProbe was used as standard for comparison.

The major objectives of this study were:

i) To analyse the reliability of measured data by (Chapter 4): (a) using the relative sensitivity

coefficient of latent heat due to the change in input parameter using the BREB and surface temperature techniques; the relative sensitivity coefficient of soil water content due to the variation in input parameter using a ThetaProbe was also analysed; (b) calibrating sensors from standards and accurate sensors; (c) comparing the fixed "constants" to the calculated ones; and (d) evaluating integrity of weather data by using the estimate of an extreme outliers for weather data.

ii) To evaluate the reliability of the estimated latent and sensible heat by (Chapter 5): (a) analysing the weather and fetch requirement, using mathematical models for rejecting unreliable data, and using the Bowen ratio sign (- or +) to depict probable effects of advection on the BREB-estimated latent heat; (b) analysing the effect of advection using the surface to air temperature differential, wind speed and comparative analysis between the surface temperature- and eddy correlation-estimated sensible heat; (c) comparing the BREB-and surface temperature-estimated latent heat with that estimated using the Penman-Monteith latent heat; and (d) evaluating the effect of placement height of air temperature sensors in the surface temperature-estimated sensible and latent heat.

iii) To evaluate irrigation management using surface temperature- and BREB-latent heat by (Chapters 6 and 7): (a) comparing the estimated CWSI using the Penman-Monteith method with that estimated using a combination of the surface temperature and empirical method, and combination of the surface temperature technique, the Penman-Monteith and empirical methods; and (b) comparing the ThetaProbe-estimated soil water content and irrigation requirement with that estimated using a water balance.

CHAPTER 2

ENERGY AND WATER BALANCE: THE CROP WATER STRESS INDEX AND IRRIGATION WATER REQUIREMENT

2.1 INTRODUCTION

The energy balance equation includes the net irradiance, soil heat flux density, sensible and latent heat flux density, the energy used in photosynthesis, advection and the stored energy flux density in the crop volume (Alves, 1995). The Penman-Monteith, BREB, and equilibrium evaporation theories are developed from the energy balance equation to estimate evaporation from the surface (Penman, 1948; Monteith, 1963; Stone and Horton, 1974; Savage *et al*, 1997). Eddy correlation and surface temperature technique can provide estimates of evaporation using the energy balance equation and the estimated sensible heat (Savage *et al.*, 1997).

Irrigation water requirement can be estimated directly from the energy balance equation through determination of actual and potential evaporation using the Penman-Monteith method to estimate the CWSI (Jackson *et al.*, 1981). The CWSI can also be determined using the actual, potential and non-transpiring surface to air temperature differential using empirical equations (Idso *et al.*, 1981a) or a combination of empirical and physically based equations (Penman-Monteith method and surface temperature technique) (Jackson *et al.*, 1981; O'Toole and Real, 1986 and Jalali *et al.*, 1994). The oldest technique for estimating irrigation water requirement is based on the soil water balance (Campbell and Campbell, 1982). This technique requires predetermination of the field capacity and refill point, and measurement or determination of actual soil water content or soil water potential. Estimation of soil water content can be achieved using the soil water balance in which evaporation is the prime component (Stegman, 1983; Cohen *et al.*, 1997).

The ability of the energy and water balance techniques for estimating evaporation and irrigation water requirement are reviewed in this chapter.

2.2 ENERGY BALANCE EQUATION

Micrometeorological methods for determining evaporation are based on the surface energy balance. The available energy at the surface (R_n - G) is equated to the consumption of the energy ($\lambda E + H + \mu P + A + J$). This energy balance is expressed as

$$R_n - G = \lambda E + H + \mu P + J + A \qquad 2.1$$

where R_n is the net irradiance (W m^{-2}), G is the soil heat energy flux density (W m^{-2}), λE is the latent heat energy flux density (W m^{-2}), λ is the latent heat of vaporization (J kg^{-1}), E is the water vapour flux density (kg s^{-1} m^{-2}), H is the sensible heat energy flux density (W m^{-2}), μP is the energy used in photosynthesis (W m^{-2}), μ is the quantum yield (J kg^{-1}), P is the carbon dioxide flux density (kg s^{-1} m^{-2}), J is the energy stored in the crop volume (W m^{-2}) and A being advection energy flux density (W m^{-2}).

The amount of energy utilized in photosynthesis, a maximum of 5 % of available energy, is approximately equivalent to the error one would get in measuring net irradiance (Alves, 1995). The energy stored in the crop volume (J) or in crop tissue and in the air inside the canopy is usually neglected when considering crops of a short height. Thus, neglecting these components and advection energy, the energy balance becomes as

$$R_n - G = \lambda E + H \qquad 2.2$$

The sign convention is that energy towards the cro is positive and away from the crop canopy is negative (Stone *et al.*, 1974). Rosenberg (1969a, 1969b), Blad and Rosenberg (1974) have stressed that strong advection increased latent heat to a point of using more energy than the available energy (R_n - G).

2.2.1 Penman-Monteith Equation

Monteith (1963) proposed a modification to Penman (1948) equation, under which biologically-based canopy and physically-based aerodynamic resistances were incorporated into the wind function (Steiner, 1991). A schematic illustration of the resistance models used by Monteith is shown (Fig. 2.1). Monteith (1963) assumed the surface canopy as uniform and homogeneous in the form of a big leaf surface.

Using Ohm's Law and Fig. 2.1 the sensible heat from the leaf surface to the atmosphere would encounter an aerodynamic resistance for heat (r_{ah}) defined as

$$r_{ah} = \rho_{air} Cp_{air}(T_{can} - T_{air})/H \qquad 2.3$$

where r_{ah} is the aerodynamic resistance for heat (s m^{-1}), ρ_{air} is the density of air (kg m^{-3}), Cp_{air} is the specific heat capacity of dry air at constant pressure (J kg^{-1} K^{-1}), T_{can} is the temperature of intercellular spaces (°C) and T_{air} temperature of the air in the atmosphere (°C).

Water vapour flow from the myriads of intercellular spaces to the atmosphere would encounter the stomatal resistance from intercellular space to the leaf surface and the aerodynamic resistance from the leaf surface to the atmosphere (Monteith and Unsworth, 1990). The combined resistance is defined as directly proportional to the vapour pressure differentials between the myriad of intercellular space and the atmosphere:

$$r_c + r_{av} = (\rho_{air} Cp_{air}/\gamma)[e_s(T_{can}) - e_{air}]/\lambda E \qquad 2.4$$

where r_c is the canopy resistance (s m^{-1}), r_{av} is the aerodynamic resistance to water vapour transfer (s m^{-1}), γ is the psychrometric constant (kPa $°C^{-1}$), $e_s(T_{can})$ is the saturation water vapour pressure at the intercellular temperature (kPa) and e_{air} is the actual water vapour pressure at air temperature (kPa).

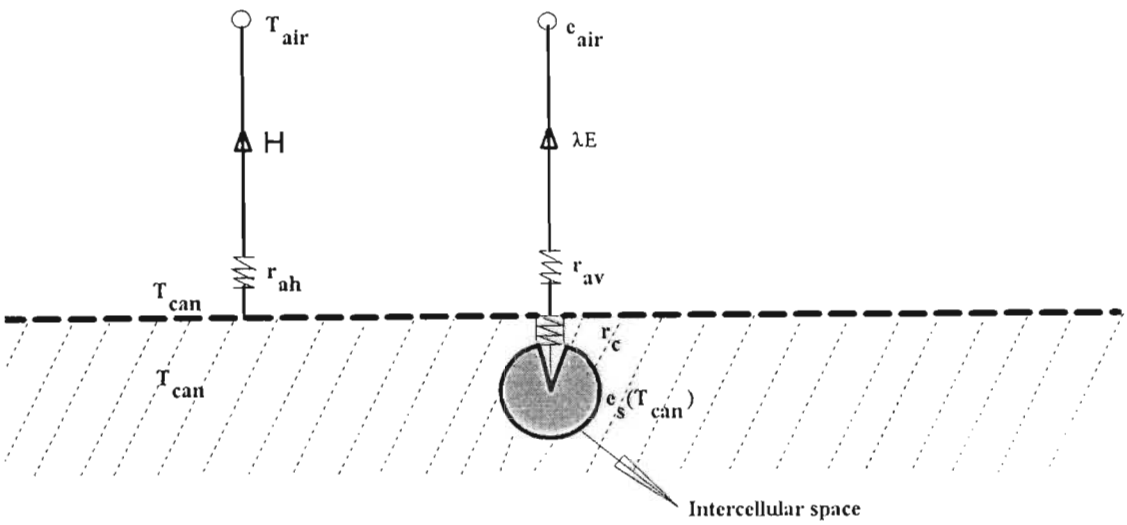

Figure 2.1 Diagram of the resistances for the transfer heat and water vapour (from Thom, 1975).

The relationship between water potential and water vapour pressure inside the intercellular spaces is defined by the Kelvin equation:

$$\psi = (RT_{can}/M_w) \ln [e_s(T_{can})/e_{airc}] \qquad 2.5$$

where R is the Universal gas constant (8.314 J K^{-1} mol^{-1}), T_{can} is the temperature in the myriad of the intercellular space, M_w is the molar mass of water (0.018 kg mol^{-1}) and e_{airc} is the vapour pressure in the myriad of the intercellular space (kPa). In Eq. 2.4, the water vapour inside the intercellular space is assumed at saturation. However, if one considers values of -4 MPa assumed for a well-watered crop (Alves, 1995) the air in the intercellular spaces would have a relative humidity of 97 %. It is also assumed that cuticular resistance is very big compared to the stomatal resistance. Therefore water flux through cuticle is neglected. Apart from the bulk stomatal resistance, one needs to consider a mixture of resistances to water vapour from the soil, plant and atmosphere within the big-leaf surface (Fig. 2.1) (Alves, 1995). Eq. 2.4 has been used to describe the diffusion of water vapour between the intercellular space for amphystomatous leaves and the atmosphere (Monteith and Unsworth, 1990).

To derive the expression for evaporation, the slope (Δ) of the saturated water vapour pressure *vs* temperature relationship (kPa) (Fig. 2.2) is needed:

$$\Delta = [e_s(T_{can}) - e_s(T_{air})]/(T_{can} - T_{air}) \qquad 2.6$$

where $e_s(T_{air})$ in kPa is the saturation water vapour pressure at air temperature (kPa). Other parameters were defined previously.

Combination of Eq. 2.6 [$e_s(T_{can}) = e_s(T_{air})+\Delta(T_{can} - T_{air})$] and Eq. 2.3 ($T_{can} = r_{ah}H/\rho_{air}Cp_{air} + T_{air}$) into Eq. 2.4 allows eliminating the "unknown" surface values, $e_s(T_{can})$ and T_{can}. The sensible heat H is eliminated by substituting Eq. 2.2 ($H = R_n - G - \lambda E$). Solving for λE and using the recommended substitutions gives the so-called Penman-Monteith equation:

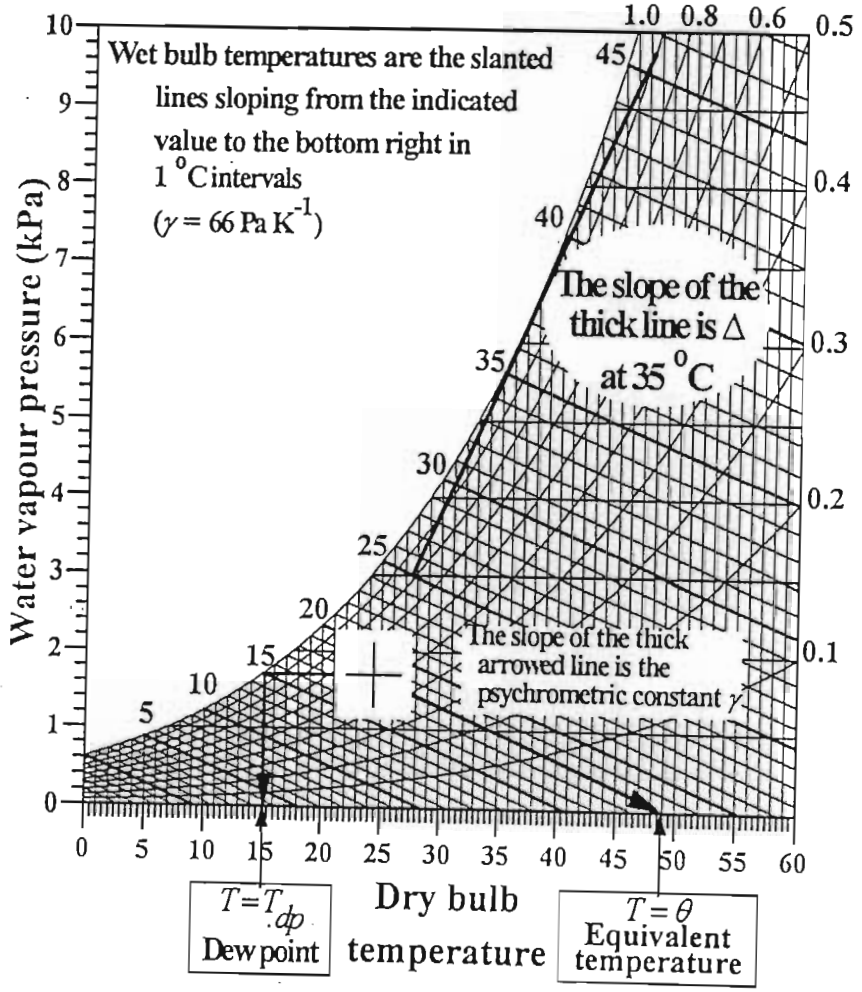

Figure 2.2 The psychrometric chart (taken from Savage *et al.*, 1997).

$$\lambda E = [\Delta(R_n - G) + \rho_{air} Cp_{air} \delta e / r_{ah}] / [\Delta + \gamma(r_{av} + r_c)/r_{ah}] \quad 2.7$$

Assuming that $r_{ah} = r_{av} = r_{am} = r_a$ (Alves, 1995) (where r_{am} is the aerodynamic resistance for momentum and r_a is the aerodynamic resistance), the Penman-Monteith equation can be reduced to

$$\lambda E_{(PM)} = [\Delta(R_n - G) + \rho_{air} Cp_{air} \delta e / r_a] / [\Delta + \gamma(1 + r_c/r_a)] \quad 2.8$$

2.2.2 Surface Temperature Equation

Surface temperatures may be used to estimate latent heat flux density using the energy balance equation (Eq. 2.2) with the sensible heat flux estimated using Eq. 2.3 (Stone *et al.*, 1974; Blad and Rosenberg, 1976b):

$$\lambda E_{(IR)} = (R_n - G) - \rho_{air} Cp_{air} (T_{can} - T_{air})/r_{ah} \quad 2.9$$

Where the index $_{(IR)}$ indicate the surface temperature (infrared) technique. Solutions for Eq. 2.9 depend on net irradiance, soil heat flux density, surface and air temperature and wind speed. For a larger remote sensing field of view (FOV), the measured surface temperature may reflect the weight of soil temperature, especially in areas with a mixture of soil and vegetation cover (Luvall and Holbo, 1986). Systematic overestimations of evaporation have been reported using this technique (Heilman and Kanemasu, 1976; Verma et al., 1976; Hatfield, 1984).

2.2.3 Crop Water Stress Index (CWSI)

The CWSI is defined in terms of the actual and potential evaporation which can be calculated using the Penman-Monteith method and the surface temperature technique (Jackson *et al.*, 1981, Campbell and Norman 1990):

$$CWSI = 1 - \lambda E_a / \lambda E_p \quad 2.10$$

where λE_a is the actual and λE_p the potential latent heat flux density. Actual latent heat can be estimated from Eq. 2.8 and Eq. 2.9 using measurements or estimates of water vapour pressure deficit (VPD), canopy and aerodynamic resistances, and the surface to air temperature differential. Similarly, potential evaporation can be determined using measurements or estimates of the potential VPD, canopy and aerodynamic resistances, and surface to air temperature differential. The actual to potential evaporation ratio estimated using the Penman-Monteith method was deduced (Jackson *et al.*, 1981; Campbell and Norman, 1990) as

$$\lambda E_a/\lambda E_p = \{[\Delta(R_n - G) + \rho_{air}\, Cp_{air}\, \delta e/r_a]/[\Delta + \gamma(1 + r_c/r_a)\,]\}/\{[\Delta(R_n - G) + \rho_{air}\, Cp_{air}\, \delta e/r_a]/[\Delta + \gamma(1 + r_{cp}/r_a)]\} = [\Delta+\gamma(1+r_{cp}/r_a)]/[\Delta+\gamma(1+r_c/r_a)] \quad 2.11$$

This ratio was used to estimate the CWSI as follows (Jackson *et al.*, 1981; Campbell and Norman, 1990):

$$CWSI=1-\lambda E_a/\lambda E_p = [\gamma(1+r_c/r_a)-\gamma(1+r_{cp}/r_a)]/[\Delta+\gamma(1+r_c/r_a)] \quad 2.12$$

The expression above relates a stress index to the fractional change in canopy resistance. Derivation of Eq. 2.12 assumes that net irradiance, soil heat flux and VPD will be the same under water stress conditions and under non-water-stressed conditions. Soil heat flux is dependent on soil water content, so its magnitude will be larger under well-watered soil conditions than under drier conditions. The net irradiance depends on longwave emitted from the surface and subsequently on the absorptivity, emissivity and reflectivity characteristic of the surface which again depend on water availability of the surface. In Eq. 2.12 the ratio $\lambda E_a/\lambda E_p$ varies from 1 for well-watered crop ($r_c = r_{cp}$) to 0 for water stressed crop ($r_c \rightarrow \infty$) with CWSI varying from 0 to 1.

The CWSI can also be estimated using the actual, potential and non-transpiring (or upper limit) surface to air temperature differential (Idso *et al.*, 1981a, b; Jackson *et al.*, 1981; Hatfield, 1983; Campbell and Norman 1990):

$$CWSI = [(T_{can} - T_{air})_a - (T_{can} - T_{air})_p]/[(T_{can} - T_{air})_u - (T_{can} - T_{air})_p] \quad 2.13$$

where $(T_{can} - T_{air})_a$ is the actual measured or estimated surface to air temperature differential (°C), $(T_{can} - T_{air})_p$ is the non-water-stressed baseline or the lower limit of the surface to air temperature differential under potential conditions (°C) and $(T_{can} - T_{air})_u$ is the non-transpiring surface to air temperature differential or the upper limit of the surface to air temperature difference when VPD = 0 kPa. The subscripts $_{a, p}$ and $_u$ refer to actual, potential and stress conditions, respectively.

2.2.3.1 Estimating Surface to Air Temperature Differential

The empirical potential surface to air temperature differential $(T_{can} - T_{air})_{pe}$ is obtained by linear regression of the $(T_{can} - T_{air})$ (Y) *vs* vapour pressure deficit (VPD) (X) (Ehrler, 1973; Idso *et al.*, 1981a) or VPD (X_1) and solar irradiance (X_2) (Jalali *et al.*, 1994) for a well-watered crop under cloudless conditions:

$$(T_{can} - T_{air})_{pe1} = a + b\ VPD \quad 2.14$$

$$(T_{can} - T_{air})_{pe2} = c + d\ VPD + eR_n \quad 2.15$$

where the subscript $_{e1}$ and $_{e2}$ refer to empirical Eq. 2.14 and Eq. 2.15. These relationships are believed to be unique for the crop and independent of the location where the crop is grown. Reported relationships for different crops are shown (Table 2.1 and Fig. 2.4). However, one needs to observe that there is an auto-self-correlation between $(T_{can} - T_{air})_{pe1}$ and VPD through air temperature and saturated water vapour pressure in Eq. 2.14 and Eq. 2.15. Additional auto-self-correlation is also observed in Eq. 2.15 between surface temperature and the outgoing longwave component of net irradiance.

The non-transpiring surface to air temperature differential (Eq. 2.14) corresponds to the intercept *a* of the regression if the intercept is negative (Idso *et al.*, 1981a; Idso, Reginato, Reicosky and Hatfield, 1981). However, if the intercept is positive, Idso *et al.* (1981a) recommend computation

of $(T_{can} - T_{air})_u$ as follows: i) define the average air temperature and calculate the surface temperature as air temperature plus the intercept; ii) calculate the saturated vapour pressure differential between canopy surface and air, $VPG = e_s(T_{can}) - e_s(T_{air})$. Then estimate $(T_{can} - T_{air})_u$ by substituting VPG into Eq. 2.14 with a wind correction factor (O'Toole and Hatfield, 1983) as

$$(T_{can} - T_{air})_{ue1} = a + bVPG + a' + b'U \qquad 2.16$$

where a' and b' are the intercept and slope of the regression between $(T_{can} - T_{air})_u$ and wind speed (U) (Table 2.2). The upper limit $(T_{can} - T_{air})_{ue2}$ for Eq. 2.15 is a function of net irradiance (Jalali *et al.*, 1994)

$$(T_{can} - T_{air})_{ue2} = f + gR_n \qquad 2.17$$

where $f = -2.59\ ^0C$ and $g = 0.0191\ ^0C\ W^{-1}\ m^2$ with an r^2 of 0.872 for cloudless conditions. With these empirical relationships, advection is not accounted for. Advection would alter the interaction between the surface to air temperature differential (Y) and VDP (X) or VPD (X_1) and net irradiance (X_2) that would exist due vertical flux only. Horizontal transport of water vapour into the field would also alter the relation reported in Eqs. 2.14 and 2.15. A graph with the potential (lower baseline) and non-transpiring (upper baseline) surface to air temperature differential is shown (Fig. 2.4). A CWSI can be determined from this graph using a measurement of actual surface to air temperature differential at a given VPD. The ratio of the vertical distance between the potential line and the point PWSI (BC) and the distance between the potential line and the non-transpiring line (AC) gives the CWSI (Idso *et al.*, 1981a). Interestingly, the regressions for the same crop for different soil and weather conditions were similar (Fig. 2.4).

The actual, potential and non-transpiring surface to air temperature differentials can be estimated using the Penman-Monteith approach (Jackson *et al.*, 1981, Jackson, 1982, Hatfield, 1983). Combining H (Eq. 2.3), λE (Eq. 2.4) and $e_s(T_o)$ (Eq. 2.6) into Eq. 2.2 and solving for surface to air

Table 2.1 Response of the potential surface to air temperature differential (Y) as influenced by water vapour pressure deficit (X) or water vapour pressure deficit (X_1) and net irradiance (X_2) for various crops (Idso, 1982).

Common Name	Scientific Name	Conditions	n	I	b	r	S_{yx}	S_I	S_b
Alfalfa	*Medigo sativa L.*	Sunlit	229	.51	-2.92	0.953	0.65	0.11	0.041
Barley	*Hordeum vulgars L.*	Sunlit, pre-heading	34	2.01	-2.25	0.971	0.17	0.22	0.098
		Sunlit, post-heading	72	1.72	-1.23	0.860	0.40	0.24	0.087
Bean	*Phaseolus vulgaris L.*	Sunlit	265	2.91	-2.36	0.978	0.72	0.11	0.031
		Shaded	65	-1.57	-2.11	0.973	0.39	0.17	0.064
Beet	*Beta vulgaris L.*	Sunlit	54	5.16	-2.30	0.982	0.46	0.16	0.060
Chard	*Beta vulgaris L. (Cicla)*	Sunlit	69	2.46	-1.88	0.955	0.58	0.17	0.071
Corn	*Zea Mays L.*	Sunlit, no tassels	97	3.11	-1.97	0.985	0.32	0.10	0.035
Cotton	*Gossipuim hirsutum L*	Sunlit	181	1.49	-2.09	0.971	0.38	0.13	0.038
Cowpea	*Vignia catjang Walp*	Sunlit	60	1.32	-1.84	0.991	0.34	0.14	0.034
Cucumber	*Cucumis sativus L.*	Sunlit	109	4.88	-2.52	0.962	0.82	0.23	0.069
		Shaded	59	-1.28	-2.14	0.982	0.57	0.19	0.054
Fig tree	*Ficus carica L.*	Sunlit	119	4.22	-1.77	0.924	0.66	0.21	0.068
Guyate	*Parthenium argentatum*	Sunlit	62	1.87	-1.75	0.928	0.89	0.31	0.094
Kohlrabi	*Brassica oleracea caulorapa communis DC*	Sunlit	70	2.01	-2.17	0.979	0.46	0.13	0.054
Lettuce leaf	*Lactuca scariola L*	Sunlit	89	4.18	-2.96	0.993	0.63	0.03	0.021
Pea	*Posmum sativum L*	Sunlit	85	2.74	-2.13	0.951	0.54	0.17	0.076
Potato	*Solanum tuberasum L.*	Sunlit	26	1.17	-1.83	0.922	0.67	0.45	0.157
Pumpkin	*Cucurbita Pepo L.*	Sunlit	76	0.95	-1.93	0.978	0.46	0.22	0.048
		shaded	89	-1.32	-2.10	0.985	0.47	0.14	0.039
Rutabaga	*Brassica napo brassica*	Sunlit	91	3.75	-2.66	0.988	0.54	0.14	0.044
	Ruta baga A.P. DC	Shaded	53	-0.50	-2.51	0.913	0.86	0.37	0.157
Soybean	*Glicina max L. Merr.*	Sunlit	125	1.44	-1.34	0.897	0.83	0.18	0.060
Squash, hubbard	*Cucurbita pepo L.*	Sunlit	90	6.91	-3.09	0.983	0.80	0.22	0.062
		Shaded	11	2.12	-2.83	0.993	0.65	0.44	0.113
Sqyash,zuchini	*Cucurbita pepo L.*	Sunlit	87	2.00	-1.88	0.935	0.38	0.17	0.036
Sugar beet	*Beta vulgaris L.*	Sunlit	47	2.50	-1.92	0.898	0.78	0.40	0.140
Sunflower	*Helianthus annuus L.*	Sunlit	53	0.66	-1.95	0.979	0.39	0.14	0.054
Tomato	*Lycopersicum suculentum Mill*	Sunlit	103	2.86	-1.96	0.936	0.64	0.13	0.033
Turnip	*Brassica rapa L.*	Sunlit	129	1.94	-2.26	0.979	0.63	0.14	0.042
Water lily	*Nuphar lateum Sibth. & Sm.*	Sunlit	36	8.99	-1.93	0.866	0.65	0.86	0.192
		Shaded	Not applicable to curvilinear relationship						
Wheat, produra	*Triticum durum Desf*	Sunlit, pre-heading	161	3.33	-3.25	0.947	0.63	0.15	0.87
		Sunlit, post-heading	56	2.88	-2.11	0.939	0.53	0.28	0.105

n = number of data points, I = Intercept, b = slope, r = correlation coefficient, S_{yx} = standard error of estimate of Y on X, S_I = standard error of the regression coefficient I, and S_b = standard error of the regression coefficient b, for the linear equation $Y = I + bX$, with temperature expressed in °C and vapour pressure in kPa.

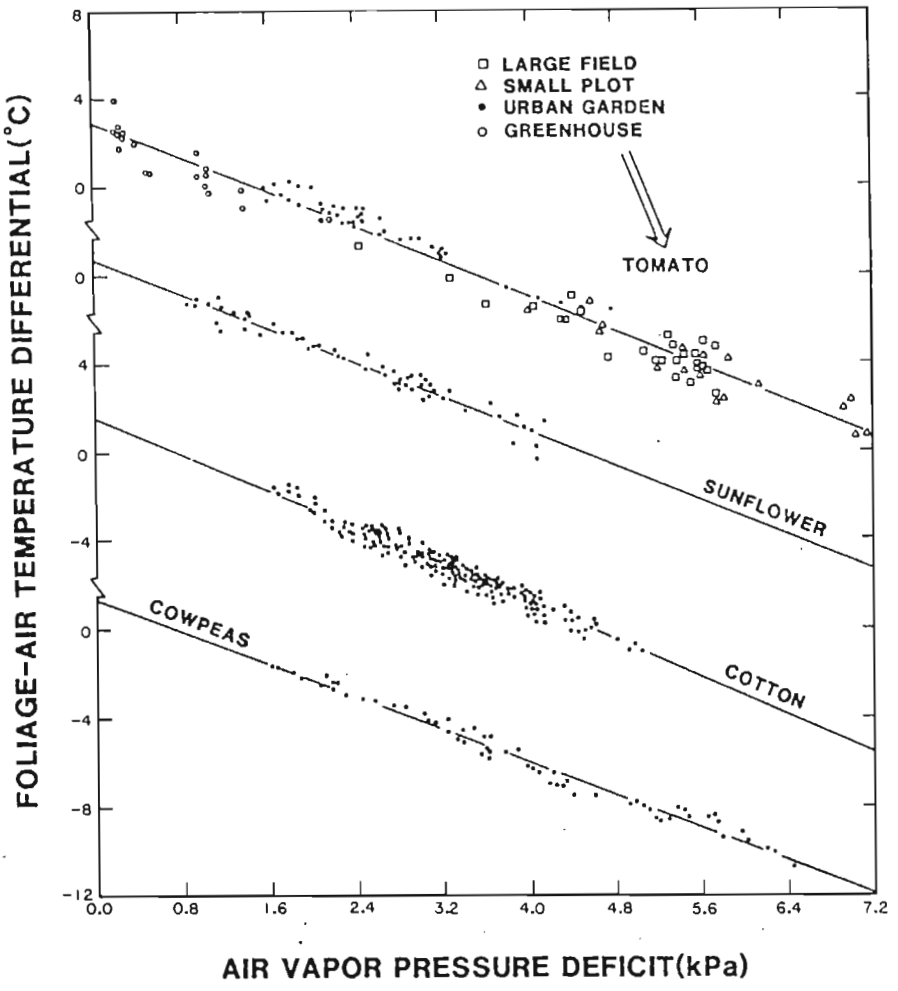

Figure 2.3 The regression of the surface to air temperature differential for the same crop under different soil and climatic conditions (Idso, 1982).

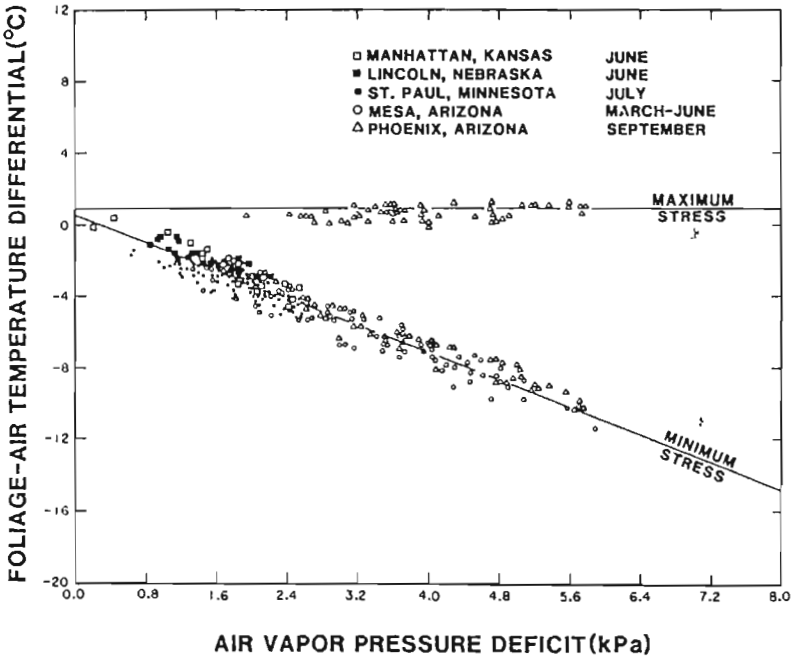

Figure 2.4 The potential surface to air temperature differential *vs* VPD and the non-transpiring surface to air temperature differential for alfalfa at variety of site across the US (Idso, 1982).

Table 2.2 Response of estimated non-transpiring surface to air temperature differential (Y) as influenced by wind speed (O'Toole and Hatfield, 1983).

Crop	Intercept	slope	r	n
Sorghum	1.89	-1.38	0.71	348
Corn	2.32	-1.38	0.63	207
Bean	0.79	-0.31	0.22	196

temperature differential yields:

$$(T_{can} - T_{air})_a = r_a(R_n - G)\gamma(1 + r_c/r_a)/\rho_{air}\, Cp_{air}[\Delta + \gamma(1 + r_c/r_a)] - VPD/[\Delta + \gamma(1 + r_c/r_a)] \quad 2.18$$

$$(T_{can} - T_{air})_p = r_{ap}(R_n - G)\gamma(1 + r_{cp}/r_{ap})/\rho_{air}\, Cp_{air}[\Delta + \gamma(1 + r_{cp}/r_{ap})] - VPD/[\Delta + \gamma(1 + r_{cp}/r_{ap})] \quad 2.19$$

$$(T_{can} - T_{air})_u = r_{astress}(R_n - G)/\rho_{air}\, Cp_{air} \quad 2.20$$

where $r_{astress}$ is the aerodynamic resistance under water stressed conditions. Use of the Penman-Monteith approaches requires estimates of r_c and r_a for $(T_{can} - T_{air})_a$ and $\lambda E_{a(PM)}$, r_{cp} and r_{ap} for $(T_{can} - T_{air})_p$ and $\lambda E_{p(PM)}$, and $r_{astress}$ for $(T_{can} - T_{air})_u$. Eq. 2.20 is used to estimate the non-transpiring surface to air temperature differential when $r_c \rightarrow \infty$ (Jackson, 1982). The surface to air temperature differential from Eqs 2.18 and 2.19 can be used to theoretically estimate the actual and potential evaporation using the surface temperature technique (Eq. 2.9).

2.2.3.2 Extreme Canopy and Aerodynamic Resistances

O'Toole and Real (1986) and Jalali *et al.* (1994) estimated r_{cp}, r_{ap} and $r_{astress}$ by coupling empirically-based equations (Eqs 12 to 15) and the energy balance approaches (Eqs 2.18 to 2.20). The resulting equations, depending on the regression used, were as follows:

$$r_{ap1} = a\, \rho_{air}\, Cp_{air}/[(R_n + G)(1 + b\Delta)] \quad 2.21$$

$$r_{ap2} = e\, \rho_{air}\, Cp_{air}/(1 + d\Delta) \quad 2.22$$

$$r_{astress} = 0.0191\, \rho_{air}\, Cp_{air} \quad 2.23$$

$$r_{cp1} = -r_{ap}\,(1 + b(\Delta + \gamma)/b\gamma \quad 2.24$$

$$r_{cp2} = -r_{ap}\,(1 + d(\Delta + \gamma)/d\gamma \quad 2.25$$

The r_{cp} and r_{ap} resistances are the theoretical canopy and aerodynamic resistances one would get under potential conditions. The $r_{astress}$ is the aerodynamic resistance under water stressed conditions. Since the linear regressions represented by Eqs 2.14 to 2.17 are assumed unique for each crop under cloudless conditions, the estimated r_{cp}, r_{ap} and $r_{astress}$ values from Eqs 2.21 to 2.25 will also be crop specific. However, one needs to remember all assumptions for the formulation of the shortened energy balance and the Penman-Monteith equations for actual and potential conditions. On the other hand, these estimates will approach real values if the r^2 values of Eqs. 2.14 and 2.15 are large. The empirical relationship needs also to be determined under a full canopy cover.

2.2.4 Actual Canopy and Aerodynamic Resistances

The physiological resistance of the Penman-Monteith equation is commonly related to canopy resistance and consequently to the stomatal resistance of the leaves. However, this resistance includes the surface soil resistance to water vapour (r_s), the aerodynamic resistance from the soil to the leaf surface (single leaf surface) (r_u), the aerodynamic resistance from the leaves to leaf surface (single leaf surface) (r_b) and the canopy resistance to water vapour (r_c) (Massman, 1992) (Fig 2.5). The

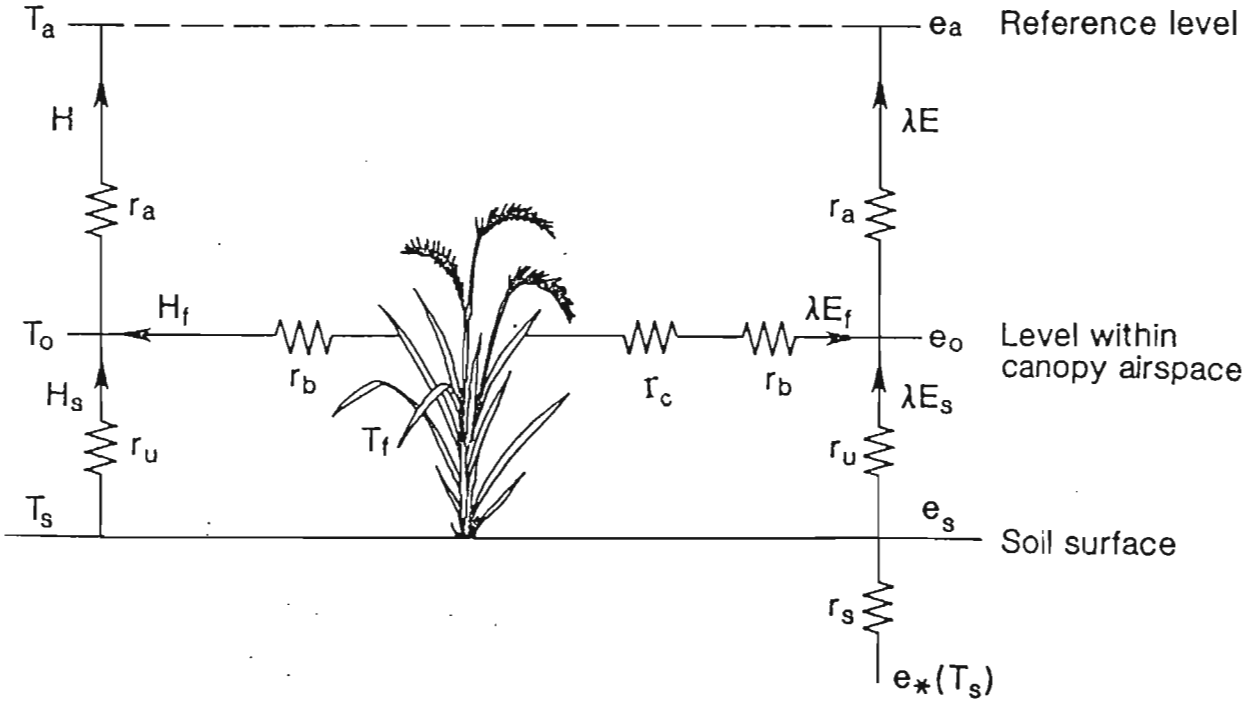

Figure 2.5 A schematic representation of resistances involved in the bulk (canopy) resistance for the transfer of water vapour (Massman, 1992).

Penman-Monteith Eq. 2.8 (Malek *et al.*, 1991; Lindroth, 1993) can be used to determine this global canopy resistance

$$r_c = [\Delta(R_n - G) + \rho_{air}\, Cp_{air}\, \delta e/r_a]/\lambda E - \Delta - \gamma \qquad 2.26$$

where λE can be measured using a lysimeter or eddy correlation techniques. Since only 50 % of the leaf area index (LAI) accounts for the transpiration process, expressions (Allen *et al.*, 1989; Alves, 1995) dependent on stomatal resistance have been used for determining the canopy resistance of a crop:

$$r_c = r_l/(0.5LAI) \qquad 2.27$$

where r_l is the mean stomatal resistance of the leaves well exposed to solar irradiance.

Most of the empirical equations for canopy resistance have been related to solar irradiance, air temperature, VPD, water potential of the leaf, soil water potential and soil water content. The empirical expression reported by Mascart *et al.* (1991) combined the potential canopy resistance r_{cp} (Eqs 2.21 and 2.22), the variation of solar irradiance R_s and the water stress due to water deficits in the rooting zone θ_{rootZ} to estimate the actual canopy resistance as

$$r_c = r_{cp}\, [F_1(R_s) + F_2(\theta_{rootZ})]\, F_3 \qquad 2.28$$

In Eq. 2.28, $F_1(R_s) = R_{so}/(1 + R_s)$ is the solar irradiance function, R_{so} is the solar irradiance of a clear sky (W m^{-2}) (Section 4.3.1), R_s is the observed solar irradiance (W m^{-2}), $F_2(\theta_{rootZ}) = 1.2\, \theta_{wilting}/(0.9\theta_{rootZ} + 0.1\theta_{surfL})$ is the soil water function, $\theta_{wilting}$ is the soil water content at wilting point ($m^3\ m^{-3}$) and θ_{surfL} is the soil water content at the soil surface ($m^3\ m^{-3}$). The term $F_3 = P_s/h$ is the shelter function, where P_s is the factor accounting for leaf shadowing at a crop height h.

Allen *et al.* (1989), Steiner, Howel and Scheineder (1991) and Alves *et al.* (1995) estimated the aerodynamic resistance as an inverse function of wind speed:

$$r_a = \ln [(z_m - d) / z_{om}] \ln [(z_h - d)/z_{ov}] / (k^2 U_z) \quad 2.29$$

where U_z is the wind speed in m s^{-1} at height z_m (m) above the surface, d is the zero-plane displacement height (d=0.67h where h=crop height in m), z_{om} is the surface roughness length for momentum (z_{om} = 0.123h in m), z_{oh} is the surface roughness lengths for water vapour and heat transfer (z_{oh} = 0.0123h in m), k is the von Karman's constant (taken as 0.41) and z_h is the heights for water vapour pressure and air temperature measurements (m).

Analysis of Eq. 2.29 suggests that the flow of water vapour or heat would be easier when the surface is rougher and when there is strong wind (Alves, 1995). Determination of zero-plane displacement height d and surface roughness length is complex since they require profile measurement of wind speed. Empirical expressions based on crop height have been used to determine the parameters (Allen *et al.*, 1989; Alves, 1995). Eq. 2.29 assumes an equality between aerodynamic resistance for water vapour and for heat flux. This can only be observed under neutral conditions when there is no predominance of vertical motion. For unstable condition there is a predominance of the upward vertical velocity over the horizontal due to a strongly heated surface. As a result, the aerodynamic resistance for heat will be smaller than that for water vapour. The opposite may occur under stable conditions when there is a predominance of descending air.

2.2.5 Equilibrium Evaporation

The Penman-Monteith equation (Eq. 2.8) can be written as

$$\lambda E = [\Delta r_a (R_n - G) + \rho_{air} c_p \delta e]/[\Delta r_a + \gamma(r_c + r_a)] \quad 2.30$$

Dividing λE by available energy (R_n - G) yield:

$$\lambda E/(R_n - G) = [\Delta r_a + \rho_{air} c_p \delta e/\gamma(R_n - G)]/[\Delta r_a + \gamma(r_c + r_a)] \quad 2.31a$$

where the term

$$\rho_{air} c_p \delta e/(R_n - G) = r_i \quad 2.31b$$

is the so-called quasi-resistance (Savage *et al.*, 1997). This is so called because it cannot be depicted using a diagram. The quasi-resistance is directly proportional to VPD (δe) and inversely proportional to available energy ($R_n - G$) (Savage *et al.*, 1997). That is, Eq. 2.31a can be written in resistance form as

$$\lambda E = (R_n - G)(\Delta r_a + \gamma r_i)/[\Delta r_a + \gamma(r_c + r_a)] \quad 2.32$$

Stomatal resistance of a crop will be related to soil water availability. It increases when the soil is dry and decreases when the soil is well supplied with water. Aerodynamic resistance will be high when wind speed is low and small when wind speed is strong. From Eq. 2.32 and taking into consideration the variations of the canopy, aerodynamic and quasi- resistance according to the prevailing weather conditions one can diagnose different cases of the Penman-Monteith equation. For example, the equilibrium case is defined as a weak flow of humid air over a crop well supplied with water from irrigation or rain. Weak flow implies larger aerodynamic resistance, humid air implies smaller quasi-resistance and soil well supplied with water implies smaller stomatal resistance. Substitution of these resistances into Eq. 2.32 gives the equilibrium evaporation:

$$\lambda E = (R_n - G)\Delta/(\Delta + \gamma) \quad 2.33$$

Equilibrium evaporation assumes a potential canopy resistance of zero. This is somewhat different to the true canopy resistances under potential evaporation. However, Eq. 2.33 has been used

irradiance, soil heat flux density, and constant values of Δ and γ. Metelerkamp (1993) and Savage *et al.* (1997) used Eq. 2.33 to estimate evaporation during the period when their BREB technique did not provide reliable estimates of evaporation due to the difficulty of measuring water vapour pressure gradients using a cooled mirror.

2.2.6 Eddy Correlation

The eddy correlation technique is based on fluctuations in the vertical wind speed, air temperature, and water vapour pressure in the constant boundary layer (Monteith and Unsworth, 1990). The sensible heat flux for an averaged time can be written as

$$H = \rho_{air} Cp_{air} \overline{Tw} \qquad 2.34$$

The over bar indicates time-averaged values (typically 10 to 30 minutes). Since the instantaneous values can be expressed as the sum of the average and its fluctuations Eq. 2.34 becomes

$$H = \rho_{air}Cp_{air} (\overline{T} + T') (\overline{w} + w') = (\rho_{air}Cp_{air} \overline{Tw} + \rho_{air}Cp_{air} \overline{T}\overline{w'} + \rho_{air}Cp_{air} \overline{T'}\overline{w} + \rho_{air}Cp_{air} \overline{T'w'}) \qquad 2.35$$

The term $\rho_{air}Cp_{air}Tw'$ is zero because the fluctuations associated with T can make no net transport. The terms $\rho_{air}Cp_{air}Tw$, $\rho_{air}Cp_{air}T'w$ also equate 0 because, for sufficiently long periods of time over horizontally uniform terrain, the quantity of ascending air is approximately equal to the quantity descending. Thus, the mean value of the vertical velocity will be negligible (Rosenberg *et al.*, 1983), that is $\rho_{air}Cp_{air} \overline{T'}\overline{w} = 0$. Thus, Eq. 2.35 becomes

$$H = \rho_{air}Cp_{air} \overline{T'w'} \qquad 2.36$$

A flux of heat towards the surface arises when eddies moving towards the surface contain air at higher temperature than the average(Monteith and Unsworth, 1990). However, assumption of $\rho_{air}Cp_{air}\ \overline{T'w} = 0$ is not observed when the vertical flux of air is humid which is a normal occurrence (Monteith and Unsworth, 1990). Similar analysis can also be done to estimate latent heat using eddy correlation. However, Savage *et al.* (1995) using KH20 sensors showed that the sonic instrument was not sufficiently accurate for a high frequency measurement of absolute humidity. The latent heat flux density has been determined indirectly from the estimated eddy correlation sensible heat using the energy balance equation:

$$\lambda E_{(EC)} = (Rn - G) - \rho_{air}Cp_{air}\ \overline{T'w'} \qquad 2.37$$

where the index $_{(EC)}$ indicate eddy correlation. However, Schotanus *et al.* (1983) and Kaimal and Gaynor (1991) also reported difficulties in the measurement of temperatures using sonic sensor due to fluctuations in both humidity and wind speed observed in neutral and stable conditions when temperature fluctuations are negligible. Schotanus *et al.* (1983) provided correction factors for the product w'T'. However, when properly applied, the technique provides reasonably accurate estimates of fluxes more directly over different surfaces and under varying conditions than does the surface temperature technique (McMillen, 1988). This estimate can then be used as a standard to compare values of sensible heat estimated using other techniques. Direct measurement of sensible heat and latent heat can be used to estimate the exchange coefficients (refered to in the following section) and aerodynamic resistances for heat and water vapour transfer.

2.2.7 Bowen Ratio Energy Balance (BREB)

According to Fick's Law of diffusion, the latent heat (λE) and the sensible heat energy flux density (H) is related to the product of the exchange coefficient and to the entities concentration gradient as

$$\lambda E = (\rho_{air}c_p/\gamma)K_v\ \partial e/\partial z \approx (\rho_{air}c_p/\gamma)K_v\ (e_{air2} - e_{air1})/(z_2 - z_1) \qquad 2.38$$

$$H = (\rho_{air} c_p K_h)\, \partial T/\partial z \approx (\rho_{air} c_p K_h)\, (T_{air2} - T_{air1})/(z_2 - z_1) \qquad 2.39$$

where K_v and K_h are exchange coefficients for latent and sensible heat transfer ($m^2\ s^{-1}$) respectively, e_{air1} and e_{air2} and T_{air1} and T_{air2} are water vapour pressure (Pa) and air temperature (°C) at level z_1 and z_2 respectively. Bowen (1926) introduced the ratio β, generally known as the Bowen ratio, which is the proportionality coefficient between H and λE,

$$\beta = H/\lambda E \approx [(\rho_{air} c_p K_h)(T_{air2} - T_{air1})/(z_2 - z_1)]/[(\rho_{air} c_p/\gamma) K_w (e_{air2} - e_{air1})/(z_2 - z_1)] \qquad 2.40$$

Following the application of the Similarity Principle (SP) (Savage *et al.*, 1997) the two exchange coefficients are assumed equal ($K_h = K_v$) and their ratio is therefore unity. The SP can only hold under neutral conditions, observed only during dawn and dusk (Tanner, 1963). During periods of high evaporation, values of β are small and acceptance of SP when K_h and K_v are not markedly different will not lead to serious error in the estimation of latent heat (Savage *et al.* 1997). The SP can also hold under windy conditions close to the rough surface when forced convection overcomes free convection due to excess friction (Tanner, 1963 and Savage *et al.*, 1997). In this case the lower level should be set at least 3-5 times the height of the roughness elements of the canopy (Tattari *et al.*, 1995). Larger errors can be expected when the surface is dry, λE is small and β values are large. However, acceptance of the Similarity Principle simplifies Eq. 2.40 so that β can be calculated using measurement of air temperature and vapour pressure at two levels in the atmosphere:

$$\beta = H/\lambda E \approx \gamma\, [(T_{air2} - T_{air1})/(e_{air2} - e_{air1})] \qquad 2.41$$

Metelerkamp (1993) estimated K_h and K_v using Eqs. 2.38 and 2.39 by measuring the profile air temperature and water vapour pressure. He also used latent heat measured using standard lysimeter and sensible heat using the energy balance equation. The eddy correlation technique can also be used to measure sensible heat and latent heat required to estimate the exchange coefficients.

To calculate the flux terms using the BREB technique, the simplified surface energy balance (Eq. 2.2) is required which may be combined with Eq. 2.41 to yield

$$\lambda E = (R_n - G)/(1 + \beta) \quad 2.42$$

$$H = (R_n - G)/(1 + 1/\beta) \quad 2.43$$

The accuracy for measuring energy fluxes using these equations will depend on the validity of assumptions for the shortened energy balance equation and computation of the Bowen ratio from measurement of the profile entities.

2.2.7.1 BREB Requirement and Limitation

The entities must be measured within the boundary layer and in the portion of the equilibrium boundary sublayer, implying the absence of horizontal gradients (Heilman, Brittin and Neale, 1989; Nie, Flitcroft and Kanemasu, 1992; Tattari *et al.*, 1995). The extent of the equilibrium sub-layer (δ_m') is 5 to 10 % of an internal boundary layer:

$$\delta_m' = 0.1\ x^{0.8}\ z_o^{0.2} \quad 2.44$$

where x is the fetch and z_o is the surface roughness length (Heilman *et al.*, 1989). An illustration of the planetary boundary layer is shown (Fig. 2.6). On the other hand, the lower sensor must be installed above the surface by three to five times the height of the roughness elements. Heilman *et al.* (1989) successfully used the equipment with a fetch-to-height of 20:1, much less than the often-quoted value of 100:1.

Eqs 2.42 and 2.43 give infinite latent and sensible heat flux density when β approaches -1. This case is observed when $H = -\lambda E$ or $-H = \lambda E$ during sunset and sunrise as net irradiance diminishes and the available energy becomes less. It can also be observed during rain and the oasis case when a strong mass of dry air flows over an irrigated crop, resulting in sensible heat flux strongly negative (Cellier

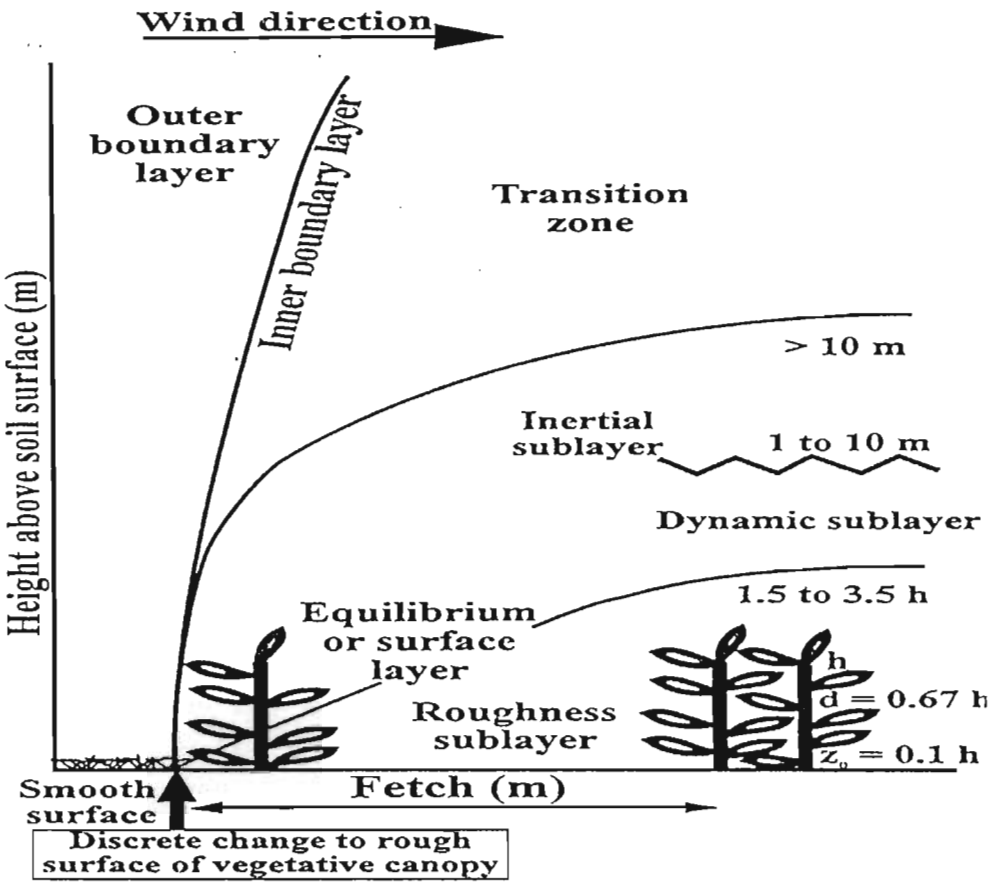

Figure 2.6 The planetary boundary layer (Thom (1975) taken from Savage *et al.*, 1997).

and Olioso, 1993). This fact becomes important because Eqs 2.42 and 2.43 give large values of sensible and latent heat when existent conditions suggest small latent and sensible heat. There is then a need to exclude data of temperature and water vapour pressure in which $-1.25 < \beta < -0.75$ (Cellier and Olioso, 1993 and Savage *et al.*, 1997).

Data are also inconclusive when the vapour pressure and air temperature difference fall within the dew point mirror and thermocouple resolution limits (Savage *et al.*, 1997). This situation may be observed during equilibrium evaporation when profile differentiations of water vapour pressure becomes limited due to sensor resolution. Condensation of water in/on the air intake tubing, filters and thermocouples preclude any meaningful measurement of fluxes (Savage *et al.*, 1997 and Tattari *et al.*, 1995) during dew, rain and irrigation. Meaningful use of the BREB is seldom obtained during nighttime, due to the deposition of dew and the small differential between air temperature and water vapour pressure measured at different heights. Accordingly, only measurements taken during daytime

are used to compute fluxes using the BREB technique (Nie *et al.*, 1992 and Savage *et al.*, 1997).

A mathematical expression by Ohmura (1982) discards unreliable data caused by model and sensor limitation using the BREB technique. The simplified expressions for deriving Ohmura rejection limits are discussed by Savage *et al.* (1997). They stated that the difference between the measured profile equivalent temperature ($\delta\theta$) and the true profile equivalent temperature difference ($d\theta$)[1] is less than twice the resolution limit in equivalent temperature $E(\theta)$:

$$|\delta\theta - d\theta| < 2E(\theta) \qquad 2.45$$

where $\delta\theta = \delta T + \delta e/\gamma$, $d\theta = dT + de/\gamma$ and $E(\theta) = E(T) + E(e)/\gamma$, T is the air temperature and e is the water vapour pressure. The ratio β, can then be calculated as

$$\beta = \gamma d\theta/de - 1 \qquad 2.46$$

which means that the ratio is -1 if $d\theta = 0$. By substituting the respective values and expressions into Eq. 2.45 and after subtracting all components from $\delta e/\gamma$, the limit within which the measured temperature difference, δT, are considered unreliable for computing fluxes is obtained as

$$-2[E(T) + E(e)/\gamma] - \delta e/\gamma < \delta T < +2[E(T) + E(e)/\gamma] - \delta e/\gamma \qquad 2.47$$

Although simple in theory, the BREB technique is seldom used accurately to estimate latent heat under different weather conditions. It is common to substitute the rejected BREB data using the average between the proceeding and subsequent data (Malek *et al.*, 1991) or using equilibrium evaporation (Savage *et al.*, 1997).

---

[1]The equivalent temperature θ (K) was defined by Savage (1996) as $\theta = T + e/\gamma$ where T (K) = T (°C) + 273.16 and e (kPa) is the water vapour pressure.

2.2.8 Parameters for Assessing Micrometeorological Determination of Evaporation

2.2.8.1 Density of Air

Air density is normally taken as constant with a value of 1.12 kg m^{-3}. However, this parameter is affected by altitude (h_l), air temperature, water vapour pressure and atmospheric pressure (P_o). An expression relating air density to different factors is given (Savage et al., 1997),

$$\rho_{air} = [\ -e(M_d - M_w) + M_d P_o]/(RT_{air} + M_d g h_l) \qquad 2.48$$

Since M_d is 0.028964 kg mol^{-1} (the molar mass of dry air), M_w is 0.018101534 kg mol^{-1} (molar mass of water vapour), R is 8.31451 J K^{-1} mol^{-1} (universal gas constant) and assuming a fixed value of gravitational acceleration (it is dependent on altitude and latitude) of 9.7922 m s^{-2} Eq. 2.48 can be rewritten as

$$\rho_{air} = (\ -0.0109866e + 28.969P_o)/[8.3145(T_{air} + 273.15) + 0.2836h_l] \qquad 2.49$$

The above expression ignores the importance of carbon dioxide density.

2.2.8.2 Specific Heat Capacity of Air

Specific heat capacity can be calculated according to Savage *et al.* (1997) as

$$Cp_{air} = 7/2\ (R/M_d) + (4R/M_d)[e/(P - e)] + \delta Cp \qquad 2.50$$

where $\delta Cp_{air} = 1.256(1 + T_{air}/40)(1 + e/e_s)$ is dependent on atmospheric pressure, air temperature and fractional relative humidity. When constants are substituted Eq. 2.50 is simplified to,

$$C_p = 1004.72 + 1148.3\ [e/(P\text{-}e)] + 1.256\ (1 + T_{air}/40)(1 + e/e_s) \qquad 2.51$$

where $P = P_0 - \rho_{air} g\ h$ is the atmospheric pressure of the site. The saturation water vapour pressure

is calculated from air temperature as

$$e_s = 0.6108 \exp[17.2694\ T_{air}/(237.3 + T_{air})] \quad 2.52$$

The psychrometric chart (Fig. 2.2) can also be used to estimate the saturation water vapour pressure. A constant value of 1004 J kg^{-1} K^{-1} has been used. However, Eq. 2.51 shows that Cp varies with the temperature, water vapour pressure and atmospheric pressure. For example at T_{air} = 20.50 °C and e_s = 1445.9 Pa the specific heat capacity will be 1024.5 J kg^{-1} K^{-1} while for T_{air} = 24.45 and e_s = 2124.4 the specific heat capacity of the air is 1033.2 J kg^{-1} K^{-1}.

2.2.8.3 Psychrometric Constant

The psychrometric constant γ at sea level pressure and air temperature of 0 °C is about 0.0655 kPa K^{-1}. This value is considered as constant and used to compute energy transfer. However, Allen, Smith, Perrier and Perreira, *et al.* (1994) and Savage et al. (1997) calculated the psychrometric constant as

$$\gamma = C_p P/\varepsilon\lambda \quad 2.53$$

where $\varepsilon = M_w/M_d = 0.018081534/0.028964 = 0.621807$. The latent heat of vaporization (J kg^{-1}) is calculated using a regression based on air temperature (T_{air}) as

$$\lambda = 2500.95 - 2.36679\ T_{air} \quad 2.54$$

At 20 °C λ is 2.453 kJ kg^{-1}. In the psychrometric chart (Fig. 2.2) the psychrometric constant is the slope magnitude of the wet bulb temperature lines.

2.2.8.4 Slope of the Saturation Vapour Pressure *vs* Temperature Relationship

The slope of the saturation water vapour pressure *vs* temperature curve (Fig.2.2) can be calculated

Because IRT is seldom used in routine meteorological measurement, it is necessary to estimate Δ. McArthur (1990) used Eq. 2.6 and 2.18 to estimate Δ and T_{can} by iteration. In the first step he used Δ based on air temperature T_{air} to estimate T_{can}

$$\Delta = 4098.02862\ e_s/(237.3 + T_{air})^2 \qquad 2.55$$

A new value of Δ is calculated by substituting T_{can} in Eq. 2.6. This procedure is repeated *n* times until the successive values of T_{can} and Δ are insignificantly different from the previous values.

2.3 SOIL WATER BALANCE

Soil water techniques are one of the oldest methods for scheduling irrigation (Campbell and Campbell, 1982). These techniques require predetermined values of field capacity and the refill point. They also require an estimate or field measurement of the actual soil water content/potential. The difficulty in applying the method lies in finding automated, precise, non-destructive and *in situ* measurement techniques for soil water measurement. The laboratory method and neutron probe fail to satisfy these requirements. However, the first is still used as standard technique. Radiative hazards and high costs restrict the use of the neutron probe. The tensiometer, the resistance and heat dissipation blocks can fulfil the above requirement. However, the tensiometer can only measure soil water potential between saturation and -80 kPa. For tension above -80 kPa, air entry into the tensiometer system perturb meaningful measurement. The ML1 ThetaProbe (Delta-T Devices, Cambridge, England) as well as other so-called time-domain reflectometry (TDR) and frequency-domain reflectometry (FDR) techniques can provide a continual, precise and non-destructive measurement of soil water content under field conditions. However, soil variability constitutes a problem in using the technique for scheduling irrigation for a large agriculture area.

Micrometeorological methods for measuring evaporation may also be used for scheduling irrigation. Estimation of soil water content can be done by using the soil water balance in which evaporation is a prime component (Stegman, 1983; Cohen *et al.*, 1997). This way of estimating soil water content

can offer an automated and non-destructive technique of determining irrigation water requirements. In addition, a large area can be monitored using this technique, in particular when using a remote sensing technique to estimate evaporation. However, different evaporation techniques would estimate different amounts of evaporation when performed under similar soil, crop and climatic conditions. The soil water content can be estimated from a soil water balance (Pleban and Israeli, 1989; Villalobos and Fereres, 1989; Azhar, Murty and Phien 1992) as:

$$\theta_{va} = \theta_{vi-1} - (\lambda E - P_o - I_o)/RD \qquad 2.56$$

where θ_{va} is the actual soil water content ($m^3\ m^{-3}$), θ_{vi-1} is the soil water content of the previous day ($m^3\ m^{-3}$), λE is the evaporation (mm), P_o is the effective precipitation (mm), I_o is the effective irrigation (mm) and RD is the depth of the rooting zone (mm).

In monitoring the soil water balance the water content is computed daily by subtracting water lost by evaporation and adding water gain by rainfall or irrigation. The soil water content of the first day can be measured or assumed as the soil water content at field capacity if any rain or irrigation has occurred two to three days before the start of an irrigation process. Otherwise, one can use a laboratory method to measure the soil water content on the first day. Irrigation and rain can be easily measured using a raingauge (in case of sprinkler irrigation). However, effective irrigation and rain are not easily estimated since one needs to account for intercepted water on the canopy, poor distribution (in the case of irrigation) and runoff losses. Evaporation can be measured using methods reported above.

Eq. 2.56 allows evaluation of evaporation measurement techniques using soil water content sensors. However, the equation assumes a negligible surface runoff into and from the field in question and vertical flux of water up or down the lower depth of the rooting zone. These assumptions can be met when the surface is flat, the water table is far from the rooting depth and irrigation water is applied without causing deep percolation. Nevertheless, these assumptions can be easily violated under

rainfed conditions, when deep percolation due to excess rain cannot be controlled.

2.3.1 Timing of Irrigation

The timing of irrigation is dependent on the farmer objectives and physical constraints (Pleban and Israeli, 1989). The general approach for the timing of irrigation will depend on a refill point (soil water content or soil water potential) (Singh *et al.*, 1995), a fixed interval, a fixed irrigation amount or a crop water stress index (CWSI). The refill point is usually taken as a fraction (say 65 %) of plant available water. The timing of irrigation can be retarded according to actual or forecast rain.

2.3.2 Amount of Irrigation

For practice, full irrigation of the amount of water to be applied can be calculated using an approach by Singh, Boivin, Kirkpatrick and Hum (1995):

$$I = RD\ (FC - RP)/E_i \qquad 2.57$$

where I is the gross irrigation (mm), RP is the refill point or the critical soil water content for the day in question ($m^3\ m^{-3}$), E_i is the irrigation efficiency and FC is field capacity ($m^3\ m^{-3}$) and RD is the depth of the rooting zone in mm. The amount of irrigation calculated using Eq. 2.57 can be further modified depending on whether deficit irrigation (< 100 %) or over-irrigation (>100 %) is being practised due to a shortage in water availability or a leaching requirement respectively. The crop, soil, weather and economic factors also limit the amount of irrigation to be applied. The amount of applied irrigation is dependent on the delivery capacity of an irrigation system.

2.3.3 Dielectric Technique for Measurement of Soil Water Content

One way of checking the estimated soil water content and irrigation water requirement using a soil water balance is to use a fast, precise, automated, non-destructive and *in situ* measurement technique. The ML1 ThetaProbe as well as other so-called time-domain reflectometry (TDR) and frequency-domain reflectometry (FDR) techniques can fulfil such requirements under field conditions.

However, dielectric-based techniques (TDR and FDR) are influenced by factors that affect the dielectric constant of soil components other than water. For example, the effect on TDRs of clay, organic matter and bulk density has been reported by Topp *et al.* (1980), Roth, Schulin, Fluher and Attinger (1990), and Jacobsen and Schjonning (1993a, b). High clay content leads to a higher specific surface which restricts the rotational freedom of water molecules, so that its dielectric constant is lower than that of free water because of strong retention in the soil matrix (Jacobsen and Schjonning, 1993a, b). A temperature effect has been reported by Topp, Davis and Annan (1980) while an iron influence on the dielectric constant has been discussed by Robinson, Bell and Batchelor (1994). Robinson found that the presence of magnetite in a mineral soil could cause an uncertainty of up to 60 % in estimation of soil water content using dielectric technique. Roots, earthworm channels, cracks and stones can also cause small variations in water content estimated using the TDR technique (Jacobsen and Schjonning, 1993b).

The ThetaProbe is essentially a frequency domain probe that depends on the frequency shift induced by energy stored in wet soils in response to a 100 MHz signal. The frequency shift is dependent on the apparent dielectric constant of the soil which is determined by soil water content. A fifth order polynomial of the sensor's output voltage V can be used to estimate the square root of the apparent dielectric constant (ε) of the soil as (Delta-T Devices, 1995):

$$\sqrt{\varepsilon} = 1 + 6.19V - 9.72V^2 + 24.35V^3 - 30.84V^4 + 14.73V^5 \qquad 2.58$$

The soil water content is calculated from the dielectric constant using soil calibration constants a_o and a_1 as

$$\theta_v = (\sqrt{\varepsilon} - a_o)/a_1 \qquad 2.59$$

where $a_o = \sqrt{\varepsilon_o}$ is the square root of the dielectric constant of dry soil calculated using the voltage output of dry soil and Eq. 2.58, and a_1 is the difference between the square root of the dielectric

constant of saturated ($\sqrt{\varepsilon_w}$) and dry ($\sqrt{\varepsilon_o}$) soil divided by the soil water content at saturation

$$a_1 = (\sqrt{\varepsilon_w} - \sqrt{\varepsilon_o})/\theta_{vs} \qquad 2.60$$

The square root of the dielectric constant of soil at saturation is also calculated using Eq. 2.58 for water saturated soil. Factory values for a_1 and a_o of 8.4 and 1.6 for mineral soils and 7.8 and 1.3 for organic soils are used. Since the factory calibration does not always provide accurate estimates of soil water content, the user needs to recalibrate the sensors for soil specific conditions. The calibration process is a tool to minimize the error that an inaccurate sensor would cause in the observed data.

CHAPTER 3

MATERIALS AND METHODS

3.1 SITE DESCRIPTION

A cabbage crop (*Brassica oleracea* var. *capitata*, cv. conquistador) was grown on "Vita Farm," Tala Valley (latitude ≈ 29^0 50' S, longitude ≈ 30^0 30' E and altitude ≈ 900 m), in KwaZulu-Natal, South Africa. Data for the study were collected 60 days after planting between 8 September and 28 October 1996. At this time the crop had fully covered the soil. The field had a slope of 3 % in the N-W direction. The site layout is shown in Fig. 3.1. The field was bordered on the north by a spinach crop, on a N-W by grass and on the S-E by a recently ploughed plot. A cucumber crop was later grown in this plot. A 0.75 m inter-row and 0.25 m intra-row spaces was North-South oriented.

Sensible heat and latent heat were determined using the Bowen ratio energy balance and surface temperature techniques. Penman-Monteith latent heat was used to compare latent heat estimated using the above-mentioned techniques. Three days measurements of sensible heat using eddy correlation were used to compare sensible heat determined using the surface temperature technique. The soil was ploughed to a 250 mm depth. Soil water content was determined using frequency domain reflectometry technique. The soil water content was measured at different depths in the cabbage rooting depth. Soil water content determined by using the ThetaProbe was also used to compare soil water contents determined using a soil water balance method. Determination of irrigation water requirements was performed using the ThetaProbe and the soil water balance soil water content. A raingauge was used to monitor water from sprinkle irrigation and rain required in the water balance equation. Pesticide sprays were applied to the crop every 15 days. A deep application of fertilizer was performed at the beginning of the season and further fertilizers were applied by a fertigation. The weather station measured solar and net irradiance, soil heat flux density, soil temperature, surface temperature, air temperature and water vapour pressure at two levels, soil

water content, wind speed and direction, rain and irrigation amounts. Two dataloggers were used, the Campbell Scientific 21X for the eddy correlation and Campbell Scientific CR7X for the remaining equipment. Sensors and dataloggers were powered by batteries. The station and aerial sensors used are shown in Fig. 3.2.

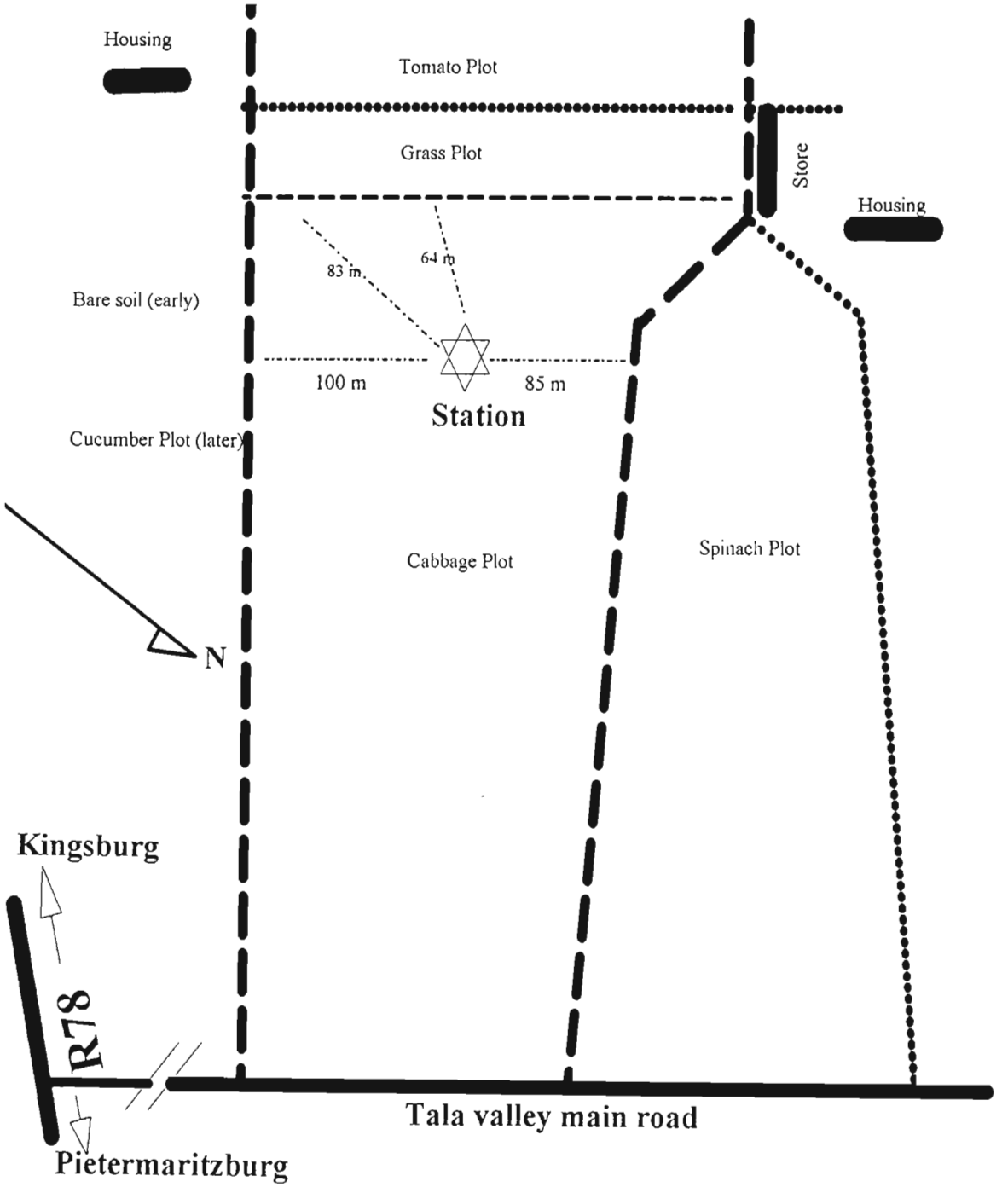

Figure 3.1 A diagram of the experimental site at Vita Farm.

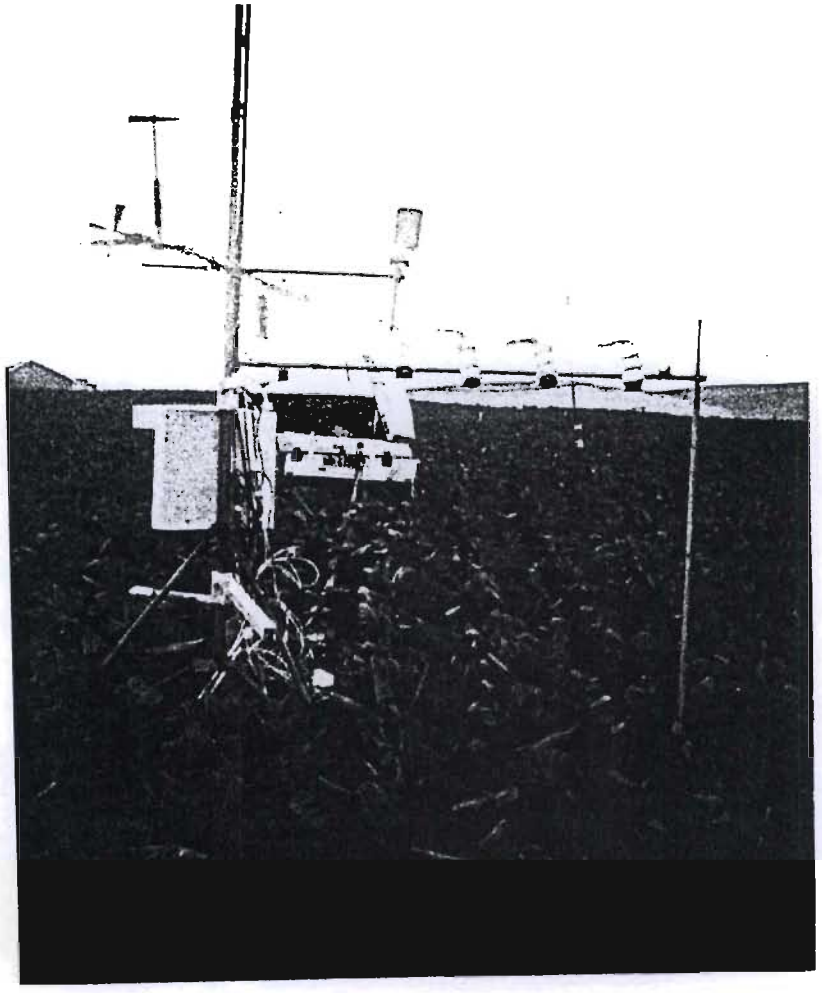

Figure 3.2 -Photograph representing the stand with aerial sensors and equipment.

3.2 DATALOGGER AND POWER SUPPLY

The CR7X datalogger was installed in metal box housed in a trailer. Both the metal box and trailer had its door facing south to minimize entry of direct solar radiation. The trailer was also used to protect the instruments against theft. The 21X datalogger together with 3-D eddy sonic anemometer/thermometer cases were sealed in a box. The interior of the loggers was kept dry using silica gel.

The 21X datalogger has eight analog inputs which are capable of eight differential (H and L = positive and negative) or 16 single-ended (H or L and ground = positive and negative) measurements (Fig. 3.3). The single ended option is less accurate than the differential measurement, but allows more sensors to be used. Six analog outputs are available, of which four are switches and two are continuous. There are pulse counter channels of eight bit or 2 of sixteen bit. The pulse option can

a

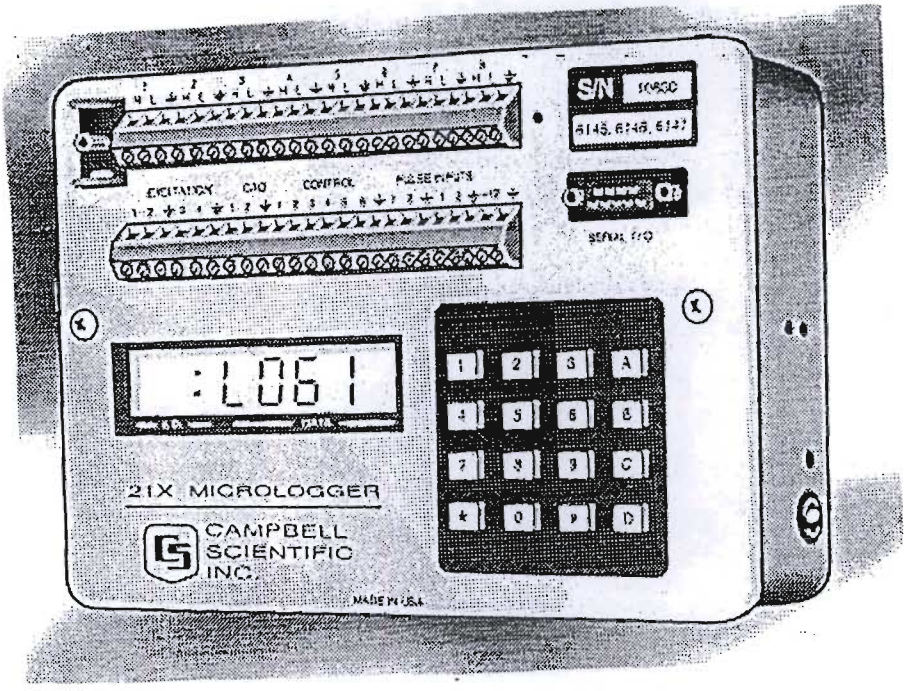

b

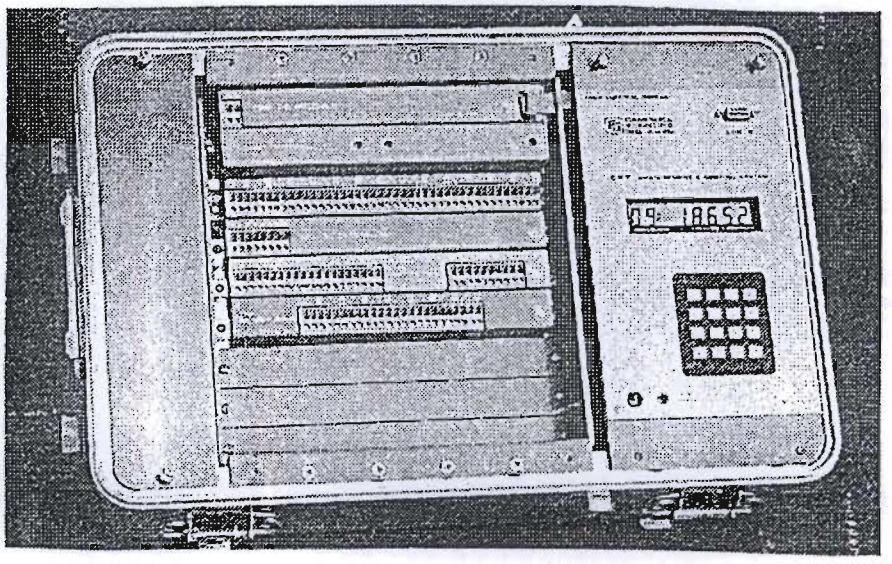

Figure 3.3 The 21X (a) and CR7X (b) Campbell Scientific dataloggers used in Tala Valley experiment (taken from Campbell Scientific Inc., manual).

be selected according to the sensor used, as switch closure, high frequency pulse or low level AC mode. Six digital control ports of 0.1 to 5 V are available. The number of analog input and output channels, pulses and ports in a CR7X datalogger can vary because the datalogger contains 7 card slots which can accommodate and combine input and output cards according to the users needs (Fig. 3.3b). In addition, the CR7X contains its own processor card and a precision analog interface card. A thermistor at the analog inputs terminal provides reference junction compensation for thermocouple measurements of temperature. The 9-pin serial I/O port provides communication between the datalogger and the data storage peripherals (such as SM192/716, tape, modem, printer

or computer via RS232 cable).

3.2.1 Program and Data Transfer

Programming and monitoring can be done by using the keyboard. Automated or semi-automated programming and monitoring can be achieved using the PC208 Datalogger Support Software containing EDLOG, SMCOM, TERM and TELCOM. A program can be written on a PC using EDLOG and downloaded to the logger using TERM software via wire, telephone or radio frequency (RF). The EDLOG program can be copied to a Storage Module (SM) using SMCOM via the SC 532. This program is later downloaded to the logger using the command *D 71A 18 A (if the program is stored in SM area 8). If the storage module (SM192 or SM716) is connected when the logger is powered-up, the program will automatically be loaded when it is stored in area 8.

Data retrieval included an on-line output of the final storage data to a SM. Data were collected by connecting the SM to the PC via RS232, using the SMCOM software. The command *9 30 A 1A A 3A was used to transfer data from the datalogger to the SM. There was a need to leave a peripheral storage device connected to a datalogger to avoid losing data when the datalogger electronic "ring" was overwritten due to a long interval for data collection. In this case a program instruction P96 30[2] (Appendix 3.1: Table 1, instruction number 13, T13) was keyed to allow automated transfer of output data to the SM. The programs were transferred from the logger to SM using the command *D 71 A 28 A (if the program is to be stored in SM area 8). Data can also be retrieved using some form of telecommunications link, radio frequency, telephone, short haul modem, multi-drop interface, or satellite. The PC208 TELCOM program automates this process for compatibles.

[2]P will be used to indicate the datalogger program instructions, while T will be used to indicate the table instruction number.

3.2.2 Programming

The programs used in the field for measurements and calibration of instruments are given (Appendix 3.1 and 3.2). Schematic wiring of the sensors to the loggers, batteries and earthing rod of the colour-coded wire are also shown (Appendix 3.3 a/b). The Campbell Scientific Bowen ratio system provided the program required to determine sensible and latent heat using a 21X datalogger. However, the program was converted to a CR7X datalogger and additional sensors were incorporated using a programming procedure available in the Campbell Scientific manual. In the field, a prompt sheet for the 21X and CR7X dataloggers allowed quick programming and monitoring of the loggers (Appendix 3.4).

Instructions are characterized in processing instructions (P30-P66), output processing instructions (P69-P82) and control instructions (P85-P98). Programs are entered in Table 1 and Table 2. Subroutines, called from Table 1 and 2, are entered in subroutine Table 3. Table 1 and Table 2 have independent execution intervals, entered with an allowable range of 0.0125 to 6553 seconds. In Appendix 3.1, Table 1 had a 1 s execution interval and Table 2 a 10 s execution interval. Two tables were used in the CR7X to allow measurement of sensors having different time response. For example, some had nearly instantaneously time constant (such as thermocouples and cooled mirror Dew-10 sensors) and others had retarded response to environment changes (such as the net radiometer and soil heat flux plates). The smallest interval used in this experiment was 0.2 s to measure eddies using a sonic anemometer/thermometer (Appendix 3.2). Subroutine Table 3 was executed only when called from Tables 1 and 2. Each program instruction (P) has a limited execution time and the sum of the execution times of all instructions must not be greater than the execution interval of the table to avoid overruns of the execution intervals. The output intervals for the CR7X and 21X were set at 20 min to facilitate a later processing of data from two different dataloggers. However, one needs to know that they were average data calculated using different number of samples since they measured using different execution intervals.

3.2.3 Power Supply

The datalogger can function using supply voltage between 9.6 and 15 V. Typical current drain for the CR7X datalogger is 3.5 to 6 mA for quiescent, 16 mA during processing and 100 mA during analogue measurement. Typical current drain for the 21X datalogger is 1 mA for quiescent, 25 mA for processing and 60 mA for analogue measurement. The datalogger provides an internal D-cell battery with 2.5 mA h. This battery can supply power for the voltage measurement, processing and storage of information. For field measurement a 12 V external battery is required. An AC operated battery charger can be included in the system to maintain full charge on the batteries where AC power is available.

A pair of batteries was connected in parallel to power the sensors and another pair was also connected in parallel to power the CR7X datalogger. Similarly, a pair of batteries in parallel was used to power the card cage containing eddy correlation electronics and another pair was used to power the DC converter and an 21X datalogger for eddy correlation technique. Although parallel connection of batteries provided a greater lifetime for the batteries, batteries were replaced every 10 days. Used batteries were charged in the laboratory using a battery charger. To avoid losing program and data, the batteries were removed and replaced one at a time to leave one connected to the datalogger and sensors at all times. To minimize current drain, a subroutine was introduced into the system to switch off the solenoid valve controlling air flow, as well as cooled mirror and pump of the BREB system during nighttime since no measurements were required at these times. The ground of the datalogger and the common ground of the two pairs of batteries for sensors and datalogger was earth grounded using a lightning rod. This protected the sensors and dataloggers against lightning.

Good electrical contact between the sensors and the terminal connectors is essential for successful measurement of micrometeorological element. Wire connections were soldered when the connections were located outside the trailer and strip connectors were used when the connections were located inside the trailer. To reduce thermally-induced electrical noise, all wires were inserted inside a thermal insulator tubing (Keen's Electrical, PMB, RSA). The trailer containing the dataloggers and batteries

as well as the insulation tubing preventing wires from heating is shown in Fig. 3.4.

3.3 MICROMETEOROLOGICAL SENSORS

3.3.1 Net Radiometer

The net radiometer used (Fritschen-type, model Q7.1, REBS, Seattle, WA, USA) has a spectral response between 0.25 and 60 μm and a time constant of 30 s. The sensor has a high output 60 junction thermopile with a nominal resistance of 4 ohms which generates a millivolt signal proportional to net irradiance. The thermopile is mounted in a glass reinforced plastic with a built-in level. The black paint absorbs the internally reflected radiation.

To avoid shading, the sensor was installed with its head facing north and the support arm facing south. The sensor was mounted horizontally using a spirit level with the down dome facing downwards and the upper dome facing upward. The instrument was mounted at 1.8 m height above the ground to allow the sensor to sense the emitted longwave from soil and crop surface, and the

Figure 3.4 The trailer containing loggers and battery, and the insulation tubing preventing sensor wires from heating.

reflected solar irradiance from the surface. This distance was also enough to avoid the negative effect of its own shadow. The net radiometer domes (windshield) were cleaned every 15 days using distilled water and a camel's hair brush and dried using a soft facial tissue. Silica gel was replaced when its colour changed from blue-white to pink.

A differential output voltage instruction P2 (Appendix 3.1, Table 2, T61) was used to accurately measure the thermopile output voltages due to its significant contribution to the energy budget. To convert the thermopile voltage (V_{therm}) to W m^{-2} a factor of 9.38 W m^{-2} mV^{-1} was used for V_{therm} greater or equal to zero (T62 and T63) and 11.75 W m^{-2} mV^{-1} for V_{therm} less than zero (T64 and T66). During the night the measured net irradiance will be negative since there is a predominance of the outgoing longwave irradiance from the surface to the atmosphere. Use of a negative multiplier for V_{therm} smaller than zero, such as recommended by the manufacturer, would result in a positive net irradiance at nighttime in contrast to negative net irradiance. Manufacturer calibration factors were used, except for the sign, because the sensor was new.

3.3.2 Soil Heat Flux Plates and Soil Thermocouples

Two soil heat flux plates (Middleton Instruments, Model CN3, Australia) were buried at a depth of 80 mm. Four thermocouples connected in parallel were used to average the heat stored in the soil layer above the plates. Two thermocouples were set at 20 mm and the other two at 60 mm depths. A diagrammatic representation of installation of the soil heat flux plates and soil thermocouples for determination of soil heat flux density is shown (Fig. 3.5). A hoe and spade were used to cut the soil in vertical and horizontal positions. The soil was replaced carefully into the hole with intent to restore the pre-existing conditions and make good contact between sensors and soil.

A single ended voltage measurement (P1) (table 2, T67) was used to sense the output voltage of the soil heat flux plates due to its relatively insignificant contribution to the energy balance. The measurements were converted to W m^{-2} using a factor of 49 W $^{-2}mV^{-1}$. The soil heat flux density G was calculated as the sum of the measured soil heat flux using plate (G_p) and that stored in the layer

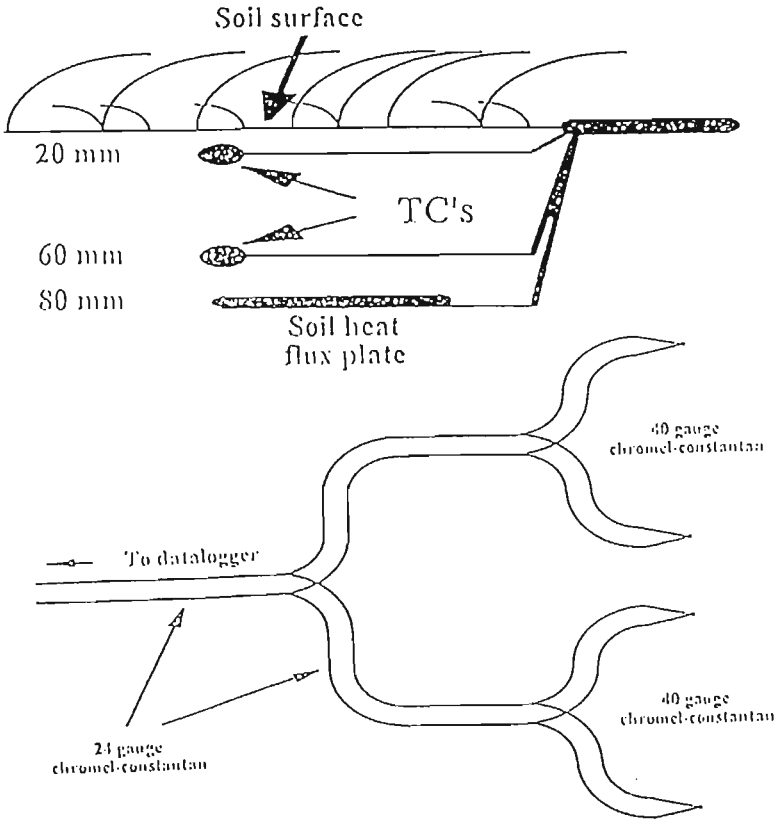

Figure 3.5 A diagram representing the installation of soil heat flux plates and soil thermocouples for determining of soil heat flux density (Savage *et al.*, 1997).

above the soil heat flux plate (G_{stored}) calculated from the soil thermocouples as

$$G = G_p + G_{stored} \qquad 3.1$$

The stored heat varies with changes in soil temperature (dT_{soil}) during a time interval, the soil bulk density (ρ_{bsoil}), the depth of the layer (Δz), the specific heat capacity of the soil (Cp_s) and water (Cp_w), and the soil (ρ_{bsoil}/ρ_{soil}) and water (θ_{va}) fraction in the soil system (ρ_{soil} refers to solid soil particle density). All these parameters are related as follows (Fuchs and Tanner, 1968; Hillel, 1982):

$$G_{stored} = \rho_{bsoil}\, \Delta z\, dT_{soil}[(\rho_{bsoil}/\rho_{soil})Cp_s + \theta_v Cp_w] \qquad 3.2$$

The soil bulk density was determined as described (Section 3.4.1), the particle density (ρ_{soil}) of 2650 kg m^{-3} was assumed as constant for mineral soil (Hillel, 1982). A constant value of 2000 J kg^{-1} K^{-1} and 4190 J $kg^{-1}K^{-1}$ was used for specific heat capacity of the dry soil and water, respectively. The soil atmosphere component in the transfer of heat was neglected. A differential thermocouple temperature

measurement was used (P14) (Appendix 3.1, Table 2, T68) for the chromel-constantan thermocouple since G_{stored} was a major contributor to Eq. 3.1. The temperature difference between two consecutive measurements was also calculated using datalogger processing (Appendix 3.1, table 2, T69 to T80).

3.3.3 Chromel-Constantan Thermocouples

Air temperature was measured at two heights using two 76 μm diameter chromel-constantan thermocouples supplied with the Campbell Scientific Inc. Bowen ratio system (Anon, 1991). Thermocouples were so fine that an absolute temperature error caused by radiation and wind was minimized. Thus, no aspirator or shield was required. However, to reduce data loss due to hail, rain or high wind speed, two thermocouple wires were connected in parallel as shown (Fig. 3.6). The lower thermocouple, set at 200 mm from the crop surface, used a differential temperature measurement (P14) since this temperature was later used as a reference for the upper thermocouple measurement. The lower thermocouple used the panel temperature as reference temperature (Appendix 1, table 1, T4). The upper thermocouple, set at 1000 mm above the crop, used a single-ended temperature measurement (P13) (Appendix 3.1, Table 1, T3). The differential temperature was obtained between the lower and the upper temperature measurement (Appendix 3.1, Table 1, T6).

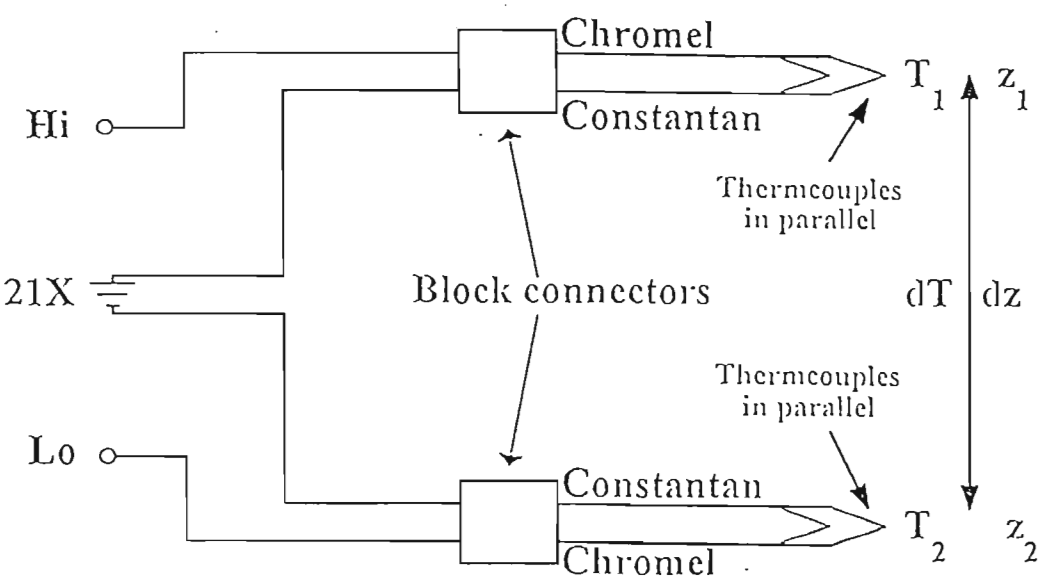

Figure 3.6 Thermocouple wire mounted in parallel to prevent losses of data when one is broken (taken from Savage *et al.*, 1997).

The average between the lower and the upper temperatures, taken as the temperature at 600 mm above the crop was used as the temperature of the site. The resolution of the thermocouple is ± 0.001 °C but the datalogger temperature resolution is only ± 0.006 °C. Sensors were checked for spider webs to avoid deposition of dew which could invalidate measurements. Furthermore, webs on one thermocouple but not on the other would result in an inaccurate air temperature difference measurement due to radiation absorption.

The average temperature between the lower and the upper sensors was calibrated in the field against the accurately measured temperature using sonic technique of the eddy correlation technique (Section 3.2.9). The eddy correlation sensor was set at mid-distance between the lower and upper thermocouple so as to measure air temperature at the same level. A regression between the averaged thermocouple temperature (Y) and the sonic thermometer was used to calibrate the chromel-constantan thermocouple.

3.3.4 Cooled Mirror Dew-10 Sensors

The cooled mirror hygrometer, a modified General Eastern Dew-10 sensor, involves the Peltier cooling of a mirror on which water is condensed (Fig. 3.7). At the point of condensation, the mirror temperature corresponding to the dew point temperature is measured (Savage *et al.*, 1996). The water vapour concentration was measured at 200 and 1000 mm above the crop surface for the lower and upper arm using a single cooled mirror dew-10 hygrometer.

The dewpoint temperature is obtained using a resistance thermometer detector (RTD) in a four wire full bridge (P6) (Appendix 3.1, table 1, T5). The P6 instruction measures the ratio between excitation voltage and the measured voltage times 1000, (1000 V_x/V_s). Since $1000V_x/V_s = 1000[R_s/(R_s + R_1) - R_3/(R_2 + R_3)]$ and R_1, R_2 and R_3 are known one can estimate the unknown resistance R_s using the datalogger bridge transform instruction P59 (Appendix 3.1, table 1, T7). This instruction gives the ratio between the PRT at actual temperature and PRT at 0 °C, (R_s/R_0). The program instruction P16 (Appendix 3.1, table 1, T8) uses this ratio to estimate temperature following the expression R_s/R_0

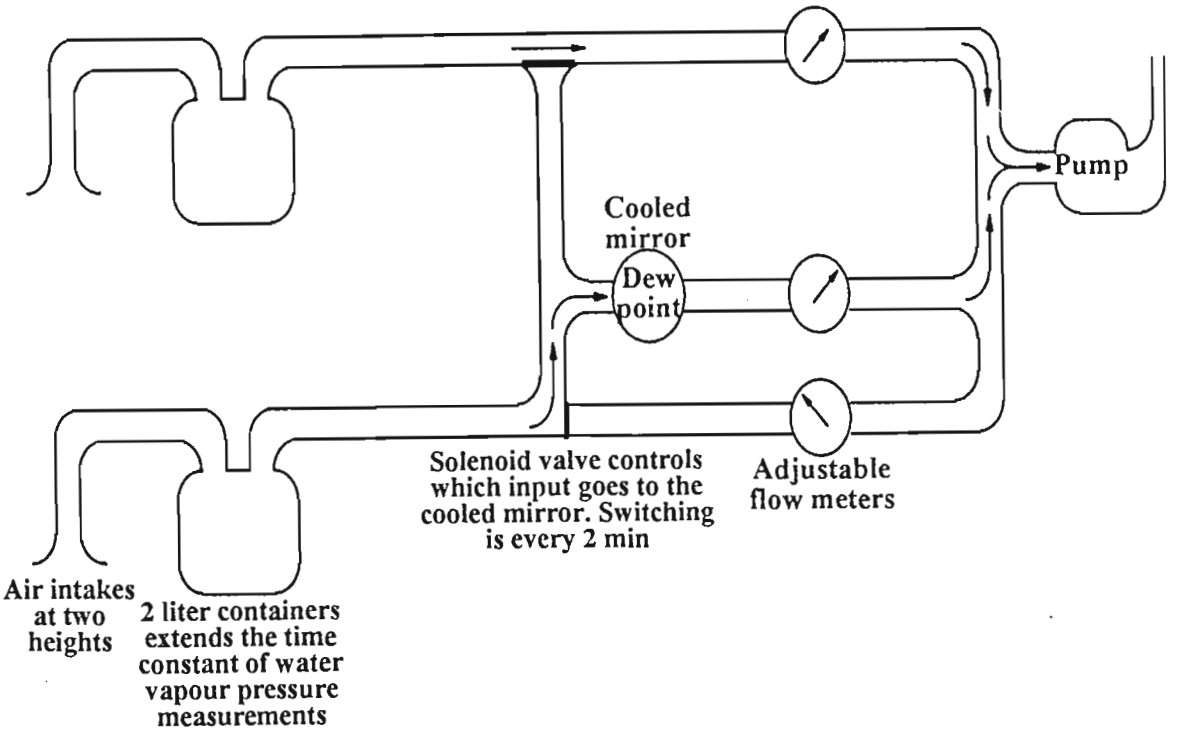

Figure 3.7 Diagram of the Bowen ratio water vapour pressure measurement circuit. Datalogger-controlled solenoid valves, switched every 2 minutes, pass air from one of the two levels to a single cooled dew point mirror. The two intakes were 800 mm apart (Savage *et al.*, 1997).

$= (1 + \alpha T)$ or $R_s = R_o + R_o \alpha T$. This relationship can be expressed in a linear regression form between temperature (X) and the resistance (Y) with intercept R_o and slope $R_o\alpha$. The R_o, $R_o\alpha$ and α are constants. The water vapour pressure is calculated using the 5th order polynomial instruction P56 (Appendix 3.1, table 1, T9).

Air was drawn from both heights through inverted 25 mm filter holders fitted with a 1 μm pore size teflon filter to exclude liquid water and dust from entering the system. The system was equipped with an aspiration pump of which the flow was regulated by a rotameter. Two litre mixing chambers were included in each line which yield a 5 minute time constant for a flow rate of 0.4 l /min (Fig. 3.7).

The relay cable was connected to ports 1 and 2 to switch every 2 min the flow of air from one height to the other using solenoids (Appendix 3.1, table 1, T42 to T59). Use of the same sensors to measure dew points at both lower and upper level allowed the offset of any systematic error which would result from using two sensors. In the range of dew points observed, 20 to 30 seconds were required

for the cooled mirror to stabilize on the new dew point. So, about 90 to 100 seconds were used to make measurement for an individual level. The relay cable was used to turn the pump and the mirror on or off using port 3 and 4, and flag 6 and 7. The resolution of the datalogger dewpoint temperature measurement was ± 0.003°C over ± 35°C range. The limitation was the stability of the Dew-10, which was approximately 0.05 yielding an error of 0.01 kPa in water vapour pressure. The Dew-10 sensor required frequent setting of the bias and cleansing of the mirror. Weekly intervals were used to clean and set the bias. Detail on mirror cleaning and bias setting is found in Appendix 3.1.

The Bowen ratio cooled mirror sensor was calibrated using the LI-COR L610 Dewpoint Calibrator (in Section 3.3.5). The LI-COR LI610's outflow tubing was connected to the cooled mirror inflow tubing. Laboratory observation showed that forcing the Dew-10 cooled mirror to measure a dew point temperature higher than the panel temperature would cause malfunctioning of the system. Thus the calibrator was set to increase the temperature by 1 °C from 0 °C to panel temperature menus 1 °C and restarted.

3.3.5 LI-COR 610 Dewpoint Calibrator

This equipment (Fig. 3.8) has a standard dew point temperature from which other sensor are calibrated. The instrument allows an airstream with a known dew point to be supplied to the sensor to be calibrated (Savage *et al.*, 1997). Adjustment of airstream with a known dew point can be achieved manually or automatically using a datalogger. This equipment was used in the laboratory to check the accuracy of the cooled mirror.

3.3.6 PC207RH Humidity Sensor

The Campbell Scientific PC107/207 for temperature and relative humidity measurement uses a Fenwal UUT51J1 thermistor configured for Campbell Scientific dataloggers. The program instruction P11 provides a 4 V AC excitation, makes a single-ended measurement and linearizes the results using a fifth order polynomial, with a multiplier of 1 and offset of 0. Instruction P12 provides 4 V AC excitation, makes a single-ended measurement, calculates relative humidity using a fifth order

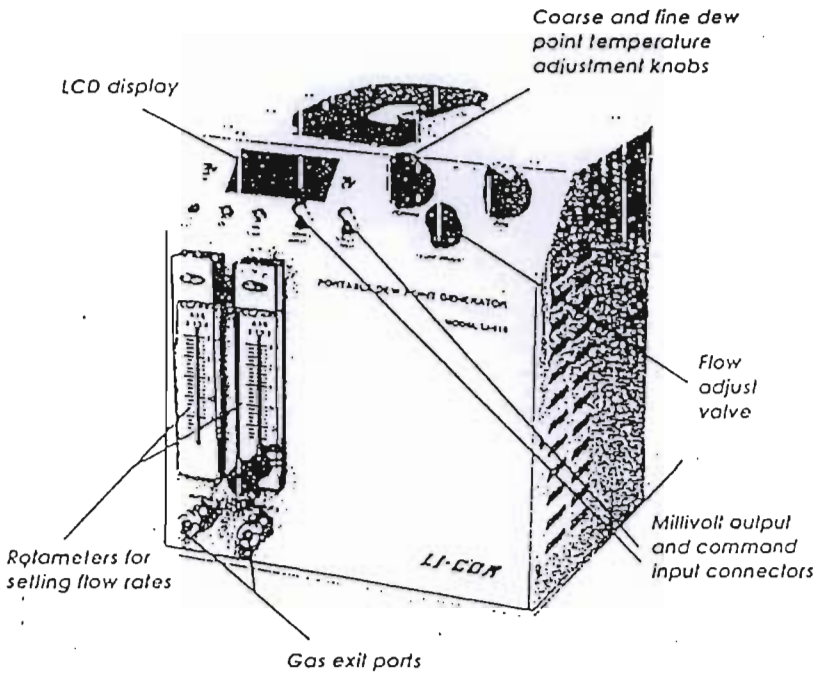

Figure 3.8 The LI-COR L610 Dewpoint Calibrator (taken from LI-COR, Inc. Manual, 1991).

polynomial with a multiplier of 0.01 and offset of 0. Details for the programming is described in Appendix 3.1 (table2, T4 to T11). Two sensors were used of which only one was functional. The working sensor was installed in a radiation shield.

The PC107 temperature sensor was calibrated in the field (Vita Farm) using the sonic thermometer temperature (Section 3.2.9). Both the PC107 sensor and 3-D sonic thermometers were set to measure air temperature at the same level. A regression line between the PC107 (Y) and 3-D sonic thermometer data was developed. The PC207RH relative humidity sensor was calibrated in the field using the Dew-10 cooled mirror.

3.3.7 Infrared Thermometer

Four IRT's (Model 4000ALCS, Everest Interscience Inc., Fullerton, CA, USA) were used to measure the crop surface temperature. Sensible heat and latent heat were estimated using the crop surface temperature using Eq. 2.3 and Eq. 2.9, respectively. The IRT temperature was also used to determine

Δ (Eq. 2.6). The sensors were installed at 1.8 m above the cabbage crop yielding a spot diameter of approximately 0.16 m. The sensors were connected single-endedly (P1) and were powered by two 12 V batteries connected in parallel. Details on programming are shown (Appendix 3.1, table 2, T4). To avoid radiation and temperature effects on the measurements, insulation covered with aluminium foil was wrapped around the sensor.

Calibrations of the IRTs were performed in the laboratory by sealing perforated plastic caps on their viewing holes. Thermocouples were inserted into the perforation and all IRT's were sealed in a cooler box. The cooler box was first cooled in a cold room, measurement comparisons performed, and then heated to 30 °C in another laboratory and further measurement comparisons obtained.

3.3.8 Propeller Anemometer

A three-dimensional propeller anemometer (Model-08234, WeatherTronic, West Sacramento, CA, USA) was used to measure wind speed and to compute the aerodynamic resistance required in the Penman-Monteith method and the surface temperature technique (Eqs. 2.3, 2.8 and 2.9). The sign of the Bowen ratio and the wind speed were used to observe the advective influence on measurements of evaporation. The propeller anemometer had a very linear response for winds above 1 m s^{-1}. The programming procedure to measure wind speed is presented (Appendix 3.1, table 2, T14 to T40).

3.3.9 Tridimensional Sonic Anemometer

The vertical wind speed and air temperature fluctuation required for determining sensible heat using the eddy correlation technique was measured using the three-axis sonic anemometer/thermometer (Model SWS-211/V, Applied Technologies, Boulder, CO, USA) connected to the aluminium card cage microprocessors. The DC voltage (12 V) and the digital signals were also connected to this card cage. The digital signal cable was also connected to the D-A converter. Details on the procedure used for wiring and programming is described in Appendix 3.3b.

3.3.10 Other Sensors

A raingauge was used to measure irrigation every 10 seconds and totalized every 20 minutes. The sensor (unidentified Japanese sensor) had a resolution of 0.5 mm. The measured cumulative rain and irrigation were used to evaluate irrigation water requirement. Solar irradiance was measured using the same execution and average intervals. This was used to observe the cloudiness of the day and used in Eq. 2.28 to compute canopy resistance. Solar irradiance was also used in Eq. 4.15.

3.4 USE AND CALIBRATION OF THE THETAPROBE FOR SOIL WATER CONTENT MEASUREMENT

3.4.1 Determination of Soil Bulk Density

Bulk density was determined using a core method (Blake and Hartge, 1986). Undisturbed soil cores, with diameters of 100 mm and thicknesses of 80 mm, were taken from the midpoint of depth ranges 0 to 150, 150 to 300, 300 to 450 and 450 to 600 mm. Four samples were taken for each depth to minimize a poor performance owing to soil variability. The samples were dried at 105 °C in the oven for 24 hours and the mass of dry soil in kg (M_{ds}) was determined. The bulk density (kg m^{-3}) was calculated as follows,

$$\rho_{bsoil} = M_{ds}/V = M_{ds}/(\pi r^2 h) \qquad 3.3$$

where V is the volume of the container (m^3), r is the radius and h is the height of the container (m).

3.4.2 Laboratory Determination of soil Water Content

Volumetric soil water content (θ_v) was determined gravimetrically using the following equation (Hillel, 1982)

$$\theta_v = \theta_m \rho_{bsoil}/\rho_w = [(M_{ws} - M_{ds})/M_{ds}]\rho_{bsoil}/\rho_w \qquad 3.4$$

where θ_m is the mass soii water content ($m^3\ m^{-3}$), $\rho_w = 998$ kg m^{-3} is the density of water, M_{ws} is the mass of wet soil, M_{ds} is the mass of oven dry soil and M_c is the mass of the container. All mass are expressed in kg.

3.4.3 Laboratory Determination of Soil Water Potential

The soil cores were saturated and subjected to various suctions on a porous tension table with a hanging column of water to study water retention characteristics at six suctions between 0 and 10 kPa (Avery and Bascomb, 1974). The volumetric soil water contents for each soil water potential were determined. Before replacing the cores on the porous plate for the next pressure equilibrium step, the plate was wet to ensure good contact between the ceramic plate, filter paper and soil. A detailed description of the equipment and procedures are found in Klute (1986). The suction applied was calculated using the expression

$$P = \rho_w g h \qquad 3.5$$

where $\rho_w = 998$ kg m^{-2}, $g = 9.81$ m s^{-2} and h the height of the hanging column. Retentivity characteristics at matric potentials of -30 and -100 kPa were determined using undisturbed soil cores and pressure-plate extractors (SoilMoisture Equipment Co., Santa Barbara, California). Pressure plate apparatus was also used to determine water retention at -800 kPa.

3.4.4 Particle Size Analysis and Organic Matter Content

Ten millilitres of calgon dispersing agent was added to 20 g of soil and dispersed mechanically using an ultrasonic probe. The sand fraction was collected by passing the suspension through a 0.053 mm sieve into a 1 litre sedimentation cylinder. It was oven dried and then sieved through a nest of sieves of 0.5 for coarse (coSa), 0.25 for medium (meSa) and 0.106 mm for fine (fiSa). Sand diameter less than 0,106 was characterized as very fine (vfiSa) grades. The suspension of clay and silt was made up to 1 litre by adding distilled water. A 20 ml sample was taken from the cylinder at zero time after agitation to determine the coarse silt (coSi), fine silt (fiSi) and clay. At 4 minutes and 35 seconds

another sample was taken at a depth of 100 mm to determine silt and clay. Further samples were taken after 5 hours and 43 minutes at a depth of 75 mm to determine clay content. Time and depths were determined using Stoke's law for a room temperature of 22 °C. Samples were taken using a pipette and dried in the oven for 24 hours at 105 °C. Calculation of percentages for different particle size fractions was performed as described in Appendix 3.5a.

Organic matter content was determined by adding 10 ml of the potassium dichromate solution (1 N ($K_2Cr_2O_7$) and 20 ml c.H_2SO_4 into a 0.5 g sample (that has previously air-dried, grinded and passed through a 0.5 mm sieve) contained in a 500 ml Erlenmeyer flask. The solution was left to stand for 20 minutes after which a 170 ml deionized water, 10 ml of 85 % H3PO4, 0.2 g NaF and 5 drops of ferroin indicator was added. After adding each chemical product the solution was mixed by swirling. This procedure was also performed for a blank sample. The blank sample flask was titrated using ferrous ammonium sulphate ($Fe(NH_4)_2(SO_4)_2$). The titre volume for which the blank sample turned from dark green-blue to dark brownish black was noted and used to estimate the concentration of the ferrous ammonium sulphate used. The titre volume for which the soil sample solution was turned to a dark brownish black was also noted and used to estimate the percentage organic carbon and subsequent organic matter using a factor. The performed calculations are shown in Appendix 3.5b.

3.4.5 ThetaProbe

Five ThetaProbes (Type ML1, Delta-T Devices) (Fig. 3.9) were used in a cabbage field to measure soil water content every 10 s and average for 20 min intervals at depths of 30, 80, 160, 240 and 350 mm. The deeper sensors were buried horizontally while the surface sensor was buried vertically. Sensors were connected to a CR7X datalogger and sensed using a differential voltage instruction (P2). Measured voltages were transformed to volumetric soil water content using Eqs 2.59 and 2.60. The factory-supplied calibration parameters a_1 and a_o values allowed the direct calculation of soil water content using the datalogger polynomial instruction (P55). The procedures used to program the sensors are presented in Appendix 3.1 (table 2, T1 and T2).

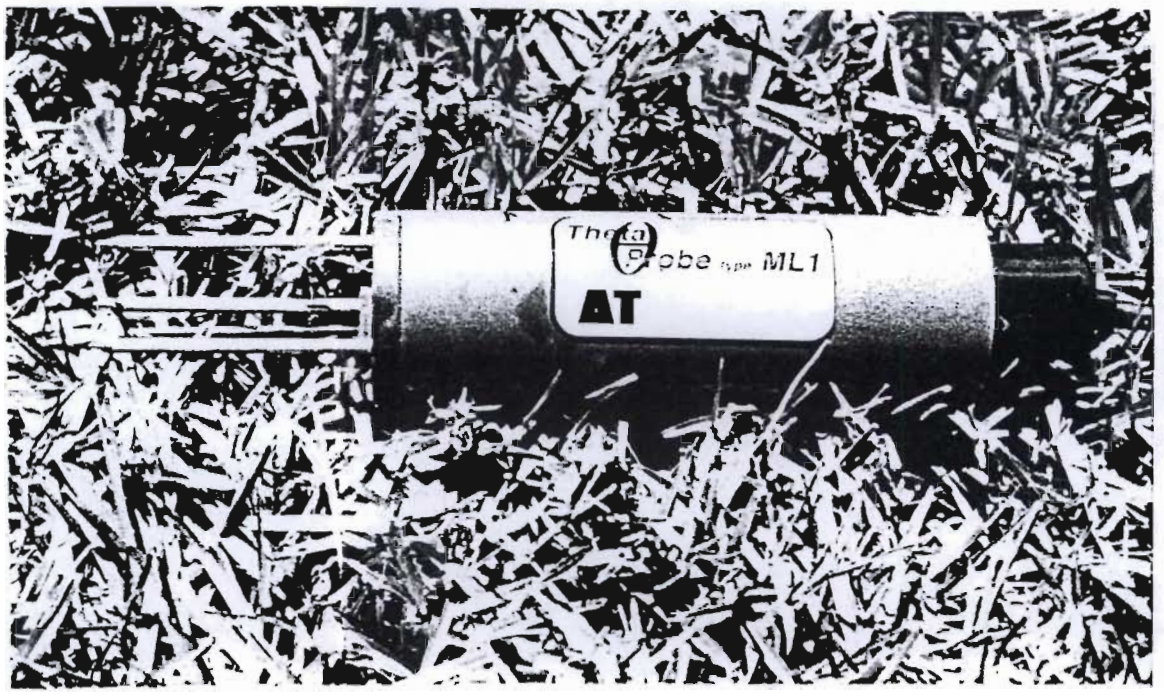

Figure 3.9 The ThetaProbe, a frequency domain reflectometry technique used to measure soil water content.

The ThetaProbe was also calibrated for the soil at the site. Undisturbed soil core samples were collected as described previously. Soil was saturated and ThetaProbe reading of voltage and estimated soil water contents were taken between saturation and air dry soil water content. Measurements were taken every two days to encompass a range of soil water contents during a drying process. After each voltage and soil water determination, the mass of the soil core was taken to determine the laboratory soil water content. Linear regression was used to compare predicted volumetric soil water contents using the factory-supplied constants (a_o and a_1 supplied by the factory) and a soil -estimated constants (a_o and a_1 determined as described in Section 2.2.3) to the measured values. Also, for each voltage and soil water content determination, soil temperature was measured using a copper-constantan thermocouple.

The temperature dependence of the sensor's voltage was determined by inserting the sensors into a soil core of known volumetric soil water content fully enclosed by an aluminum foil to avoid evaporation of water. The sensor was artificially heated using a heater wire. Chromel-constantan thermocouples were used to measure the temperature variation of the sensor and soil. The experiment

was repeated for known volumetric water contents of 0.15, 0.34 and 0.42 $m^3 m^{-3}$. An analysis of the influence of soil bulk density and soil texture was performed by using the regression between the estimated soil water content (Y) and the measured soil water content (X) of each depth (since they have different bulk density and texture). A stepwise inclusion of bulk density (X_1) and clay content (X_2) was used to observe the increase in r^2 caused by bulk density or clay content, and by combined effect of bulk density and clay content.

3.5. DATA HANDLING AND PROCESSING

The PC208 Datalogger Support Software contains SPLIT software for the general purpose of data processing. After loading, SPLIT requests information necessary to find, split, process and store the data into a specified file. This program allowed joining the data from two tables into one file with a continued row in an output file that can be used in a spreadsheet. The SPLIT parameter file for data collected using the CR7X is shown (Appendix 3.6).

The Name/s of input DATA FILE (s) is the name of the file that contains the datalogger data or the split created file. Name of OUTPUT FILE to generate is the name of the output file which may contain the extension PRN to facilitate the import to the QPRO software. START reading in and STOP reading are used to specify a starting and ending point, while COPY from is used to specify the row of the old file to be copied to a new file. SELECT element # (s) in is used to specify which elements from the original array or processed values to include in the output file. HEADING for report and VARIABLES names are used to include reports of what the file is about and what each column represents, respectively. The remaining calculations were conducted using QPRO. Equations used in this experiment are also referred in the Results and Discussions section. The so-called microclimate constant for assessing evaporation were calculated rather than use of fixed values.

CHAPTER 4

SENSITIVITY ANALYSIS, SENSOR CALIBRATION AND THE INTEGRITY OF WEATHER DATA

4.1 INTRODUCTION

In this chapter, the relative sensitivity coefficient and the error for estimating the surface temperature and BREB latent heat due to error in input parameters was estimated using analytical and experimental procedures. The relative sensitivity coefficient and error for the estimate of soil water content due to input parameters using ThetaProbe was also determined. The calibration of the infrared thermometers (IRT), air temperature and actual water vapour sensors is discussed in relation to the accuracy in measuring the respective variables and subsequent estimate of latent heat. An analysis of the accuracy of the estimated latent heat using fixed *vs* calculated constants was also performed in relation to various microclimate techniques for determining evaporation. Integrity and quality of the measured data were analysed using computation of the extreme outliers for weather data measurement.

4.2 SENSITIVITY AND ERROR ANALYSIS

4.2.1 Introduction

Following Saxton (1975), Beven (1979) and Alves (1995), the sensitivity of estimating an output parameter F to changes in input parameters x_1, x_2, to x_n can be developed as a function:

$$F = f(x_1, x_2, \ldots, x_n) \tag{4.1}$$

by first writing

$$F + \Delta F = f(x_1 + \Delta x_1, x_2 + \Delta x_2, \ldots, x_n + \Delta x_n) \tag{4.2}$$

Expanding Eq. 4.2 in Taylor series and ignoring squares, products, and higher power leads to

$$\Delta F = (\partial F/\partial x_1)\,\Delta x_1 + (\partial F/\partial x_2)\,\Delta x_2 +,\ldots, (\partial F/\partial x_n)\,\Delta x_n \qquad 4.3$$

where the partial differentials $(\partial F/\partial x_1)$, $(\partial F/\partial x_2)$ to $(\partial F/\partial x_n)$ indicate the dimensional sensitivity coefficients to which an absolute error in an input parameters Δx_1, Δx_2 to Δx_n may be multiplied to obtain an error in output parameter F. The relative error in F, x_1, x_2, to x_n can be calculated as

$$\xi F = \Delta F/F \qquad 4.4a$$

$$\xi x_1 = \Delta x_1/x_1 \qquad 4.4b$$

$$\xi x_2 = \Delta x_2/x_2 \qquad 4.4c$$

$$\xi x_n = \Delta x_n/x_n \qquad 4.4d$$

Substituting Eqs 4.4a to 4.4d into Eq. 4.3 provides a general equation for estimating the relative change in an output parameter due to relative changes of the input parameters as

$$\xi F = (\partial F/\partial x_1)\,(x_1/F)\,\xi x_1 + (\partial F/\partial x_2)\,(x_2/F)\,\xi x_2 +,\ldots, (\partial F/\partial x_n)\,(x_n/F)\,\xi x_n. \qquad 4.5$$

The expressions within brackets $(\partial F/\partial x_1)\,(x_1/F)$, $(\partial F/\partial x_2)\,(x_2/F)$ and $(\partial F/\partial x_n)\,(x_n/F)$ are the relative sensitivity coefficients (RSC) due to variation in input parameters x_1, x_2, and x_n. The RSC is also called the dimensionless sensitivity coefficient. From Eq. 4.5 one can estimate the RSC using experimental determination of the relative error in input and output parameters as

$$(\partial F/\partial x_1)\,(x_1/F) = \xi F/\xi x_1 = \mathrm{RSC}_{x1} \qquad 4.6a$$

$$(\partial F/\partial x_2)\,(x_2/F) = \xi F/\xi x_2 = \mathrm{RSC}_{x2} \qquad 4.6b$$

$$(\partial F/\partial x_n)\,(x_n/F) = \xi F/\xi x_n = \mathrm{RSC}_{xn} \qquad 4.6c$$

A negative coefficient would indicate that there is an underestimate of F when the input parameter

is overestimated. However, the RSC is not a good indication of the significance of x_1, x_2, to x_n if either x_1, x_2, x_n and F tend to zero independently, or the range of values taken by x_1, x_2, to x_n is small in relation to its usual magnitude. Equations reported above also assume that there are no interactions between input parameters (Alves, 1995).

4.2.2 Bowen Ratio Energy Balance Technique

The RSCs for latent heat using the BREB method (Eq. 2.42) due to variation in net irradiance (R_n), soil heat flux density (G) and Bowen ratios (β) are given:

$$RSC_{\lambda E(BREB)\text{-}Rn} = (\partial\lambda E/\partial R_n)\,(R_n/\lambda E) = R_n/(R_n - G) \quad 4.7a$$

$$RSC_{\lambda E(BREB)\text{-}G} = (\partial\lambda E/\partial G)\,(G/\lambda E) = -G/(R_n - G) \quad 4.7b$$

$$RSC_{\lambda E(BREB)\text{-}\beta} = (\partial\lambda E/\partial\beta)\,(\beta/\lambda E) = -\beta/(1 + \beta) = -H/(R_n - G) \quad 4.7c$$

The relative error in latent heat using the BREB technique was estimated as the sum of the relative errors obtained due to variations of (R_n), (G) and (β). Model and instrumental shortcomings of the BREB technique for measuring evaporation were discussed by Metelerkamp (1993) and Savage *et al.* (1997). The estimated RSC of latent heat due to the use of net irradiance, soil heat flux and Bowen ratio for cloudless days are shown (Fig.4.1). The average RSC for the net irradiance was 1.09 during daytime. That is, assuming a 2.25 % error in net irradiance measurement, following Metelerkamp (1993), one would expect only a 2.45 % error in latent heat. The average RSC of latent heat due to soil heat flux was -0.094 during the daytime and cloudless conditions, while it was large and positive during the nighttime and cloudy conditions. For a 20 % error in soil heat flux density (Metelerkamp, 1993), one would expect only an average of a 2 % error in latent heat.

Metelerkamp (1993) and Savage *et al.* (1997) have analysed the error in latent heat due to error in β determination by examining the error in the estimate of *de* and *dT*. These authors reported a small error in latent heat for a small value of $|\beta|$. In their analysis they assumed a constant psychrometric

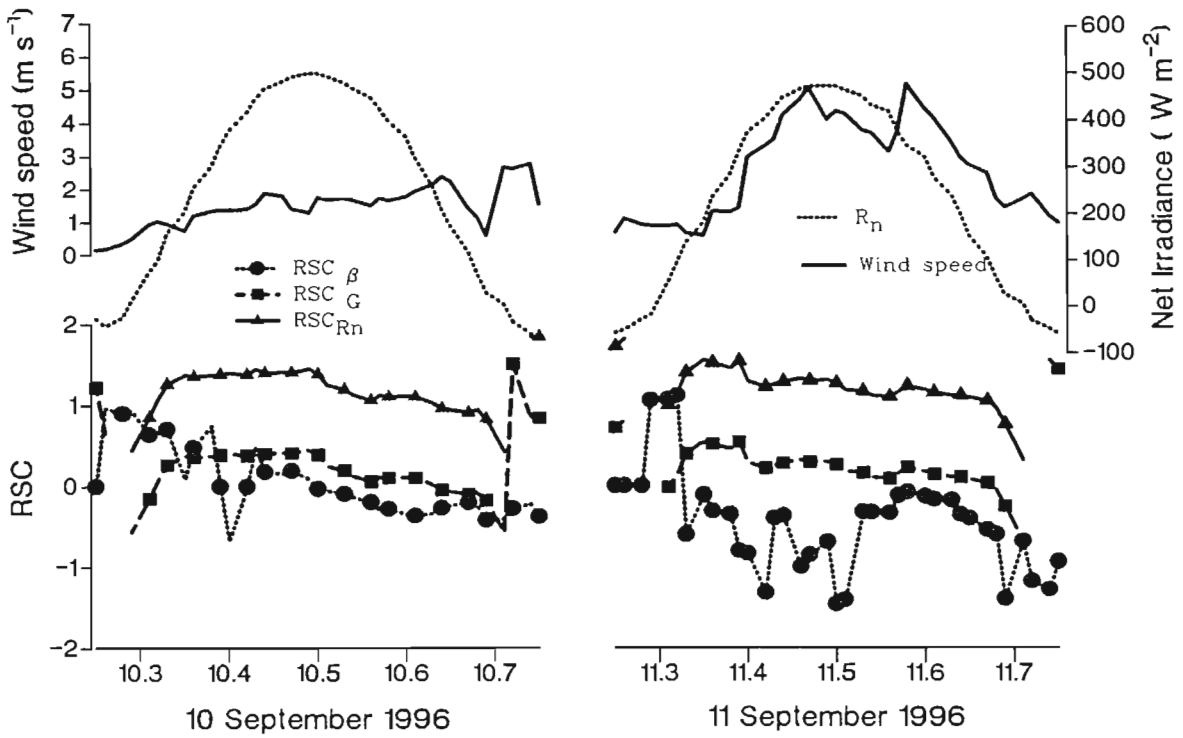

Figure 4.1 The estimated RSC of latent heat due to the use of net irradiance, soil heat flux and Bowen ratio for cloudless days (10 and 11 September 1996)

"constant" and the observance of the Similarity Principle between sensible and latent heat exchange coefficients. Use of a fixed γ of 0.0655 kPa K^{-1} in place of calculated γ underestimated the latent heat by 0.3 %. The γ was overestimated by 3 % and the average RSC was 0.1. The RSC of latent heat due to β was negative and large in magnitude on cloudy days, while it approached zero during solar noon on cloudless days. However, during periods of sensible heat advection on cloudless days, error in latent heat would be 10 % for a 10 % error in β. The average RSC for latent heat due to β on a cloudless day was -0.14, and on a cloudless day together with the influence of a sensible heat advection was -1.

4.2.3 Surface Temperature Technique

The relative error in latent heat ($\xi\lambda E_{(IR)}$) due to relative error in the surface to air temperature differential $\xi(T_o - T_{air})$, aerodynamic resistance ξr_a, soil heat flux density ξG and net irradiance ξR_n can be written as follows:

$$\xi\lambda E_{(IR)} = [\partial\lambda E_{(IR)}/\partial(T_{can} - T_{air})]\ [(T_{can} - T_{air})/\lambda E_{(IR)}]\ \xi(T_{can} - T_{air}) + (\partial\lambda E_{(IR)}/\partial r_a)\ (r_a/\lambda E_{(IR)})\ \xi r_a + (\partial\lambda E_{(IR)}/\partial G)\ (G/\lambda E_{(IR)})\ \xi G + (\partial\lambda E_{(IR)}/\partial R_n)\ (R_n/\lambda E_{(IR)})\ \xi R_n \quad 4.8$$

where the relative sensitivity coefficients (RSC) are obtained as

$$RSC_{(To - Tair)} = \partial\lambda E_{(IR)}/\partial(T_{can} - T_{air})]\ [(T_{can} - T_{air})/\lambda E_{(IR)}] = -\rho_{air}\ Cp\ (T_{can} - T_{air})/[(R_n + G)r_a - \rho_{air}\ Cp\ (T_{can} - T_{air})] \quad 4.9a$$

$$RSC_{ra} = (\partial\lambda E_{(IR)}/\partial r_a)\ (r_a/\lambda E_{(IR)}) = \rho_{air}\ Cp\ (T_{can} - T_{air})/[(R_n + G)r_a - \rho_{air}\ Cp\ (T_{can} - T_{air})] \quad 4.9b$$

$$RSC_G = (\partial\lambda E_{(IR)}/\partial G)\ (G/\lambda E_{(IR)}) = R_n\ r_a/[(R_n + G)r_a - \rho_{air}\ Cp\ (T_{can} - T_{air})] \quad 4.9c$$

$$RSC_{Rn} = (\partial\lambda E_{(IR)}/\partial R_n)\ (R_n/\lambda E_{(IR)}) = -R_n\ r_a/[(R_n + G)r_a - \rho_{air}\ Cp\ (T_{can} - T_{air})] \quad 4.9d$$

Field measurements and an error analysis by Verma *et al.* (1976) indicated that the latent heat estimated by using the surface temperature technique was sensitive to errors in crop temperature measurement under non advective conditions. The relative error in latent heat due to a 2.5 % error in net irradiance and a 20 % error in soil heat flux density measurement (Metelerkamp, 1993), the soil heat flux, net irradiance and latent heat are shown (Fig. 4.2). The average error in latent heat due to error in net irradiance and soil heat flux measurement was below 1 % throughout the daytime during period of intensely sensible heat advection such as on 11 and 12 September. On a normal cloudless day, the error in latent heat was underestimated during the morning period and overestimated during the afternoon period, averaging -1 %.

Thus, the estimated error in latent heat may certainly result from the surface to air temperature differential and aerodynamic resistance. The experimentally determined-RSC of latent heat using the surface temperature technique due to a change in air temperature was 2.5 resulting in a 25 % error in latent heat if air temperature was overestimated by 10 %. To estimate latent heat to within 10 %, the error in air temperature should not exceed 4 %, provided there was no error introduced by other input parameters. The average RSC of 7.0 corresponded to an average error in latent heat of about 7 % due to an error in the surface temperature of 1 % The RSC values varied and were very large

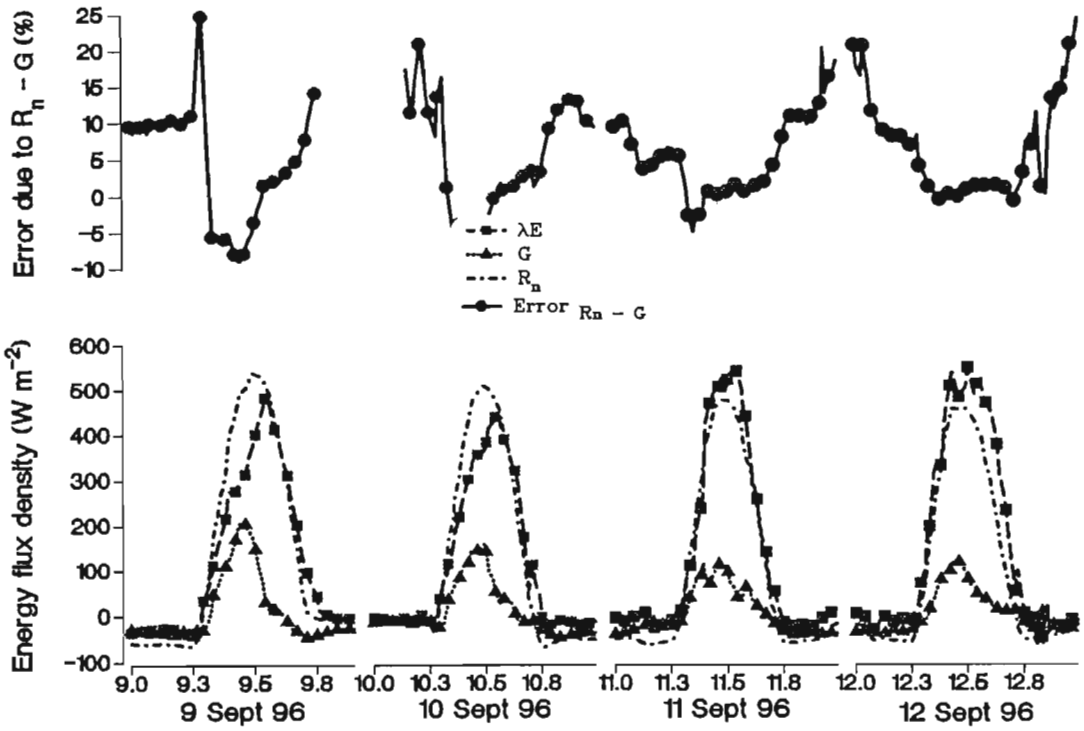

Figure 4.2 The Relative error in latent heat due to 2.5 % error in net irradiance and 20 % error in soil heat flux measurement, the soil heat flux density, net irradiance and latent heat variation.

during the nighttime suggesting that the nighttime use of IRT is impractical. An RSC value of 0.2 for latent heat due to the error in the surface to air temperature differential (T_{can} - T_{air}) was obtained using the experimental method and the analytical method. Unfortunately, no error in the measurement of air and surface temperatures was assessed during the experiment. Similarly, no error in estimating aerodynamic resistance (Eq. 2.29) and error in measuring wind speed using the 3-D wind propeller was determined.

4.2.4 Soil Water Content Measurement Using the ThetaProbe

Profile measurement of soil water content was required to compare soil water content and irrigation water requirements estimated using the soil water balance. The RSC of soil water content is analysed according to Eq. 2.59 as

$$\xi\theta_V = (\partial\theta_V/\partial\varepsilon)\,(\varepsilon/\theta_V)\,\xi\varepsilon + (\partial\theta_V/\partial a_o)\,(a_o/\theta_V)\,\xi a_o + (\partial\theta_V/\partial\, a_1)\,(a_1/\theta_V)\,\xi a_1 \qquad 4.10$$

where

$$RSC\ \varepsilon = (\partial\theta_V/\partial\varepsilon)(\varepsilon/\theta_V) = \sqrt{\varepsilon}/\ [2(\sqrt{\varepsilon} - a_o)] \quad 4.11a$$

$$RSC_{a1} = (\partial\theta_V/\partial a_1)(a_1/\theta_V) = -1 \quad 4.11b$$

$$RSC_{ao} = (\partial\theta_V/\partial a_o)(a_o/\theta_V) = -a_o/(\sqrt{\varepsilon} - a_o) \quad 4.11c$$

are the individual RSC's in soil water content due to variation in the dielectric constant (ε), constants a_o and a_1 respectively. An average RSC of 5, -1 and -0.5 for soil water content due to change in the estimated soil dielectric constant, constant a_1 and constant a_o were obtained respectively. For a 1 % error in dielectric constant, a_1 or a_o the soil water content would be overestimated by 5 % and underestimated by 1 % and 0.5 % respectively. Thus, the resultant 20 % overestimate of soil water content (to be discussed in Section 7.2) using the ThetaProbe appears to have been caused by a 4 % overestimation of the dielectric constant of the soil, if one considers the calibration Eq. 2.59 accurate for estimating soil water content. The estimated RSC's using factory-supplied and soil-estimated calibration parameters are shown (Fig. 4.3).

4.3 SENSOR CALIBRATION AND USE OF FIXED vs CALCULATED "CONSTANTS"

Chromel-constantan thermocouples were more accurate than the PC107 air temperature sensor (Table 4.1, columns 2 and 3). Statistical evidence suggests use of PC107 only when calibrated in relation to the sonic thermometer or chromel-constantan thermocouple. The PC107 sensor overestimated air temperature by 18 %, with a maximum error during the nighttime and minimum during the daytime. A comparative study of the IRT sensors (Table 4.1, column 4, column 5, column 6 and column 7), using the 95 % and 99 % confidence limits, showed that there was no difference between sensors IRT#1 and IRT# 3. Sensors IRT#2 and IRT#4 were statistically different from sensors IRT#1 and IRT#3 and different each other. Uncalibrated IRTs measured different canopy temperatures under similar weather conditions when the four sensors were directed toward the cabbage canopy. An

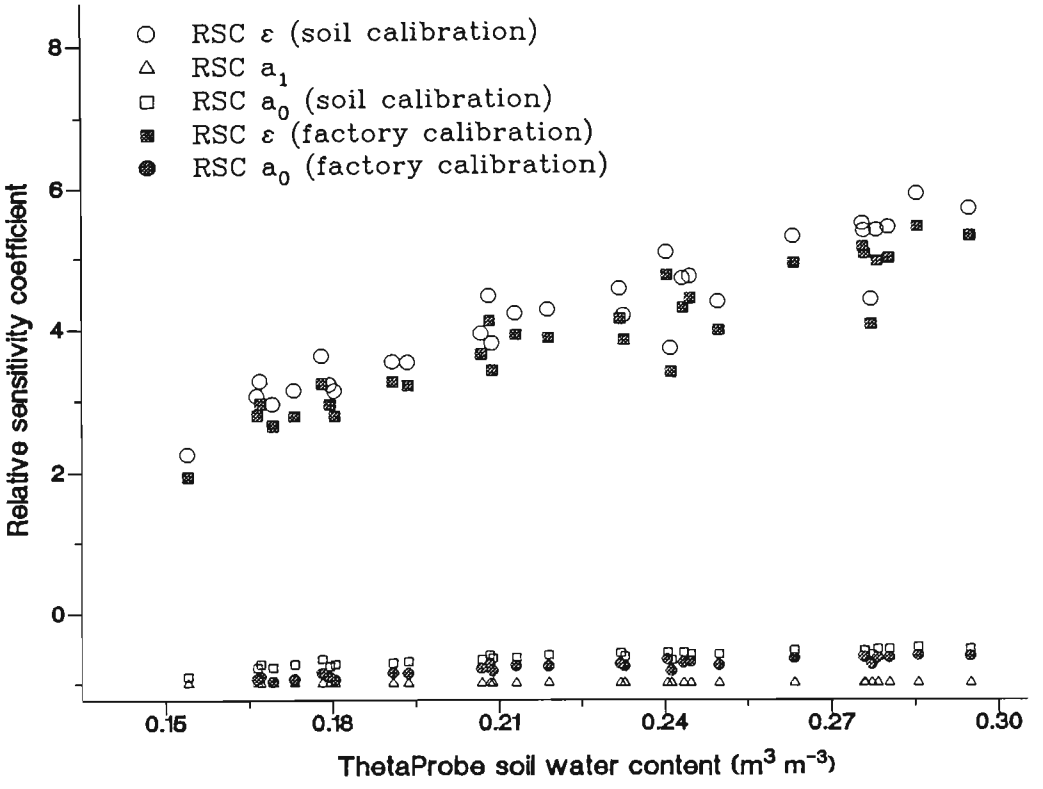

Figure 4.3 The estimated relative sensitivity coefficient of soil water content determined using the ThetaProbe due to a change in the apparent dielectric constant and calibration constants (a_1 and a_0)

average IRT temperature was used to estimate latent heat to compensate for the differences between sensors. Use of an uncalibrated IRT would have overestimated the surface crop temperature by 1.0 % on a cloudless day.

The calibration statistics of both cooled mirror and PC207 RH sensors against the DewPoint Calibrator are shown (Table 1, column 8 and column 9). The r^2 for the cooled dewpoint mirror was 0.996 (standard error of 0.12 kPa). Although the slope and intercept values were not within the 95 % confidence limits, the slope, the intercept and the bias of the cooled dewpoint mirror sensor were very close to the expected values of 1 and zero. The cooled dewpoint mirror was, therefore, an accurate sensor for measuring water vapour pressure provided the bias and the cleaning of the mirror were performed frequently and the system had no air leaks. The PC207 RH sensor was less accurate than the cooled dewpoint mirror, measuring actual water vapour pressure to within 11 %.

Use of an uncalibrated PC207 RH sensor to measure air temperature and actual water vapour pressure would have introduced a 73 % error in water vapour pressure deficit and a consequent error in the Penman-Monteith latent heat of 25 %. Such large errors would exclude any possibility of using the uncalibrated PC207 RH sensor for measuring air temperature and actual water vapour pressure. Use of an uncalibrated air temperature sensor (PC107) and the surface (IRT) temperature sensors would cause more than 200 % error in (T_o - T_{air}) and about 40 % error in latent heat. The difference (T_o - T_{air}) determined using uncalibrated IRT and T107 sensors was negative throughout the experiment while that determined with calibrated and an accurate sensor was negative during the day and positive during the nighttime. If this difference, for uncalibrated sensors, was used to determine the Stress Degree Day (Jackson, Reginato and Idso, 1977) or crop water stress index (Jackson, 1982), one would say that the crop was never water stressed. It is necessary to calibrate both air and canopy surface temperature sensors against standard sensors to reduce errors.

4.3.1 Fixed "Constant" *vs* Calculated "Constant"

A summary of fixed and calculated constant, the percentage error and the relative sensitivity coefficient of latent heat due to variation in constants are shown (Table 4.2). The calculated density of air (Eq. 2.49) ranged between 1.09 kg m^{-3} at a high temperature to 1.17 kg m^{-3} at a low temperature. If the constant 1.12 kg m^{-3} was used, the density would be underestimated during the nighttime by 1.5 % and overestimated during daytime by 1 %. The specific heat capacity is assumed to be 1004 J kg^{-1} K^{-1}. However, values between 1009 J kg^{-1} K^{-1} and 1070 J kg^{-1} K^{-1} were calculated (Eq. 2.51). On average, use of a fixed Cp would underestimate the parameter by 2.5 %. A constant psychrometric constant (γ) value of 0.065 kPa K^{-1} has been used to calculate latent heat using the Bowen ratio technique, and the equilibrium evaporation and Penman-Monteith methods. In this experiment, fixing γ at 0.065 Pa K^{-1} overestimated the calculated value (Eq. 2.53) by 3 % during the daytime.

An accurate estimate of Δ using Eq. 2.6 requires the measurement of air temperature and surface temperature. Chromel-constantan thermocouples and calibrated IRTs were used to accurately

estimate T_{air} and T_o. The value of Δ was also calculated using Eq. 2.55 recommended by Monteith and Unsworth (1990) and Savage *et al.* (1997) for T_{air} less than 40 °C. The error between the calculated Δ using Eq. 2.6 and Eq. 2.55 was 2 % resulting in only 0.5 % error in equilibrium evaporation and 0.2 % errors Penman-Monteith evaporation. Saxton (1975) found an RSC value of 0.2 for evaporation due to a variation in Δ in a modified Penman (1948) model. The soil bulk density of the experiment was 1500 kg m^{-3} which corresponded to a Cp_s value of 1132 J kg^{-1} K^{-1}. Using 840 J kg^{-1} K^{-1} (Bowen ratio manual) would underestimate the Cp_s by 26 %, the G_{stored} by 14 % and G by 10 %. The error in Cp_s was dependent on soil bulk density and temporal soil temperature change. The error in latent heat due to using 840 J kg^{-1} K^{-1} amounted to 0.3 % for equilibrium evaporation and the BREB, 0.4 % for the Penman-Monteith, 1 % for surface temperature and 2 % for the eddy correlation latent heat.

Fixed constants were also used together to observe if their combined effect would increase the error in the latent heat compared to using calculated values. For instantaneous latent heat values, the error can exceed 20 % of latent heat due to the use of fixed constants. Using the equilibrium evaporation, Bowen ratio, surface temperature and eddy correlation techniques and the Penman-Monteith method, the error in daily integrated latent heat values is small due to morning underestimates cancelling the afternoon overestimates. The latent heat and corresponding errors introduced by using fixed constants are shown (Fig. 4.4). Total errors in daily latent heat was 0.4 % for the equilibrium evaporation, 0.3 % for the BREB technique, 1 % for the surface temperature technique, -0.8 % for the Penman-Monteih method and 5 % for the eddy correlation technique. Under cloudy conditions and when higher accuracy is required it is recommended that the calculated constants rather than fixed constants be used for the calculations of latent heat.

Table 4.1 Calibration of micrometeorological sensors: column 2-PC107 *vs* sonic thermometer; column 3- chromel-constantan thermocouple (Tc) *vs* sonic thermometer; column 4 to 7-IRT#1 to IRT#4 *vs* chromel-constantan thermocouple; column 8-PC207 RH *vs* Dew-10 mirror; and column 9-Dew-10 mirror *vs* dew point calibrator.

column 1	column2	column3	column4	column5	column6	column7	column8	column9
	Thermoc *vs* sonicThe oC	PC107Th *vs* sonicThe oC	IRT#1 *vs* Thermoc oC	IRT#2 *vs* Thermoc oC	IRT#3 *vs* Thermoc oC	IRT#4 *vs* Thermoc oC	PC207 *vs* Dew-10 kPa	Dew-10 *vs* DP Calibra oC
n	45	309	863	863	863	863	144	421
slope	1.03	1.32	1.06	1.01	1.06	1.06	0.89	0.96
r^2	0.94	0.95	0.99	0.99	0.99	0.99	0.64	1
$t^*=r[(n-2)/(1-r^2)]^{0.5}$	25	72	251	238	241	253	16	956
Intercept (°C, kPa)	-0.22	-3.13	-1.19	0.54	-1.21	-1.48	0.27	0.51
Syx (°C, kPa)	0.77	1.06	0.21	0.21	0.22	0.21	0.21	0.12
meanX	24.84	18.55	28.11	28.14	28.05	28.13	1.88	9.7
SEb	0.04	0.018	0.004	0.004	0.004	0.004	0.056	0.001
Slope Confidence Limit 99%	0.92, 1.13	1.27, 1.36	1.05, 1.07	1.00, 1.02	1.05, 1.08	1.05, 1.07	0.75, 1.04	0.959, 0.964
Slope confidence Limit 95%	0.95, 1.11	1.28, 1.35	1.05, 1.07	1.00, 1.02	1.06, 1.07	1.05, 1.07	0.78, 1.00	0.96, 0.964
SEa	0.2	0.03	0.02	0.02	0.02	0.02	0.11	0.01
Intercept confid limit 99%	-0.5, 0.58	-3.22, -3.04	-1.24, -1.13	0.49, 0.60	-1.27, -1.15	-1.54, -1.43	-0.01, 0.54	0.48, 0.54
Intercept confid limit 95%	-0.36, 0.44	-3.2, -3.07	-1.23, -1.14	0.5, 0.59	-1.25, -1.16	-1.53, -1.44	0.06, 0.48	0.53, 0.53
MSEunsy	24.98	2501.23	38.14	38.1	41.22	37.6	259.82	6.05
MSEsyst	10.65	2659.82	168.77	582.09	326	65.88	233.78	28.94
% unsy	70.12	48.46	18.43	6.14	11.22	36.34	52.64	17.28
% syst	29.88	51.54	81.57	93.86	88.78	63.66	47.36	82.72
Bias b	-0.47	-2.72	-0.43	-0.82	-0.61	-0.26	-0.06	-0.14
t test (Table t)	2.01	1.96	1.96	1.96	1.96	1.96	1.96	
sum x^2	355	8666	2489	2463	2452	2485	6	
c^2	0.0064	0.0003	0.0001	0.0001	0.0001	0.0001	0.0348	
$1-c^2$	0.9936	0.9997	0.9999	0.9999	0.9999	0.9999	0.9652	
meanY	25.33	21.19	28.54	28.97	28.66	28.39	1.94	
min	10.99	16	12.3	12.7	12.1	12.1	1.79	-0.01
max	30.18	36.8	32	32.2	32.1	31.9	3.1	21

Table 4.2 A summary of fixed and calculated constants, the percentage error for using fixed "constant", the relative sensitivity coefficients and the resultant error in latent heat due to the change in micrometeorological constants.

CONSTANTS	Fixed constant	Calculated constant (day-time)			% Error in using fixed constant	Relative sensitivity coefficient					% Error in latent heat				
		Min	Max	Avg		PM	IR	EC	EE	BREB	PM	IR	EC	EE	BREB
Density of air (kg m^{-3})	1.12	1.09	1.17	1.11	1.00	0.4	0.1	0.2			0.3	0.1	0.2		
Specific heat capacity of the air (J kg^{-1} K^{-1})	1004	1009	1070	1029	2.50	0.4	0.1	-0.8			0.9	0.3	-2.0		
Psychrometric constant (Pa K^{-1})	65.5	62.0	65.00	64.0	2.30	-0.5			-0.3	0.1	0.5			0.5	0.2
Slope of saturation w.v.p. vs Tair (Pa K^{-1})	0.14	0.08	0.23	0.14	2.00	0.1			0.3		0.2			0.5	
Specific heat capacity of soil (J kg^{-1} K-1)	840			1132	25.80	0.0	0.0	0.1	0.0	0.0	1.0	1.0	2.0	0.3	0.3

Where PM = Penman-Monteith, IR = Infrared thermometer, EE = eddy correlation and BREB = Bowen Ratio

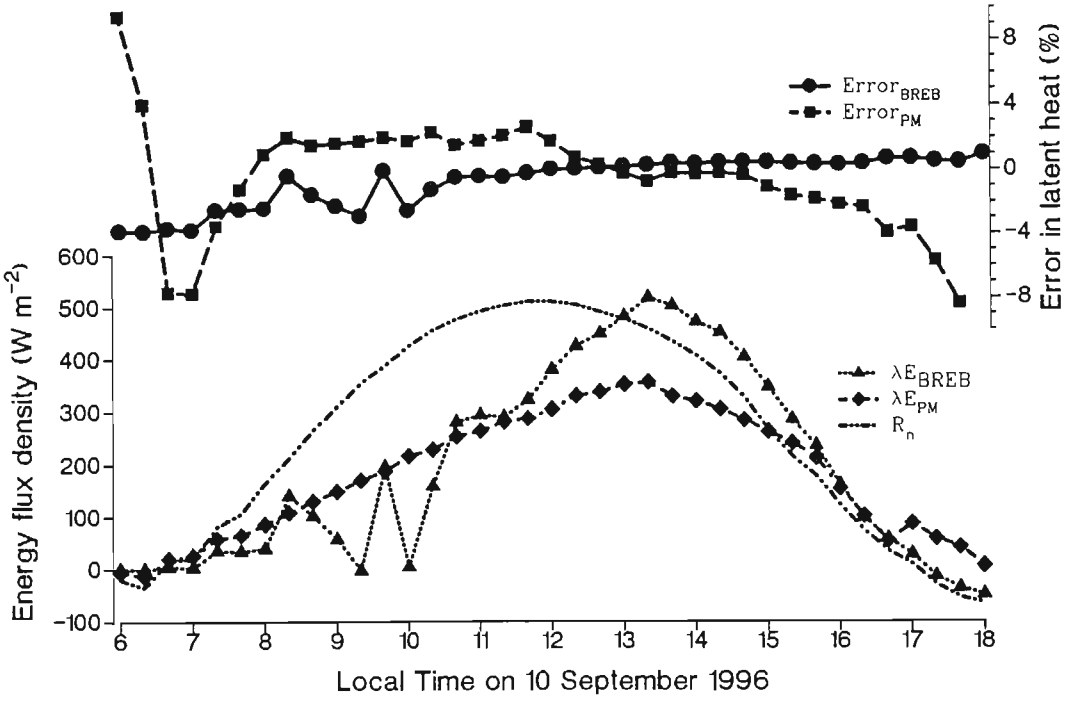

Figure 4.4 The latent heat and corresponding errors introduced by using fixed constants.

4.4 INTEGRITY OF WEATHER DATA

Assesing the integrity and quality of weather data allows detection of the error in data measurement due to the poor performance of sensors. Assessment of the integrity includes computation of extreme outliers for weather data measurements (Allen, 1996). Measured data should be within the extreme outliers. On the other hand, use of the rejection criteria can also be used to test the integrity of data. For example, the computation of negative water vapour pressure deficit or relative humidity higher than 100 % suggested that air and/or dew point temperature is being measured inaccurately. The integrity of data can also be achieved by comparing measurement of the experimental sensors to the standard sensors.

4.4.1 Solar Irradiance

The pyranometer operation and accuracy was evaluated by plotting the 20 min measurements of solar irradiance against computed solar irradiance expected under clear sky conditions. Allen (1996)

estimated the solar irradiance of clear sky (R_{so}) as the product between a clearness factor (K_T) and extraterrestrial solar irradiance (R_a) as follows:

$$R_{so} = K_T R_a \quad 4.12$$

The extraterrestrial solar irradiance is computed following Savage (1991) as

$$R_a = R_{sc} [1 + 0.033 \cos (2\pi n / 365)] \cos \underline{\theta} \quad 4.13$$

where R_{sc} is solar constant (1353.7 W m^{-2}), [1 + 0.033 cos (2πn / 365)] is the relative distance between earth and sun, n is the day of the year and $\underline{\theta}$ is the zenith angle. The cos $\underline{\theta}$ is computed (Savage, 1991) as

$$\cos \underline{\theta} = \sin \delta \sin \varphi + \cos \delta \cos \varphi \cos \omega \quad 4.14$$

where $\delta = -23.45 \sin [360(284 + n)/365]$ is solar declination (rad) for a southern hemisphere, φ is the latitude (rad), $\omega = 15 (12 - t)$ is the sunset hour angle (rad) and t is local time (h). The estimate of the clearness index was discussed by Allen (1996). A constant clearness index of 0.75 was used to estimate the solar irradiance for clear sky (Fig. 4.5). The measured solar irradiance was closely correlated to the estimated one. A non-linearity of the curve was caused by the variation of the clearness index because of change in clarity coefficient, sun angle, water vapour and precipitable water in the atmosphere (Allen, 1996).

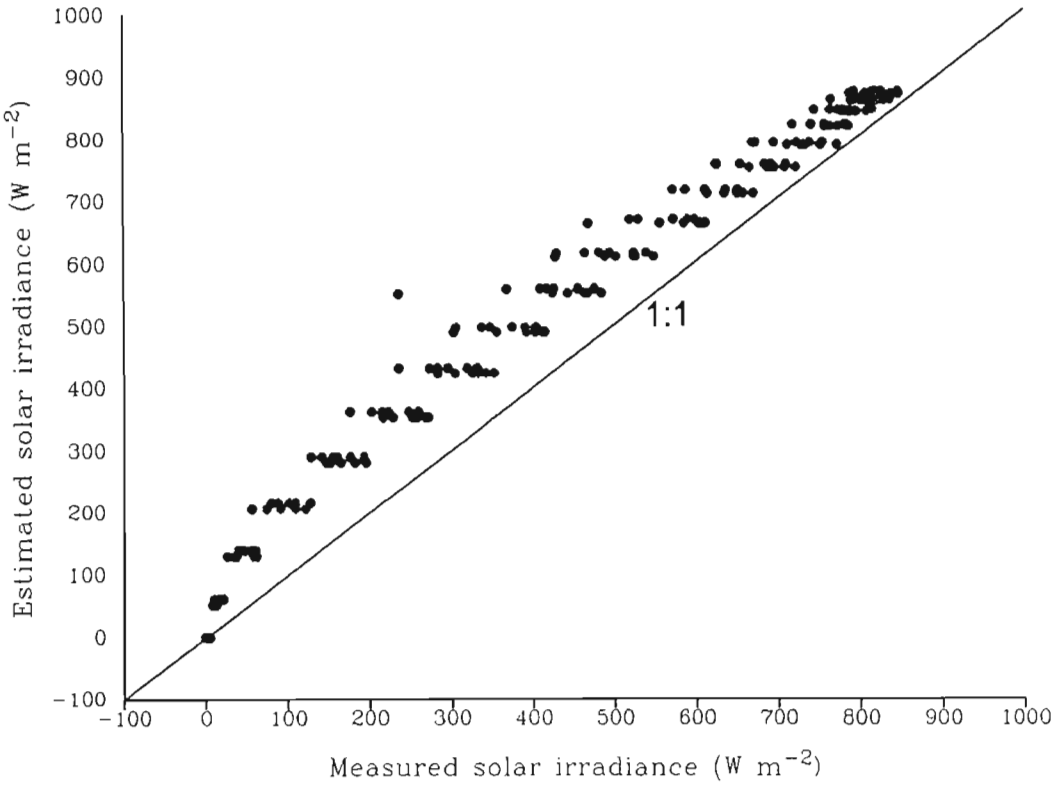

Figure 4.5 Comparison of the measured and the estimated solar irradiance for clear sky.

4.4.2 Net Irradiance

An equation by Allen (1994) was used to estimate net irradiance (R_n):

$$R_n = 0.77R_s - [a_c(R_s/R_{so}) + b_c](a_1 + b_1 e)\, T_{air} \qquad 4.15$$

where R_s is solar irradiance, R_{so} is the solar irradiance for clear sky, $a_c = 1.35$ and $b_c = -0.35$ are the slope and intercept of the correlation between the ratio (R_s/R_{so}) (X) and the cloudiness factor (Y), $a_1 = 0.34$ and $b_1 = -0.14$ are the intercept and slope of the correlation between emissivity of the surface (Y) and the square root of actual vapour pressure (e_a) (X). The measured net irradiance compared favourably with the estimated net irradiance. The difference between the measured and the estimated net irradiance increased at solar noon (Fig. 4.6). The use of a negative multiplier of -11.5 W m^{-2}mV^{-1} recommended by the manufacturer would give positive net irradiance at nighttime and a subsequent overestimate of latent heat. Nighttime net irradiance should be negative because there is a

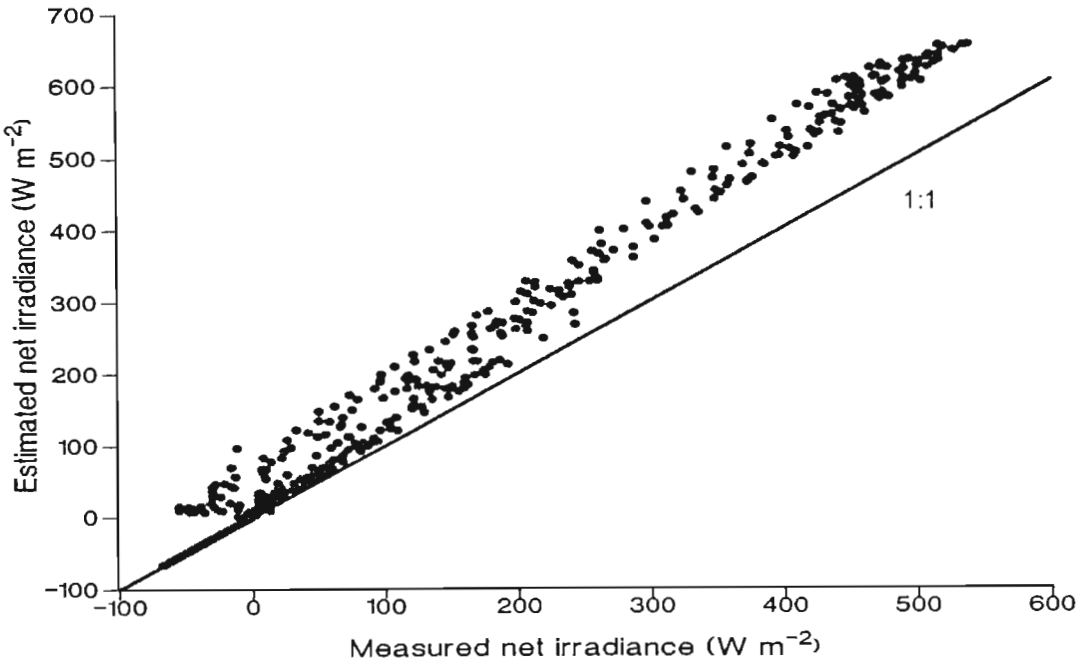

Figure 4.6 Comparison between the measured and the estimated net irradiance.

predominant flux of terrestrial longwave irradiance from the surface to the atmosphere, except when there is an influence of advection. Data were corrected using a positive multiplier of 11.5 W m^{-2} mV^{-1}.

4.4.3 Soil Heat Flux Density

Soil heat flux density was estimated as 10 % of net irradiance during daytime and 50 % during nighttime. The plot of the estimated values *vs* the measured values are shown in Fig. 4.7. The measured soil heat flux density was close to the estimated values during nighttime more so than during daytime at solar noon. At solar noon the measured soil heat flux density was above 150 W m^{-2} during cloudless days in the early stages of the experiment (8, 9 and 10 September) and was less than or equal to 150 W m^{-2} later on. The maximum estimated soil heat flux at solar noon on a cloudless day was 50 W m^{-2}.

4.4.4 Surface Temperature

The surface temperature can be estimated using Eq. 2.18 (Jackson *et al.*, 1981). The plot of estimated surface temperature and the average measured surface temperature using four IRTs are shown (Fig.

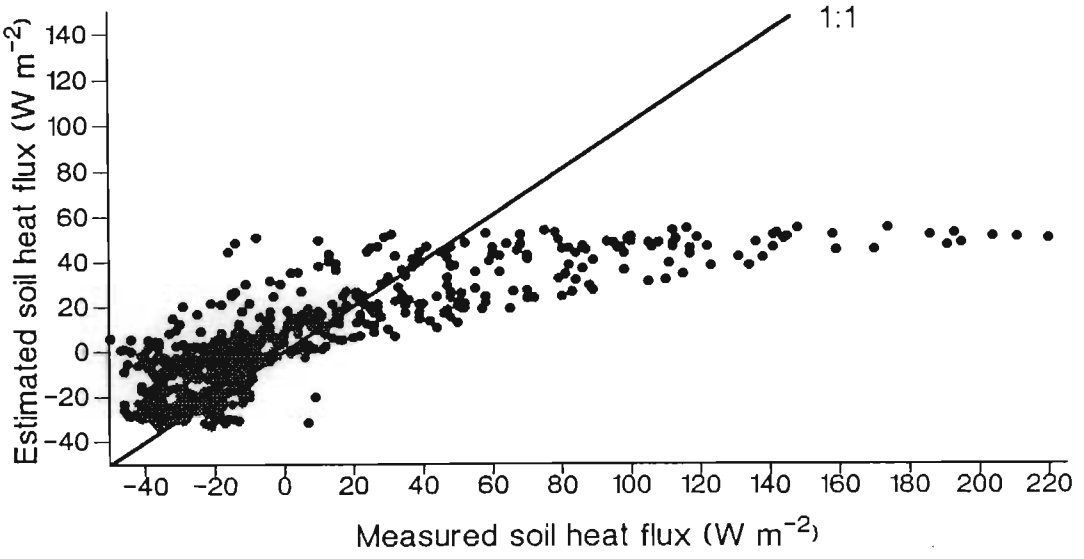

Figure 4.7 Comparison between the measured and estimated soil heat flux.

4.8). The measured surface temperature tended to be overestimated for temperature below 14 °C and underestimated for temperature above this value. In terms of the integrity of the data one may expect an influence of additional factors not incorporated in Eq. 2.18. For example, such a situation could be observed if there was sensible heat advection. However, Eq. 18 would fail to estimate the surface temperature under highly variable weather conditions due to moving clouds because of time response of a plant to weather change compared to the response of the sensors. If a line graph was used, the line indicating the measured surface temperature would appear smoother than the estimated surface temperature which is more responsive to variation in available energy. There were also some estimated surface temperature values smaller than the measured values during a period of rain, irrigation or dew on 15, 24 and 25 September, and on 2, 3, 4 and 6 October during the nighttime.

4.4.5 Water Vapour Pressure and Air Temperature

The integrity of the measurement of water vapour pressure and air temperature can be checked indirectly by transforming the water vapour pressures to relative humidity [RH = (e/e_s)*100] or to water vapour pressure deficit (VPD = e_s - e_a). The first relation should not exceed 100 % and the

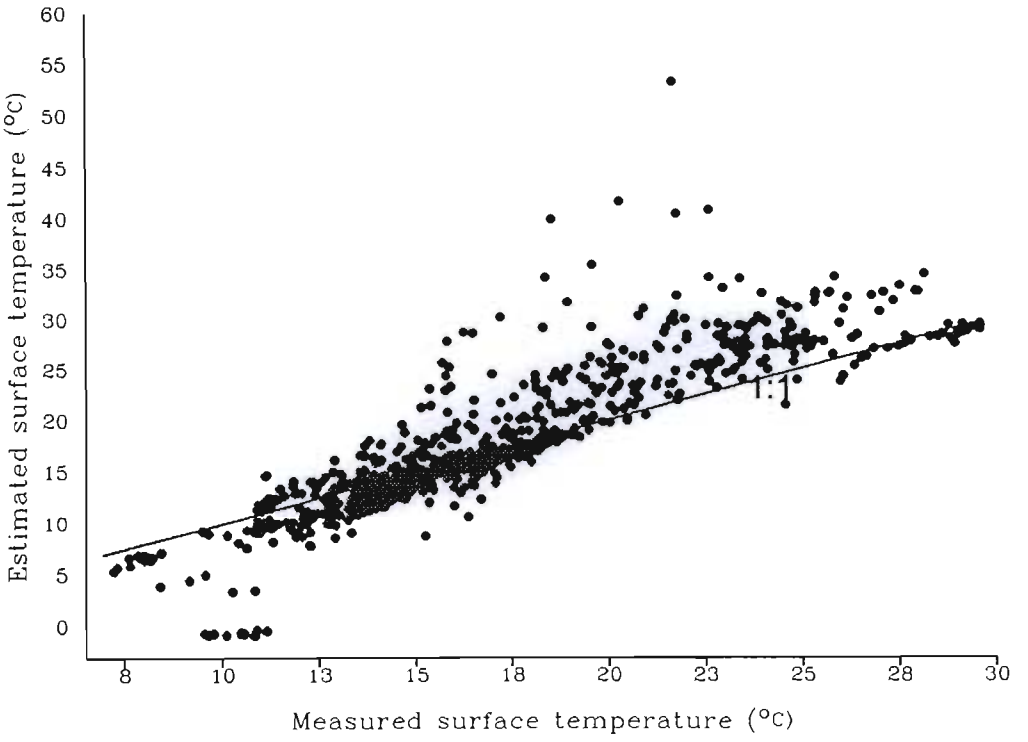

Figure 4.8 Comparison between the measured and estimated surface temperature.

second relation should not be negative. Observation of RH > 100 or VPD < 0 implies that the dew point temperature was above ambient temperature, an abnormal measured data. The VPD observed in this experiment is shown in Fig. 4.9. The values of VPD were positive during the daytime and negative during the nighttime when the pump was off. So, there was poor measurement of air temperature or dewpoint during the nighttime. The cooled mirror was disconnected during the nighttime to conserve battery power. The data are therefore not reported. The deposit of dew on the cooled mirror and on thermocouple wire could affect accuracy to measurement of the dewpoint and air temperatures. Some negative VPDs were observed during the daytime on 12, 13, 14 and 15 October owing to the malfunctioning of the cooled mirror. Latent heat calculated using the BREB technique and the Penman-Monteith method would be affected if these measurements of water vapour pressure were used.

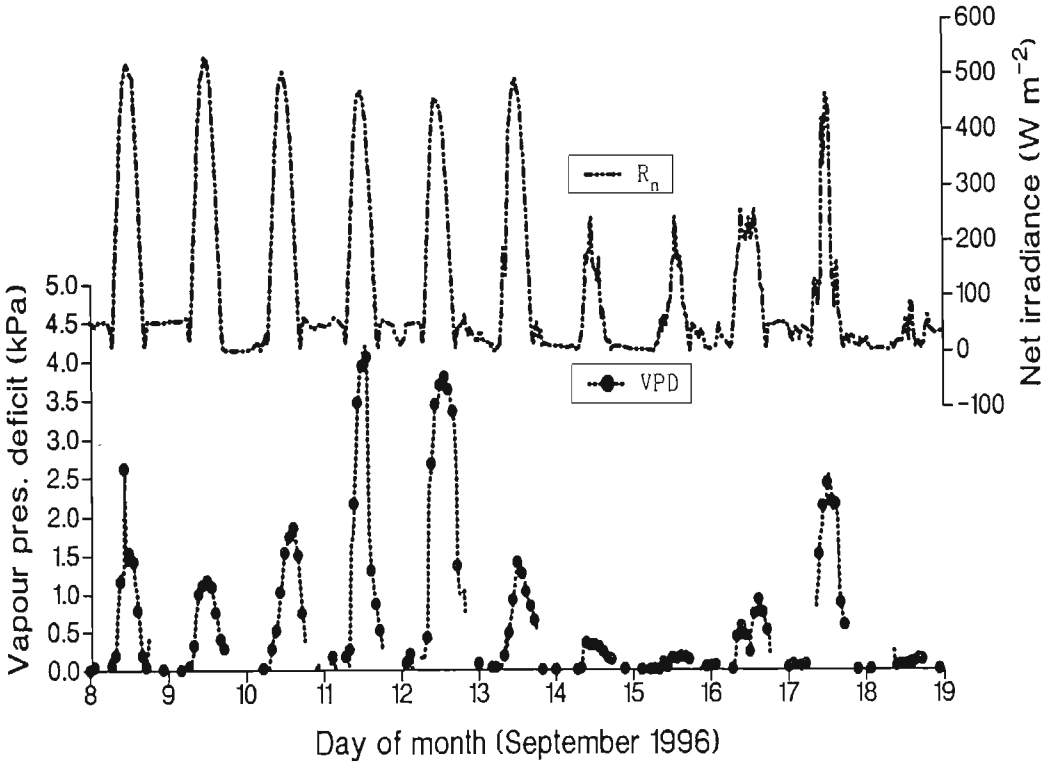

Figure 4.9 The observed water vapour pressure deficit for 10 days in September

4.5 CONCLUSIONS

A RSC and error analysis suggested that less than a 5 % and 1 % error in latent heat determined using the BREB and surface temperature technique respectively would result from using measured net irradiance and soil heat flux density. The error would result from a poor estimate of β and the surface to air temperature differential. The performance of the ThetaProbe depended on the accuracy of the sensor to estimate the dielectric constant. This is because a 1 % error in the dielectric constant would overestimate soil water content by 5 %. The PC207 RH sensor was discarded in this experiment and substituted by the average air temperature and vapour pressure measured using thermocouples and the cooled mirror. The error in measuring such parameters by using the PC207RH was very large. The error in measuring surface temperature using IRT was negligible. The use of fixed constants does contribute to a very small error in the estimated latent heat. Integrity of weather data suggested that solar and net irradiance were measured accurately while soil heat flux was overestimated. The

estimated surface temperature seemed to depend on other input energy not accounted for in the Penman-Monteith equation, while water vapour pressure deficit was poorly estimated on the last 5 days of the experiment.

CHAPTER 5

PERFORMANCE OF THE MICROMETEOROLOGICAL TECHNIQUES FOR MEASURING EVAPORATION

5.1 INTRODUCTION

In this chapter, an analysis is performed in relation to the accuracy for estimating the Bowen ratio. The Bowen ratio is used to detect the occurrence of advection. A rejection criterion is used to discard unreliable data caused by model and equipment shortcomings. A comparative analysis using the linear regression is performed between the estimated latent heat using the BREB technique and the Penman-Monteith method. The surface temperature technique is also evaluated over a cabbage crop. In this technique, the occurrence of advected energy is analysed using the observation of the surface to air temperature differential and wind speed. The error in latent heat is analysed using comparative analysis between the latent heat estimated using the surface temperature, and the Penman-Monteith method and the BREB technique. The sensible heat estimated using the surface temperature technique is evaluated in relation to the sensible heat estimated using the eddy correlation technique. The effect of placement height of air temperature sensors required to compute sensible heat and latent heat using the surface temperature technique is also analysed. A daily variation of the energy balance components as estimated using the BREB and surface temperature technique is performed.

5.2 BOWEN RATIO ENERGY BALANCE TECHNIQUE

5.2.1 Introduction

Unlike other microclimate techniques, the Bowen ratio energy balance method does not require information on the vertical wind speed and the aerodynamic properties of the surface to estimate the total evaporation required in irrigation scheduling. A technique for scheduling irrigation should be accurate and capable of measuring evaporation throughout the day, during the growth and development stages of a crop under different climatic conditions. The BREB method has been compared to the standard lysimeter and was found to provide good estimates of latent and sensible heat (Savage *et al.*, 1997). The BREB has the advantage of being portable compared to a fixed lysimetric measurement.

However, the performance of the BREB has been questioned for a protracted period of monitoring of latent and sensible heat. For example, Tattari *et al.* (1995) found 47 % of daily data to be unreliable when using the BREB technique due to condensation water inside the air intake tubing and filters of the instrument. But Iritz and Lindroth (1994) successfully used the BREB technique to measure nighttime and daytime evaporation using a thermometer interchange system. Cellier and Olioso (1993) improved the performance of the BREB system by fitting inside the tubing for water vapour pressure measurement a heater wire to warm the air when relative humidity approached 90 %. Malek and Bingham (1993), used a Campbell Scientific Bowen Ratio System which was able to provide an accurate measurement of the profile entities throughout the daytime and nighttime. Usually, all nighttime data and some daytime data are rejected. These data require to be estimated by averaging the proceeding and subsequent measurement (Malek and Bingham, 1993) or by using the equilibrium evaporation to estimate the rejected data (Savage *et al.*, 1997).

From the analysis of the sensitivity, error and integrity of weather data (in Section 4.2.2), the error in latent heat determined by using the BREB technique would result from a poor estimate of β. On the other hand, the cooled mirror measured poorly the dewpoint temperature in the last 5 days of the

experiment (Section 4.4.5). In addition, there was indication of the occurrence of advection in the field. The advection was defined as the process of energy and mass transport in the horizontal plane in a downwind direction (Rosenberg *et al.*, 1983). Rosenberg (1969a, 1969b) and Blad and Rosenberg (1974) found that strong advection increased latent heat to a point of using more energy than that supplied by available energy (R_n -G).

The BREB technique was used to measure the latent heat under advection (Blad and Rosenberg, 1974). Rosenberg (1969a) found that the BREB underestimated total evaporation under advection conditions. In this sub-chapter, the accuracy for estimating the Bowen ratio is discussed. A rejection criterion was used to discard unreliable data caused by model and equipment limitation. The estimated latent heat using the BREB is compared to that estimated using the Penman-Monteith method.

5.2.2 Weather Conditions and Fetch Requirement

A summary of the daily air temperature, water vapour pressure, relative humidity and wind speed is presented in Table 5.1. Irrigation was observed on 8, 16, 22 and 29 September with 11.5, 21.5, 32 and 16.5 mm respectively. Rain was recorded 17 times in 36 days during the experiment. Strong south-easterly wind was observed during the afternoons. The morning wind was predominantly from the south while in the evening it was north-west.

The site detail was presented in Section 3.1. When the data were collected, the crop was at a height of 300 mm. The lower arm containing air temperature and water vapour pressure sensors was installed 200 mm above the canopy surface, *i. e.* about 5 times more than the roughness length (Heilman *et al.*, 1989; Metelerkamp, 1993). The upper arm was installed at 800 mm above the lower sensor so that it was not more than 1 m from the canopy ground (Savage *et al.*, 1990) but sufficient for detecting a large enough profile difference in air temperature and water vapour pressure. The estimated thickness of the internal boundary layer was 20 m and that of the equilibrium sublayer (Eq. 2.44) was about 2.1 m. Thus, a fetch of 100:1 in the south easterly direction for this experiment

Table 5.1 - Summary of daily air temperature, water vapour pressure, relative humidity and wind speed observed during the experiment.

Day of Month	Air Temperature	Water v Pressure	Relative Humidity	Wind speed	Day of Month	Air Temperature	Water v Pressure	Relative Humidity	Wind speed
September	°C	kPa	%	m s^-1		°C	kPa	%	m s^{-1}
8	23	2.08	70	1.70	27	18	1.43	69	1.95
9	22	1.86	71	2.25	28	23	1.69	61	1.50
10	25	M 2.10	67	1.21	29	27	1.98	57	1.70
11	28	1.70	51	1.75					
12	M 29	m 1.14	m 31	M 2.75	October				
13	21	1.60	67	1.83	2	14	1.49	93	2.02
14	14	1.35	85	1.58	3	16	1.74	93	1.82
15	13	1.43	93	1.77	4	21	2.06	84	1.53
16	21	1.91	77	m 1.16	5	17	1.80	93	2.04
17	24	1.57	55	2.37	6	25	2.21	72	2.42
18	m 12	1.25	93	1.86	7	21	1.02	82	2.57
19	16	1.18	65	1.84	8	18	1.96	96	1.35
20	18	1.30	62	1.98	9	14	1.51	95	2.13
21	24	1.50	53	1.60	10	17	1.65	87	1.65
22	13	1.35	93	1.82	11	22	1.37	56	1.35
23	16	1.56	83	2.04	12	19	1.31	63	2.04
24	24	1.58	56	2.21	13	19	2.69	M 100	1.91
25	19	1.86	84	1.93	14	26	2.35	M 100	2.12
26	16	1.36	76	1.99	15	15	1.85	M 100	2.86

M = maximum and m = minimum

(predominant wind direction) was higher than the minimum 20:1 recommended fetch (Heilman *et al.*, 1989). The two height measurements of air temperature and water vapour pressure were within the equilibrium sublayer.

5.2.3 Analysis of the Estimated Bowen Ratio

The determination of the Bowen ratio β(Eq. 2.41) requires the psychrometric constant (γ), the sensible and latent heat exchange coefficients (K_h and K_v) and the profile measurement of air temperature and water vapour pressure. The accuracy of the BREB technique for determining sensible and latent heat depend on the accuracy for estimating β. The error in latent heat due to using a fixed psychrometric constant γ (0.065 kPa K^{-1} at 20 °C and at sea level) was reported to be very small (in Section 4.1.6). However, the use of the calculated values is recommended to suppress an additional error from the already existing theoretical and instrumental error of the technique. Unfortunately, neither an eddy correlation nor a lysimeter was available when the BREB was applied to estimate the sensible and latent heat exchange coefficient. The Similarity Principle between sensible

and latent heat exchange coefficient was applied to simplify the BREB determination of latent and sensible heat.

In spite of the suitability of the Similarity Principle, the estimate of β was seldom accurate. Data were collected from 08h00 to 18h00 to minimize the error in β estimates that one would get due to model and sensor limitations during nighttime. However, an error of β could still not be avoided during the daytime measurement of the profiles entities.

A plot of air temperature and water vapour pressure differences and the recorded wind speed on 9, 10, 11, and 12 September is shown (Fig. 5.1). Air temperature and water vapour pressure differential should be positive during daytime for lapse conditions. However, an inversion of air temperature (negative *dT*) was observed during the afternoons when the wind speed was high on 9 and 10 of

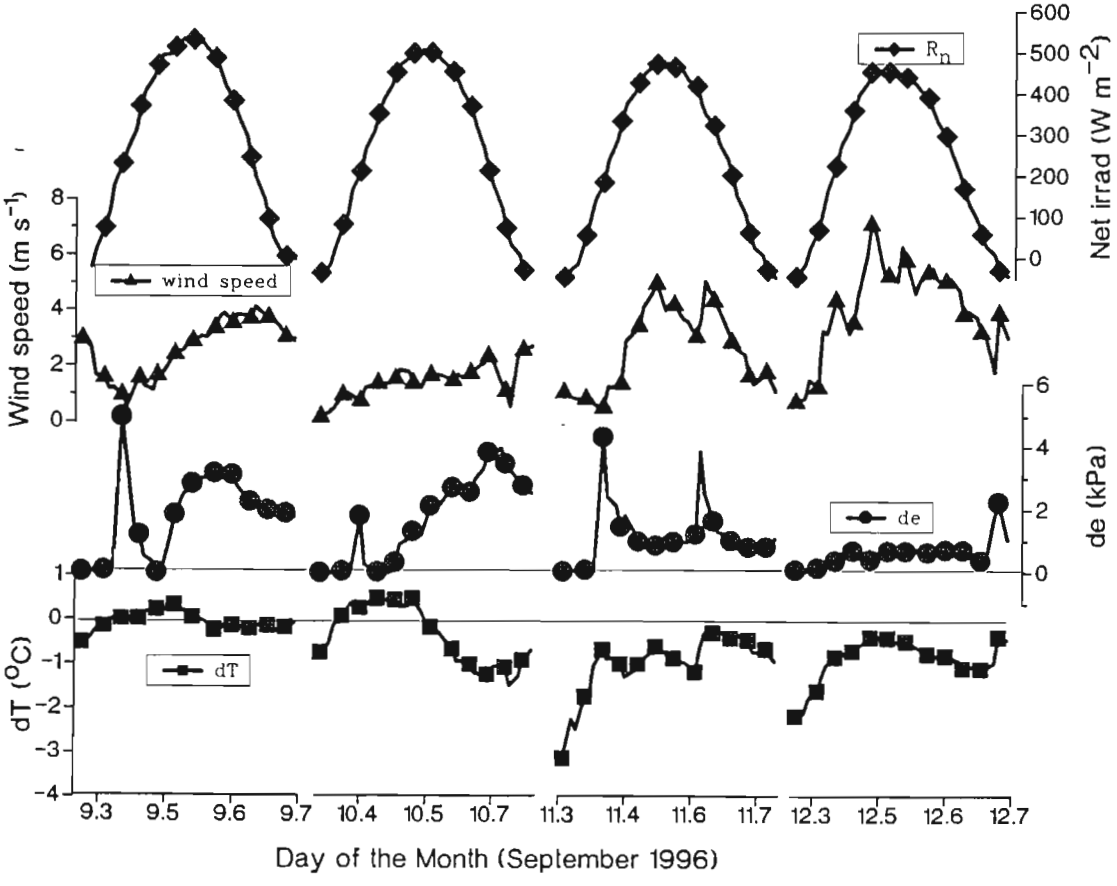

Figure 5.1 Variation of air temperature differential *dT* and vapour pressure differential *de* between the 200 and 1000 mm heights above the canopy surface. The measured wind speed and net irradiance are also shown.

September and throughout the day on 11 and 12 September. It is thought that the wind transported warm and dry air over a rapidly transpiring and cooled cabbage crop. This situation is observed under sensible heat advection conditions. Negative *de*'s were observed during the early morning period. It is thought that wind flow could advect dew water deposited on crop surfaces of the upwind field to the downwind field. The *de* was small under windy conditions on 11 and 12 September.

A plot of the variation of β, net irradiance and wind speed is shown (Fig. 5.2). Negative values of β are usually indicative of advection of sensible heat energy from the upwind field. The β value was positive during the morning period, while it was negative during the afternoon on 9 and 10 September. The β was negative throughout 11 and 12 September. Negative β and dT were in concordance, and this was observed during strong wind. The upwind field was not fully covered when the experiment was carried out. Uncovered and dry soil of the upwind field generated sensible

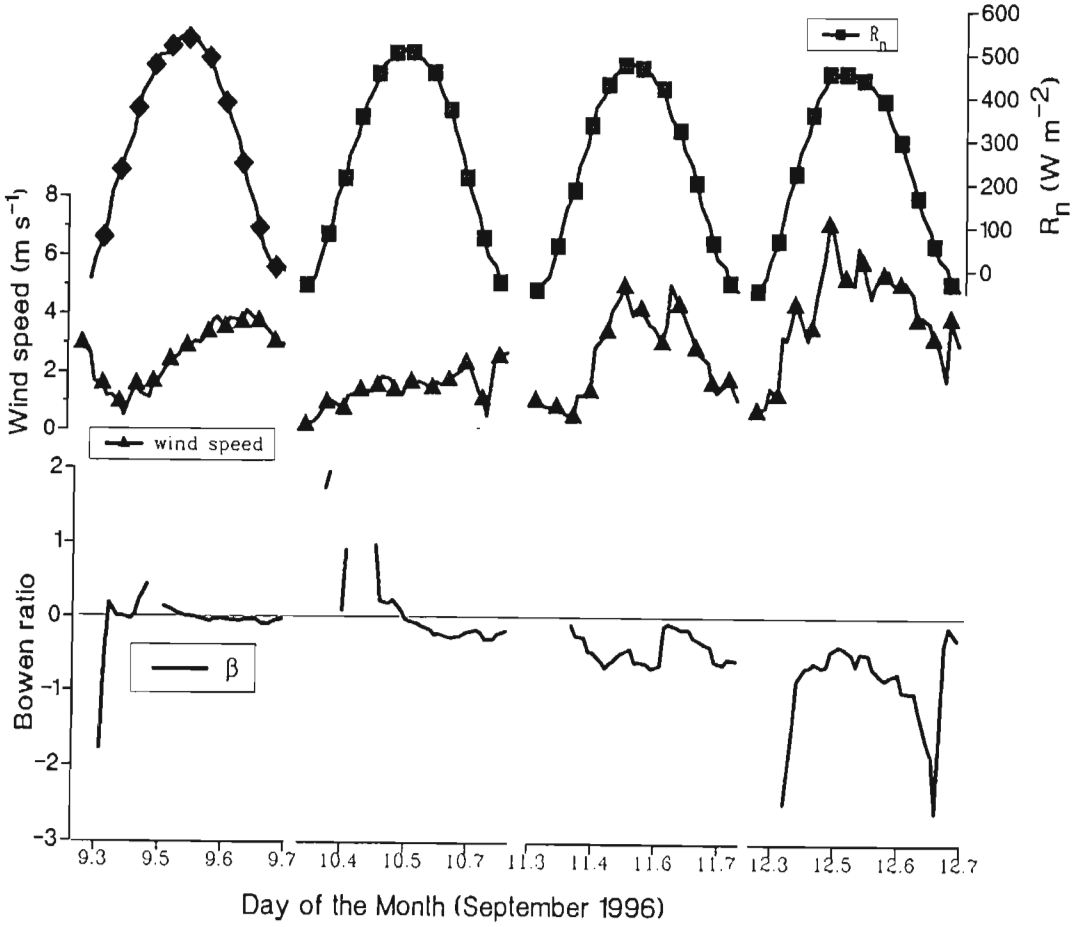

Figure 5.2 Variation of the Bowen ratio (β), net irradiance (R_n) and wind speed for non-advection (9 and 10 September) and advection (11 and 12 September) days.

heat which was transported to the neighbouring fields in the downwind field. It is unfortunate that one of the first assumptions, regarding negligible advection energy, (in section 2.1, paragraph 2) was violated and this would have a negative impact on the performance of the BREB.

5.2.4 Rejected Data

Eq. 2.47 was used to discard unreliable data due to model (β approaching -1) and equipment limitation. The BREB equipment was not operated during the nighttime to conserve battery voltage. The chromel-constantan thermocouple resolution was 0.006 °C and the cooled mirror resolution limit was 0.003 °C which corresponds to actual water vapour pressure of 0.01 kPa. Transient clouds could shade a sensor at a height and not both of them simultaneously. This would cause dissimilarity in incident radiation over the thermocouple sensors in the lower and upper arms. Most data were rejected because of *de* being within the resolution limit. This situation was observed when the sensors were wet because of dew, rain and irrigation water being deposited on the filter and when there was advection. For example, in the period between 30 September and 12 October the mixing bottle collapsed because teflon filters were blocked, possibly by water or pesticide. It is thought that during this time the water vapour pressure being measured was being sucked through the hole of the mixing bottle and not from the filters at the upper and lower heights. To avoid further blocking, the teflon filters were replaced with Gelman filters.

The upper and the lower limit of Eq. 2.47, the dT and the wind speed are shown in Fig. 5.3. Data were rejected when the dT was within the limit and accepted when outside of the rejection limit. Large amounts of data were rejected on 12 September when there was a strong influence of sensible heat advection. The β value on 12 September was between -1.3 and -0.6 (Fig. 5.2) which resulted in a very large amount of latent and sensible heat. Although the data were acceptable on 11 September, another day with strong advection, the dT was very close to the upper limit of the rejection limit. No daytime data were rejected on 9 and 10 September during the afternoon when there was also an indication of advection. Early morning rejection would result due to *de* being within the resolution limit on 9 September (see also Fig. 5.1). Unfortunately, advection energy was not

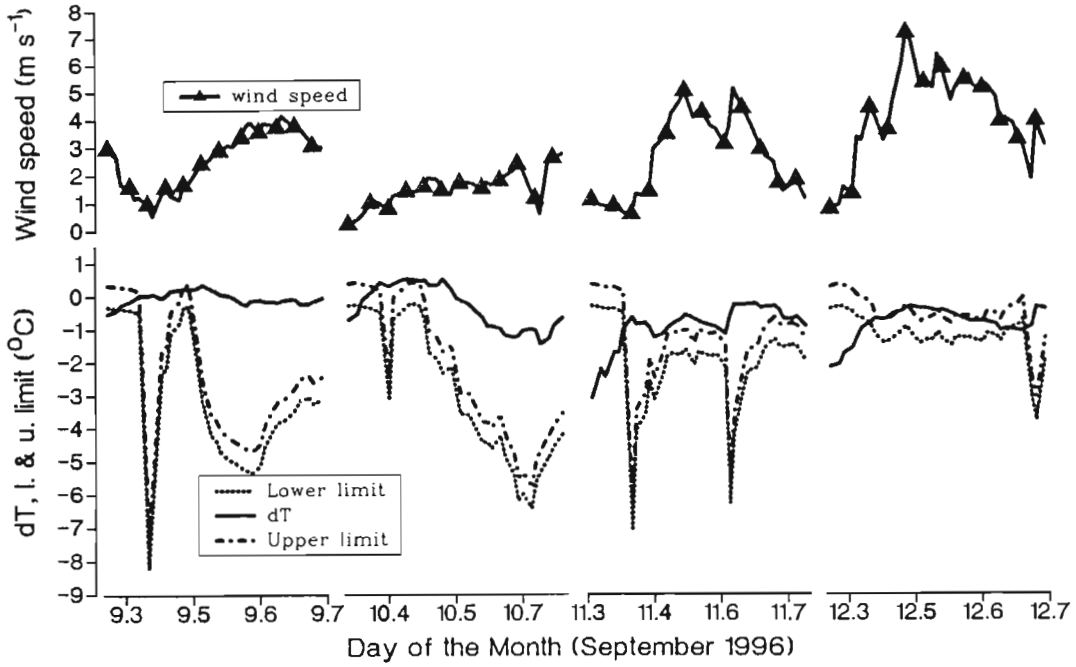

Figure 5.3 The upper and the lower limit for rejecting unreliable data. Values of dT are rejected if there are between upper and lower limits. Also shown is the wind speed as an indication of advection.

quantified. Wind speed was the only indicator of advection. Advection increased with increasing wind speed and *vice versa*.

Wet sensors were also the source of poor performance of the cooled mirror in the early morning due to water being deposited from dew, irrigation or rain. The problem with wet sensors is that energy input is not immediately sensed by the sensors; it is rather used to evaporate the condensed water on sensors and crop. On average, 3 hours were necessary for the sensor to dry and start providing valid measurement after rain or irrigation on 8 and 18 September, and 8 and 9 October. Tattari *et al.* (1995) found about 1 to 3 hours sufficient for the sensor to provide reliable gradient measurements after being wet.

Eq. 2.47 excluded data from $-1.55 \leq \beta \leq -0.6$, a limit relatively wider than the usually recommended limit of $-1.25 \leq \beta \leq -0.75$ by Savage *et al.* (1997). The wideness of the limit increased at a lower end due to sensible heat advection and at the upper end during sunset and sunrise, and on cloudy days. By screening data during nighttime due to sensor limitation one has only 40 % of the hours of the

daily measurement data using the BREB technique. About 30 % of daytime data were rejected, *i.e.* the BREB performed well in only about 35 % of the experimental period. Iritz and Lindroth (1994) reported 46% of the total numbers of days to be useful for calculation of evaporation using the BREB technique. Tattari *et al.* (1995) found about 53% of daytime data to be reliable.

The advection condition and high water vapour pressure deficits can increase the nighttime latent heat. So, a well-performed technique should also measure evaporation during the nighttime. Some authors (Malek, Bingham and McCurdy, 1990; Malek, Bingham and McCurdy, 1991; Cellier and Olioso, 1993; Iritz and Lindroth, 1994) were able to measure fluxes during the nighttime using the BREB technique. However, the performance of the BREB for this study would be poor during the nighttime.

5.2.5. Latent and Sensible Heat of the BREB

The estimate of latent heat using the BREB (Eq. 2.42) has been reported to agree with the latent heat measured using standard lysimetric method (Malek and Bingham, 1993). The BREB technique *per se* was not able to provide good estimates of latent and sensible heat energy during the daytime. Rejected data were estimated using equilibrium evaporation (Eq. 2.33) assuming that a weak flow of humid air was crossing over well watered cabbage crops (Savage *et al.*, 1997). Averaging the preceding and subsequent measurements (Malek *et al.*, 1990; Malek *et al* 1991) was also used to estimate rejected data during daytime. One of the greater disadvantages of the BREB technique is the use of other methods to estimate about 65 % of the rejected data (nighttime and daytime). For example, in this particular experiment, data were rejected when a strong flow of dry air was flowing over an irrigated crop or over a stressed crop (in the early stage the crop was stressed). Thus, one would use a Penman-Monteith for an oasis case or for a desert case to estimate the discarded data.

Measured net irradiance and soil heat flux density, and estimated latent and sensible heat flux density for 20 min intervals are shown (Fig. 5.4). Latent heat was larger than the net irradiance on 11 and 12 September. It is thought that the utilized extra energy was extracted from the air. On 10

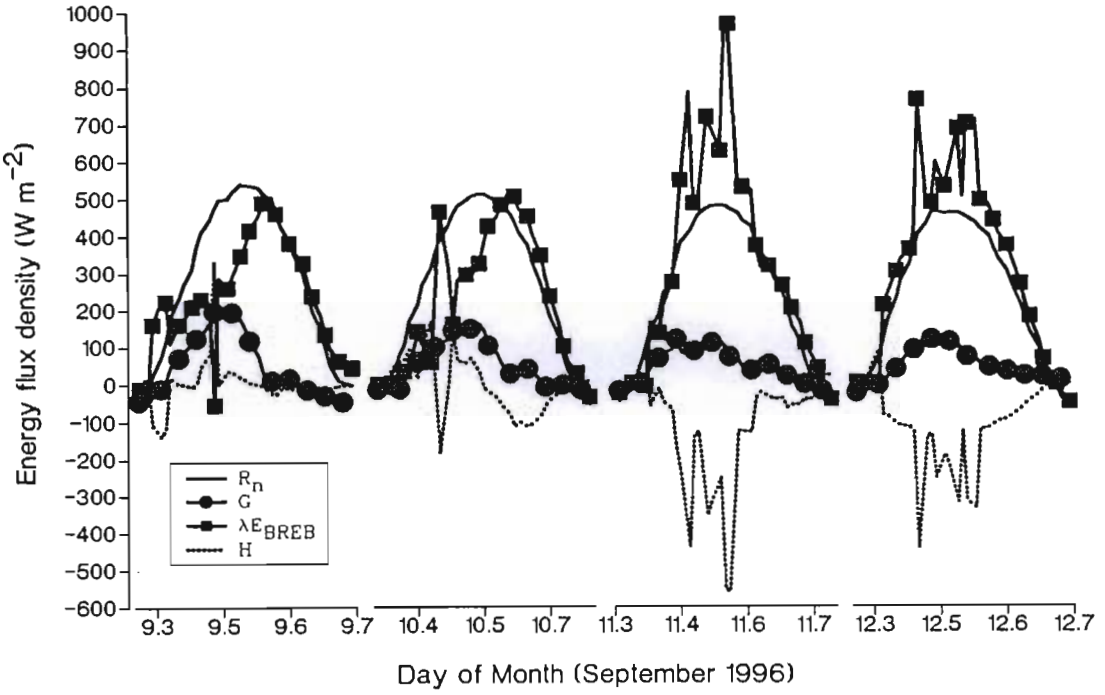

Figure 5.4 Measured net irradiance and soil heat flux density, and estimated latent and sensible heat flux density for 20 min intervals for non-advection (on 9 and 10) and advection (on 11 and 12) days.

September latent heat was large during the afternoon due to advection. Most of the data had high latent heat during afternoons. Normally, during the daytime, the sensible heat will be transferred from the warm ground or crop surface to the cooler air above (Rosenberg *et al.*, 1983). But instantaneous observation of the ratio between sensible heat (H) and available energy (R_n - G) showed that the ratio was negative during the afternoon period, *i.e.* there was a converse situation and sensible heat was being transferred from the air to the surface. This was an effect of consumption rather than generation of energy from the experimental site (Rosenberg *et al.*, 1983).

Latent heat estimated using the BREB technique and the Penman-Monteith method were compared (Fig. 5.5). The slope of 1.197, standard error of estimated Y of 69.1 and the r^2 of 0.82 was obtained using the regression between the BREB and the Penman-Monteith latent heat. The BREB technique overestimated the latent heat in the majority of cases by 17 %. The dispersion of the estimated latent heat using the BREB compared to the Penman-Monteith was large when latent heat was above 200 W m^{-2}.

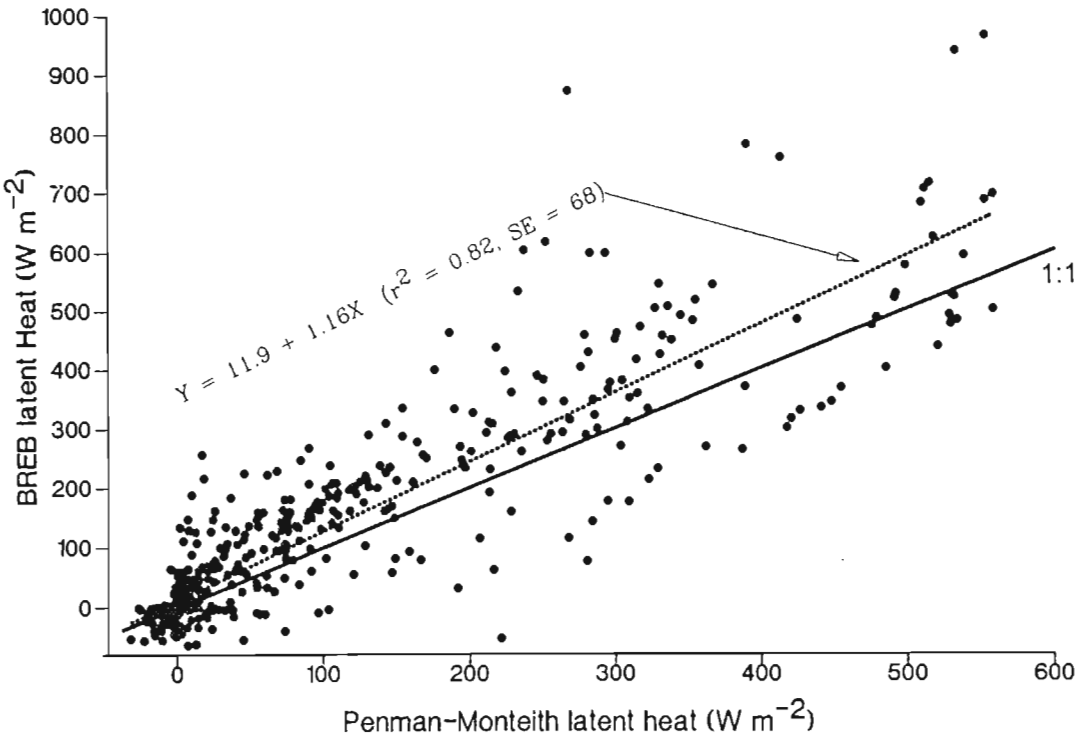

Figure 5.5 The BREB Latent heat vs Penman-Monteith latent heat flux density for 8 to 18 September 1996. Each point represents a 20 min period.

5.2.6 Conclusions

In this experiment, the Bowen ratio was calculated accepting the Similarity Principle and excluded nighttime data. However, an error of β could still not be avoided during the daytime measurement of the profiles entities because of wet sensors and presence of convection and stable conditions where the Similarity Principle could not be observed. Negative values of β were observed when there was strong wind and this was an indication of sensible heat advection from the upwind field. It is unfortunate that one of the first assumptions of the energy balance equation, regarding negligible advection energy, was not fulfilled. Data were rejected during morning, and strong advection periods. They were also rejected when the sensors were wet because of rain and irrigation. Most data in which the Bowen ratio was between -1.5 and -0.6 were discarded for computing the latent heat. In this experiment only 35 % of the experimental period was accepted for latent and sensible heat estimates using the BREB technique. Latent heat was larger than the net irradiance during advection periods. Comparative analysis showed that on average the BREB overestimated latent heat by 17 % compared to the Penman-Monteith latent heat. However, both the Penman-Monteith and the BREB latent heat

were affected by advection, a component of the energy balance equation assumed negligible.

5.3 SURFACE TEMPERATURE TECHNIQUE

5.3.1 Introduction

The surface temperature technique combines the integrated response of a crop to prevailing weather and soil conditions. It is therefore, an important tool for estimating evaporation and crop water requirement. The technique does not require canopy resistance and water vapour pressure deficit as does the Penman-Monteith method. It also does not require profile measurement of water vapour pressure and air temperature as does the Bowen ratio method.

The surface temperature technique can be accomplished with an IRT, an air-borne or satellite radiometer (Hatfield, 1983). The technique can estimate latent heat to within 10 % (Hatfield, 1984) when compared to a standard lysimeter under a full canopy cover. Blad and Rosenberg (1976a) found that the method could give good results under conditions of sensible heat advection where the BREB underestimated total evaporation by 20 %. The technique is based upon the assumptions that transpired water evaporates and cools the leaves below the temperature of the surrounding air. Thus, the canopy will warm if little water is transpired and cool if much water is transpired (Jackson, 1982). Verma *et al.* (1976) used the technique under advection conditions and found that it could estimate latent heat to within 9.6 %.

The surface temperature technique was evaluated for cabbage crop. The occurrence of advection is analysed using the surface to air temperature differential and wind speed. The surface temperature latent heat is compared to the Penman-Monteith and the BREB latent heat, while the surface temperature sensible heat is compared to the eddy correlation technique. The effect of placement height of air temperature sensors for sensible and latent heat estimate is also analysed using three heights.

5.3.2 Surface to Air Temperature Differential

A summary of daily weather conditions was presented in Section 5.2.2. The surface to air temperature differential is the driving force for heat flow (Eq. 2.3). It determines the sign and magnitude of sensible heat flux density. A negative surface to air temperature differential yields negative sensible heat and indicates a consumption of the energy by the crop. The positive surface to air temperature differential and subsequent sensible heat indicated generation of the energy from the crop surface.

The surface to air temperature differential (T_{can} - T_{air}), wind speed, water vapour pressure and net irradiance for cloudless days are shown (Fig. 5.6). The crop surface was more than 4 °C cooler compared to the air at 600 mm above the canopy surface during cloudless days, windy days and in the presence of a strong water vapour pressure deficit. The magnitude of $(T_{can}-T_{air})_{am}$ seemed to be

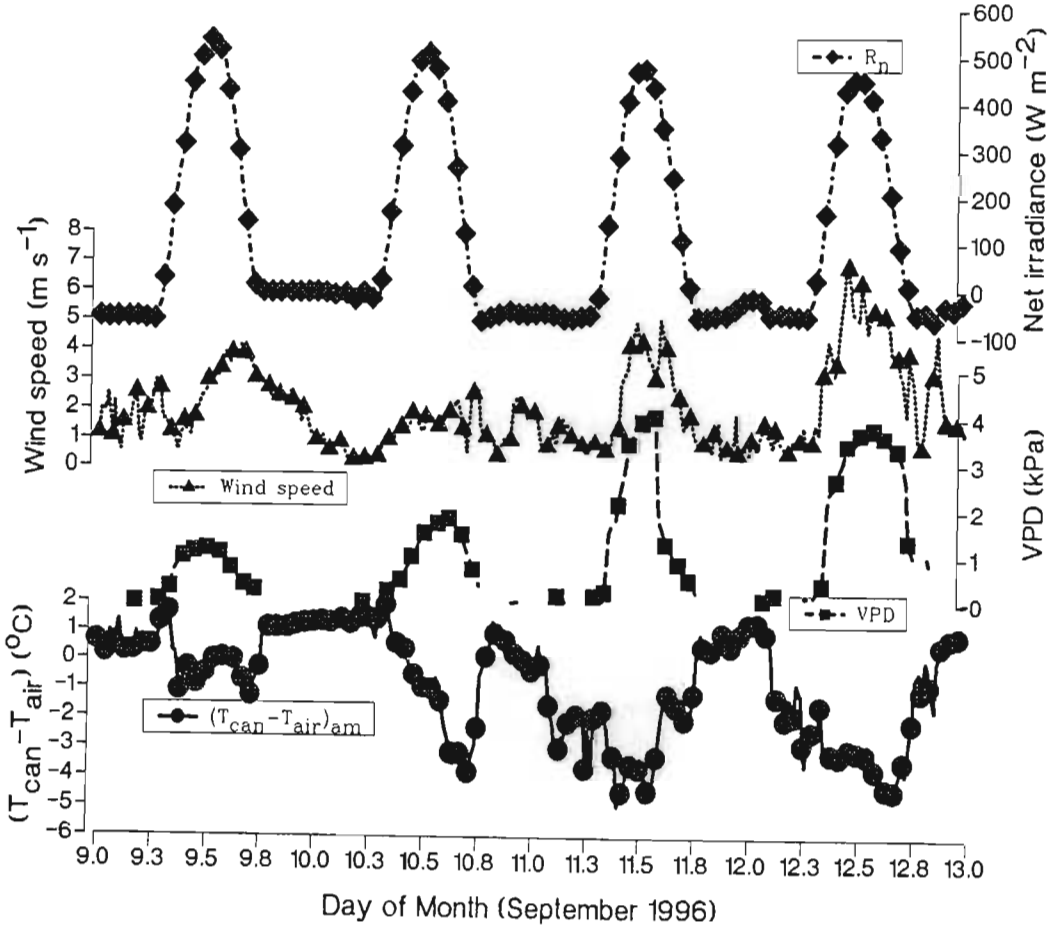

Figure 5.6 Variation of the surface to air temperature differential, wind speed, water vapour pressure and net irradiance for cloudless days with and without strong wind speed.

influenced more by wind speed than by VPD. For example, on 11 and 12 September wind was strong throughout the day, the magnitude $(T_{can}-T_{air})_{am}$ being larger with increases in wind speed and *vice versa*. The negative surface to air temperature differential was also large during most afternoon periods due to increases in wind speed.

However, on 9 September (as on 20 and 25 September, and 7 and 8 October) cloudiness conditions were similar to those observed on 10 September while wind speed was greater than that observed on 10 September. Nevertheless, the magnitude of $(T_{can}-T_{air})_{am}$ being smaller than expected due to an increase in wind speed (Fig. 5.6). There was a large amount of water vapour over the cabbages on 9 September. It is thought that the wind transported water vapour on 9 September and not sensible heat from the upwind field to the experimental field. The crop surface of the upwind field was possibly wet due to rain or irrigation. However, the upwind field was irrigated independently and no strict control of irrigation was maintained. Net irradiance also affected the magnitude and sign of the surface to air temperature differential, increasing the consumption processes under cloudless conditions and increasing the generation of sensible heat under cloudy conditions.

Aerodynamic resistance was estimated using Eq. 2.29. It appears that the consumption of sensible heat advection by the crop will increase during periods of strong wind carrying sensible heat advection. This is because of reduction in aerodynamic resistance and the increase in the magnitude of the surface to air temperature differential. However, the consumption process will be attenuated if there is water vapour advection.

5.3.3 Latent and Sensible Heat

Sensible heat (Eq. 2.3), latent heat (Eq. 2.9), net irradiance and soil heat flux at 20 min intervals are shown (Fig. 5.7). Latent heat was larger than net irradiance throughout 11 and 12 September and during the afternoon on 9 and 10 September. Additional energy was probably taken from the air, the

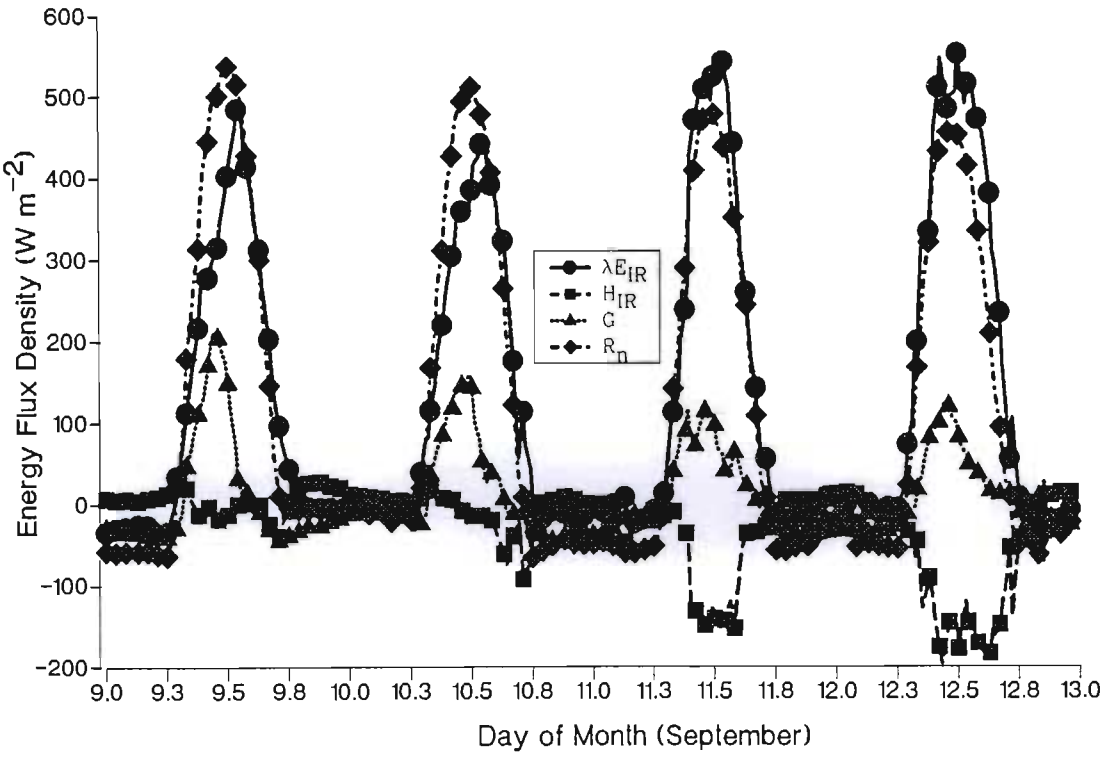

Figure 5.7 Variation of the estimated sensible and latent heat flux density using the surface temperature technique, net irradiance and soil heat flux density at 20 min intervals.

advected sensible heat from the upwind field. These observations are in concordance with that reported for the surface to air temperature differential. An r^2 of 0.96 and 0.94 was obtained when the estimated latent heat using the surface temperature technique, and that using the BREB technique and the Penman-Monteith method were regressed respectively. The slope of 1.57 and 1.17 indicated that there was approximately a 57 % and a 17 % overestimate of latent heat when using the surface temperature technique compared to the BREB and the Penman-Monteith respectively. The intercept for both the BREB and the Penman-Monteith was forced to 0 and the standard error was 31 and 37 W m^{-2} respectively. A plot of latent heat determined by using the surface temperature *vs* the latent heat determined using the Penman-Monteith method indicated that the surface temperature technique overestimated latent heat consistently, except for latent heat above 500 W m^{-2} (Fig. 5.8). This analysis, includes nighttime and daytime data between 9 September and 16 September.

The "energy closure", the ratio between the expenditure of energy [$H_{IR}+\lambda E_{(BREB)}$ or $H_{IR}+\lambda E_{(PM)}$,

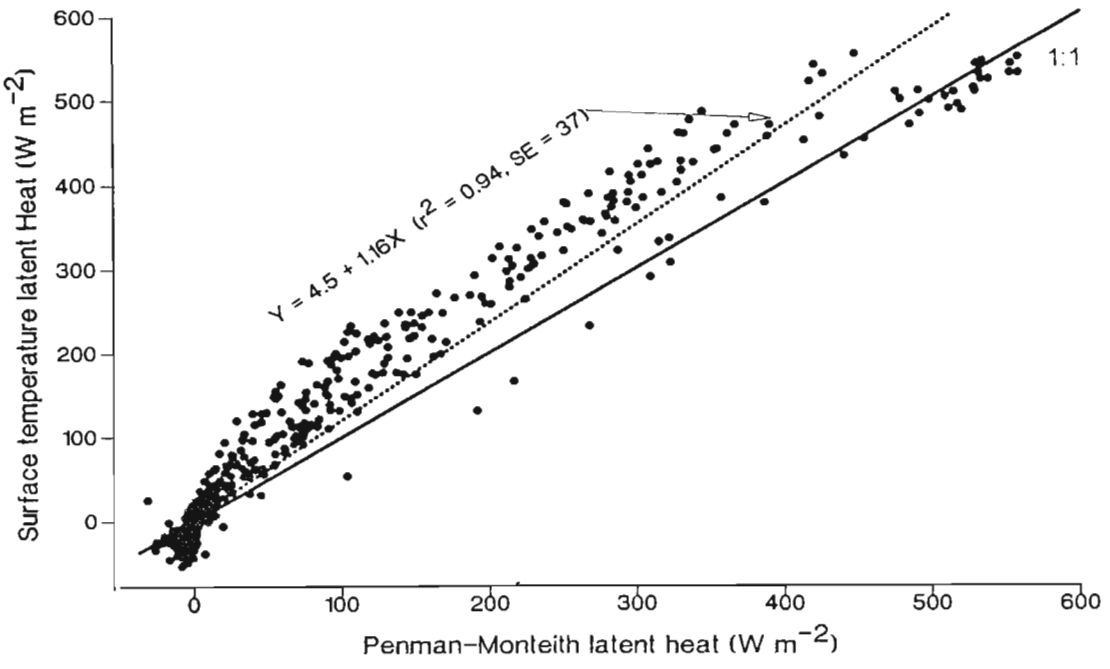

Figure 5.8 A plot of latent heat determined using the surface temperature *vs* latent heat determined using the Penman-Monteith method.

taking the BREB and Penman-Monteith as standard determinations] and available energy (R_n - G) was used to analyse the accuracy of the surface temperature technique to estimated sensible heat (Fig. 5.9). The energy closure was around 0.7 and 0.75 on cloudless days without marked influence of sensible heat advection when using the latent heat estimated using the BREB technique and the Penman-Monteith method as standard respectively. The closure was 0.4 and 1.1 during periods of strong influence of sensible heat advection on 11 and 12 September when the latent estimated using the BREB technique and the Penman-Monteith method was used as standard respectively. Thus, the estimated sensible heat using Eq. 2.3 was underestimated by 25 and 30 % during cloudless days without marked influence of sensible heat advection when compared to the Penman-Monteith method and the BREB technique. However, during periods with strong influence of sensible heat advection the surface temperature technique underestimated the sensible heat by 60 % in relation to the BREB and overestimated by 10 % in relation to the Penman-Monteith. The reason for this disparity is that neither the Penman-Monteith nor the BREB was accurate for estimating latent heat under advection conditions.

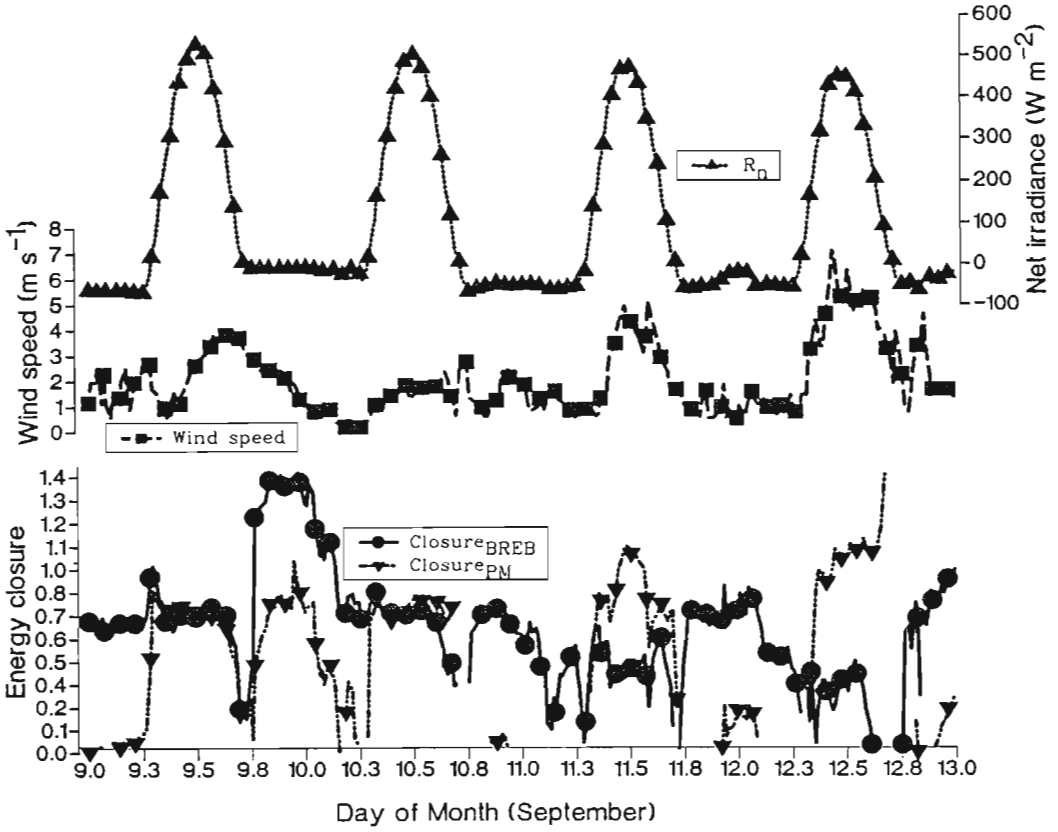

Figure 5.9 "Energy closure" between the expenditure of energy [$H_{IR}+\lambda E_{BREB}$ or $H_{IR}+\lambda E_{PM}$, taking the BREB and the Penman-Monteith as standard determination] and available energy (R_n - G).

5.3.4 Error Analysis

The eddy correlation method (Eq. 2.36) is an accurate technique for measuring sensible heat energy flux density. An r^2 of 0.2 (n = 216) was obtained between the correlation of sensible heat estimated using the surface temperature technique (Y) and eddy correlation technique (X_1) on 27, 28 and 29 October under variable cloud conditions. The slope and the intercept were very far from reaching the expected value of 1 and 0 according to the 95 % confidence interval. Inclusion of the wind speed (X_2) into the regression analysis increased the r^2 to 0.42 and the intercept approached the expected value of 0. That is, the measured sensible heat using the surface temperature technique was driven by sensible heat advection reflected in wind speed. The estimated sensible heat using the surface temperature technique under advection was underestimated by 70 % compared to 60 % reported above when the BREB technique was used as standard technique during advection conditions.

This comparison was performed when the cabbage crop was at maturity, assuming a high canopy

resistance and consequent generation of sensible heat energy from the crop rather than consumption of sensible advection by the crop. Plotting the two estimates of sensible heats, wind speed and net irradiance (Fig. 5.10) confirmed that there was generation of sensible heat when using the eddy correlation technique while there was heat consumption when using the surface temperature technique. It can be said that, under advection, sensible heat estimated using the surface temperature technique is driven by sensible heat from upwind field and not completely by the microclimate created by the interaction between the crop and atmosphere over the crop. Thus, a strong correlation between the surface to air temperature differential and VPD required to estimate the non-water-stressed baseline and consequent CWSI (Idso *et al.*, 1981a, b) is not likely to be found under such conditions.

The RSC sensitivity coefficient of latent heat due to change in input parameters was discussed (Section 4.1.3). It was reported that the estimated error in latent heat would certainly result from an error in the surface to air temperature differential and aerodynamic resistance. Thus, the 57 % overestimate in latent heat reported above under advection conditions may be caused by these factors. This value is much larger than the 9.6 % error reported by Verma *et al.* (1976) for their experiment.

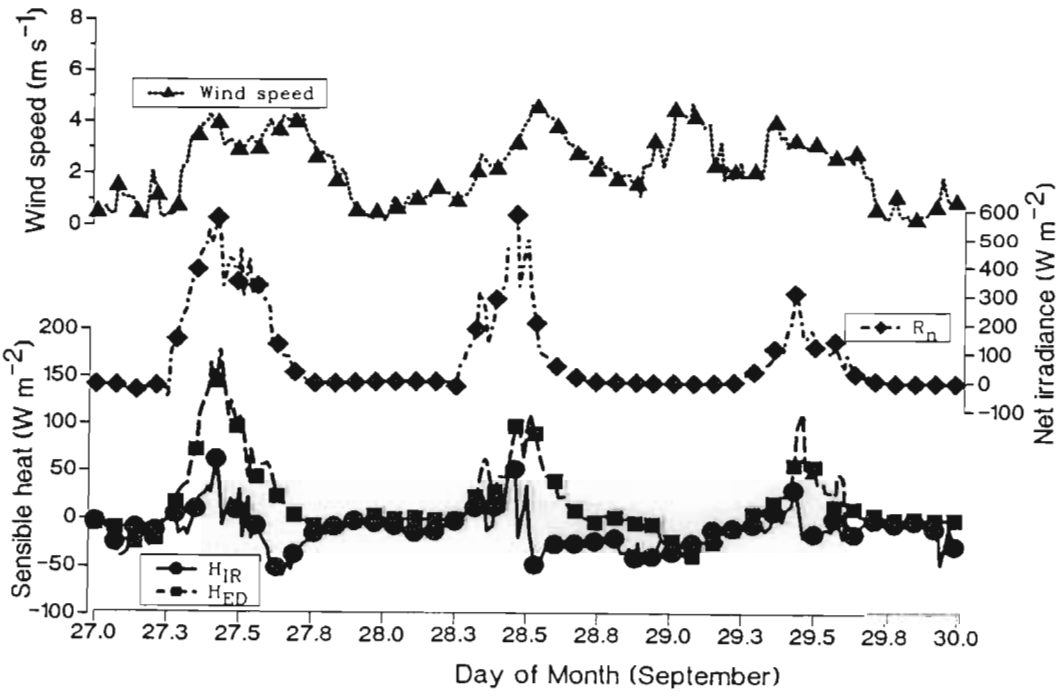

Figure 5.10 The Variation of sensible heat flux density estimated using surface temperature and eddy correlation techniques, wind speed and net irradiance for the last days of the cabbage growth.

5.3.5 Effect of Placement Height of Air Temperature Sensors

The IRT can provide acceptable measurement of the surface temperature up to a distance of 154 m above the crop surface (Jackson, 1982). However, air temperature sensors need to be installed at an appropriate height so that they detect the air temperature under the influence of the surface. Air temperatures measured at 200 mm, 1000 mm and the average between of 600 mm above the crop surface, are plotted (Fig. 5.11a). There was an inversion condition during periods of intense sensible heat advection. The lower sensor measured lower temperatures than the upper sensors. The difference was about 0.5 °C between air temperature measured at 200 mm and 600 mm height and 1 oC between 200 mm and 1000 mm. The difference between the surface to air temperature

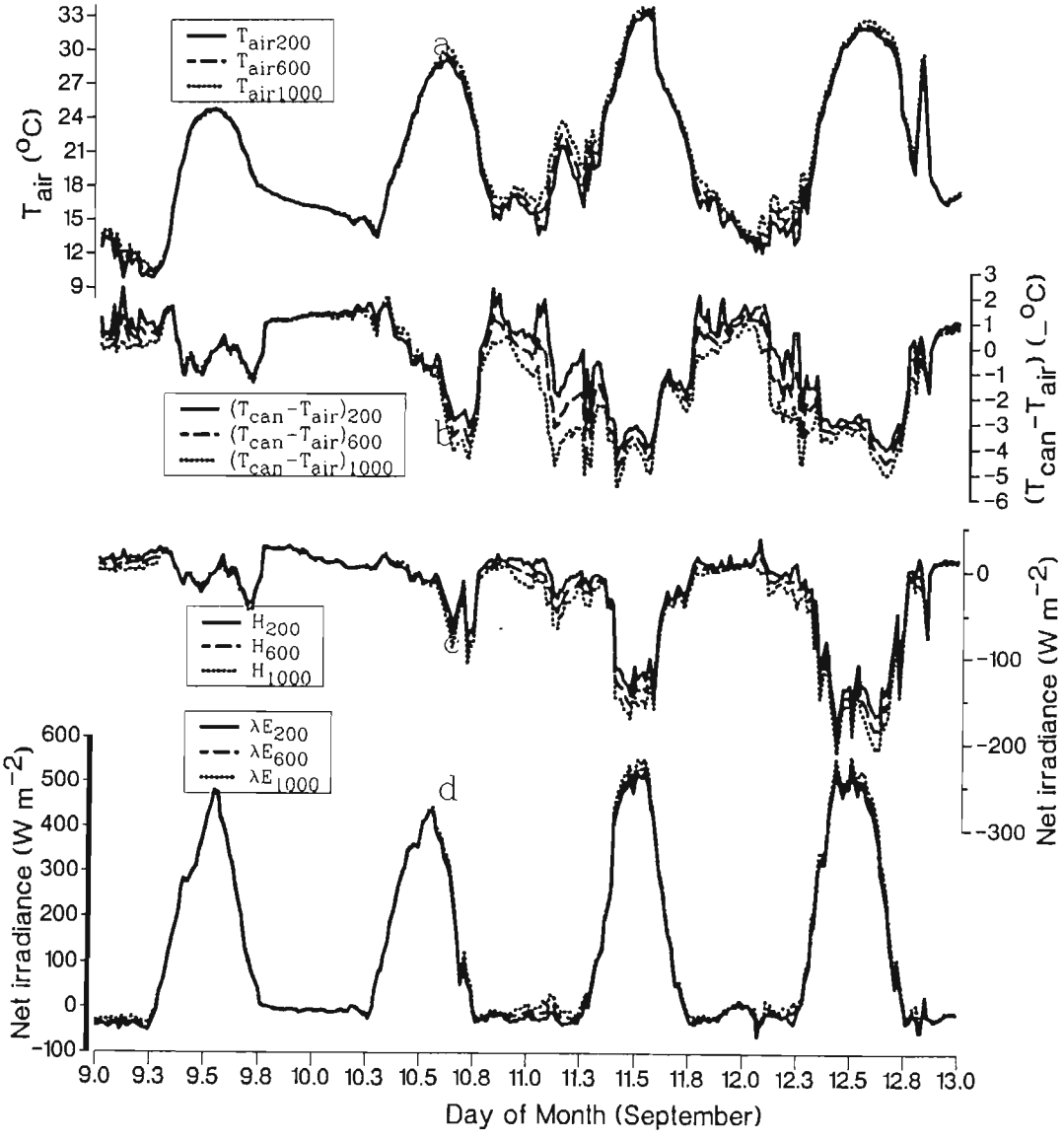

Figure 5.11 Variation of air temperature, surface temperature, sensible heat and latent heat for air temperature measured at 200, 600 and 1000 mm above the canopy surface.

differential was -0.5 °C between the sensors at 200 mm and 600 mm heights and -1 °C between 200 mm and 1000 mm (Fig. 5.11b)

Sensible heat and latent heat estimate using air temperature measured at 200 mm, 600 mm and 1000 mm above the crop canopy are shown (Fig. 5.11c, d). During cloudless days and intense influence of sensible heat advection, sensible heat was higher in magnitude at an upper height than at a lower height. The difference was 25 W m^{-2} between the measurement at 200 mm and 600 mm and 50 W m^{-2} between 200 mm and 1000 mm. This resulted in smaller latent heat when the sensor was set at lower height. The difference in latent heat between the extreme sensor was not more than 30 W m^2.

5.3.6 Conclusions

The surface to air temperature differential was very large in magnitude when there were strong wind speed and drier conditions in the upwind field, while it was small in magnitude when there was a lighter wind speed and wetter surface in the upwind field. The surface temperature latent heat was overestimated when it was compared with the Penman-Monteith and BREB latent heat. An analysis of the energy closure taking the Penman-Monteith and BREB as standards, suggested that the surface temperature technique overestimated the consumption of sensible heat from the air. This observation was also confirmed when the eddy correlation technique was used to evaluate the sensible heat estimated using the surface temperature technique. The effect of placement height of air temperature sensors suggested that the consumption of sensible heat would be overestimated if the sensor was placed far from the crop surface. This overestimation in consumption of sensible heat would result in overestimation of latent heat using the surface temperature technique.

5.4 DAILY VARIATIONS OF ENERGY BALANCE COMPONENTS COMPARATIVE ANALYSIS

The daily net irradiance, soil heat, latent and sensible heat flux density measured using the BREB and surface temperature techniques are shown (Fig. 5.12 a, b, c and d) together with sensible and latent

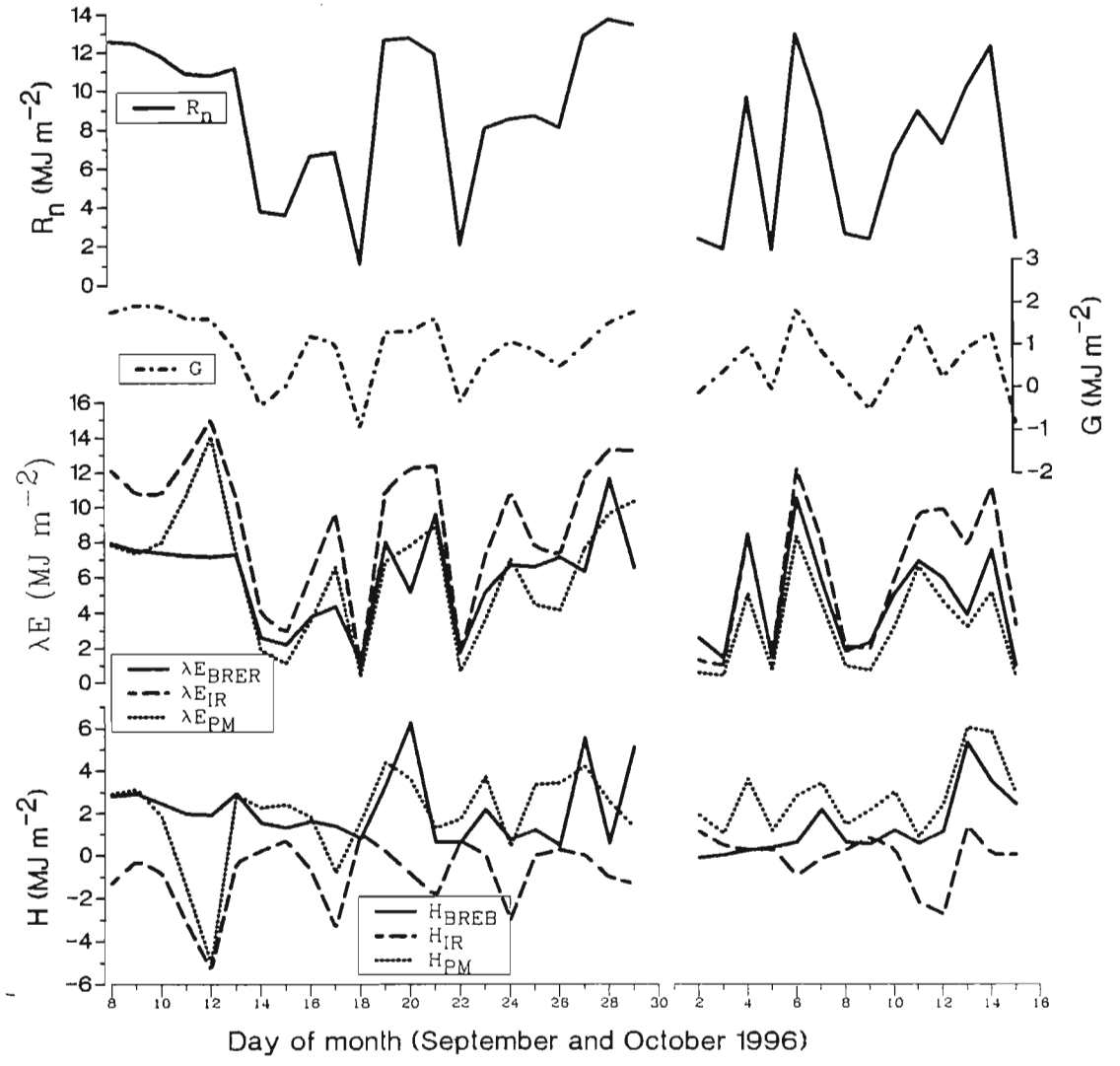

Figure 5.12 The daily energy density of the energy balance components estimated using the BREB and surface temperature techniques and the Penman-Monteith method.

heat flux density estimated using the Penman-Monteith method. The daily soil heat flux density change was dependent on the daily change in net irradiance. For cloudless days the soil heat flux density was 14 % of the net irradiance in comparison to 10 % reported by Allen (1996). The consumption of sensible heat energy was large when the surface temperature technique was used compared to when the BREB technique or the Penman-Monteith method was used. As a consequence the daily latent heat estimated using the surface temperature technique was larger than that estimated using the BREB technique and the Penman-Monteith method. The BREB latent heat was more closely related to the Penman-Monteith latent heat than to the surface temperature latent heat.

The daily relationship $\lambda E/(R_n - G) = 1/(1+\beta) > 1$ (Rosenberg, 1969a; Blad and Rosenberg, 1974; Blad and Rosenberg, 1976a; Rosenberg *et al.*, 1983), a *prima facie* evidence of sensible heat advection (Rosenberg *et al.*, 1983) was used to evaluate advection. Unfortunately, this relation is not always a sign of occurrence of advection as contested by Savage *et al.* (1997). This relation can be observed at low values of available energy, low vapour pressure and high temperature. Daily plot (Fig. 5.13) of the relation showed that there were 19 days with a predominance of sensible heat advection when using the surface temperature technique compared to 3 when using the Penman-Monteith method and 2 when using the BREB.

In this relationship the positive $[\lambda E/(R_n - G) - 1]$ value indicates the fraction of the advection of sensible heat used to evaporate water. For example, it is assumed that advection contributed more than 66 % on 12 September to evaporate water if one considers the latent heat estimated using the

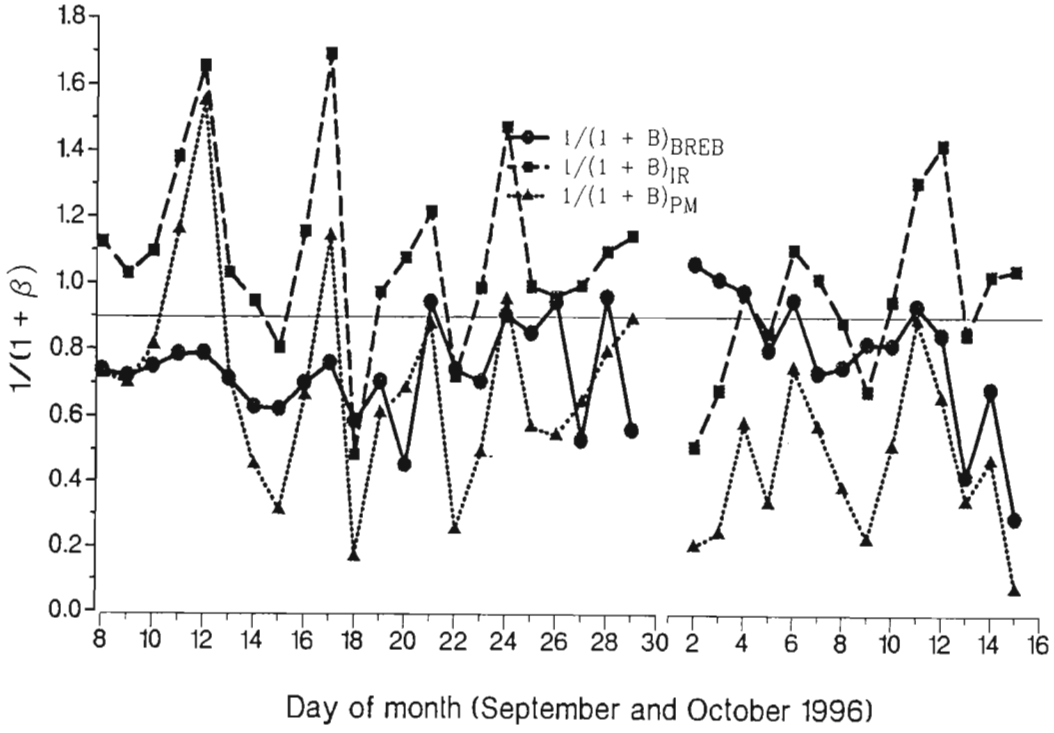

Figure 5.13 The daily relationship $\lambda E/(R_n - G) = 1/(1 + \beta) > 1$ showing the influence of advection on latent heat determined using the BREB and surface temperature techniques, and the Penman-Monteith method.

surface temperature technique. Blad and Rosenberg (1974) reported a 20 % of advected sensible energy contribution to evaporate water and as much as 40 % for a single day. For this analysis one assumes that all available energy was used to evaporate water.

Davenport and Hudson (1967) found that, under advection, evaporation was high over the leading edge. It decreased within the field to an equilibrium value at the wet area of an infinite extent due to the absorption of advected energy and reduction of wind speed by drag force exerted by crop roughness. It is thought that the equilibrium value due to leading effect under advection was observed behind 100 m downwind in this experiment if taking into consideration the surface temperature latent heat. The effect of advection in increasing evaporation rates can be minimized by first planting the upwind field to increase the drag force against wind and reduce generation of sensible heat by bare soil. Irrigation should also start in the upwind field so that wet and cool air from the upwind field is carried to the field under study. There is a need to consider setting up a windbreak to attenuate the wind effect in the transport of sensible and latent heat advection.

Evaporation for the entire period was 117 for the surface temperature technique, 80 for the BREB technique and 74 mm the Penman-Monteith method. That is, the surface temperature technique overestimated evaporation by 50 % in relation to the BREB and 60 % in relation to the Penman-Monteith evaporation. Most workers have reported the technique to overestimate evaporation (Heilman and Kanemasu, 1976; Hatfield, 1984). The advection into the field was the cause of such a large overestimate of latent heat when using the surface temperature technique.

CHAPTER 6

DETERMINING THE CROP WATER STRESS INDEX USING SURFACE TEMPERATURE TECHNIQUE AND PENMAN-MONTEITH METHOD

6.1 INTRODUCTION

One of the advantages of the surface temperature technique in relation to the BREB technique is the possibility to estimate the crop water stress index (CWSI). However, the estimate of the CWSI from the surface temperature technique and the Penman-Monteith method requires reliable estimates of the potential (minimum) canopy resistance and actual canopy resistance. A combination of the empirical and Penman-Monteith equations has been used successfully to estimate the potential canopy resistance (Jackson *et al.*, 1981; O'Toole and Real, 1986; Jalali *et al.*, 1994). Actual canopy resistance can be estimated using the Penman-Monteith equation (Lindroth, 1993; Malek *et al.*, 1991). An empirical equation (Mascart *et al.*, 1991) based on the potential canopy resistance, solar irradiance and soil water content has been used for estimating actual canopy resistance. The equation relating actual aerodynamic resistance to wind speed has been widely used (Allen *et al.*, 1989; Alves *et al.*, 1995).

The estimate of the actual and potential evaporation from the surface temperature technique and the Penman-Monteith method can be used to estimate the CWSI. The simplicity and possibility of scanning regional surface temperature using a remote sensing technique constitute an advantage for the surface temperature technique because regional actual and potential evaporation and CWSI can be determined. However, an estimate of latent heat using the surface temperature technique must be compared to that estimated using the Penman-Monteith method because the method still requires further refinement to estimate evaporation or CWSI. The only precise method of estimating crop water stress using the surface temperature technique consisted in determining the difference between the surface temperature of the field under study and that of a well-watered area of the same crop

(Jackson, 1982; Hatfield, 1983). However the technique was not widely used because of difficulty in maintaining a well-watered crop. Further research in determining the crop water stress involved coupling the surface temperature and air temperature to determine the Stress Degree Day (Jackson *et al.*,1977).

Additional progress for estimating the crop water stress using the surface to air temperature differential and meteorological factors were developed by normalising the Stress Degree Day (Idso *et al.*, 1981a; Idso, 1982). Meanwhile Idso *et al.* (1981a) linked the surface to air temperature differential to a vapour pressure deficit, Jalali *et al.* (1994) linked it to vapour pressure deficit and net irradiance. However, none of these authors addressed the problem of auto-self correlation existing between the surface temperature differential and the water vapour pressure deficit or net irradiance (Savage 1997, personal communication). These workers estimated the CWSI as the ratio of the differences between the actual and the potential surface to air temperature differentials and the difference of the non-transpiring and potential surface to air temperature differentials. The actual surface to air temperature differential would be measured, the potential and non-transpirirng surface to air temperature differentials would be estimated from regression analysis (Hatfield, 1983; O' Toole and Hatfield, 1983). A more developed theory, linking most micrometeorological factors to the surface to air temperature differential was later developed to estimate the actual, potential and non-transpiring surface to air temperature differentials (Jackson *et al.*, 1981).

In this chapter an empirical equation was used to estimate the canopy resistance. The potential and non-transpiring surface to air temperature differentials were estimated using an empirical equation based on the surface temperature technique. The Penman-Monteith method was also used to estimate such parameters and the actual surface to air temperature differential. The actual and potential evaporation is determined using the surface temperature technique and the Penman-Monteith method. A series of combinations was made to estimate the CWSI using the measured and empirical estimate of the surface to air temperature differentials, and actual and potential evaporation determined using the surface temperature technique and the Penman-Monteith method.

6.2 ACTUAL, POTENTIAL AND NON-TRANSPIRING SURFACE TO AIR TEMPERATURE DIFFERENTIAL

The regression between $(T_{can} - T_{air})_{pe1}$ and VPD (Eq. 2.14) for a well watered cabbage crop is shown (Table 6.1) with that reported (Idso, 1982) for kohlrabi (*Brassica oleracea*), rutabaga *(brassica napo-brassica*) and turnip (*Brassica rapa L.*). Data were collected 1 to 3 days after irrigation and only for which solar irradiance greater than 230 W m^{-2} were considered in this regression. An average air temperature of 21.73 ^{0}C was used to estimate the non-transpiring surface to air temperature differential, and the average estimated canopy surface temperature was 22.84 ^{0}C. The water vapour pressure difference between the crop surface and the air at 600 mm above the crop surface was 0.18 kPa. Using this value and wind correction factors (Table 2.2) for beans, the computed non-transpiring surface to air temperature differential was 2.8 ^{0}C (Eq. 2.16). The regression incorporating net irradiance (Eq. 2.15) was used to observe if there was an improvement for estimating $(T_{can} - T_{air})_{pe2}$ from micrometeorological variables. This regression line is also shown in Table 6.1. A non-transpiring surface to air temperature of 4.81 ^{0}C was calculated (Eq. 2.17).

Poor correlation between $(T_{can} - T_{air})_{pe1}$ and VPD were observed for data collected at 20 min intervals from 11h00 to 14h00. There were possibly other meteorological factors determining the variations

Table 6.1 The regression of the potential surface to air temperature differential (Y) as influenced by vapour pressure deficit (X) or vapour pressure deficit (X_1) and net irradiance (X_2). Data for the experiment (the last two rows) were poorly correlated due to sensible and latent heat advection.

Common Name	Scientific Name	Conditions	n	I	Slope1	Slope2	r^2	Syx	SEI	SESlope1	SESlope2	Authors
Kohlrabi	*Brassica Oleracea*	Sunlit	70	2.01	-2.17		0.979	0.46	0.13	0.053		Idso (1982)
Rutabaga	*Brassica napo-brassica*	Sunlit	91	3.75	-2.66		0.988	0.54	0.14	0.044		Idso (1982)
Ruta-baga		Shaded	53	-0.5	-2.51		0.913	0.86	0.37	0.157		Idso (1982)
Turnip	*Brassica rapa L.*	Sunlit	129	1.94	-2.26		0.979	0.68	0.14	0.042		Idso (1982)
Bermudagrass				0.58	-1.4	0.0066	0.889					Jalali *et al.* (1994)
Cabbage	*Brassica oleracea Capitata*	semi-shaded	89	1.12	-1.78		0.41	1.28		0.225		Experiment
Cabbage	*Brassica oleracea Capitata*	semi-shaded	89	-1.46	-2.23	0.0075	0.63	1.03		0.192	0.001	Experiment

of $(T_{can} - T_{air})_{pe1}$ rather than a single VPD (Ehrler, 1973). Although the introduction of net irradiance improved the regression, the r^2 value was smaller than the values reported by Idso (1982) and Jalali *et al.* (1994). This was caused certainly due to the influence of advection. As stressed in Chapter 5, there was presence of both sensible heat and water vapour advection into the field under study. Daily analysis using the surface temperature technique showed that there were 19 days whose latent heat was affected by advection of sensible heat in comparison to 3 and 2 days when using the BREB technique and the Penman-Monteith method.

Sensible heat advection can affect directly the values of the surface to air temperature differential. Water vapour advection into the field can reduce the water vapour pressure deficit. All these interferences may have affected the correlation between $(T_{can} - T_{air})_{pe1}$ (Y) and VPD (X) or $(T_{can} - T_{air})_{pe2}$ and VPD (X_1) and net irradiance (X_2) that would exist due to the interaction between the crop and microclimate above the crop within the field. The potential and the non-transpiring surface to air temperature differential estimated using Idso *et al.* (1981a) and Jalali *et al.* (1994) approaches are plotted *vs* VPD (Fig. 6.1). The plotting of the potential surface to air temperature difference estimated using net irradiance and VPD as independent variable against VPD show the data scattered below the regression line between potential surface to air temperature differential and VPD. The lower line of the region (of data resulting from the regression incorporating net irradiance) would be 2.5 oC lower than the regression line between potential surface to air temperature differential and VPD. The estimated non-transpiring surface to air temperature differential using Eq. 2.17 was about twice as large than that estimated using the regression between $(T_{can} - T_{air})_{pe1}$ and VPD taking into account the wind correction factor. It is thought that the potential and non-transpiring surfaces to air temperature differential for the cabbage were not found in this experiment.

The estimated potential canopy and aerodynamic resistances (according to Jackson *et al.*, 1981; O'Toole and Real, 1986; Jalali *et al.*, 1994) using a combination of the Penman-Monteith and empirical Eqs. 2.14 and 2.15 were used to estimate the potential surface to air temperature differential $(T_{can} - T_{air})_p$ (Eq. 2.19). The aerodynamic resistance under water stressed conditions $r_{astress}$

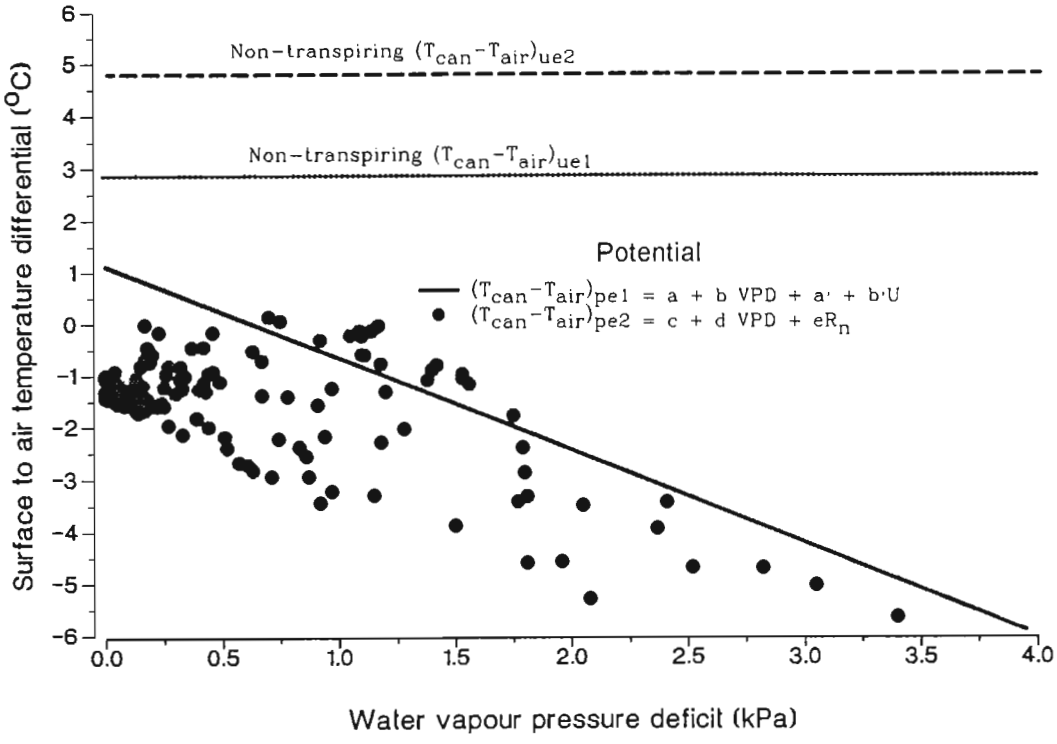

Figure 6.1 The potential and the non-transpiring surface to air temperature differential estimated using the regressions between the surface to air temperature differential (T_{can} - T_{air}) vs vapour pressure deficit (VPD)(O'Toole and Hatfield, 1983) or vapour pressure deficit (VPD) and net irradiance (R_n)(Jalali *et al.*, 1994).

(Eq. 2.23) was used to estimate the non-transpiring $(T_{can} - T_{air})_u$ while the actual canopy (Eq. 2.28) and aerodynamic (Eq. 2.29) resistance were used to estimate the actual $(T_{can} - T_{air})_a$ (Eq 2.18). The estimated actual, potential and non-transpiring surface to air temperature differential are shown (Fig. 6.2) for data collected at 20 min intervals. The normal occurrence of $(T_{can} - T_{air})_u > (T_{can} - T_{air})_a > (T_{can} - T_{air})_p$ was observed at about 11h00 to sunset. During cloudy days the $(T_{can} - T_{air})_a$ was above the non-transpiring surface to air temperature differential. The actual and lower limit of the $(T_{can} - T_{air})$ was positive for most of the daytime except when there was marked presence of advection on 11 and 12 September. The actual surface to air temperature differential should be negative during daytime due to transpiration cooling of the crop surface.

The correlation between the estimated (Y) and measured actual $(T_{can} - T_{air})$ resulted in a $r^2 = 0.124$, intercept of 0.73 and slope of 0.625. This correlation was relatively poor because the actual surface

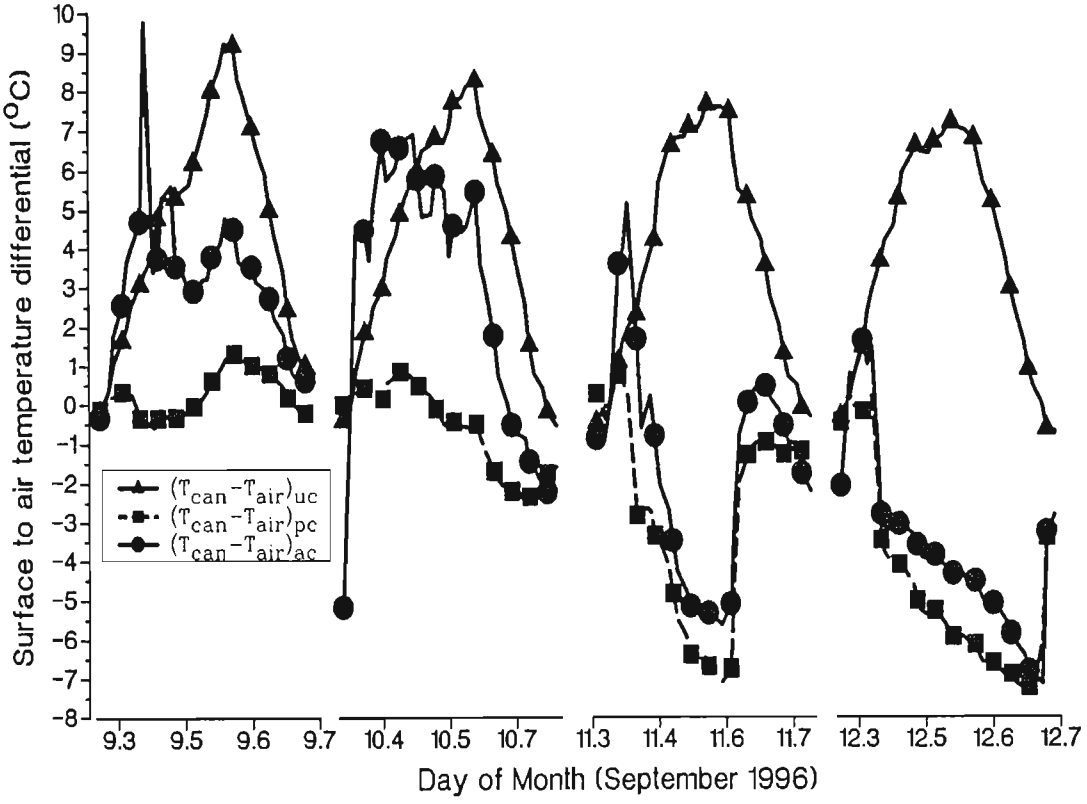

Figure 6.2 The actual ($_{ac}$), potential ($_{p}$) and non-transpiring ($_{uc}$) surface to air temperature differential estimated using the Penman-Monteith approach.

to air temperature differential was estimated using the potential canopy and aerodynamic resistances determined by using a poorly correlated empirical equation (Eqs 2.14 and 2.15). The estimate would have been improved if advection was taken into consideration. Unfortunately no attempt was made to estimate sensible heat and water vapour advection into the field. A maximum r^2 of 0.33 was found between the linear regression of the surface to air temperature differential and VPD (Eq. 2.14) with surface temperature and actual water vapour pressure obtained randomly. The intercept was -1.2, the slope -4.02 and standard deviation of 7.2. This indicate that there is an autoself-correlation between the surface to air temperature differential and water vapour pressure deficit because of presence of air temperature in the surface to air temperature differential (T_{can} - T_{air}) and in the saturated water vapour pressure of the VPD {VPD = es - e = 0.6108 exp[17.2694 T_{air}/(237.3 + T_{air})] - e}. That is, the surface to air temperature differential can be correlated to VPD if the r^2 is larger than 0.33. Thus, an r^2 of 0.43 reported in this experiment (Table 6.1) can be attributed to the autoself-correlation between surface to air temperature differential and VPD. The autself-correlation

of the non-water-stressed-baseline may be strong when the regression Eq. 2.15 is used. In this equation there is straight relationship between the surface to air temperature and saturated water vapour pressure deficit. Additional autoself-correlation is (T_{can} - T_{air}) and net irradiance [$R_n = R_{ns} + R_{nl} = R_s + f(\varepsilon_a - \varepsilon_{vs})\,\sigma\,T_{air}^4$, where R_{ns} is the net solar irradiance, R_{nl} is net longwave irradiance, f is the cloudiness factor, ε_a effective emissivity of the atmosphere, ε_{vs} is the emissivity by vegetation and soil and σ the Stefan-Boltzmann constant (Allen *et al.*, 1994)].

6.3 AERODYNAMIC AND CANOPY RESISTANCE

Latent heat estimated using the BREB technique was used in Eq. 2.26 to estimate the canopy resistance(Eq. 2.26) (Malek *et al.*, 1991). There was poor performance because a negative estimate of canopy resistance was observed. Alves *et al.* 1996 had similar observations. Physical interpretation by these authors suggested that the negative canopy resistance can be obtained using the Penman-Monteith equation when the evaporating surface is located above the "big leaf" (= d + $Z_{ohv,}$. when using Eq. 2.29 for r_a), certainly at the top of the canopy. Since it was not the aim of this work to discuss the performance of different techniques for estimating canopy resistance, the Penman-Monteith-based equation for estimating canopy resistance was discarded. Detailed discussion on the performance of the Penman-Monteith equation for estimating canopy resistance was given by Alves *et al.* (1996).

Use of an empirical equation based on solar irradiance, soil water content and potential canopy resistance (Mascart *et al.*, 1991) (Eq. 2.28) gave reasonable results for estimating canopy resistance. However, there was a need to estimate the potential canopy and aerodynamic resistance (according to Jackson *et al.*, 1981; O'Toole and Real, 1986; Jalali *et al.*, 1994) of a cabbage crop using Eqs 2.21, 2.22, 2.24 and 2.25. The average of the estimated potential aerodynamic and canopy resistance using intercept and slope of Eq. 2.14 were 6.9 and 36.0 s m^{-1} respectively. Nevertheless, use of the intercept and slope of Eq. 2.15 resulted in larger potential aerodynamic and canopy resistance of 15.5 and 50 s m^{-1} respectively. The 20 min variations of r_{cp} and r_{ap} estimated using the two regression data are shown (Fig. 6.3). The r_{cp} was slightly larger during early morning, late afternoon and on cloudy

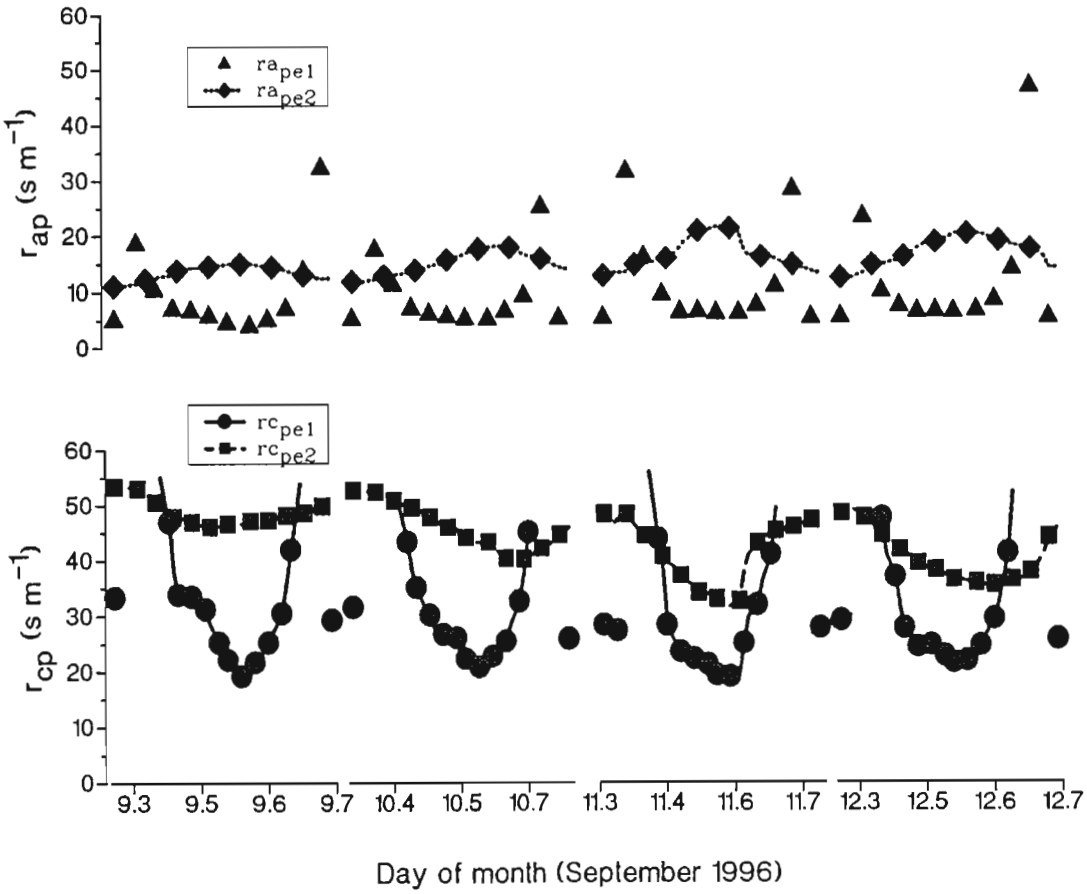

Figure 6.3 The 20 min variations of potential canopy (r_{cp}) and aerodynamic (r_{ap}) resistance estimated using a combined equation between statistical regression and the Penman-Monteith method.

days. Since there was good agreement when incorporating net irradiance into the regression for the surface to air temperature estimate (Eq. 2.15), the 50 s m^{-1} was taken as the canopy resistance of the cabbage crop under potential water conditions. O'Toole and Real (1986) found a potential canopy and aerodynamic resistance of 60 and 16 s m^{-1} for a fig tree while Jallali *et al.* (1994) found 79 and 13 s m^{-1} for Bermuda grass. It is interesting to observe that the estimated values were consistent and that the method could be trusted provided there was a good correlation between $(T_{can} - T_{air})_{pe1/2}$ and VPD or VPD and net irradiance.

The estimated actual canopy and aerodynamic resistance using Eqs 2.28 and 2.29 are shown (Fig. 6.4). The canopy resistance was large in the early morning, late afternoon and on cloudy days than at solar noon and cloudless days. The increase in actual canopy resistance between 12 and 16

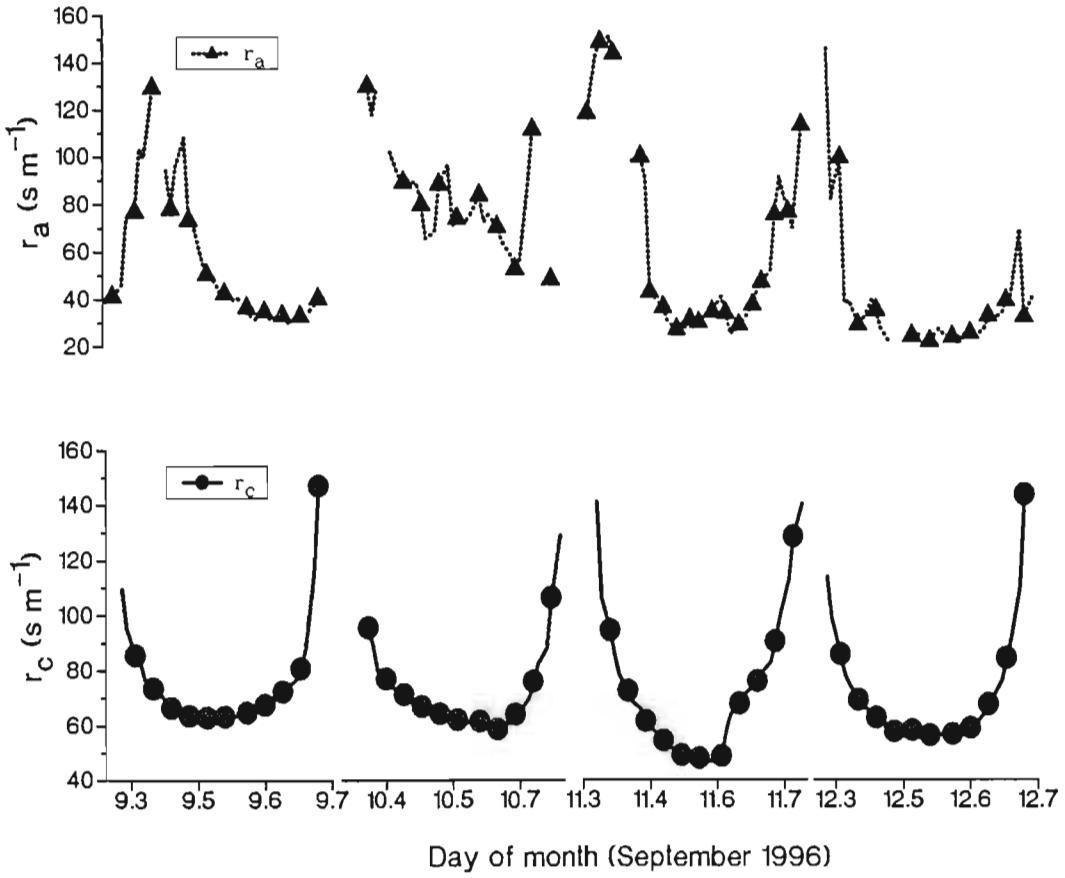

Figure 6.4 The variation of the actual canopy (r_c) and aerodynamic (r_a) resistance

September was due to a combination of decreased soil water availability and to cloudy conditions. The soil water content was below the refill point during this period (Chapter 7). The values of the canopy resistance varied between 69 and 600 s m^{-1}. Since the minimum canopy resistance should be 50 s m^{-1} for potential conditions, one may assume that the shelter function F_3 (Eq. 2.28) was 50/69 = 0.72. The estimated actual canopy resistance was corrected using this factor.

There was a small aerodynamic resistance during afternoon and throughout the day on 11 and 12 September because of high wind speed. For example, on 12 September it reached values less than 17 m s^{-1}. The $r_{astress}$ = 22 s m^{-1}, the aerodynamic resistance under water stressed conditions estimated (Eq. 2.23) for this experiment was larger than 10 s m^{-1} found by Jackson *et al.* (1981) for wheat but close to 20 s m^{-1} found by Jalali *et al.* (1994) for Bermuda grass. Although r_{cp}, r_{ap} and $r_{astress}$ for a crop have been used successfully to estimate the CWSI, no investigation was performed to relate such

estimates to the nature of the dynamic of canopy and aerodynamic resistance. For example, the estimated aerodynamic resistance using Eq. 2.29 for a well watered and water stress period was different from the r_{ap} and $r_{astress}$. These resistances were used to estimate the actual, potential and non-transpiring surface to air temperature differentials (Jackson *et al.*, 1981), potential and actual evaporation, and the CWSIs.

6.4 ACTUAL AND POTENTIAL EVAPORATION

The Penman-Monteith potential evaporation ($\lambda E_{p(PM)}$) was estimated using r_{cp} = 50 s m^{-1} and r_{ap} = 15.5 s m^{-1} (Eqs 2.21 and 2.22) while the Penman-Monteith actual evaporation was estimated using r_c and r_a. as

$$\lambda E_{p(PM)} = [\Delta(R_n - G) + \rho_{air} Cp_{air} \delta e/r_{ap}]/[\Delta + \gamma(1 + r_{cp}/r_{ap})] \quad 6.1a$$

$$\lambda E_{a(PM)} = [\Delta(R_n - G) + \rho_{air} Cp_{air} \delta e/r_a]/[\Delta + \gamma(1 + r_c/r_a)] \quad 6.1b$$

The potential surface to air temperature differential determined by using the regression of Eqs 2.14 and 2.15, and Eq. 2.19 were used to estimate potential evaporation using the surface temperature technique as:

$$\lambda E_{pe1(IR)} = (R_n - G) - \rho_{air} Cp_{air} (T_o - T_{air})_{pe1}/r_{ap1} \quad 6.2a$$

$$\lambda E_{pe2(IR)} = (R_n - G) - \rho_{air} Cp_{air} (T_o - T_{air})_{pe2}/r_{ap2} \quad 6.2b$$

$$\lambda E_{pc(IR)} = (R_n - G) - \rho_{air} Cp_{air} (T_o - T_{air})_{pc}/r_{ap2} \quad 6.2c$$

The measured and calculated $(T_{can} - T_{air})_a$ (Eq. 2.18) were used to estimate actual latent heat using the surface temperature method:

$$\lambda E_{am(IR)} = (R_n - G) - \rho_{air} Cp_{air} (T_{can} - T_{air})_{am}/r_a \quad 6.3a$$

$$\lambda E_{ac(IR)} = (R_n - G) - \rho_{air} Cp_{air} (T_{can} - T_{air})_a/r_a \quad 6.3b$$

The potential and actual Penman-Monteith latent heat ($\lambda E_{p(PM)}$ and $\lambda E_{a(PM)}$) was taken as standard for comparing potential and actual evaporations calculated using the surface temperature technique.

Actual evaporations, $\lambda E_{a(PM)}$, $\lambda E_{am(IR)}$ and $\lambda E_{ac(IR)}$ are presented together with the measured net irradiance (Fig. 6.5). As expected the $\lambda E_{a(PM)}$ and $\lambda E_{ac(IR)}$ were the same since the r_c and r_a used to estimate $(T_{can} - T_{air})_a$ and subsequently $\lambda E_{ac(IR)}$ are similar to those used to estimate $\lambda E_{a(PM)}$. The $\lambda E_{am(IR)}$ was larger and the difference from the $\lambda E_{a(PM)}$ and $\lambda E_{ac(IR)}$ was larger during periods of sensible heat advection than during typical cloudless days. From previous discussion it was found that the calculated $(T_{can} - T_{air})_a$ did not reflect the real characteristics of a fully transpiring crop since it was a producer of sensible heat because of positive $(T_{can} - T_{air})_a$. Sensor calibration and error analysis (section 4.1.3) for the site suggested that the surface and air temperature measurement using IRT and chromel-constantan thermocouples were accurate and that they could be trusted for determining reliable $(T_{can} - T_{air})_a$. So, an equality between latent heat estimated using the Penman-Monteith

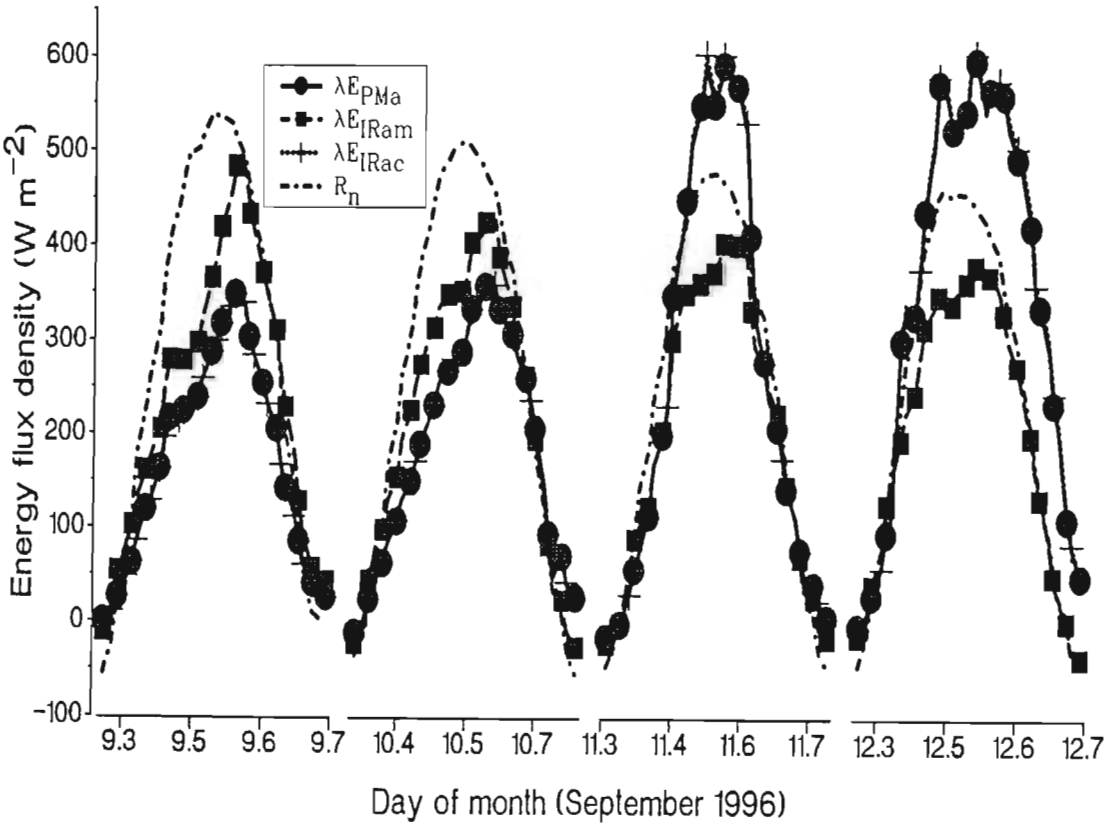

Figure 6.5 Actual evaporation estimated using the Penman-Monteith method and surface temperature technique with actual measured and calculated surface to air temperature differential.

method and the surface temperature technique with the calculated surface to air temperature differential can only suggest that the Penman-Monteith did not perform well either. Both the Penman-Monteith method and the surface temperature technique did detect the increase in evaporation rates due to sensible advection from the upwind field on 11 and 12 September.

The estimated potential evaporation using the Penman-Monteith and the surface temperature technique at 20 min intervals are shown (Fig. 6.6). The $\lambda E_{pc(IR)}$ estimated using the Penman-Monteith calculated $(T_{can} - T_{air})_p$ was well matched to the $\lambda E_{p(PM)}$ and both were smaller than that estimated using $(T_{can} - T_{air})_{pe1/2}$ from empirical equations. Empirical equations based on the regression of $(T_{can} - T_{air})_{pe1}$ *vs* VPD resulted in large potential evaporation because of small calculated potential aerodynamic resistance. Potential latent heat was larger than the net irradiance during advection period. It appears that if the correlation coefficient between the surface to air temperature differential (Y) and VPD (X) or VPD (X1) and net irradiance (X2) was larger the estimated evaporation would be equal to that estimated using the Penman-Monteith method.

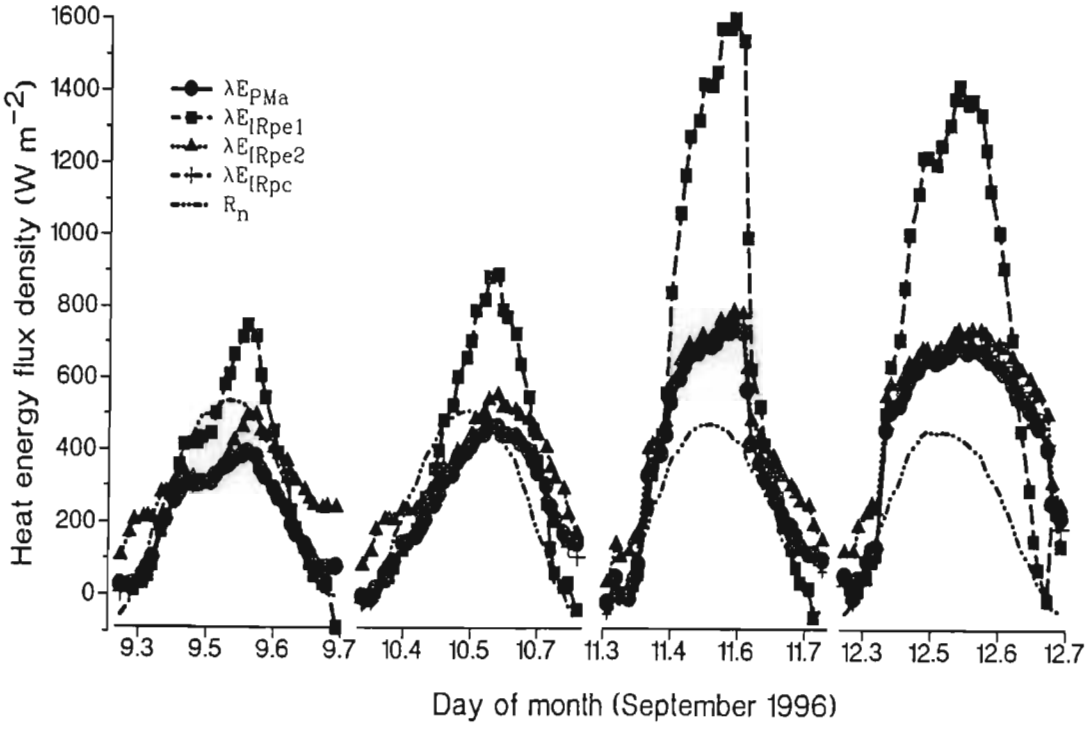

Figure 6.6 Variation of the estimated potential evaporation using the Penman-Monteith method and the surface temperature technique for 20 min intervals.

The actual to potential latent heat ratio can indicate the status of soil and crop water stress. This ratio must be between 0 for a severely water stressed crop and 1 for well watered crops. Values outside of this range can only indicate a wrong calculation or an unreliable method was used to estimate either actual evaporation, or potential evaporation, or both actual and potential evaporation. The ratios $\lambda E_{a(PM)}/\lambda E_{p(PM)}$, $\lambda E_{am(IR)}/\lambda E_{pe1(IR)}$, $\lambda E_{am(IR)}/\lambda E_{pe2(IR)}$ and $\lambda E_{ac(IR)}/\lambda E_{pcIR)}$ are shown in Fig. 6.7. The ratio $\lambda E_{a(PM)}/\lambda E_{p(PM)}$ and $\lambda E_{ac(IR)}/\lambda E_{pccIR)}$ was much the same, decreasing along a depletion period. The ratio $\lambda E_{am(IR)}/\lambda E_{pe1(IR)}$ and $\lambda E_{am(IR)}/\lambda E_{pe2(IR)}$ were within the limit at solar noon during cloudless days. Small r^2 for estimating the surface to air temperature differential using the regressions (Eqs. 2.14 and 2.15) may justify such a poor estimate of the ratio $\lambda E_{am(IR)}/\lambda E_{pe1(IR)}$ and $\lambda E_{am(IR)}/\lambda E_{pe2(IR)}$. These ratios were very responsive to advection.

6.5 CROP WATER STRESS INDEX (CWSI)

Eq. 2.13 was used to estimate the crop water stress index based on measured and estimated actual surface to air temperature differentials and estimated potential (Eqs 2.14, 2.15 and 2.19) and non-

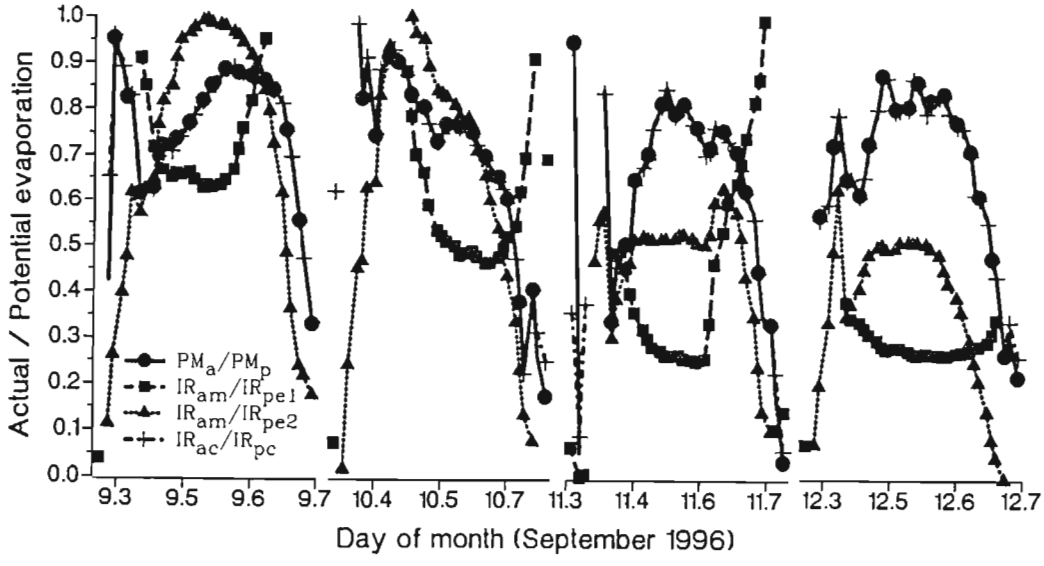

Figure 6.7 Variation of the ratio between actual evaporation and potential evaporation using the Penman-Monteith method ($\lambda E_{a(PM)}/\lambda E_{p(PM)}$) and the surface temperature technique ($\lambda E_{am(IR)}/\lambda E_{pe1(IR)}$, $\lambda E_{am(IR)}/\lambda E_{pe2(IR)}$ and $\lambda E_{ac(IR)}/\lambda E_{pCIR)}$).

transpiring (Eqs 2.16, 2.17 and 2.20) surface to air temperature differential as follows:

$$CWSI_{Te1} = [(T_{can} - T_{air})_{am} - (T_{can} - T_{air})_{pe1}]/[(T_{can} - T_{air})_{ue1} - (T_{can} - T_{air})_{pe1}] \quad 6.4a$$

$$CWSI_{Te2} = [(T_{can} - T_{air})_{am} - (T_{can} - T_{air})_{pe2}]/[(T_{can} - T_{air})_{ue2} - (T_{can} - T_{air})_{pe2}] \quad 6.4b$$

$$CWSI_{Tc} = [(T_{can} - T_{air})_{a} - (T_{can} - T_{air})_{p}]/[(T_{can} - T_{air})_{u} - (T_{can} - T_{air})_{p}] \quad 6.4c$$

Eq. 2.12 was used to estimate $CWSI_{EPM}$, $CWSI_{Ee1}$, $CWSI_{Ee2}$ and $CWSI_{Ec}$ using the ratio $\lambda E_{a(PM)}/\lambda E_{p(PM)}$, $\lambda E_{am(IR)}/\lambda E_{pe1(IR)}$ and $\lambda E_{am(IR)}/\lambda E_{pe2(IR)}$ and $\lambda E_{ac(IR)}/\lambda E_{pc(IR)}$:

[3]

$$CWSI_{EPM} = 1 - \lambda E_{a(PM)}/\lambda E_{p(PM)} \quad 6.5a$$

$$CWSI_{Ee1} = 1 - \lambda E_{am(IR)}/\lambda E_{pe1(IR)} \quad 6.5b$$

$$CWSI_{Ee2} = 1 - \lambda E_{am(IR)}/\lambda E_{pe2(IR)} \quad 6.5c$$

$$CWSI_{Ec} = 1 - \lambda E_{ac(IR)}/\lambda E_{pcCIR)} \quad 6.5d$$

The $CWSI_{PM}$ using $\lambda E_{a(PM)}/\lambda E_{p(PM)}$ was used as standard for comparing the other method though taking into account the uncertainty of the accuracy of the Penman-Monteith method for estimating actual evaporation under advection.

The daily $CWSI_{Te1}$, $CWSI_{Te2}$ and $CWSI_{Tc}$ are plotted together with the standard $CWSI_{EPM}$ (Fig. 6.8) for the average of data collected between 11h00 and 14h00. The $CWSI_{Te1}$, $CWSI_{Te2}$ was below the standard $CWSI_{EPM}$. They reached negative values during cloudless days when the estimated $(T_{can} - T_{air})_{pe1/2}$ using regressions (Eqs 2.14 and 2.15) were larger than the measured $(T_{can} - T_{air})_{a}$. The $CWSI_{Tc}$ and $CWSI_{Te2}$ were larger than the $CWSI_{EPM}$ when the estimated $(T_{can} - T_{air})_{p}$ was larger than the $(T_{can} - T_{air})_{u}$ on cloudy days. The CWSI should be between 0 for a well-watered crop and 1 for water stressed crop. Thus, the CWSI so determined could not be used for an interpretation of the crop and

[3]The indexes $_{e1}$ correspond to calculation involving the regression equation between the surface to air temperature differential (Y) and the VPD (X), while the index $_{e2}$ involve VPD (X_1) and net irradiance (X_2) as independent variables.

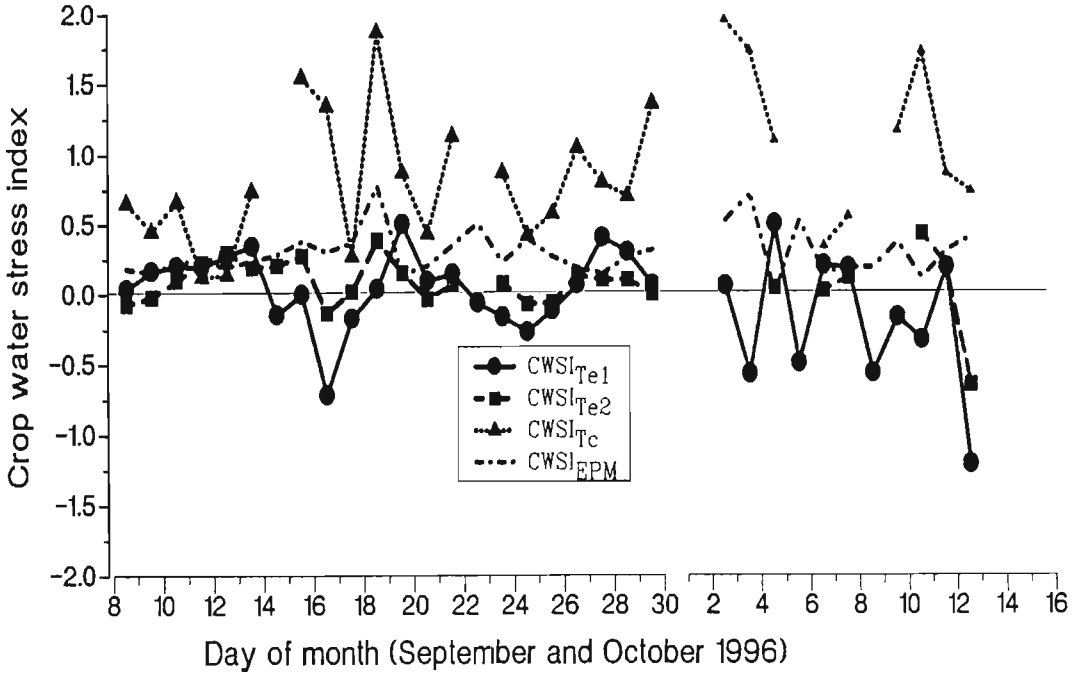

Figure 6.8 The daily variation of $CWSI_{Te1}$, $CWSI_{Te2}$, $CWSI_{Tc}$ determined using the surface to air temperature differential and the standard $CWSI_{EPM}$ for the average of data collected between 11h00 and 14h00.

soil water status.

The $CWSI_{Ee1}$, $CWSI_{Ee2}$ and $CWSI_{Ec}$[4] are also plotted in conjunction with the standard $CWSI_{EPM}$ (Fig. 6.9). As expected the $CWSI_{Ec}$ was much the same as the $CWSI_{EPM}$ for reasons discussed previously. The $CWSI_{Ee2}$ was improved compared to $CWSI_{Te2}$, being closer to the 0.75 during the drying period and zero during the rewetting period. Thus, the CWSI can be acceptably estimated using Eq. 2.12, with actual and potential evaporation estimated using the Penman-Monteith method and the surface temperature technique. The $(T_{can} - T_{air})_a$ and $T_{can} - T_{air})_p$ for such estimates can be obtained using a combination method between the Penman-Monteith and a well correlated empirical regression equation.

[4]$CWSI_T$ is related to the crop water stress index calculated using the surface to air temperature differential ratio, while $CWSI_E$ is related to the evaporation ratio.

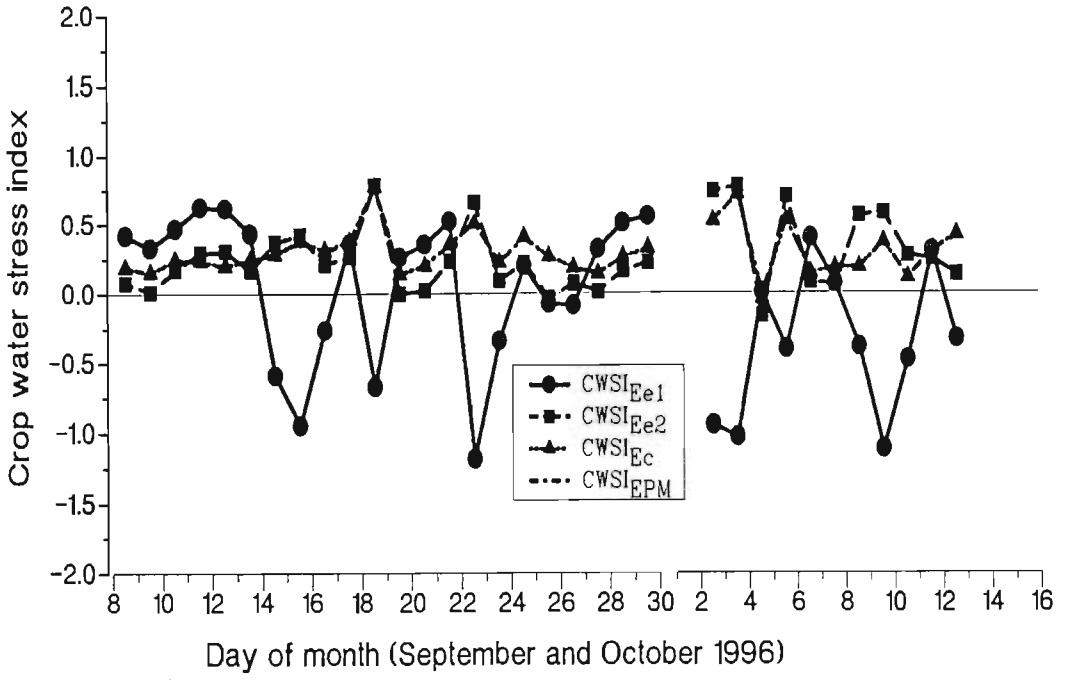

Figure 6.9 The daily variations of $CWSI_{Ee1}$, $CWSI_{Ee2}$ and $CWSI_{Ec}$ determined using actual and potential latent heat from surface temperature technique and the standard Penman-Monteith latent heat.

6. 6 TIMING OF IRRIGATION USING THE CWSI

The most common purpose of irrigation is to alleviate crop water stress by the timely application of water. On the other hand if CWSI can be used to evaluate the timing of irrigation, one could relate the CWSI to soil water content. Successful irrigation scheduling using the CWSI would solve many problems related to using soil water content. The CWSI would estimate the timing of irrigation for a regional scale if a satellite or an air-borne technique was used to measure surface temperature.

The $CWSI_{PM}$, the average soil water content of the rooting zone, the canopy resistance and the recorded rain and irrigations are shown (Fig. 6.10). An r^2 value of 0.021 was calculated between the standard $CWSI_{PM}$ and the depth-averaged soil water content. This poor correlation between $CWSI_{PM}$ resulted because the crop sensed the effect of applied water into the soil one to four days after rain or irrigation. For example, for the irrigation applied on 16 September the CWSI reached its minimum (non-water-stressed condition) on 20 September. The field capacity and the refill point for the soil were 0.292 and 0.237 $m^3\ m^{-3}$ respectively. The refill point is the soil water content below which crop

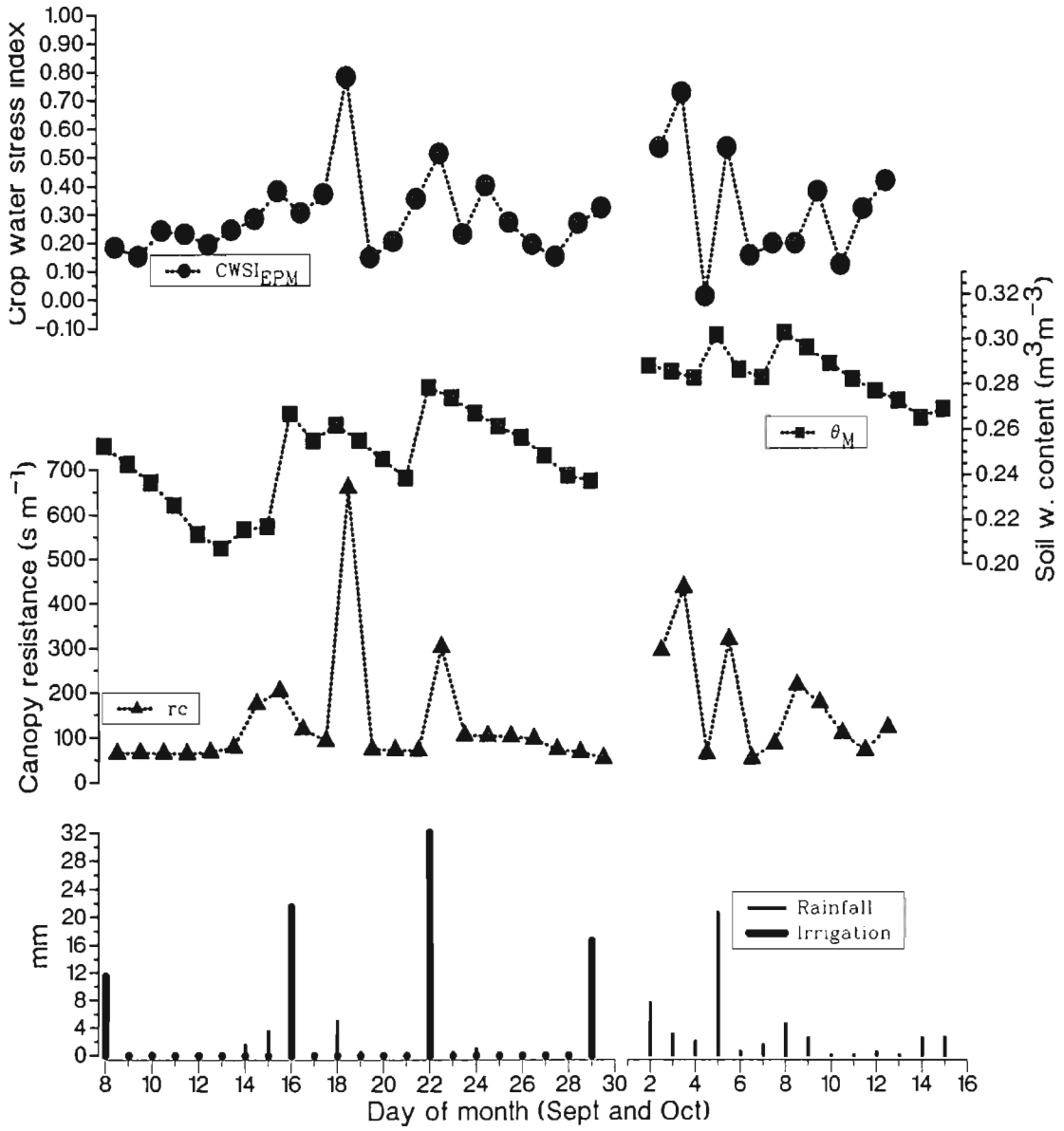

Figure 6.10 The daily variation of the CWSI, the depth-averaged soil water content, the canopy resistance and the recorded rain and irrigation.

growth is measurably decreased. Irrigation should be applied when soil water content is at refill point. A range of $CWSI_{PM}$ between 0.25 and 0.35 would be related to the refill point soil water content or to a canopy resistance of 70 s m^{-1}. Jalali *et al.*(1994) found a refill CWSI of 0.16 for Bermuda grass corresponding to actual canopy resistance of 125 s m^{-1}. Wanjura, Upchurch and Mahan (1992) reported a CWSI of 0.1 to 0.2 corresponding to the refill point. The CWSI was much correlated with with the canopy resistance than with the soil water content. A value $r^2 = 0.488$ was found when the $CWSI_{PM}$ was related to canopy resistance.

6.7 CONCLUSIONS

Agricultural water management was analysed using the CWSI. This index was calculated using the actual to potential evaporation ratio estimated from the Penman-Monteith method and the surface temperature technique. The estimated and measured actual surface to air temperature differential, the estimated potential and non-transpiring surface to air temperature differential were also used to estimate the CWSI using the Penman-Monteith, surface temperature and empirical approaches. The estimate of the CWSI using both techniques was inaccurate because of poor correlation between the surface to air temperature differential and the water vapour pressure deficit (or water vapour pressure and net irradiance). However, use of CWSI estimated by the actual to potential evaporation ratio ($CWSI = 1 - \lambda E_a/\lambda E_p$) was comparable to the standard CWSI determined using the Penman-Monteith approach. The actual canopy resistance was estimated acceptably using an empirical equation based on potential canopy resistance, solar irradiance, soil water content and the shelter factor. A 50 s m^{-1} was estimated for potential (minimum) canopy resistance of the cabbage crop. Soil water content was poorly correlated to CWSI, while the canopy resistance was well correlated.

CHAPTER 7

INFLUENCE OF EVAPORATION TECHNIQUES ON IRRIGATION WATER REQUIREMENT USING A SOIL WATER BALANCE METHOD

7.1 INTRODUCTION

Soil water techniques represent some of the oldest methods for scheduling irrigation (Campbell and Campbell, 1982). Their use requires predetermined values of the field capacity, wilting point and refill point soil water content or potential. In addition, the actual soil water content must be measured or estimated.

Field capacity or the upper limit, has been discussed and defined by Gear *et al.* (1977), Campbell and Campbell (1982), Ratliff, Ritchie and Cassel (1983), Schulze *et al.* (1985), Hillel (1982) and Savage, McInnes and Heilman (1996). Uncertainty of the exact value and the precise method for its determination have been reported by these workers. However, the index has a useful application in scheduling irrigation. It indicates the soil water content at which drainage rate from a pre-wetted soil is considered to be negligibly small (Gear, Rdansfield and Campbell, 1977; Campbell and Campbell, 1982; Ratliff *et al.*, 1983). A fixed value of soil water content corresponding to a matric potential between -10 and -33 kPa has been used by those authors to identify field capacity. The term drained upper limit has been used specifically to define the highest field-measured water content of the soil after it had been thoroughly wetted and allowed to drain until the drainage becomes practically negligible or after the decrease in the soil water content was about 0.1 to 0.2 % per day (Ratliff *et al.*, 1983). Ratliff *et al.* (1983) reported that 2 to 12 days after saturation were required for the soil to reach the drained upper limit depending on soil texture and depth.

A refill point is the soil water content below which crop growth is measurably decreased (Campbell and Campbell, 1982). This is the point where irrigation must start in order to avoid yield decline, and

is usually in the -50 to -100 kPa matric potential ranges. The wilting point has been used to identify the field-measured water content of the soil after the plant had stopped extracting water and was at or near premature death or became dormant as a result of water stress (Ratliff *et al.* 1983; Savage *et al.*, 1996). The soil water potential at this stage can be less than the -1500 kPa value but the difference in soil water content corresponding to these soil water potentials is small (Ratliff *et al.* 1983; Savage *et al.*, 1996).

The ideal instrument for measurement of soil water content or potential for assessing irrigation water requirement should be automated, precise, non-destructive and an *in situ* technique. It should also have a low degree of spatial dependence. The gravimetric and neutron probe methods fail to satisfy these requirements, although the gravimetric method is still used as a standard technique. Radiation hazard and high cost restrict the use of the neutron probe. The tensiometer, the resistance and heat dissipation blocks can meet the above requirement. However, some of these techniques cover a limited range of soil water potential. For example, the tensiometer has an upper limit of approximately -80 kPa due to the entry of the air into the system for suctions above this value. The ML1 ThetaProbe (Delta-T Devices, Cambridge, England) as well as other so-called time-domain reflectometry (TDR) and frequency-domain reflectometry (FDR) techniques can provide a continual, precise, non-destructive and *in situ* measurement of soil water content under field conditions. However, soil variability constitutes a problem for the widespread application of the technique for scheduling irrigation for large areas.

Micrometeorological methods for measuring evaporation are potential techniques for estimating irrigation water requirement. Soil water content can be estimated using the soil water balance in which evaporation is the prime component (Stegman, 1983; Cohen *et al.*, 1997). This method of estimating soil water content can offer an automated, precise, non-destructive and *in situ* technique for determining crop water requirements. In addition, large areas can be monitored, in particular when using a remote sensing technique to estimate evaporation. However, the performance of each evaporation technique may affect the accuracy in the estimated soil water content using a soil water

balance method. For example, different values of evaporation were reported in Chapter 6 when the surface temperature and BREB technique, and the Penman-Monteith method were used over a cabbage crop for the same weather and soil conditions.

A simple graph showing a plot of soil water content variation with time, with the refill point indicated, has been successfully used for forecasting the date of the next irrigation (Gear *et al.*, 1977; Campbell and Campbell, 1982). A certain proportion of the plant available water or a refill point (Cary and Fisher, 1983a and 1983b; Campbell and Campbell, 1982) has been used to start irrigation. So, some aspects of irrigation scheduling, such as when to start, how much water to apply and the prediction of the day for the next irrigation, could be determined easily by using a water content sensor or soil water content estimated using the water balance method.

In this chapter the ThetaProbe is calibrated for the site described in Section 3.4.5 using the factory-supplied and soil-estimated parameters. The influence of the bulk density, clay content and temperature on the soil water content measurement by the sensor is analysed. The soil water content variation for different depths of the rooting zone is also reported. The estimated soil water content using the soil water balance method with evaporation measured using the surface temperature and BREB technique, and the Penman-Monteith method are compared with the average soil water content measured using the ThetaProbe. The timing and the amount of irrigation are estimated using the measured and estimated soil water content.

7.2 CALIBRATION AND SOIL WATER CONTENT DETERMINATION USING THE THETAPROBE

Selected soil physical characteristics of the soil from the site for the four depths are shown in Table 7.1. The lowest soil bulk density was in the 450 to 600 mm layer and the highest between 300 and 450 mm. The average was 1546 kg m^{-3}. A particle density of 2650 kg m^{-3} for mineral soil was assumed (Hillel, 1982). The soil water content at saturation measured gravimetrically was 0.406 m^3

Table 7.1 Physical characteristics of four strata of the soil studied.

Depth	Bulk density	Water retention (m^3m^{-3}) vs kPa			Particle size distribution			Gravel	Organic Matter
mm		Saturation	Field Capacity	Refill Point	Clay	Silt	Sand		
	kg m^{-3}	0 kPa	-10 kPa	-100 kPa	%	%	%	%	%
0-150	1508	0.402	0.292	0.233	36	23	40	2.1	3.3
150-300	1595	0.412	0.289	0.230	35	24	41	3.4	3.3
300-450	1604	0.394	0.294	0.241	33	27	40	15.3	2.9
450-600	1476	0.414	0.291	0.253	46	15	39	8.7	2.8
Mean	1546	0.406	0.292	0.239	38	22	40	7.4	3.1

m^{-3} and at -10 kPa was 0.292 m^3 m^{-3}. The soil water content corresponding to -10 kPa was taken as the field capacity as recommended by Schulze *et al.* (1985). The refill point, determined in the laboratory using -100 kPa was 0.237 m^3 m^{-3}. Particle size distribution showed the soil to be a clay loam. The soil had a coarse layer of iron/manganese concretions in the 300 to 450 mm layer. The organic matter of the soil was 3.1 %.

Statistical equations by Snedecor and Cochran (1980) provide a method for estimating independent variable X (laboratory) from dependent variable Y (ThetaProbe soil water content), referred to as a prediction of X from Y, from a Y *vs* X relationship having a slope *b* and intercept *I:*

$$X = [(Y - I)/b]/(1 - c^2) \qquad 7.1$$

where $c^2 = (1/\sum x^2)(tS_{y.x}/b)^2$, $x = X - \overline{X}$, t is the student t, $S_{y.x}$ is the standard error of Y on X.

7.2.1 Factory Calibration vs Soil Calibration

The factory-supplied parameters for calibrating mineral soil, where a_o = 1.6 and a_1 = 8.4, were used to estimate soil water content (Eq. 2.60). The soil-estimated parameters, a_o = 1.411 and a_1 = 11.09, were used to estimate soil-calibrated soil water content. The dielectric constant of the dry soil was 2.1 that of saturated soil was 23.1.

The linear calibration for the total depth is shown (Fig. 7.1). The linear regression statistics for θ_v determined using the factory-supplied or soil-estimated parameters *vs* θ_v determined gravimetrically in the laboratory for individual depth and total depth are shown (Table 7.2). Unfortunately there was difficulty in measuring soil water content between 0 and 0.15 $m^3\ m^{-3}$ because the probe could not be pushed into the hard soil for these low water contents. The 300 to 450 mm layer had the lowest r^2 (Table 7.2) probably due to the presence of the coarse lateritic material. Iron minerals have been reported by Robinson *et al.* (1994) to affect the apparent dielectric constant measurement using the TDR technique for soil water measurement. However, analysis of the 95 % confidence limit showed that there was no significant difference between different layers. It was therefore decided to pool all the data and use one regression relationship for all depths between 0 and 600 mm.

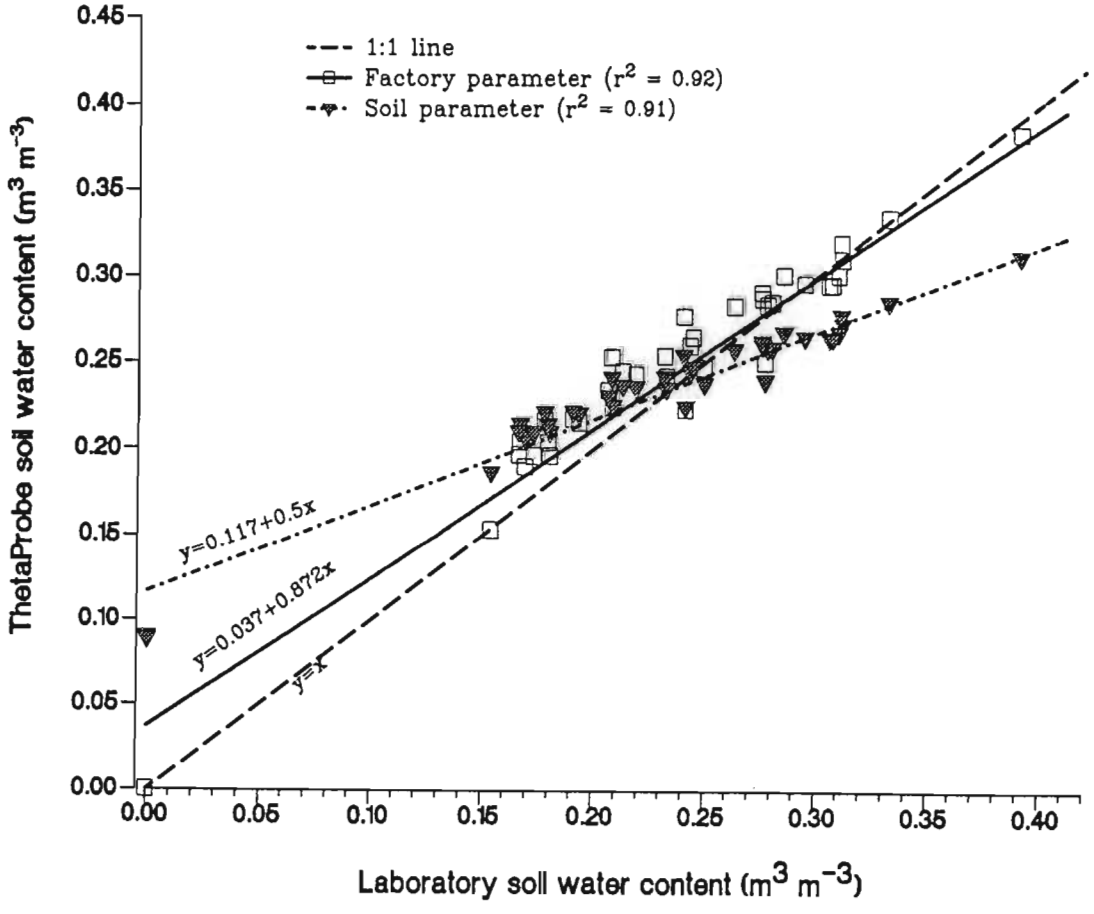

Figure 7.1 Laboratory calibration of the ThetaProbe soil water content using the factory - supplied and the soil-estimated parameters *vs* the laboratory soil water content on soil samples removed from the study site.

There was a somewhat improved correlation of soil water content estimates when factory-supplied parameters were used compared to soil-estimated parameters. There was a significant difference between the two estimates (Table 7.2). The poor performance of the sensor for estimating soil water content using soil-determined calibration constants may be caused by the soil variability and sampling error. On average, θ_v could be estimated to within 0.034 $m^3\ m^{-3}$ when using soil-estimated parameters and 0.02 $m^3\ m^{-3}$ when using factory-supplied parameters. Both soil and factory calibrations gave smaller errors compared to the maximum error of 0.05 $m^3\ m^{-3}$ specified by the manufacturer. The standard deviations for volumetric water content of 0.21 (factory-calibration) and 0.13 (soil-calibration) were within the range of 0.005 to 0.023 found by Jacobsen and Schjonning (1993a) using a TDR technique. An error 0.034 $m^3\ m^{-3}$ is about 66 % of the difference between field capacity and refill point (Table 7.1). That is, the error for estimating irrigation water requirement using the difference between the field capacity and refill point would be about 66 %. The estimate of soil water content indices (saturation, air entry, field capacity, refill point and wilting point) using the ThetaProbe and related percentage errors for the factory-supplied and soil-estimated parameters are shown in Fig. 7.2a. The soil water content at air entry (-5kPa) was determined as reported by Gregson *et al.*(1987), Ahuja and Williams (1991) and Williams *et al.* (1992). A wilting point 0.21 $m^3\ m^{-3}$ was estimated using empirically based equation[5] based on the clay and silt content, and the bulk density (Schulze *et al.*, 1986). Other soil water content indices were estimated using the laboratory method (in 3.4.2 and 3.4.3). The error in the estimated soil water content increased with decreasing soil water content. Both factory-supplied and soil-estimated parameters resulted in an average error of more than 20 %.

An attempt was made to recalibrate the sensors (see Eq. 7.1 and the statistics from Table 7.2: column 10 and column 11) to improve the regression (column 12 and column 13). The slope, intercept and bias of the recalibrated sensors were closer to the ideal slope of 1, and intercept and bias of 0. The r^2 was much the same, while the standard error of the predicted Y values for each X value increased

[5] $\theta_{v(-1500\ kPa)} = 0.062 + 0.00322Clay + 0308Silt - 0.026\rho_b$, where clay and silt is in % and ρ_b in Mg m^{-3}

Table 7.2 Regression analysis between the gravimetric soil water content (X) and the estimated soil water content using the factory-supplied (Y) or the soil-estimated parameters for individual and the entire soil layers (X).

column 1	column 2	column 3	column 4	column 5	column 6	column 7	column 8	column 9	column 10	column 11	column 12	column 13
Depth	0 -150		150 - 300		300 - 450		450 - 600		0 - 600		0 - 600	
	factory	soil	factory	soil	factory	soil	factory	soil	factory	soil	factory	soil
											Recalibration	
n	24	24	24	24	23	23	7	7	78	78	78	78
r^2	0.943	0.933	0.96	0.949	0.845	0.84	0.981	0.973	0.92	0.91	0.92	0.91
t	19.041	17.453	23.412	20.21	10.686	10.488	16.071	13.356	29.523	27.786	29.523	27.786
slope ($m^3\ m^{-3}/m^3\ m^{-3}$)	0.874	0.498	0.889	0.509	0.805	0.457	1.023	0.607	0.872	0.5	1.005	1.005
intercept ($m^3\ m^{-3}$)	0.037	0.118	0.034	0.116	0.05	0.126	0.015	0.099	0.037	0.117	0	0
Syx ($m^3\ m^{-3}$)	0.018	0.011	0.015	0.01	0.03	0.017	0.016	0.012	0.021	0.013	0.025	0.026
$SumX^2$	1.512	1.512	1.492	1.492	1.505	1.505	0.375	0.375	4.884	4.884	4.884	4.884
SEb	0.046	0.029	0.038	0.025	0.075	0.044	0.064	0.045	0.030	0.018	0.034	0.036
Slope Confidence Limit 99%	0.774, 1.003	0.417, 0.578	0.782, 0.996	0.439, 0.58	0.592, 1.018	0.333, 0.58	0.766, 1.28	0.424, 0.791	0.794, 0.95	0.452, 0.548	0.915, 1.094	0.91, 1.101
Slope Confidence Limit 95%	1.779, 0.969	0.439, 0.557	0.81, 0.968	0.457, 0.561	0.648, 0..961	0.366, 0.547	0.859, 1.187	0.49, 0.724	0.813, 0.931	0.465, 0.536	0.937, 1.072	0.933, 1.077
SEa	0.012	0.007	0.009	0.006	1.608	0.04	0.015	0.011	0.007	0.005	0.009	0.009
Intercept Confidence Limit 99%	-0.004, 0.069	0.098, 0.138	0.007, 0.061	0.098, 0.133	-4.502, 4.601	0.011, 0.24	-0.045,0.074	0.056, 0.141	0.018, 0.056	0.105, 0.129	-0.022, 0.022	-0.024, 0.024
Intercept Confidence Limit 95%	-0.013, 0.061	0.103, 0.133	0.014, 0.054	0.103, 0.129	-3.293, 3.393	0.042, 0.209	-0.023, 0.053	0.072, 0.126	0.022, 0.052	0.108, 0.126	-0.017, 0.017	-0.018, 0.013
MSEunsy	0.007	0.003	0.005	55.945	0.018	141.977	0.001	2.473	0.031	0.012	0.058	0.185
MSEsyst	0.003	0.037	0.003	1.758	0.006	0.00	0.003	0	0.015	0.131	0.013	0.455
%Unsy	66.492	6.615	58.744	96.953	99.376	100	32.520	100	66.891	8.076	81.648	28.87
% Syst	33.508	93.385	41.256	3.047	0.624	0	67.480	0	33.109	91.924	18.352	71.13
Biasb	-0.007	0.002	-1.286	0.105	-16.019	0.08	-0.212	-0.308	-0.007	0.001	-0.001	-0.001
t test	2.06	2.06	2.06	2.06	2.6	2.06	2.31	2.31	1.98	1.98	1.98	1.98
MeanX ($m^3\ m^{-3}$)	0.238	0.239	0.237	0.237	0.242	0.242	0.211	0.211	0.237	0.237	0.237	0.237
MeanY ($m^3\ m^{-3}$)	0.245	0.237	0.244	0.236	0.245	0.236	0.230	0.227	0.243	0.235	0.238	0.238
$Sumx^2$	0.146	0.146	0.148	0.004704	0.155	0.01892	0.0651	0.507	0.515	0.513	0.515	0.513
c^2	0.01175	0.014	0.007768	0.329074	0.037308	0.325105	0.020575	0.003828	0.004547	0.005	0.004547	0.005
$1-c^2$	0.98825	0.986	0.992232	0.670926	0.962692	0.674891	0.979425	0.996172	0.995453	0.995	0.995453	0.995

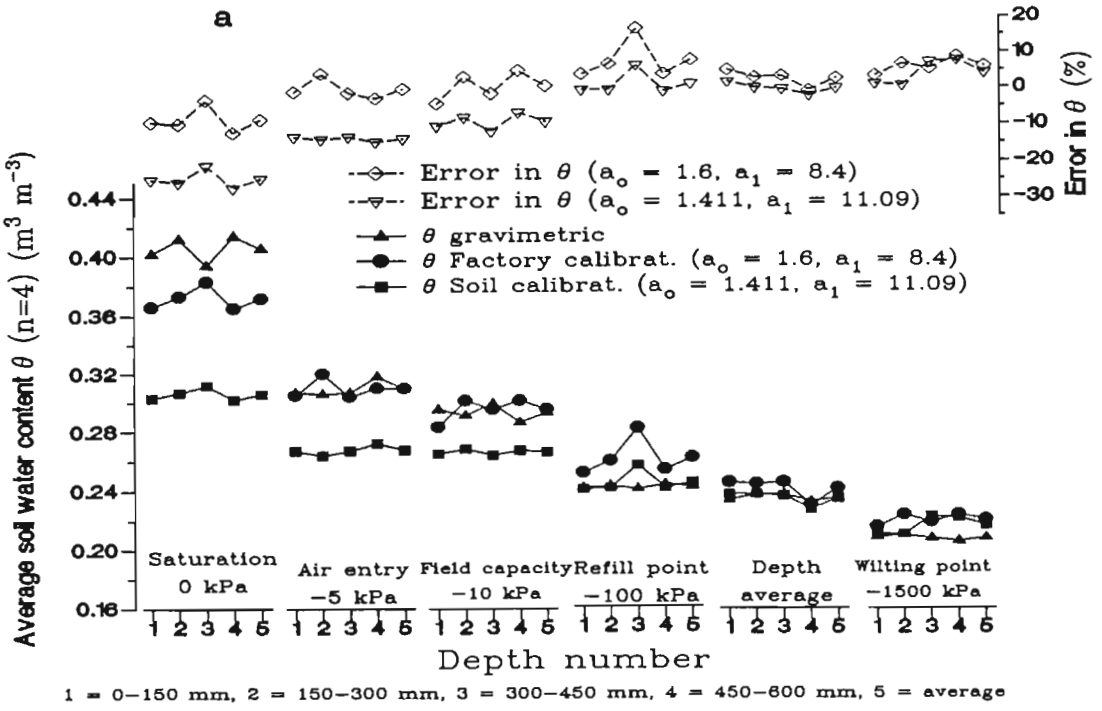

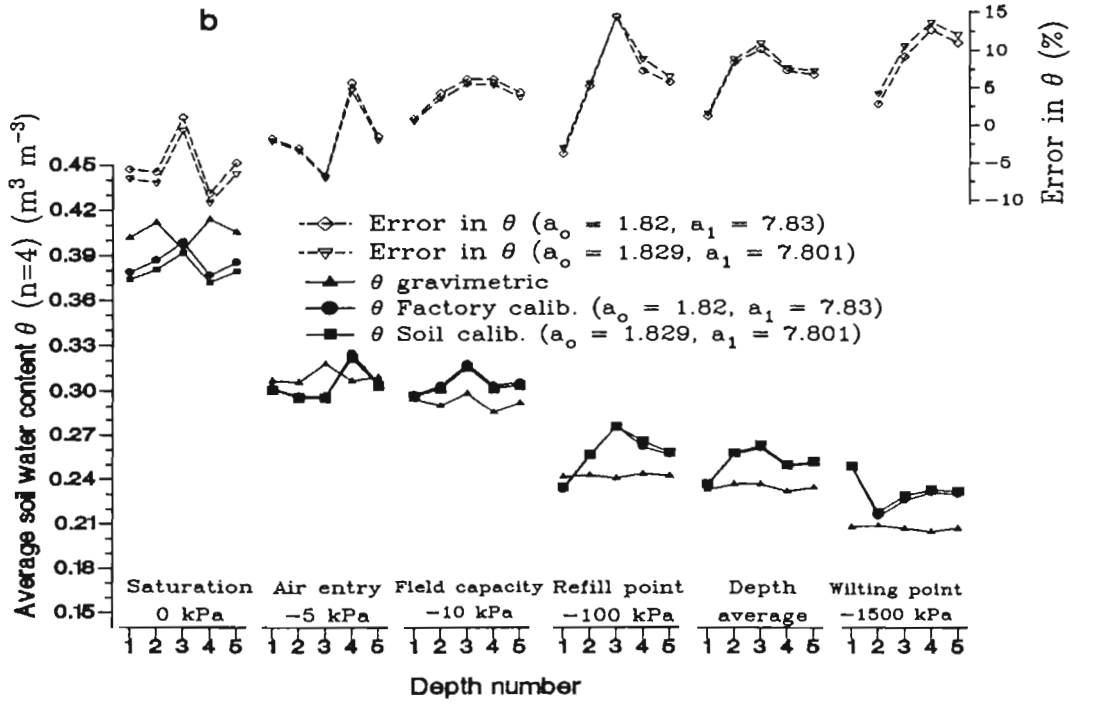

Figure 7.2 (a) The estimated soil water content indices using the ThetaProbe with the factory-supplied (a_0 =1.6 and a_1 = 8.4) and soil-estimated (a_0 = 1.411 and a_1 = 11.09) parameters, and the corresponding error. (b) The estimated soil water content indices using the recalibration of the ThetaProbe with the adjustment of the factory-supplied parameters (a_0 = 1.83 and a_1 = 7.82) and adjustment of the soil-estimated parameters (a_0 =1.83 and a_1 = 7.33) and the corresponding error .

for both factory and soil calibration. Using the recalibration procedure, soil water content could be estimated to within 0.020 $m^3\ m^{-3}$ for both soil-estimated and factory-supplied parameters. There was an improvement for the soil-estimated parameters. The estimated percentage errors for different soil water content indices are presented (Fig. 7.2b). The errors decreased, compared to those shown in Fig. 7.2a, for both the factory-supplied and the soil-estimated parameters. For a better estimate of θ_v in the field, the factory-supplied parameters were used rather than the soil-estimated parameters because the r^2 value was slightly greater.

So, the "best fit" expression to estimate soil water content using the ThetaProbe in this experiment (clay loam soil) was

$$\theta_{v\text{-adjust}} = [(\theta_v - I)/b]/(1 - c^2) \qquad 7.2$$

where $c^2 = (1/\Sigma x^2)(tS_{yx}/b)^2 = 0.0046$, the slope b = 0.872 and the intercept I = 0.037 $m^3\ m^{-3}$. A regression between the $\theta_{v\text{-adjus}}$ (X) and $\sqrt{\varepsilon}$ (Y) gave an intercept of 1.83 and slope of 7.82. The intercept and slope of the regression between $\theta_{v\text{-adjus}}$ (X) and $\sqrt{\varepsilon}$ (Y) correspond to a_o = 1.83 and a_1= 7.82 of the calibration constants (See Eq. 2.60) in comparison to a_o of 1.6 and a_1 of 8.4 provided by the manufacturer. The r^2 of the regression was 1 and the standard error of the estimate of Y was 0.03. The values a_o = 1.829 and a_1 = 7.329 were obtained for the $\theta_{v\text{-adjus}}$ adjusted from soil-estimated parameters, the r^2 was 1 and standard error was 0.001.

7.2.2 Temperature, Soil Bulk Density and Soil Texture Effects on ThetaProbe

The relative sensitivity coefficient of soil water content due to the change in the dielectric constant, constant a_1 and constant a_o (Eq. 2.60) was discussed in section 4.1.4. The error in soil water content due to the temperature variation between 12 and 18 °C was not more than 0.015 $m^3\ m^{-3}$ for the surface soil layers and not more than 0.005 $m^3\ m^{-3}$ for the deeper layers. Topp *et al.* (1980) also had satisfactory results for temperature between 10 and 30 °C.

In this experiment, the soil water contents were estimated accurately for those layers with a high clay

content and low bulk density (Tables 7.1 and 7.2). The r^2 of the linear regression between the ThetaProbe-estimated soil water content (Y) and the laboratory soil water content (X) was 0.92. Combining bulk density or clay content with the laboratory soil water content (X_1 and X_2) increased r^2 to 0.921 and 0.921 respectively. Combining the bulk density and clay content with the laboratory soil water content (X_1, X_2 and X_3) increased r^2 to 0.927. The change in soil bulk density and clay content of different layers had a very small effect on the sensor-determined soil water content. Thus, the possibility of including bulk density and clay content into the calibration (Eq. 2.59 and 2.60) was not pursued. Similar conclusions were also found by Topp *et al.* (1980) and Jacobsen and Schjonning (1993b) for TDR using soil samples that included a wider textural class and bulk density than those used in this experiment. However, it is recommended that more research be done on the effect of the bulk density, texture, temperature and other soil physical characteristics on the estimates of the dielectric constant of the soil.

7.2.3 Sub-Hourly Measurement of Soil Water Content

The soil was irrigated on 8, 16, 22 and 29 of September (corresponding to 60, 68, 74 and 81 days after planting) with 11.5, 21.5, 32 and 16.5 mm water respectively. There were 17 rainfall events in 36 days of the experiment. Irrigation and rain were recorded using a tipping bucket raingauge with a resolution of 0.5 mm. The drying process was monitored by measuring soil water content every 10 s and averaging every 20 min.

On 8 September the cabbage crop was probably extracting water in the layer situated between 120 to 200 mm depths and on 15 September from 120 to 200 and 200 to 280 mm layers. These layers had lower water contents than other layers, except for some very dry conditions when the surface layer had similar water content to those layers (see Fig.7.3). The rapid decrease of soil water in the 120 to 200 mm and later the 200 to 280 mm depths can be attributed to root extraction of water (Phene *et al.*, 1987).

Abrupt decreases in soil water content of the order of 0.01 $m^3\ m^{-3}$ were observed in the high water

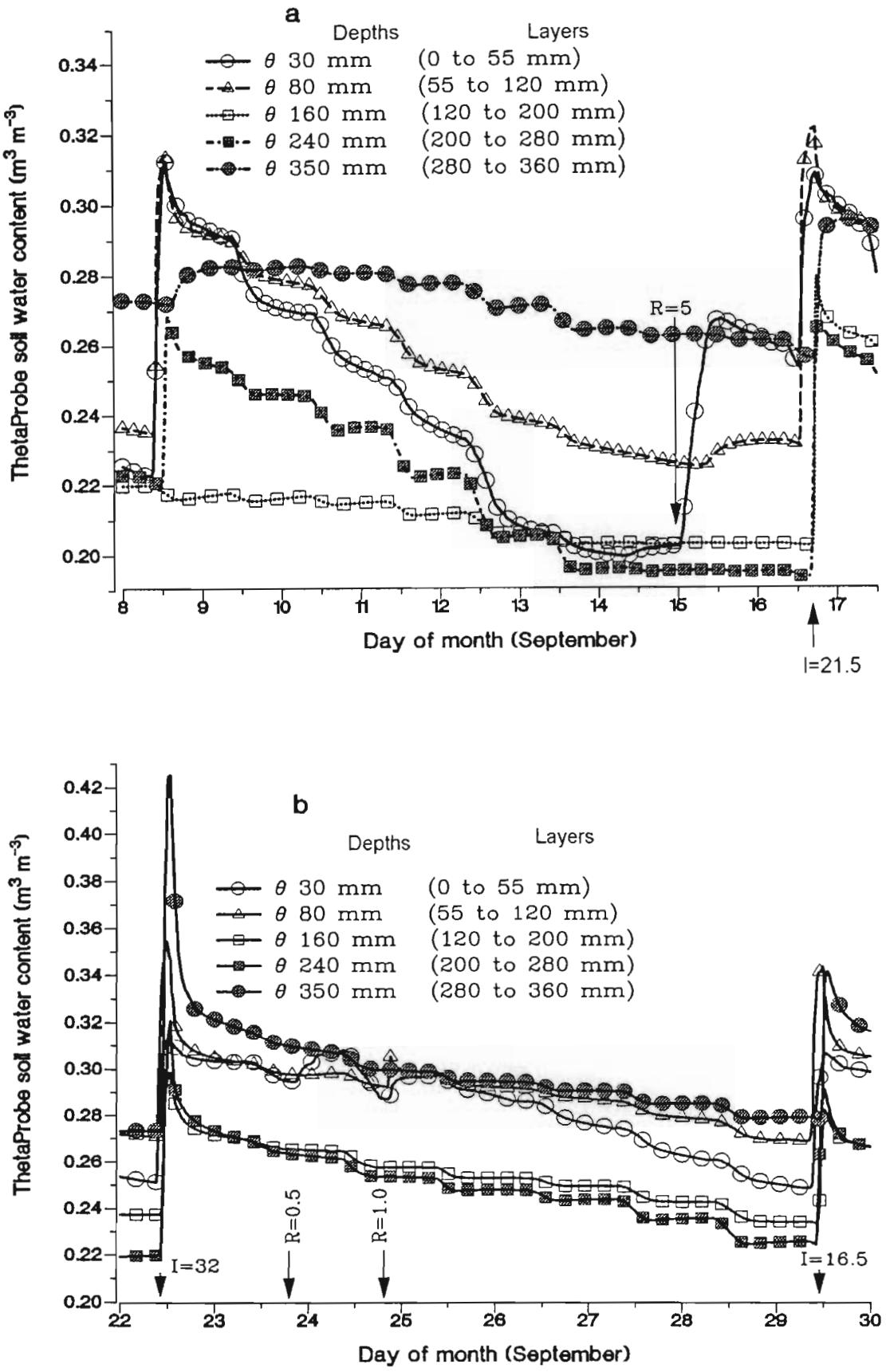

Figure 7.3 The 20 minute variation of the soil water content measured using ThetaProbe at 30, 80, 160, 240 and 320 mm depths between 8 and 16 September (a) and between 22 and 29 September (b). Also shown are the rain and irrigation event.

extraction layers at noon during the active crop growth stages (Fig. 7.4). At this stage the absorption rate was certainly greater than the unsaturated hydraulic conductivity required to replenish water from the low soil water extraction layer. The decreases were also observed in the morning when more than 3 days had passed after irrigation or rain. There was also recovery in soil water content during the night for the high water extraction layer when the soil water content was below 0.24 m^3 m^{-3} (Fig. 7.4), while the low water extraction layers lost water continuously. The rate of water uptake was highest in the high water extraction layers creating lower water potentials in this layer compared to the zone of low water extraction. The resultant soil water potential gradient induced water movement from the low to high water extraction layers (Hillel, 1982). It is thought that this flow of water was also assisted by the hydraulic lift of soil water from a zone of high potential to that of low potential through the root system (Molz and Peterson, 1976).

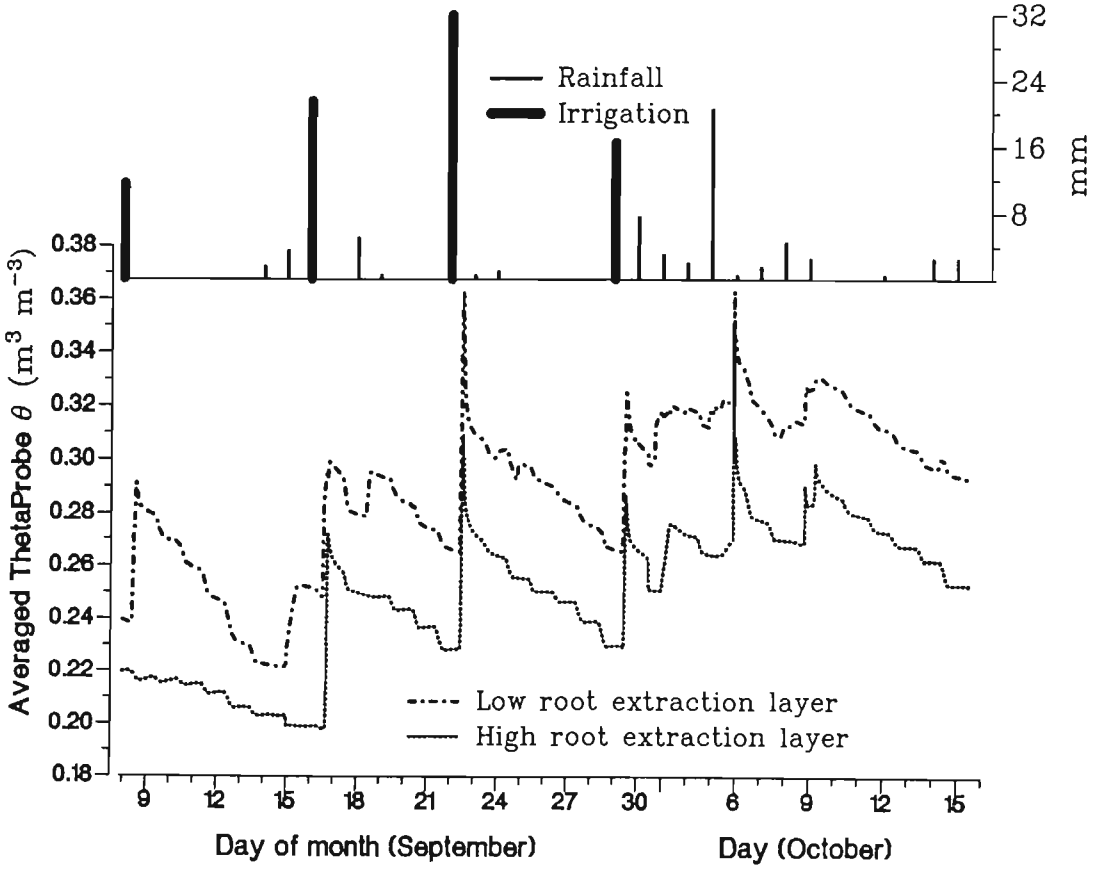

Figure 7.4 Variation in the average soil water content of the layer of higher and low root extractions. There was r^2 value of 0.84 for the soil water content between the two layers.

The surface depths (30 mm to a lesser extent 80 mm) experienced a sharp decrease in soil water content compared to lower depths (Fig. 7.3). The coarse plinthic layer below 300 mm depth is likely to have acted as a barrier for water movement from the underlying layers to the upper layer which showed greater water extraction (Clothier *et al.*, 1977). For example, there was no indication of water extraction in the layer of high water extraction (120 to 200 mm and 200 to 280 mm) between 13 and 16 September (Fig. 7.3a) despite a large amount of soil water in the underlying layer. During this period soil water content of the high water extraction layer was below the wilting point. A 5 mm rain added into the soil on 15 September did not change the soil water content of the high water extraction layers because of very dry overlying layers.

7.3 ESTIMATING CABBAGE WATER REQUIREMENT USING A SOIL WATER BALANCE

The daily measurements of latent heat estimated using the Bowen ratio energy balance and surface temperature technique, and the Penman-Monteith method together with the net irradiance are shown (Fig. 7.5). The latent heat estimated by using the surface temperature technique was overestimated by 60 % compared to that estimated using the Penman-Monteith method. The latent heat estimate using the BREB technique was closely correlated to the latent heat estimated using the Penman-Monteith method. As can be seen, latent heat using the surface temperature technique was larger than the net irradiance much of the time. The estimated amounts of evaporation are shown (Table 7.3: columns 21 to 23). Irrigation requirements were estimated using the soil water balance method in which evaporation calculated from these three micrometeorological methods is the prime component. The accuracy of the estimated irrigation requirements using the soil water content calculated from water balance equation using the surface temperature, BREB and Penman-Monteith evaporation are compared to that estimated using the ThetaProbe.

7.3.1 Estimating Soil Water Content Using the a Soil Water Balance Method

Soil water contents estimated using the shortened soil water balance (Eq. 2.56) with evaporation

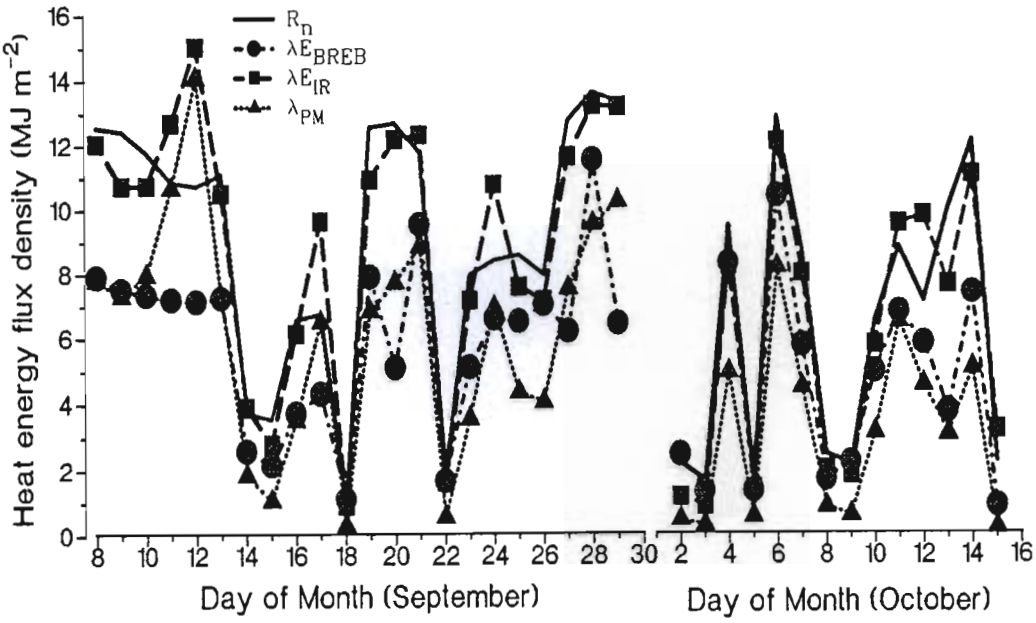

Figure 7.5 Variation of the daily latent heat measured using the Bowen ratio energy balance (λE_{BREB}), surface temperature technique (λE_{IR}) and the Penman-Monteith (λE_{PM}) method. Also, shown is the net irradiance.

calculated using the BREB and surface temperature technique, and the Penman-Monteith method are shown (Fig. 7.6, Table 7.3: columns 7 to 10). These soil water contents represent the depth-averaged soil water content between 0 and 300 mm depth. The regressions between the estimated and the measured soil water content are given in Table 7.4. There was a relatively better correlation between the measured and the estimated soil water content using the BREB and Penman-Monteith evaporation in the soil water balance equation than using surface temperature evaporation. The soil water contents estimated by using the BREB and Penman-Monteith evaporations were very close. Analysis of the 95 % confident limit showed that there was no significant difference between the two soil water contents. However, there was a significant difference between the soil water content estimated using the surface temperature and Penman-Monteith evaporations.

The soil water content derived from the BREB and Penman-Monteith evaporations underestimated the measured soil water content during the early stage of the experiment (8 to 22 September) and overestimated it during the later stage of the experiment. The soil water content derived from the

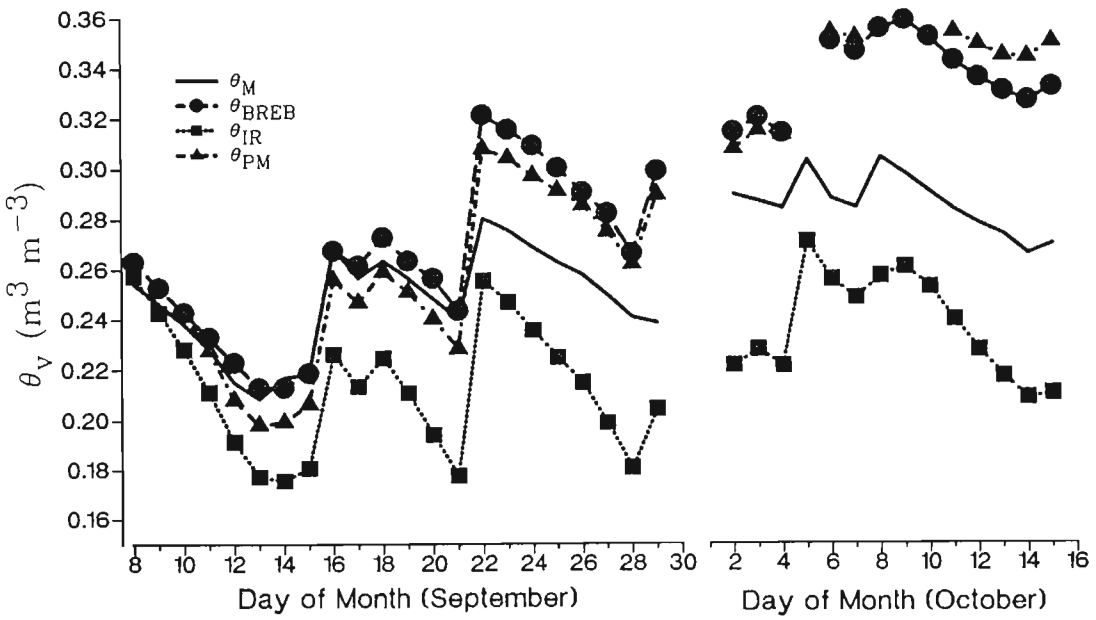

Figure 7.6 Variation of the estimated and measured soil water content during the experimental period.

surface temperature evaporation was considerably lower than that determined using the BREB and Penman-Monteith evaporation throughout the experiment. This soil water content was also smaller in relation to that measured using the ThetaProbe. If the ThetaProbe was taken as an accurate sensor for measuring soil water content and that Eq. 2.59 and assumptions used were correct, one can say that the BREB technique and the Penman-Monteith method overestimated evaporation between 8 and 22 September and underestimated evaporation in later stage of the experiment (Fig. 7.6). However, it is thought that in later stage of the experiment there was considerable drainage not accounted in the shortened soil water balance equation. On the other hand, measurement from the Penman-Monteith method and the BREB technique could not be trusted between 3 October and the end of the experiment because of malfunctioning of the Dew-10 cooled mirror. The soil water content using surface temperature technique was consistently lower even in later stage when there was excess rain.

An average difference of 0.069 m^3 m^{-3} was found between soil water content estimated using evaporation determined from the surface temperature technique and the Penman-Monteith method. This difference is larger than 0.055 m^3 m^{-3}, the difference between field capacity and the refill point soil water content. This indicated that a larger error could result in irrigation scheduling estimated

Table 7.3 The estimated amounts of evaporation, soil water content, amount of irrigation and the day for the start of irrigation for 36 days period.

column 1	column 2	column 3	column 4	column 5	column 6	column 7	column 8	column 9	column 10	column 11	column 12	column 13	column 14	column 15	column 16	column 17	column 18	column 19	column 20	column 21	column 22	column 23
D of year	D ay of month	R mm	R_{ef} mm	I mm	I_{ef} mm	SWC_m $m^3\ m^{-3}$	SWC_{BREB} $m^3\ m^{-3}$	SWC_{IR} $m^3\ m^{-3}$	SWC_{PM} $m^3\ m^{-3}$	SWC_{BRED} $m^3\ m^{-3}$	SWC_{IR} $m^3\ m^{-3}$	SWC_{PM} $m^3\ m^{-3}$	I_{SWCm} mm	$I_{SWCBREB}$ mm	I_{SWCIR} mm	I_{SWCPM} mm	$I_{SWCBREB}$ mm	I_{SWCIR} mm	I_{SWCPM} m m	E_{BREB} mm	E_{IR} mm	E_{PM} mm
						THETAP ROBE	$\theta_{vs} = \theta_{vi}$ - (Eλ-P_o - I_o)/RD with recorded P and I			$\theta_{vs} = \theta_{vi}$ - (Eλ-P_o - I_o)/RD recorded P & simulat I			I = RD (FC - θ_{vs}), RD = 300 mm I = 300 (0.292 - RP) = 21 mm				I = RD (FC - θ_{vs}) with simulated θ_{vs} (col. 11-13)			EVAPORATION		
						0.232							24				24					
252	8	0.0	0.0	11.5	8.6	0.262	0.250	0.244	0.250	0.221	0.216	0.221	12	17	19	17	28	31	28	3.2	4.9	3.2
253	9	0.0	0.0	0.0	0.0	0.254	0.240	0.230	0.240	0.305	0.303	0.306	15	21	25	21	-5	-4	-5	3.1	4.4	3.0
254	10	0.0	0.0	0.0	0.0	0.246	0.230	0.215	0.229	0.295	0.288	0.295	18	25	31	25	-1	2	-1	3.0	4.4	3.3
255	11	0.0	0.0	0.0	0.0	0.236	0.220	0.198	0.214	0.285	0.271	0.280	22	29	38	31	3	8	5	3.0	5.1	4.4
256	12	0.0	0.0	0.0	0.0	0.222	0.210	0.178	0.195	0.275	0.251	0.261	28	33	45	39	7	16	13	3.0	5.9	5.8
257	13	0.0	0.0	0.0	0.0	0.215	0.200	0.164	0.185	0.265	0.237	0.251	31	37	51	43	11	22	17	3.0	4.3	3.0
258	14	1.5	1.1	0.0	0.0	0.223	0.200	0.163	0.186	0.265	0.309	0.252	28	37	52	42	11	-7	16	1.1	1.6	0.8
259	15	3.5	2.6	0.0	0.0	0.225	0.206	0.168	0.194	0.271	0.314	0.259	27	35	50	39	8	-9	13	0.9	1.1	0.4
260	16	0.0	0.0	21.5	16.1	0.277	0.254	0.213	0.243	0.266	0.305	0.254	6	15	32	20	10	-5	15	1.5	2.5	1.4
261	17	0.0	0.0	0.0	0.0	0.264	0.248	0.200	0.234	0.260	0.293	0.245	11	17	37	23	13	-0	19	1.8	3.8	2.7
262	18	5.0	3.8	0.0	0.0	0.271	0.260	0.212	0.246	0.271	0.304	0.258	8	13	32	18	8	-5	14	0.4	0.4	0.1
263	19	0.5	0.4	0.0	0.0	0.264	0.250	0.198	0.238	0.262	0.290	0.249	11	17	38	22	12	1	17	3.2	4.5	2.8
264	20	0.0	0.0	0.0	0.0	0.255	0.243	0.181	0.227	0.255	0.274	0.239	15	20	44	26	15	7	21	2.1	5.0	3.2
265	21	0.0	0.0	0.0	0.0	0.247	0.230	0.164	0.215	0.242	0.257	0.298	18	25	51	31	20	14	-2	3.9	5.0	3.6
266	22	0.0	0.0	32.0	24.0	0.289	0.308	0.242	0.294	0.239	0.255	0.297	1	0	20	0	21	15	-2	0.7	0.7	0.2
267	23	0.5	0.4	0.0	0.0	0.284	0.302	0.234	0.291	0.300	0.246	0.293	3	0	23	1	-3	18	-1	2.1	2.9	1.5
268	24	1.0	0.8	0.0	0.0	0.277	0.295	0.222	0.284	0.294	0.296	0.286	6	0	28	3	-1	-2	2	2.7	4.2	2.9
269	25	0.0	0.0	0.0	0.0	0.270	0.286	0.212	0.278	0.285	0.285	0.280	9	2	32	6	3	3	5	2.7	3.2	1.8
270	26	0.0	0.0	0.0	0.0	0.265	0.277	0.202	0.272	0.275	0.275	0.274	11	6	36	8	7	7	7	2.9	3.0	1.7
271	27	0.0	0.0	0.0	0.0	0.257	0.268	0.186	0.262	0.267	0.259	0.264	14	9	43	12	10	13	11	2.5	4.8	3.1
272	28	0.0	0.0	0.0	0.0	0.248	0.253	0.168	0.248	0.251	0.241	0.251	18	16	50	17	16	20	16	4.7	5.4	3.9
273	29	0.0	0.0	16.5	12.4	0.247	0.285	0.191	0.276	0.242	0.291	0.237	18	3	40	7	20	0	22	2.7	5.3	4.2
276	2	7.5	5.6	0.0	0.0	0.289	0.300	0.208	0.294	0.324	0.308	0.328	1	0	34	0	-13	-7	-15	1.0	0.5	0.2
277	3	3.0	2.3	0.0	0.0	0.297	0.306	0.214	0.301	0.330	0.315	0.336	0	0	31	0	-15	-9	-17	0.5	0.4	0.1
278	4	2.0	1.5	0.0	0.0	0.295	0.300	0.208	0.299	0.324	0.308	0.334	0	0	34	0	-13	-6	-17	3.4	3.4	2.0
279	5	20.5	15.4	0.0	0.0	0.292	0.350	0.257	0.350	0.373	0.357	0.384	0	0	14	0	-32	-26	-37	0.5	0.6	0.2
280	6	0.5	0.4	0.0	0.0	0.312	0.336	0.242	0.340	0.360	0.342	0.374	0	0	20	0	-27	-20	-33	4.3	4.9	3.4
281	7	1.5	1.1	0.0	0.0	0.296	0.332	0.235	0.338	0.356	0.335	0.372	0	0	23	0	-26	-17	-32	2.4	3.3	1.8
282	8	4.5	3.4	0.0	0.0	0.292	0.341	0.244	0.348	0.368	0.344	0.382	0	0	19	0	-29	-21	-36	0.7	0.8	0.4
283	9	2.5	1.9	0.0	0.0	0.313	0.344	0.247	0.353	0.361	0.347	0.388	0	0	18	0	-30	-22	-38	0.9	0.8	0.2
284	10	0.0	0.0	0.0	0.0	0.300	0.338	0.239	0.349	0.352	0.339	0.383	0	0	21	0	-27	-19	-37	2.0	2.4	1.3
285	11	0.0	0.0	0.0	0.0	0.298	0.328	0.226	0.340	0.345	0.326	0.374	0	0	26	0	-23	-14	-33	2.8	3.9	2.7
286	12	0.5	0.4	0.0	0.0	0.292	0.322	0.214	0.335	0.340	0.314	0.369	0	0	31	0	-21	-9	-31	2.4	4.0	1.9
287	13	0.0	0.0	0.0	0.0	0.286	0.316	0.204	0.330	0.336	0.304	0.365	2	0	35	0	-19	-5	-29	1.6	3.1	1.3
288	14	2.5	1.9	0.0	0.0	0.281	0.313	0.195	0.330	0.341	0.295	0.364	4	0	39	0	-17	-1	-29	3.0	4.5	2.1
289	15	2.5	1.9	0.0	0.0	0.273	0.318	0.197	0.336	0.340	0.297	0.370	8	0	38	0	-19	-2	-31	0.3	1.3	0.1

Table 7.4 The statistics of the regression between the estimated soil water content (Y) and the measured soil water content using ThetaProbe.

	SWC_{BREB}	SWC_{IR}	SWC_{PM}
n	36	36	36
r^2	0.88	0.58	0.84
$t^*=r[(n-2)/(1-r^2)]^{0.5}$	16.08	6.916	13.24
slope	1.66	0.78	1.88
intercept ($m^3\ m^{-3}$)	-0.17	0	-0.23
Syx ($m^3\ m^{-3}$)	0.02	0.02	0.02
$Sum(SWCm)^2$	1.619	1.619	1.619
SEb	0.13	0.14	0.19
Slope Confid. Lim. 99%	1.304, 2.016	0.395, 1.174	1.363, 2.406
Slope Confid. Lim. 95%	1.395, 1.926	0.495, 1.075	1.495, 2.270
SEa	0.028	0.03	0.04
b+SEa99%	-0.245, -0.094	-0.086, 0.079	-0.344, -0.123
b+SEa95%	-0.226, -0.113	-0.065, 0.086	-0.316, -0.151

from the soil water balance method using an inaccurate evaporation estimated using a poorly performed technique. Basic aspects of irrigation scheduling using the estimated soil water content are discussed below.

7.3.2 Timing of Irrigation

The variation of the estimated and measured soil water contents, the refill point and the soil water content at field capacity are shown (Fig. 7.7) together with the daily irrigation and rain. Irrigation must commence when soil water content is equal to or slightly below the refill point (Singh *et al.*, 1995). Haise and Hagan (1967) reported a cabbage refill point of -60 and -70 kPa for high and low evaporative demand condition while Stanley and Maynard (1990) reported -80 kPa and -180 kPa respectively. A depth-averaged soil water content of 0.237 $m^3\ m^{-3}$ (-100 kPa) was used for the refill point value, while 0.292 $m^3\ m^{-3}$ (-10 kPa) was used for field capacity.

Irrigation was applied on 8, 16, 22 and 29 September with 11.5, 21.5, 32 and 16.5 mm water

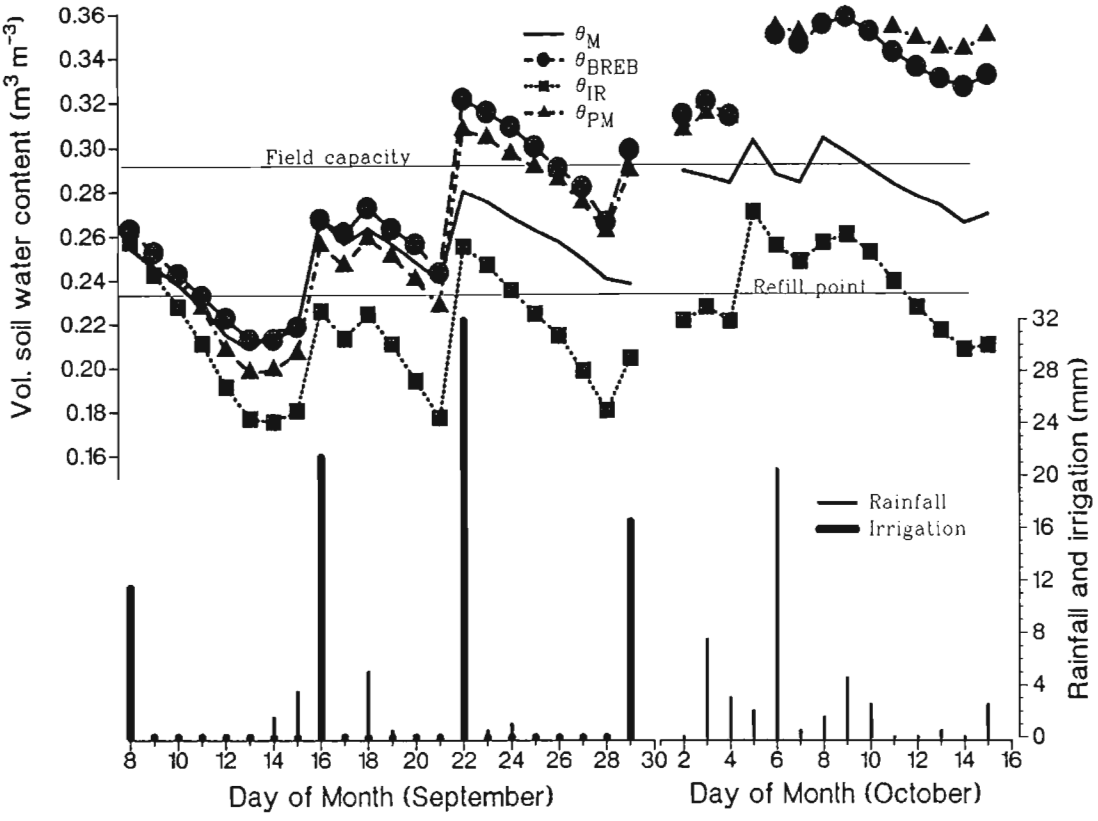

Figure 7.7 Variation of the estimated and measured soil water content, the refill point and the soil water content at field capacity. Also shown are the daily irrigation and rain.

respectively and 17 rainfall events were measured in 36 days (Table 7.3: columns 2 to 6). The estimated soil water content using water balance and evaporation derived from the surface temperature technique reached the refill point on 8 September. That is the 11.5 mm irrigation on 8 September only lasted 15 hours for the soil water content to decrease below the refill point. The timing of irrigation for this estimated soil water content would be 2 days earlier than using the measured soil water content. The soil water content estimated using the water balance and evaporation derived from the BREB technique and Penman-Monteith method would reach the refill point on 9 September. This would be one day later in relation to that estimated using water balance and evaporation calculated from surface temperature and one day earlier in relation to using the measured soil water content using ThetaProbe.

The estimated and measured soil water content were below the refill point between 9 September and 16 September and below the wilting point between 11 to 16 September. Observation of the estimated soil water content using the surface temperature evaporation method would suggest that the crop was stressed throughout the experimental period despite the input of water through irrigation and rain. However, if one had used the Penman-Monteith evaporation method, further irrigations should have been applied on 17 and 19 September. This would suggest that water applied 16 September was enough to maintain soil water content above the refill point only for about 1 day. This is because the Penman-Monteith method overestimated actual evaporation. Further irrigation would have been needed on 20 September if the BREB evaporation was used. It can be said that when overestimated evaporation is used in the water balance equation one would get early and more frequent irrigation, and *vice versa*. The amount of evaporation affected the rate of soil drying and how often there was a need to replenish the soil water content to the field capacity.

7.3.3 Amount of Irrigation

The required amount of irrigation calculated using Eq. 2.57 would be 21.2 mm per application when using 0.292 m^3 m^{-3} (-10 kPa) for field capacity and 0.237 m^3 m^{-3} (-100 kPa) for refill point (Table 7.1). It was assumed that the efficiency of irrigation was 75 %. It was also assumed that no significant percolation would occur when the actual soil water content was below or equal to the field capacity after an irrigation event. A plot of the daily water depletion (mm) (Eq. 2.57), which is in fact the amount of water to be replenished using irrigation to take the soil water content to field capacity, and the amount of applied irrigation is shown for the different methods of estimating evaporation (Fig. 7.8 and Table 7.3: column 5 and column 14 to column 17).

Irrigation amount on 9,16, 22 and 29 September would have been 24, 27, 18 and 18 mm according

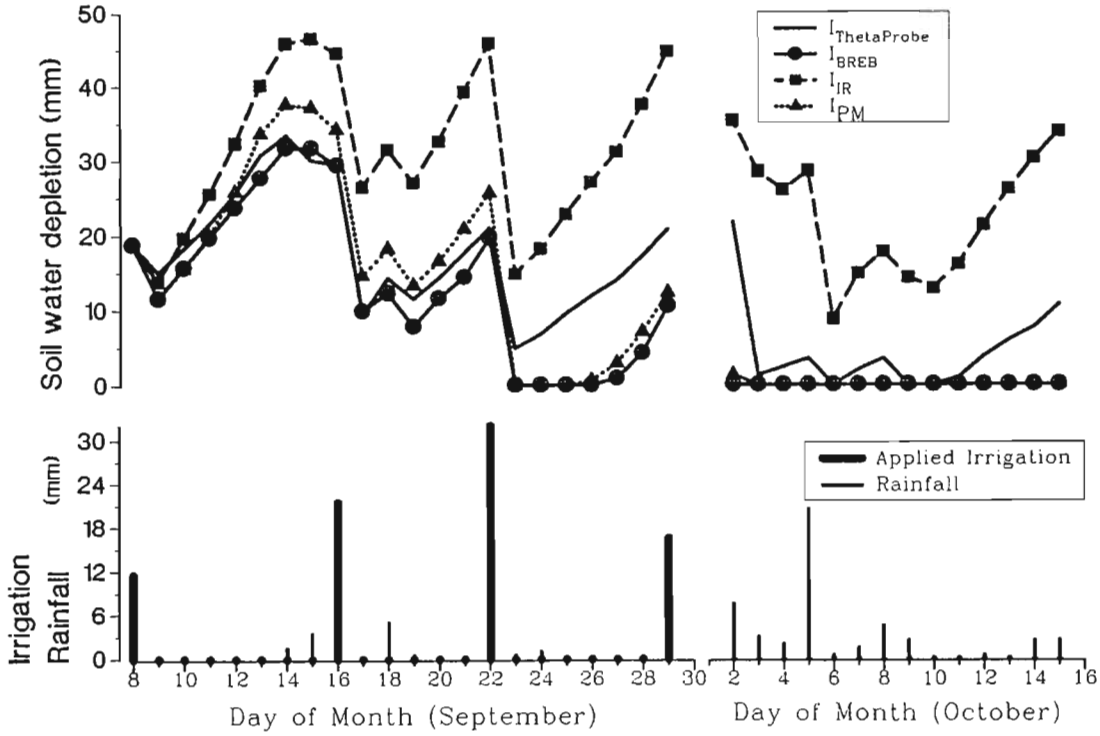

Figure 7.8 Daily variation of the estimated and measured soil water depletions (estimated irrigation) and the amount of applied irrigation during the experimental period. Applied irrigation is incorporated in the water balance equation as a gain of soil.

to the soil water content measured using the ThetaProbe. Thus, there was an over-irrigation on 22 September and under-irrigation on 9, 16 and 29 September. However, 35, 50 and 39 mm water would have been scheduled on 16 September if one have used soil water contents calculated using the water balance equation with evaporation calculated from the BREB, Penman-Monteith and surface temperature respectively. The magnitude of overestimation of irrigation amount was directly proportional to the magnitude of overestimation of evaporation. However, from 29 September this amount was underestimated by 2 and 1 mm when the BREB and Penman-Monteith evaporation were used. The amount of irrigation would have been overestimated throughout the experiment if the surface temperature evaporation was used. Thus, an inaccurate estimation of evaporation would lead to an inaccurate irrigation amount.

Another alternative was used to simulate the amount of irrigation using Eq. 2.57. In this case the irrigation would be applied after removal of about 19 to 22 mm. This equation used the actual soil water estimated by using Eq. 2.56. On the other hand, the amount of the simulated irrigation was incorporated in Eq. 2.56 as inputs in water into the soil water reservoir. Results of the estimated amount of irrigation are shown (Table 7.3: column 18 to column 20 and Fig. 7.9). Irrigation would have been applied on 8, 22, and 29 September with 28, 21 and 20 mm respectively when using soil water content estimated using water balance and evaporation calculated from BREB technique. It should also be applied three times, on 8, 20 and 29 September with 28, 21 and 22 mm respectively when using Penman-Monteith evaporation. The total amount of irrigation during the experiment would be 69 and 71 mm when using the BREB and Penman-Monteith evaporation respectively. However, if one had used an irrigation amount estimated using the water balance and evaporation estimated using the surface temperature, four irrigations would have been required on 8, 13, 23 and 28 September with 31, 22, 18 and 20 mm respectively. The total amount irrigated would have been 91 mm. This corresponds to a 30 % overestimation of the amount of irrigation in comparison to using the BREB and Penman-Monteith evaporation. In addition, irrigation would have been more frequent when using the surface temperature evaporation than when using the Penman-Monteith or the BREB evaporation. The negative soil water depletion was observed in later stage because of excess rain. If rainfall forecast between 1 and 15 October was provided effectively, one would have avoided irrigation simulated on 28 and 29 September and subsequent use of rain water that fell on the following days. The corresponding simulated soil water content would vary between approximately 0.23 and 0.31 $m^3 m^{-3}$ as shown in Table 7.3: columns 12 to 14 and Fig. 7.10). These values would correspond to the refill point and field capacity respectively. The soil water content was above the field capacity during period between 30 and 15 October.

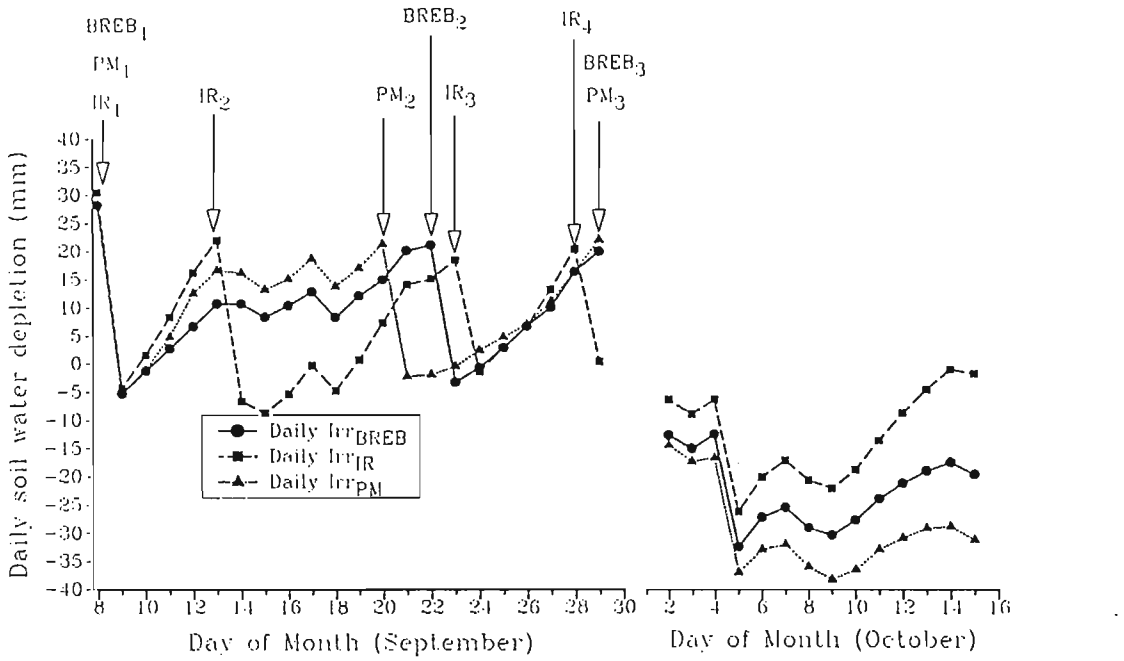

Figure 7.9 Calculated daily variation of soil water depletion estimated using the water balance equation with evaporation determined by using the surface temperature and BREB technique and Penman-Monteith method.

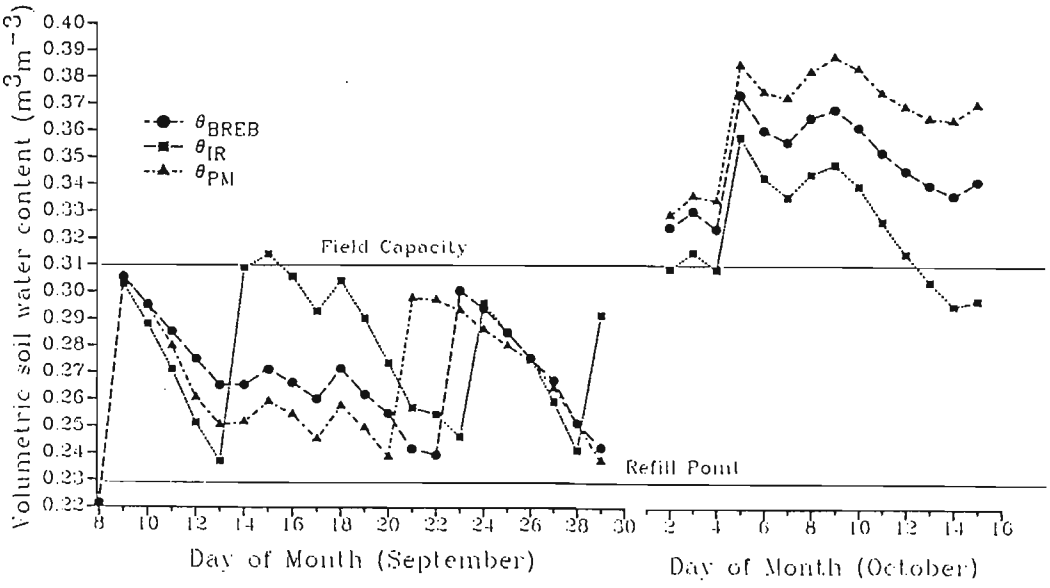

Figure 7.10 Variation of the estimated soil water contents calculated using the simulated irrigation.

7.4 CONCLUSION

There was a good correlation between the ThetaProbe soil water content determined using factory-supplied parameters and that determined using the laboratory method. Both factory-supplied and soil-estimated parameters resulted in more than 20 % overestimation of soil water content using the ThetaProbe compared to laboratory soil water content. This corresponded to estimating the soil water content to within 0.02 and 0.034 m^3 m^{-3} when using the factory-supplied and soil-estimated parameters. However, using a recalibration equation, the soil water content could be estimated to within 0.02 m^3 m^{-3} for both factory supplied and soil-estimated calibration constants. The slope, intercept and bias of the estimated soil water content was closer to the statistically expected values. The bulk density, clay content and temperature effect on the ThetaProbe showed a negligible influence on the measured soil water content.

The estimated soil water content was underestimated throughout the experiment when evaporation from the surface temperature technique was used. There was an underestimate of soil water content in the early stage and overestimate in later stage of the experiment when the BREB and Penman-Monteith evaporations were used. The reason for this was an excessive drainage during the later stage of the experiment. On the other hand the BREB and the Penman-Monteith method could not be trusted because of using inaccurate measurement of the actual water vapour pressure during the later stage. Use of the estimated soil water content using the soil water balance with overestimated evaporation would result in an too early date, a too large amount of applied water and too frequent irrigation application.

CHAPTER 8

DISCUSSION, CONCLUSIONS AND RECOMMENDATIONS FOR FUTURE RESEARCH

8.1 DISCUSSION AND CONCLUSIONS

8.1.1 Introduction

A proper irrigation water management system requires accurate, automated, non-destructive and simple techniques to measure evaporation. The BREB and the surface temperature techniques seem to fulfil these requirements. However, their performance under certain conditions is a cause for concern. The main reasons for the poor performance of technique are the fulfilment of the assumption adopted to derise the equations and sensor's limitation. The poor performance in estimating evaporation can affect the crop water stress index (CWSI) and the irrigation water requirement calculated using the water balance equation. A general discussion and conclusion on the reliability for measuring weather data, the performance of the Bowen ratio and surface temperature technique for measuring evaporation is presented in this chapter. The effect of the estimated evaporation on the CWSI and irrigation water requirement is also discussed. In addition, recommendations for future research on the improvement of the surface temperature, BREB and soil water balance techniques are shown.

8.1.2 Reliability of the Measured Weather Data

Solar irradiance and net irradiance were estimated accurately following analysis of the integrity of the weather data. However, the soil heat flux density passed the extreme outlier by 200 % during cloudless days at solar noon. It is thought that there were some electrical noises due to the temperature variation despite all precautions taken to house the wiring in a plastic tube. The chromel-constantan thermocouple for air temperature measurement agreed with the air temperature measured using an accurate sonic anemometer apparatus. The Dew-10 cooled mirror accurately measured the dewpoint temperature when it was compared to the dewpoint temperature measured using the Dewpoint Calibrator in the laboratory. However, the Dew-10 cooled mirror sensor did not provide

reliable measurement of the dewpoint during the later stage of the experiment because of wet filters after it had rained. The IRT temperature was closely correlated to the chromel-constantan thermocouple for air temperature under laboratory conditions. However, there was uncertainty as to whether the sensors did also perform well under field conditions. This is because there was not a good correlation between the measured surface temperature and the estimated assumed outlier line. There was not a significance difference between the use of fixed microclimate "constants" and those calculated. However, in this experiment the calculated "constants" rather than the fixed ones were used. In summary, data could be regarded as accurate except for the vapour pressure during some weather conditions and uncertainty about the surface temperature.

8.1.3 Bowen Ratio Energy Balance Technique

Most of the error in the latent heat estimate using the BREB would derive from the Bowen ratio measurement. This is because the analysis showed that an error in the BREB-latent heat due to a combined error of 2.5 % in net irradiance and 20 % in the soil heat flux density would not exceed 4.45 %. The Bowen ratio was calculated based on the Similarity Principle and excluded nighttime data. However, an error of β could still not be avoided during the daytime measurement of the profile entities because of the wet sensors and presence of convection and stable conditions in which the Similarity Principle could not be observed. Negative values of β were observed when there was strong wind. This was an indication of the sensible heat advection from the upwind field. It is unfortunate that one of the first assumptions of the energy balance equation, regarding negligible advection energy, was not fulfilled. Data were rejected during morning, and strong advection periods. It was also unreliable when the sensors were wet because of rain and irrigation. In this experiment only 35 % of the data were valid for determining latent and sensible heat using the BREB technique. Comparative analysis showed that the BREB overestimated latent heat by 17 % in relation to the Penman-Monteith latent heat. Thus, the main reasons for the poor performance of the BREB in this experiment were inaccurate determination of the Bowen ratio, sensors' limitation during dew, rain and irrigation period and the presence of advection.

8.1.4 The Surface Temperature Technique

The net irradiance and soil heat flux also had a little effect on the surface temperature-latent heat. An error of less than 5 % in latent heat was attributed to the use of the fixed air density and specific heat capacity, and to the use of a 2 % and 20 % error in net irradiance and soil heat flux density, respectively. The surface to air temperature differential or the aerodynamic resistance, or both, were the source of the overestimation of the latent heat using the surface temperature technique. The surface to air temperature differential was very large in magnitude when there were strong wind speeds and drier conditions in the upwind field, while it was small in magnitude when there were lighter wind speeds and a wetter surface in the upwind field.

The surface temperature-latent heat was overestimated in relation to the Penman-Monteith and BREB-latent heat. The technique generally has been reported to overestimate evaporation, although to a lesser extent than the 57 % reported in this experiment. Analysis of the energy closures, taking the Penman-Monteith and BREB as standards, suggested that the surface temperature technique overestimated the consumption of the sensible heat from the air. This observation was also confirmed when the eddy correlation technique was used to evaluate the sensible heat estimated using the surface temperature technique. The effect of placement height on air temperature measurement suggested that the consumption of the sensible heat would be overestimated if the sensor was placed far from the crop surface. This overestimation in the consumption of sensible heat would result in an overestimation of latent heat using the surface temperature technique. That is, the major problem for the good performance of the technique was the uncertainty in determining the surface to air temperature differential, the aerodynamic resistance and the presence of advection into the experimental field.

8.1.5 The Crop Water Stress Index

An investigation into the irrigation scheduling was performed using the CWSI calculated from the surface temperature or Penman-Monteith methods. Both methods require an estimate or measurement of the surface to air temperature differential, and canopy and aerodynamic resistances.

A combination of the Penman-Monteith, surface temperature and an empirical method was found to effect an accurate estimate of the CWSI. Data from the empirical equation were used to estimate the canopy and aerodynamic resistance under potential and non-transpiring conditions. These resistances were later used to estimate the latent heat or the surface to air temperature differential. However, a good correlation between the surface to air temperature differential (Y) *vs* VPD (X) or *vs* VPD (X_1) and net irradiance (X_2) was required. The correlation for this experiment was poor because of advection. The CWSI estimated using the ratio between the actual and potential evaporation was in better agreement with that determined using the Penman-Monteith method. The soil water content was poorly correlated to CWSI, while the canopy resistance was well correlated.

8.1.6 The Soil Water Balance Technique for Irrigation Scheduling

8.1.6.1 Calibration of the ThetaProbe

There was a good correlation between the ThetaProbe soil water content determined using factory-supplied parameters and that determined using the laboratory method. Both the factory-supplied and soil-estimated parameters resulted in more than 20 % overestimation of soil water content. Soil water content could be estimated to within 0.034 and 0.02 $m^3 m^{-3}$ when using the factory-supplied and soil-estimated parameters. However, using a recalibration equation, the soil water content could be estimated to within 0.02 $m^3 m^{-3}$ with a bias and intercept of 0 and slope of 1. The bulk density, clay content and temperature effect on the ThetaProbe showed a negligible influence on the measured soil water content. The average soil water content of the high water extraction layers was smaller than that of the low water extraction layers and there was strong correlation between their soil water contents. The depth-averaged soil water contents for recalibrated factory-supplied parameters were used to compare the soil water content estimated using the soil water balance.

8.1.6.2 Soil Water Balance

The irrigation water management can also be estimated using the water balance equation in which evaporation is the prime component. A comparison of the estimated soil water content using the soil water balance to that measured by using the ThetaProbe showed that there would be an

overestimation of the irrigation requirement when the evaporation component was overestimated, and *vice versa*. When the evaporation from the surface temperature technique was used, the estimated soil water content was underestimated throughout the experiment. But when the BREB and Penman-Monteith evaporation were used the soil water content was underestimated in the early stage and overestimated in the later stage of the experiment. It is thought that there was an inaccurate estimation of latent heat and soil water content using the BREB technique and Penman-Monteith method in the later stage of the experiment. This is because of the use of a poorly measured dewpoint. On the other hand, the drainage component was not taken into consideration when the soil water content was greater than the field capacity during the later stage of the experiment. Use of the estimated soil water content calculated by using the soil water balance with overestimated evaporation would result in the irrigation being applied unnecessarily early.

8.2 RECOMMENDATIONS FOR FUTURE RESEARCH

There is a need to perform more research on the surface temperature method to find out the cause for the overestimation of evaporation. The motivation for more research is the attractiveness of the simplicity of the technique and the robustness of the equipment which can be used for protracted periods without frequent maintenance. Also the method could be used for regional monitoring of evaporation using remote sensing techniques to measure surface temperature. Future research on the technique should focus on the estimate of the sensible and latent heat advection, and on the investigation of further resistances to water vapour flow from the surface to the atmosphere. An improvement of the BREB technique will depend on the possibility of estimating the BREB under adverse conditions and on the refinement of the equipment for continual measurement of the flux entities under variable weather conditions.

The soil water balance can be a solution for continual monitoring of the irrigation requirement. However, improved evaporation measurement must be accompanied by proper use of the energy balance equation. In addition, the runoff out of and into the area, the vertical flow of soil water

through the profile and the intercepted water on plant surfaces should be taken into account. The advantage of this technique is the facility in using the TDR or FDR sensors for accurate, fast and non-destructive measurement of the soil water content.

REFERENCES

Ahuja, L.R. and Williams, R.D., 1991. Scaling water characteristic and hydraulic conductivity based on Gregson-Hector-McGowan approach. *Soil Sci. Soc. Am.* J., 55, 308-319.

Allen, R. G, Jensen, M. E., Wright, J. L. and Burman, R. D., 1989. Operational estimate of reference evapotranspiration. *Agron. J.*, 81, 650-662.

Allen, R. G. 1996. Assessing intregrity of weather data for reference evaporation estimation. *J. Irrig. Drain. Eng. A.S.C.E.*, 122, 97-106.

Allen, R. G., Smith., M., Perrier, A. and Pereira, L. S., 1994. An update for the definition of reference evaporation. *ICID Bulletin*, 43, 1-92.

Alves, M. C. L., 1995. "Modelacao da evapotranspiracao cultural. Resistancia aerodinamica e do coberto".Unpublished PhD dissertation submitted to the "Instituto Superior de Agronomia, Universidade Tecnica de Lisboa", Lisbon, Portugal.

Alves, I., Perrier, A. And Pereira L. S., 1996. Aerodynamic and surface resistances of complete cover crops: How good is the "big leaf"? Paper presented at the "Evapotranspiration and Irrigation Scheduling International Conference" (Nov 3-7). ASAE/IA/ICID. San Antonio, Texas, US.

Anon (1991) Campbell Scientific Inc. Bowen Ratio Instrumentation Instruction Manual. Revision 4/91. Logan, Utah.

Avery, B. W. and Bascomb, C. L., 1974. Soil survey laboratory methods. Technical monograph No 6, Survey of England and Wales. Ministry of Agriculture and Fisheries.

Azhar, A. H., Murty, V. V. N., Phien, H. N., 1992. Modelling irrigation schedules for lowland rice with stochastic rainfall. *J. Irrig. Drain. A.S.C.E.*, 118, 36-53.

Beven, K. (1979) A sensitivity analysis of the Penman-Monteith actual evaporation estimates. *J. Hydrol.*, 44, 169-190.

Blad, B. L. and Rosenberg, N. J., 1974. Evapotranspiration by subirrigated alfalfa and pasture in the East Central Great Plains. *Agron. J.*, 66, 248-252.

Blad, B.L. and Rosenberg, N.J., 1976a. Measurement of crop temperature by leaf thermocouple, infrared thermometer and remotely sensing thermal imagery. *Agron J.*, 68, 635-641.

Blad, B.L. and Rosenberg, N.J, 1976b. Evaluation of resistance and mass transport evapotranspiration models requiring canopy temperature data. *Agron. J.*, 68, 764-769

Blake, G.R. and Hartge, K.H., 1986. Bulk density. In Campbell, G. S., Jackson, R. D., Mortland, M. M., Nielsen, D. R. and Klute, A. (Eds), Methods of Soil Analysis. Part 1; Physical and Mineralogical Methods. Agronomy No. 9, 2nd ed., 363-376. Am. Soc. Agron. Inc., Madison, Wis.

Bowen, I. S., 1926. The ratio of heat losses by conduction and by evaporation from any water surface. *Phys. Rev.*, 27, 779-787.

Campbell, G. S. and Campbell, M. D., 1982. Irrigation scheduling using soil moisture measurements: theory and practice. *Adv. Irrig.*, 1, 25-42.

Campbell, G. S. and Norman, J. M., 1990. Estimation of plant water status from canopy temperature: an analysis of the inverse problem. In Steve M. D. and Clark, J. A (Eds), Application of Remote Sensing in Agriculture, p255-271. London. .

Cary, J. W. and Fisher, H. D., 1983. Irrigation based on gypsum block for soil water suction at the 15 cm depth. International Conference on Measurement of Soil and Plant Water Status, 2, 227-231. Logan, Utah.

Cary, J. W. and Fisher, H. D., 1983b. Irrigation decision simplified with electronics and soil water sensors. *Soil Sci. Soc. Am. J.*, 47, 1219-1223.

Cellier, P. and Olioso, A., 1993. A simple system for automated long-term Bowen ratio measurement. *Agric. For. Meteorol.*, 66, 81-92.

Clothier, B. E., Scotter, D. R. and Kerr, J. P., 1977. Water retention in soil underlain by a coarse-textured layer: theory and field application. *Soil Sci.*, 123, 392-399.

Cohen, I. S., Lopes, V. L., Slack, D. C., and Gogel, M. M., 1997. Water balance model for small-scale water harvesting systems. *J. Irrig. Drain. A. S. C. E*, 123, 123-128.

Davenport, D. C. and Hudson, D.C., 1967. Changes in Evaporation rates along a 17-km transect in the Sudan Gezira. *Agric. Meteorol.*, 4, 339-352.

Delta-T Device, 1995. ThetaProbe Soil Moisture Sensor. Cambridge, England.

Ehrler, W. L., 1973. Cotton leaf temperature as related to soil water deplection and meteorological factors. *Agron. J.*, 65, 404-409.

Fuchs, M. and Tanner C. B., 1968. Calibration and field test of soil heat flux plates. *Soil. Sci. Soc. Am. Proc.*, 32, 326-328.

Gee GW, Bauder JW 1986 Particle-size analysis. In Campbel GS, Jackson RD., Mortland MM., Nielsen DR, and Klute A (eds) Methods of Soil Analysis. Part 1. Physical and Mineralogical Methods. Agronomy Monograph no. 9 2nd ed., p383-409. Madison, Wis., USA.

Gear, R. D., Rdansfield, A. S. and Campbell, M. D., 1977. Irrigation scheduling with neutron probe. *J. Irrig. Drain. A. S. C. E.*, 103, 291-298.

Gregson, K., Hector, D. J. and McGowan, M., 1978. A one-parameter model for the soil water characersitic. *J. Soil Sci.*, 38, 483-486.

Haise, H. R. and Hagan, R. M., 1967. Soil, plant and evaporation measurement as criteria for scheduling irrigation. In Hagan, R. M., Haise, H. R. and Edminster, T. W. (Eds), Irrigation of Agriculture Land. Agronomy No. 11, (30), p577-604. Am. Soc. Agron. Inc., Madison, Wis.

Hatfield, J. L., 1983. Evapotranspiration obtained from remote sensing methods. *Adv. Irrig.*, 2, 395-415.

Hatfield, J.L., 1984. Evaluation of canopy temperature evapotranspiration models over various crops. *Agric. For. Meteor.*, 32, 41-53.

Heilman, J. L., Brittin, C. L. and Neale C. M. U, 1989. Fetch requirements for Bowen ratio measurements of latent and sensible heat fluxes. *Agric. For. Meteorol.*, 44, 261-273.

Heilman, J.L. and Kanemasu, E.T., 1976. An evaluation of a resistance of the energy balance to estimate evapotranspiration. *Agron. J.*, 68, 607-611.

Hillel, D., 1982. Introduction to Soil Physics. Academic Press, Orlando, Florida.

Idso, S. B., 1982. Non-water-stressed baselines: A key to measuring and interpreting plant water stress. *Agric. Meteorol.*, 27, 59-70.

Idso, S. B., Jackson, R. D., Pinter, P. J., Reginato, R. J. and Hatfield, J. L., 1981a. Normalizing the stress-degree-day parameter for environmental variability. *Agric. Meteorol.*, 24, 45-55.

Idso, S. B., Reginato, R. J., Reicosky, D. C. and Hatfield, J. L., 1981b. Determining soil-induced plant water potential depressions in alflafa by means of infrared thermometry. *Agron. J.*, 73, 826-831.

Iritz, Z. and Lindroth, A., 1994. Night-time evaporation from a short-rotation willow stand. *J. Hydrol.*, 157, 235-245.

Jackson, R. D., 1982. Canopy temperature and crop water stress. *Adv. Irrig.* 1, 43-85.

Jackson, R. D., Idso, S. B., Reginato, R. J. and Pinter, J. R., 1981. Canopy temperature as a crop water stress indicator. *Water Resour. Res.*, 17, 1133-1138.

Jackson, R. D., Reginato, R. J. and Idso, S. B., 1977. Wheat canopy temperature: a practical tool for evaluating water requirements. *Water Resour. Res.*, 13, 651-656.

Jacobson, O.H. and Schjonning, P., 1993a. A laboratory calibration of time domain reflectometry for soil water measurement including effects of bulk density and texture. *J. Hydrol.*, 151, 147-157.

Jacobson, O.H. and Schjonning, P., 1993b. Field evaluation of time domain reflectometry for soil water measurements. *J. Hydrol.*, 151, 159-172.

Jalali-Farahani, H. R., Slack, D. C., Kopec, D. M., Mathias, A. D. and Brown, P. W., 1994. Evaluation of resistances for bermudagrass turf crop water stress index models. *Agron. J.*, 86, 574-581.

Kaimal, J.C. and Gaynor, J.E., 1991. Another look at sonic thermometer. *Boundary-Layer Meteorol.*, 56, 401-410.

Klute, A., 1986. Water retention: laboratory methods. In Campbell, G. S., Jackson, R. D., Mortland, M. M.,Nielsen, D. R. and Klute, A. (Eds), Methods of Soil Analysis. Part 1; Physical and Mineralogical Methods. Agronomy No. 9, 2nd ed., p635-662. Am. Soc. Agron., Madison, Wis.

Lindroth, A., 1993. Aerodynamic and canopy resistance of short-rotation forest in relation to leaf area index. *Boundary-Layer Meteorol.*, 66, 265-279.

LI-COR, Inc., 1991. Portable Dew Point Generator. Operating and Service Manual. Nebraska.

Luvall, J.C. and Holbo, H.R., 1986. Using the thermal infrared multispectral scanner (TIMS) to estimate surface thermal responses. International Conference on Measurement of Soil and Plant Water Status, 2, 115-120. Logan, Utah

Malek, E., 1992. Night-time evaporation *vs* day-time and 24 h evpotranspiration. *J. Hydrol.* 138, 119-129.

Malek, E., Bingham, G. E. and McCurdy, G. D., 1990. Evapotranspiration from the margin and moist playa of closed desert valley. *J. Hydrol.*, 120, 15-34.

Malek, E, Bingham, G. E. and McCurdy, G. D., 1991. Continuous measurement of aerodynamic and alfalfa canopy resistances using the Bowen ratio-energy balance and Penman-Monteith methods. *Boundary-Layer Meteorol.*, 59, 189-194.

Malek, E. and Bingham, G. E., 1993. Comparison of the Bowen ratio-energy balance and the water balance methods for the measurement of evapotranspiration. *J. Hydrol.*, 146, 209-220.

Mascart, P., Taconet, O., Pinty, J-P and Mehrez, M. B., 1991. Canopy resistance formulation and its effect in mesoscale models. a HAPEX perspective. *Agric. For. Meteorol.*, 54, 319-351.

Massman, W. J., 1992. A surface energy balance method for partitioning evaporation data into plant and soil components for a surface with partial canopy cover. *Water Resour. Res.*, 28, 1723-1732.

McArthur, A. J., 1990. An accurate solution to the Penman equation. Agric. *For. Meteorol.*, 51, 87-92

McCuent, R., 1973. The role of the sensitivity analysis in hydrology modelling. *J. Hydrol.*, 18, 37-53

McMillen, R., 1987. An eddy correlation technique with extended application to non-simple terrain. *Boundary-Layer Meteorol.*, 43, 231-245.

Meterlerkamp, B. R., 1993. The use of the Bowen ratio energy balance method for the determination of total evaporation over a grassed surface. Unpublished M. Sc. Agric. thesis. Department of Agronomy, University of Natal, Pietermaritzburg, South Africa.

Molz, F. R. and Peterson, C. M., 1976. Water transport from roots to soil. *Agron. J.*, 68, 901-904.

Monteith, J. L., 1963. Gas exchange in plant communities. In: Evans LJ (Ed.) Environmental Control of Plant Growth. pp. 99-112. Academic Press, New York.

Monteith, J. L. and Unsworth, M. H., 1990. Principles of Environmental Physics. 2nd Edition. Edward Arnold, London.

Nie, D., Flitcroft, I. E. and Kanemasu, E. T., 1992. Performance of Bowen ratio systems on a slope. *Agric. For. Meteorol.*, 59, 165-181.

Ohmura, A., 1982. Objective criteria for rejecting data for Bowen ratio flux calculations. *J. Appl. Meteorol.*, 21, 595-598.

O'Toole, J. C. and Hatfield, J. L., 1983. Effect of wind on the crop water stress index derived by infrared thermometer. *Agron. J.*, 75, 811-817.

O'Toole, J. C. and Real, J. G., 1986. Estimation of aerodynamic and crop resistances from canopy temperature. *Agron. J.*, 78, 305-310.

Penman, H.L., 1948. Natural evaporation from open water, bare soil and grass. *Proc. Roy. Soc. London A.*, 198, 116-140.

Phene, C. J., Alle, P. A., and Pierro, J., 1987. Measurement of soil matric potential and real time irrigation scheduling. International Conference on Measurement of Soil and Plant Water Status, 2, 245-265. Logan, Utah

Pleban, S. and Israeli, I., 1989. Improved approach to irrigation scheduling programs. *J. Irrig. Drain. A. S. C. E.*, 115, 577-587.

Ratliff, L. F., Ritchie, J. T. and Cassel, D. K., 1983. Field-measured limits of soil water availability as related to laboratory-measured Properties. *Soil Sci. Soc. Am. J.*, 47, 770-775.

Robinson, D. A., Bell, J. P. and Batchelor, C. H., 1994. Influence of iron minerals on the determinations of soil water content using dielectric techniques. *J. Hydrol.*, 161. 169-180.

Rosenberg, N. J., 1969a. Seasonal patterns in evapotranspiration by irrigated alfalfa in the Central Great Plain. *Agron. J.*, 61, 879-886.

Rosenberg, N. J., 1969b. Advection contribution of energy utilized in evapotranspiration by alfalfa in the East Central Great Plains. *Agric. Meteorol.*, 6, 179-184.

Rosenberg, N. J., Blad, B. L. and Verma, S. B., 1983. Microclimate: The Biological Environment. 2nd ed. John iley & Sons., New York.

Roth, K., Schulin, R., Fluher, H. and Attinger, W., 1990. Calibration of time domain reflectometry for water content measurement using a composite dielectric approach. *Water Resour. Res.*, 26, 2267-2273.

Savage, M. J., 1991. Unpublished Agrometeorology 320 courses notes. University of Natal, Pietermaritzburg.

Savage, M. J., 1996. Unpublished Agrometeorology course notes. University of Natal, Pietermaritzburg.

Savage, M. J., Everson, C. S. and Metelerkamp, B. R., 1997. Evaporation measurement above vegetated surfaces using micrometeorological techniques. Report to the Water Research Commission, by the Department of Agronomy, University of Natal. WRC Report No 349/1/97.

Savage, M. J., McInnes, K. J. and Heilman, J. L., 1995. Placement height of eddy correlation sensors above a short turfgrass surface. *Agric. For. Meteorol.*, 74, 195-204.

Savage, M. J., Ritchie, J. T., Bland, W. L., Dugas, W. A., 1996. Lower limit of soil water availability. Agron.J, 88, 44-651.

Saxton, K. E., 1975. Sensitivity analysis of the combination evapotranspiration equation. *Agric. Meteorol.*, 15, 343-353.

Schotanus, P., Nieuwstadt, F.T.M. and De bruin, H.A.R., 1983. Temperature measurement with a sonic anemometer and its application to heat and moisture fluxes. *Boundary-Layer Meteorol.*, 26, 81-93.

Schulze, R. E., Hutson, J. L., and Cass, A., 1985. Hydrological characteristics and properties of soil in Southern Africa 2. Soil water retention models. *Water S.A.*, 11, 129-136.

Singh, B., Boivin, J., Kirkpatrick, G. and Hum, B., 1995. Automatic irrigation scheduling system (AISSUM): Principles and Applications. *J. Irrig. Drain. A. S. C. E.*, 121, 43-57.

Snedecor, G. W. and Cochran, W., 1980. Statistical Methods. Seventh Edition. The Iowa State University Press. Ames, Iowa, USA.

Stanley, C. D. and Maynard, D. N., 1990. Vegetables. In Stewart, B. A. and Nielsen, D. R. (Eds), Irrigation of Agriculture Crop Agronomy No 30, (31), p921-950. Madison, Wis.

Stegman, E. C., 1983. Irrigation scheduling: applied timing criteria. *Adv. Irrig.*, 2, 1-31.

Steiner, J. L., Howel, T. A. and Scheineder, A. D., 1991. Lysimeter evaluation of daily potential models for grain sorghum. *Agron. J.*, 83, 240-247.

Stone, L.R. & Horton, M.L., 1974. Estimating evaporation using canopy temperature. *Agron. J.*, 66, 450-454.

Tanner, C. B., 1963. Basic instrumentation and measurements for plant environment and micrometeorology. Soils Bulletin 6, Dept of Soil Science, College of Agriculture, University of Wisconsin, Madison 6, Wisconsin.

Tattari, S., Ikonen, J. P. and Sucjsdorff, Y., 1995. A comparison of evapotranspiration above a barley field based on quality tested Bowen ratio data and deardorff modelling. *J. Hydrol.*, 170, 1-14.

Thom, A. S., 1975. Momentum, mass and heat exchange in plant communities. In Monteith, J. L. (ed), Vegetation and Atmosphere, 1, 57-105. Academic Press, London.

Topp, G. C., Davis, J. L. and Annan, A. P., 1980. Electromagnetic determination of soil water content. measurement in coaxial transmission lines. *Water. Resour. Res.*, 16, 574-582.

Upchurch, D. R. and Wanjura, D. F., 1991. Infrared thermometer calibration and viewing method effects on canopy temperature measurement. *Agric. For. Meteorol.* 55, 309-321

Verma, S.B., Rosenberg, N.J., Blad, B.L. & Baradas, M.W., 1976. Resistance-energy balance method for predicting evaporation: Determination of boundary layer resistance and evaluation of errors effects. *Agron. J.*, 68, 776-782.

Villalobos, F. J. and Fereres, E., 1989. A simulation model for irrigation scheduling under variable

rainfall. *Trans. of the ASAE,* 32, 181-189.

Wanjura, D. F., Uchurch, D. R., and Mahan, J. R., 1995. Automated irrigation base on Control of irrigation scheduling using temperature-time thresholds. *Trans. of ASAE*, 38, 403-409.

Williams, R. D., Ahuja, L. R. and Naney, J. W., 1992. Comparison of method to estimate soil water characteristic from soil texture, bulk density, and limited data. *Soil Science*, 153, 172-184.

APPENDICES

Appendix 3.1 The CR7X datalogger program for performing the BREB, surface temperature and Penman-Monteith techniques for determining evaporation. Also included is the program for measuring the soil water content using the ThetaProbe.

The sample Bowen ratio program supplied by the Campbell Scientific for 21X datalogger was adapted for CR7X R. Further sensors were introduced for soil water content, surface temperature, solar radiation and rainfall measurements.

2 Soil heat flux plates, input locations 16 and 17.
1 Soil temperature sensors, input location 24 for the average Tsoil and 25 for soil temperature difference. This sensors placed at a depth of 80 mm for determination of the stored heat for 0-80 mm layer.
Upper and lower TC temperature, input locations 2 and 3, while the difference between lower and upper in input location 4. **Upper and lower dew point cooled mirror,** input location 8. The actual vapour pressure input location was 9. Air intake filters changed every 2 weeks (do not touch filters. use tweezer). The coarse layer of the filter should be should be exposed to the atmosphere and the shiny layer should be on pump side.
Net radiometer, input location 15.

Important note: 1. In order to continuously check the validity of the dew point measurements, the cooled mirror sensor was calibrated in the laboratory. Further checking in the field using the T107/RH207 sensors was unsuccessful because of lack of accuracy by using this sensors. 2 The mirror was cleanliness and bias was checked weekly. 3 Battery voltage for datalogger and sensors were kept above 12 V by 10 days interval substitution.

FLAG USAGE
Set flag 6 to initiate program by switching on pump: press *6 A D 6. The response to setting the flag may not be immediate. Set flag 7 to terminate program by switching on pump: press *7 A D 7. The response to setting the flag may not be immediate. Flag 4 set high to output the current time and disable data processing and set low to resume. Press *6 A D 4 to set high to disable and low resume. Flag 1 set to disable averaging while mirror stabilizes. Flag 2 active air intake high for upper and lower for lower . Flag 3 set battery subroutine high for pump and mirror off. Flag 5 used by the program during used disable. Flag 8: high at the end of intervals while soil temperature is averaged. Flag 9: the intermediate processing flag. Mirror and pump on/off routine. Input location 29 is for minutes into day for switching on time; 30 is for minutes into days for switching off time; 31 is for current time (minutes into day). Press *A 31 A *0 to repartition input memory allocation from default of 28 input locations to 31 input locations.

PROCEDURE FOR CLENING THE MIRROR AND SETTING THE BIAS
1- Press *6 A D 4 to disable output. One have to remember then to press * A 6 D to enable output when this procedure are completed. 2- Press *6 8 A to display the dew pont temperature. 3- Slide switch SW1 down. 4- Wait 120 s until the dew point increases to the ambient temperature; 5- Switch the switch to the middle position. The red LED light should come on. If it does not, the mirror needs to be cleaned. 6- To set the mirror bias, slides the switch SW1 upwards. Wait 120 s for the dew point to increase to the ambient temperature. The light should come on. If not, turn potentiometer R34 CW until the red light just comes on. Then switch the switch to the middle position. If the light did come on, turn the potensiometer CCW until the light goes off then slowly CW until the light comes on. Then switch the switch to the middle position.

ADDITIONAL INSTRUMENTS
4 IRT's, input locations 47 to 50
1 3D propeller, input location 69 for wind speed and 70 for wind direction. Serial numbers 218 (u), 225 (v) and 240 (w). The u direction pointed roughly south (coming winds?) and v direction west. For wind less than 1 m s-1:
218 (m s-1) = 0.0124 * mV + 0.13
225 (m s-1) = 0.0124 * mV + 0.13
240 (m s-1) = 0.0124 * mV + 0.13
else
218 (m s-1) = 0.0146 * mV + 0.082
225 (m s-1) = 0.0151 * mV - 0.166
240 (m s-1) = 0.0153 * mV - 0.103
5 ThetaProbe , input location s 35 to 39 for mV and 40 to 44 for θv m3 m-3. Probes one to 4 were buried deep and horizontal, while sensors 5 buried vertically at the surface.
2 T107/RH207, input locations 51 and 55 for air temperatures, 52 and 56 for relative humidity, 53 and 57 for saturation VP, and 54 and 58 for actual VP.
4 Soil temperature, input locations 60 to 63, associated with v m3 m-3 measurement (40 to 43)
1 Raingauge, input location 71.
1 Solar radiometer, input location 59.

SENSORS CONNECTION FOR THE CR7X (appendix 3.3a).

MODES
Modes to be set prior to unattended logging: Output option: *4 11 2 (for tape and printer on and 9600 baud). * 5 yy (1) ddd (1) hhmm (1) sec (1) A. Use of (0) in place of (1) suppress the output and display zero instead. *6 A display input location listed at the end of this appendix. *7 A list the output location also listed at the end of this appendix. This can be viewed 20 minute after sensors have been connected to an operated datalogger. *8 to check data transfer prior tounattended operation, press *8 3A 3A. The tape should advance automatically. *930A 1A A 3A. The format for these data will be printable ASCII, not comma delineated ASCII.

FILE NAME CONVENTION
Row from the datalogger: C:\gastao\ data\Talavall\dd mm ytal.dat where dd is day of year, mm is month and y is year (6). Data after using SPLIT program: C:\gastao\ data\Talavall\ddmm ytal.prn

DAY OF THE YEAR CONVERSION (see appendix 3.4)

HISTORY AND SITE DETAILS (TalaValley)
On 17/09/96 (DOY 261): An active silica gel was introduced into the net radiometer sensor, cleansing of the net radiometer domes and charged battery.connected to the sensors and datalogger. Data change of the Sms: The new left connected to the datalogger and the old taken to Pietermaritzburg for data transfer. General status after data collection: good operational of the sensors and datalogger.
23/09/96 (DOY 266): Change of SM. Error display (E09). New battery (12.85) for sensors. Program downloaded. All input location and sytem operational. Filters changed. Bias adjusted and mirror cleaned. Air flow reduced from 60 to 4.5 $m^3 s^{-1}$. Replacement of the broken lower thermocouple to the newer one.
30/09/96 (DOY 274): Change of SM. Mirror cleaned and bias adjusted. General status: sensors and datalogger operational.
03/10/96 (DOY 277): Bias adjusted and mirror cleaned. Abnormal actual water vapour pressure. Broken mixing chamber (bottle).
12/10/96 (DOY 286): Change of SM Mixing bottle changed. Filters changed from microfilters to Gelman filters. The actual water vapour pressure was very unstable, varying from negative (-0.7) to positive (2.128). Over-flow of data, losing 2 days data (30/09/96 and 01/10/96).
15/10/96 DOY 289: Change of SM. The mirror cleansing and bias checking repeated in order to measure real actual vapour pressure.
16/10/96 DOY 290: Harvested
18/10/96 DOY 292: Further checking on mirror and bias.

```
{CR7}
*Table 1 Program
01: 1.0      Execution Interval (seconds)
```

MEASURE PANEL TEMP., AIR TEMPs, AND COOLED MIRROR PRT

```
01:  Panel Temperature (P17)
 1: 1        In Card
 2: 1        Loc [ PanelTemp ]

02:  Battery Voltage (P10)
 1: 10       Loc [ VBattery  ]

03:  Thermocouple Temp (SE) (P13)
 1: 1        Reps
 2: 2        5000 uV Slow Range
 3: 1        In Card
 4: 8        In Chan
 5: 2        Type E (Chromel-Constantan)
 6: 1        Ref Temp Loc [ PanelTemp ]
 7: 3        Loc [ TClower   ]
 8: 1.0      Mult
 9: 0.0      Offset

04:  Thermocouple Temp (DIFF) (P14)
 1: 1        Reps
 2: 2        5000 uV Slow Range
 3: 1        In Card
 4: 4        In Chan
 5: 2        Type E (Chromel-Constantan)
 6: 1        Ref Temp Loc [ PanelTemp ]
 7: 2        Loc [ TCupper   ]
 8: 1.0      Mult
 9: 0.0      Offset

05:  Full Bridge (P6)
 1: 1        Reps
 2: 2        5000 uV Slow Range
 3: 1        In Card
 4: 2        In Chan
 5: 1        Ex Card
 6: 1        Ex Chan
 7: 1        Meas/Ex
 8: 5000     mV Excitation
 9: 8        Loc [ Dewpoint  ]
10: .001     Mult
11: .00498   Offset
```

CALCULATE TEMP. GRADIENT, DEW POINT, AND VAPOUR PRESS.

```
06:  Z=X-Y (P35)
 1: 3        X Loc [ TClower   ]
 2: 2        Y Loc [ TCupper   ]
 3: 4        Z Loc [ TClmTCu   ]

07:  BR Transform Rf[X/(1-X)] (P59)
 1: 1        Reps
 2: 8        Loc [ Dewpoint  ]
 3: 200      Mult (Rf)

08:  Temperature RTD (P16)
 1: 1        Reps
 2: 8        R/RO Loc [ Dewpoint  ]
 3: 8        Loc [ Dewpoint  ]
 4: 1.0      Mult
 5: 0.0      Offset

09:  Saturation Vapor Pressure (P56)
 1: 8        Temperature Loc [ Dewpoint  ]
 2: 9        Loc [ ActVPBREB ]
```

OUTPUT PROCESSING

```
10:  If Flag/Port (P91)
 1: 15       Do if Flag 5 is High
 2: 0        Go to end of Program Table

11:  If time is (P92)
 1: 0        Minutes into a
 2: 20       Minute Interval
 3: 10       Set Output Flag High

12:  Resolution (P78)
 1: 1        high resolution

13:  Serial Out (P96)
 1: 30       SM192/SM716/CSM1

14:  Set Active Storage Area (P80)
 1: 1        Final Storage
 2: 110      Array ID or Loc [ _____ ]
```

User can set flag 4 to output data to current time and disable output processing while working on system.

```
15:  If Flag/Port (P91)
 1: 14       Do if Flag 4 is High
 2: 30       Then Do
```

Output data to current time

```
16:  Do (P86)
 1: 10       Set Output Flag High

17:  Set Active Storage Area (P80)
 1: 1        Final Storage
 2: 112      Array ID or Loc [ _____ ]
```

Further output

```
18:  Do (P86)
 1: 15       Set Flag 5 High

19:  End (P95)

20:  Real Time (P77)
 1: 1110     Year,Day,Hour/Minute

21:  Average (P71)
 1: 1        Reps
 2: 10       Loc [ VBattery  ]

22:  Average (P71)
 1: 2        Reps
 2: 3        Loc [ TClower   ]
```

Disable avg if on upper intake

```
23: If Flag/Port (P91)
 1: 12      Do if Flag 2 is High
 2: 30      Then Do

24: Do (P86)
 1: 19      Set Flag 9 High

25: Else (P94)

Disable avg if just switched
26: If Flag/Port (P91)
 1: 11      Do if Flag 1 is High
 2: 19      Set Flag 9 High

27: End (P95)

Dew-point and actVP from lower arm
28: Average (P71)
 1: 2       Reps
 2: 8       Loc [ Dewpoint  ]

Re-enable intermediate processing
29: Do (P86)
 1: 29      Set Flag 9 Low

Disable avg if on lower intake
30: If Flag/Port (P91)
 1: 22      Do if Flag 2 is Low
 2: 30      Then Do

31: Do (P86)
 1: 19      Set Flag 9 High

32: Else (P94)

Disable avg if just switched
33: If Flag/Port (P91)
 1: 11      Do if Flag 1 is High
 2: 19      Set Flag 9 High

34: End (P95)

Dew-point and actual VP from upper arm
35: Average (P71)
 1: 2       Reps
 2: 8       Loc [ Dewpoint  ]

*Table 2 Program
 02: 10.0     Execution Interval (seconds)

MEASURE THETAPROBE mV and θ, IRT TEMP., T107 TEMP., RH207 RH, ACTUAL AND SATURATED VP, SOLAR Irradiance, WIND SPEED, SOIL TEMP FOR THETAPROBEs, WIND DIRECTION AND RAINFALL
01: Volt (Diff) (P2)
 1: 5       Reps
 2: 8       5000 mV Slow Range
 3: 1       In Card
 4: 9       In Chan
 5: 35      Loc [ VThetaP#1 ]
 6: .001    Mult
 7: 0.0     Offset

Calculate θ using polynomial function and data from manufacturer
02: Polynomial (P55)
 1: 5       Reps
 2: 35      X Loc [ VThetaP#1 ]
 3: 40      F(X) Loc [ SWCThet#1 ]
 4: -.07143  C0
 5: .72738   C1
 6: -1.1571  C2
 7: 2.8988   C3
 8: -3.6714  C4
 9: 1.7547   C5

Measure IRT temperature
03: Volts (SE) (P1)
 1: 4       Reps
 2: 7       1500 mV Slow Range
 3: 2       In Card
 4: 4       In Chan
 5: 47      Loc [ IRT#1     ]
 6: .1      Mult
 7: 0.0     Offset
Measure temp., RH, actual and saturated VP using T107/RH207#1 sensors
04: Temp 107 Probe (P11)
 1: 1       Reps
 2: 2       In Card
 3: 19      In Chan
 4: 1       Ex Card
 5: 2       Ex Chan
 6: 51      Loc [ T107#1    ]
 7: 1       Mult
 8: 0       Offset

05: R.H. 207 Probe (P12)
 1: 1       Reps
 2: 2       In Card
 3: 20      In Chan
 4: 1       Ex Card
 5: 2       Ex Chan
 6: 1       Meas/Temp
 7: 51      Temperature Loc [ T107#1    ]
 8: 52      Loc [ RH207#1   ]
 9: .01     Mult
10: 0.0     Offset

06: Saturation Vapor Pressure (P56)
 1: 51      Temperature Loc [ T107#1    ]
 2: 53      Loc [ es#1      ]

07: Z=X*Y (P36)
 1: 52      X Loc [ RH207#1   ]
 2: 53      Y Loc [ es#1      ]
 3: 54      Z Loc [ eair#1    ]

Measure temp., RH, actual and saturated VP using T107/RH207#2 sensor
08: Temp 107 Probe (P11)
 1: 1       Reps
 2: 2       In Card
 3: 21      In Chan
 4: 1       Ex Card
 5: 3       Ex Chan
 6: 55      Loc [ T107#2    ]
 7: 1.0     Mult
 8: 0.0     Offset

09: R.H. 207 Probe (P12)
 1: 1       Reps
 2: 2       In Card
 3: 22      In Chan
 4: 1       Ex Card
 5: 3       Ex Chan
 6: 1       Meas/Temp
 7: 55      Temperature Loc [ T107#2    ]
 8: 56      Loc [ RH207#2   ]
 9: .01     Mult
10: 0       Offset

10: Saturation Vapor Pressure (P56)
 1: 55      Temperature Loc [ T107#2    ]
 2: 57      Loc [ es#2      ]

10: Z=X*Y (P36)
 1: 56      X Loc [ RH207#2   ]
 2: 57      Y Loc [ es#2      ]
 3: 58      Z Loc [ eair#2    ]

Solar radiation
12: Volts (SE) (P1)
 1: 1       Reps
 2: 4       50 mV Slow Range
 3: 1       In Card
 4: 11      In Chan
 5: 59      Loc [ Sr        ]
 6: 147.9   Mult
 7: 0.0     Offset

Soil temps.
13: Thermocouple Temp (SE) (P13)
 1: 4       Reps
 2: 2       5000 uV Slow Range
 3: 2       In Card
 4: 9       In Chan
 5: 1       Type T (Copper-Constantan)
 6: 1       Ref Temp Loc [ PanelTemp ]
 7: 60      Loc [ TsoilTh#1 ]
 8: 1.0     Mult
 9: 0.0     Offset

Wind speed and wind direction
14: Volts (SE) (P1)
 1: 3       Reps
 2: 8       5000 mV Slow Range
 3: 2       In Card
 4: 15      In Chan
 5: 64      Loc [ Umps#1    ]
 6: 1.0     Mult
 7: 0.0     Offset

15: IF (X<=>F) (P89)
 1: 64      X Loc [ Umps#1    ]
 2: 4       <
 3: 70.65   F
 4: 30      Then Do

16: Z=X*F (P37)
 1: 64      X Loc [ Umps#1    ]
 2: .0124   F
 3: 64      Z Loc [ Umps#1    ]

17: Z=X+F (P34)
 1: 64      X Loc [ Umps#1    ]
 2: .13     F
 3: 64      Z Loc [ Umps#1    ]

18: Else (P94)

19: Z=X*F (P37)
 1: 64      X Loc [ Umps#1    ]
 2: .0146   F
 3: 64      Z Loc [ Umps#1    ]

20: Z=X+F (P34)
 1: 64      X Loc [ Umps#1    ]
 2: .082    F
 3: 64      Z Loc [ Umps#1    ]

21: End (P95)

22: IF (X<=>F) (P89)
 1: 0       X Loc [ _________ ]
 2: 4       <
 3: 70.65   F
 4: 30      Then Do

23: Z=X*F (P37)
 1: 65      X Loc [ Umps#2    ]
 2: .0123   F
 3: 65      Z Loc [ Umps#2    ]

24: Z=X+F (P34)
 1: 65      X Loc [ Umps#2    ]
 2: .13     F
 3: 65      Z Loc [ Umps#2    ]

25: Else (P94)

26: Z=X*F (P37)
 1: 65      X Loc [ Umps#2    ]
 2: .0151   F
 3: 65      Z Loc [ Umps#2    ]

27: Z=X+F (P34)
 1: 65      X Loc [ Umps#2    ]
 2: -.166   F
 3: 65      Z Loc [ Umps#2    ]

28: End (P95)

29: IF (X<=>F) (P89)
 1: 66      X Loc [ Umps#3    ]
 2: 4       <
 3: 63.75   F
 4: 30      Then Do

30: Z=X*F (P37)
 1: 66      X Loc [ Umps#3    ]
 2: .0127   F
 3: 66      Z Loc [ Umps#3    ]

31: Z=X+F (P34)
 1: 66      X Loc [ Umps#3    ]
 2: .13     F
 3: 66      Z Loc [ Umps#3    ]

32: Else (P94)

33: Z=X*F (P37)
 1: 66      X Loc [ Umps#3    ]
 2: .0148   F
 3: 66      Z Loc [ Umps#3    ]

34: Z=X+F (P34)
 1: 66      X Loc [ Umps#3    ]
 2: .057    F
 3: 66      Z Loc [ Umps#3    ]

35: End (P95)

36: Z=X*Y (P36)
 1: 64      X Loc [ Umps#1    ]
 2: 64      Y Loc [ Umps#1    ]
 3: 67      Z Loc [ Umps#1sq  ]

37: Z=X*Y (P36)
 1: 65      X Loc [ Umps#2    ]
 2: 65      Y Loc [ Umps#2    ]
 3: 68      Z Loc [ Umps#2sq  ]

38: Z=X+Y (P33)
 1: 67      X Loc [ Umps#1sq  ]
 2: 68      Y Loc [ Umps#2sq  ]
 3: 69      Z Loc [ Windspeed ]

39: Z=SQRT(X) (P39)
 1: 69      X Loc [ Windspeed ]
 2: 69      Z Loc [ Windspeed ]

40: Z=ARCTAN(X/Y) (P66)
 1: 65      X Loc [ Umps#2    ]
 2: 64      Y Loc [ Umps#1    ]
 3: 70      Z Loc [ Winddirec ]

41: Pulse (P3)
 1: 1       Reps
 2: 4       In Card
 3: 1       Pulse Input Channel
 4: 2       Switch Closure
 5: 71      Loc [ Rainfall  ]
 6: .245    Mult
 7: 0       Offset

COOLED MIRROR SETTING
42: Time (P18)
 1: 0       Tenths of seconds into minute (maximum 600)
 2: 400     Mod/By
 3: 11      Loc [           ]

Check if time to enable avg
43: IF (X<=>F) (P89)
 1: 11      X Loc [         ]
 2: 4       <
 3: 100     F
 4: 21      Set Flag 1 Low

Check for disable/re-enable
If output is disabled
44: If Flag/Port (P91)
 1: 15      Do if Flag 5 is High
 2: 30      Then Do

Check if user has re-enable
45: If Flag/Port (P91)
 1: 24      Do if Flag 4 is Low
 2: 1       Call Subroutine 1

46: End (P95)

Switch cooled mirror intake every 2 mnutes
Solenoid switching every 2 minutes
47: If time is (P92)
 1: 0       Minutes into a
 2: 2       Minute Interval
 3: 30      Then Do
```

```
Disable avg when just switched to allow cooled
mirror to stabiliza on new dew point
temperature.
48: Do (P86)
 1: 11     Set Flag 1 High

Every 4 minutes
49: If time is (P92)
 1: 0      Minutes into a
 2: 4      Minute Interval
 3: 30     Then Do

Switch to upper intake
50: Set Port(s) (P20)
 1: 1      Set High
 2: 1      Ex Card
 3: 2      Port Number

Flag 2 set high while on upper
51: Do (P86)
 1: 12     Set Flag 2 High

2 minutes into 4 minute interval...
52: Else (P94)

Switch to lower arm
53: Set Port(s) (P20)
 1: 1      Set High
 2: 1      Ex Card
 3: 1      Port Number

Flag 2 low while on lower
54: Do (P86)
 1: 22     Set Flag 2 Low

55: End (P95)

56: Excitation with Delay (P22)
 1: 1      Ex Card
 2: 1      Ex Chan
 3: 0      Delay w/Ex (units = 0.01 sec)
 4: 2      Delay After Ex (units = 0.01 sec)
 5: 0.0    mV Excitation

57: Set Port(s) (P20)
 1: 00     Option
 2: 1      Ex Card
 3: 1      Port Number

58: Set Port(s) (P20)
 1: 0      Set Low
 2: 1      Ex Card
 3: 2      Port Number

59: End (P95)

MEASURE NET IRRADIANCE, SOIL
TEMP., AND SOIL HEAT FLUXT.
Measure net irradiance
60: Volt (Diff) (P2)
 1: 1      Reps
 2: 6      500 mV Slow Range
 3: 1      In Card
 4: 1      In Chan
 5: 15     Loc [ Rn      ]
 6: 1      Mult
 7: 0.0    Offset

Use 9.38 Wm-2/mV multiplier if thermopile mV
is positive.
61: IF (X<=>F) (P89)
 1: 15     X Loc [ Rn    ]
 2: 3      >=
 3: 0      F
 4: 30     Then Do

62: Z=X*F (P37)
 1: 15     X Loc [ Rn    ]
 2: 9.38   F
 3: 15     Z Loc [ Rn    ]

Use -11.38 Wm-2/mV multiplier if thermopile
mV is negative.
63: Else (P94)

64: Z=X*F (P37)
 1: 15     X Loc [ Rn    ]
 2: 11.75  F
 3: 15     Z Loc [ Rn    ]

65: End (P95)

Soil heat flux measurement
66: Volts (SE) (P1)
 1: 2      Reps
 2: 3      15 mV Slow Range
 3: 1      In Card
 4: 9      In Chan
 5: 16     Loc [ G#1     ]
 6: 49     Mult
 7: 0.0    Offset

Soil thermocouple measurement
67: Thermocouple Temp (DIFF) (P14)
 1: 1      Reps
 2: 2      5000 uV Slow Range
 3: 1      In Card
 4: 3      In Chan
 5: 2      Type E (Chromel-Constantan)
 6: 1      Ref Temp Loc [ PanelTemp ]
 7: 20     Loc [ Tsoil   ]
 8: 1.0    Mult
 9: 0.0    Offset

Soil temperature is only averaged over the last 5
minutes of output interval in order to have the
change in temp. During the interval. An average
rather than a sample is used to avvoid
perturbation by an anomalous reading)
68: If time is (P92)
 1: 15     Minutes into a
 2: 20     Minute Interval
 3: 18     Set Flag 8 High

69: If Flag/Port (P91)
 1: 18     Do if Flag 8 is High
 2: 30     Then Do

Totalize soil temperature
70: Z=X+Y (P33)
 1: 20     X Loc [ Tsoil   ]
 2: 21     Y Loc [ TsoilT  ]
 3: 21     Z Loc [ TsoilT  ]

71: Z=Z+1 (P32)
 1: 22     Z Loc [ NoOfsa]

72: End (P95)

OUTPUT AVG (TOTAL/HYSTOGRAM)
THETAPROBEs mV AND , IRTs, AIR
TEMPERATURE AND VP FROM
T107/RH207 SENSORS, SOLAR
RADIATION, SOIL TEMPERATURES FOR
THETAPROBE, WIND SPEED AND
DIRECTION, NET IRRADIANCE, SOIL
HEAT FLUX, SOIL TEMPERATURE AND
SOIL TEMPERATURE DIFFERENCE.
73: If time is (P92)
 1: 0      Minutes into a
 2: 20     Minute Interval
 3: 30     Then Do

Avg soil temperature
74: Z=X/Y (P38)
 1: 21     X Loc [ _____ ]
 2: 22     Y Loc [ _____ ]
 3: 24     Z Loc [ TsoilAvg ]

Temporal change in soil temperature
75: Z=X-Y (P35)
 1: 24     X Loc [ TsoilAvg ]
 2: 23     Y Loc [ _____ ]
 3: 25     Z Loc [ dTsoil   ]

Move current avg to previous
76: Z=X (P31)
 1: 24     X Loc [ TsoilAvg ]
 2: 23     Z Loc [ _____ ]

Set total one to zero
77: Z=F (P30)
 1: 0      F
 2: 21     Z LOC [ _____ ]

Set N counter to 0
78: Z=F (P30)
 1: 0      F
 2: 22     Z LOC [ _____ ]

79: Do (P86)
 1: 28     Set Flag 8 Low

80: Do (P86)
 1: 10     Set Output Flag High

81: Resolution (P78)
 1: 1      high resolution

82: Serial Out (P96)
 1: 30     SM192/SM716/CSM1

83: Set Active Storage Area (P80)
 1: 1      Final Storage
 2: 237    Array ID or Loc [ _____ ]

84: End (P95)

85: Real Time (P77)
 1: 1110   Year,Day,Hour/Minute

86: Average (P71)
 1: 3      Reps
 2: 15     Loc [ Rn      ]

87: Sample (P70)
 1: 2      Reps
 2: 24     Loc [ TsoilAvg ]

88: Average (P71)
 1: 29     Reps
 2: 35     Loc [ VThetaP#1 ]

89: Average (P71)
 1: 2      Reps
 2: 69     Loc [ Windspeed ]

90: Totalize (P72)
 1: 1      Reps
 2: 71     Loc [ Rainfall  ]

91: Histogram (P75)
 1: 1      Reps
 2: 15     No. of Bins
 3: 1      Closed Form
 4: 70     Bin Select Value Loc [ Winddirec ]
 5: 0      WV Loc Option [ _____ ]
 6: 0      Low Limit
 7: 360    High Limit

CALL BATTERY CHECK/PUMP &
MIRROR SUBROUTINE
92: Do (P86)
 1: 2      Call Subroutine 2

INSERT ADDITIONAL
MEASUREMENT/OUTPUT
PROGRAMMING HERE
*Table 3 Subroutines

SUBROUTINE 1 OUTPUT TIME
PROCESSING IS RE-ENABLED
01: Beginning of Subroutine (P85)
 1: 1      Subroutine 1

02: Do (P86)
 1: 25     Set Flag 5 Low

03: Do (P86)
 1: 10     Set Output Flag High

04: Set Active Storage Area (P80)
 1: 1      Final Storage
 2: 303    Array ID or Loc [ _____ ]

05: Real Time (P77)
 1: 1110   Year,Day,Hour/Minute

06: End (P95)

SUBROUTINE 2 SWITCH PUMP AND
COOLED MIRROR IN RESPONSE TO
USEFLAG OR OFF IF BATTERY IS < 11.5
VOLTS AND SWITCH ON AGAIN IF
BATTERY >12 VOLTS.
07: Beginning of Subroutine (P85)
 1: 2      Subroutine 2

08: Z=F (P30)
 1: 480    F
 2: 29     Z LOC [ _____ ]

09: Z=F (P30)
 1: 1080   F
 2: 30     Z LOC [ _____ ]

10: Time (P18)
 1: 1      Minutes into current day (maximum
1440)
 2: 0      Mod/By
 3: 31     Loc [ _____ ]

11: IF (X<=>Y) (P88)
 1: 29     X Loc [ _____ ]
 2: 1      =
 3: 31     Y Loc [ _____ ]
 4: 16     Set Flag 6 High

12: Set Port(s) (P20)
 1: 16     Set According to Flag 6
 2: 1      Ex Card
 3: 3      Port Number

13: Do (P86)
 1: 26     Set Flag 6 Low

14: IF (X<=>Y) (P88)
 1: 30     X Loc [ _____ ]
 2: 1      =
 3: 31     Y Loc [ _____ ]
 4: 17     Set Flag 7 High

15: Set Port(s) (P20)
 1: 17     Set According to Flag 7
 2: 1      Ex Card
 3: 4      Port Number

16: Do (P86)
 1: 27     Set Flag 7 Low

17: IF (X<=>F) (P89)
 1: 10     X Loc [ VBattery ]
 2: 4      <
 3: 11.5   F
 4: 30     Then Do

18: If Flag/Port (P91)
 1: 23     Do if Flag 3 is Low
 2: 30     Then Do

19: Set Port(s) (P20)
 1: 1      Set High
 2: 1      Ex Card
 3: 4      Port Number

20: Excitation with Delay (P22)
 1: 1      Ex Card
 2: 4      Ex Chan
 3: 0      Delay w/Ex (units = 0.01 sec)
 4: 1      Delay After Ex (units = 0.01 sec)
 5: 0      mV Excitation

21: Set Port(s) (P20)
 1: 0      Set Low
 2: 1      Ex Card
 3: 4      Port Number

22: Do (P86)
 1: 13     Set Flag 3 High

23: Do (P86)
 1: 10     Set Output Flag High
```

```
24: Set Active Storage Area (P80)
 1: 1       Final Storage
 2: 317     Array ID or Loc [ _____ ]

25: Real Time (P77)
 1: 1110    Year,Day,Hour/Minute

26: Sample (P70)
 1: 1       Reps
 2: 10      Loc [ VBattery  ]

27: End (P95)

28: Else (P94)

29: If Flag/Port (P91)
 1: 13      Do if Flag 3 is High
 2: 30      Then Do

30: IF (X<=>F) (P89)
 1: 10      X Loc [ VBattery  ]
 2: 3       >=
 3: 11.89   F
 4: 30      Then Do

31: Set Port(s) (P20)
 1: 1       Set High
 2: 1       Ex Card
 3: 3       Port Number

32: Excitation with Delay (P22)
 1: 1       Ex Card
 2: 4       Ex Chan
 3: 0       Delay w/Ex (units = 0.01 sec)
 4: 1       Delay After Ex (units = 0.01 sec)
 5: 0       mV Excitation

33: Set Port(s) (P20)
 1: 0       Set Low
 2: 1       Ex Card
 3: 3       Port Number

34: Do (P86)
 1: 23      Set Flag 3 Low

35: Do (P86)
 1: 10      Set Output Flag High

36: Set Active Storage Area (P80)
 1: 1       Final Storage
 2: 328     Array ID or Loc [ _____ ]

37: Real Time (P77)
 1: 1110    Year,Day,Hour/Minute

38: Sample (P70)
 1: 1       Reps
 2: 10      Loc [ VBattery  ]

39: End (P95)

40: End (P95)

41: End (P95)

42: End (P95)

End Program

-Input Locations-
1 PanelTemp 0 4 1
2 TCupper   0 1 1
3 TClower   0 2 1
4 TClmTCu   0 1 1
5 _____     0 0 0
6 _____     0 0 0
7 _____     0 0 0
8 Dewpoint  0 5 3
9 ActVPBREB 0 2 1
10 VBattery  0 5 1

11          0 1 1
12 _____     0 0 0
13 _____     0 0 0
14 _____     0 0 0
15 Rn        0 4 3
16 G#1       4 1 2
17 G#2       16 1 2
18 _____     0 0 0
19 _____     0 0 0
20 Tsoil     0 1 1
21 _____     0 2 2
22 _____     0 2 2
23 _____     0 1 1
24 TsoilAvg  0 3 1
25 dTsoil    0 1 1
26 _____     0 0 0
27 _____     0 0 0
28 _____     0 0 0
29 _____     0 1 1
30 _____     0 1 1
31 _____     0 2 1
32 _____     0 0 0
35 VThetaP#1 4 2 2
36 VThetaP#2 8 2 2
37 VThetaP#3 8 2 2
38 VThetaP#4 8 2 2
39 VThetaP#5 16 2 2
40 SWCThet#1 4 1 1
41 SWCThet#2 8 1 1
42 SWCThet#3 8 1 1
43 SWCThet#4 8 1 1
44 SWCThet#5 16 1 1
47 IRT#1     4 1 2
48 IRT#2     8 1 2
49 IRT#3     8 1 2
50 IRT#4     16 1 2
51 T107#1    0 2 2
52 RH207#1   0 2 1
53 es#1      0 2 1
54 eair#1    0 1 1
55 T107#2    0 2 2
56 RH207#2   0 2 1
57 es#2      0 2 1
58 eair#2    0 1 1
59 Sr        0 1 1
60 TsoilTh#1 4 1 1
61 TsoilTh#2 8 1 1
62 TsoilTh#3 8 1 1
63 TsoilTh#4 16 1 1
64 Umps#1    4 8 5
65 Umps#2    8 7 5
66 Umps#3    16 5 5
67 Umps#1sq  0 1 1
68 Umps#2sq  0 1 1
69 Windspeed 0 2 2
70 Winddirec 0 2 1
71 Rainfall  0 1 1
-Program Security-
0000
0000
0000
```

Appendix 3.2 The eddy correlation program and information card used in Vita Farm experiment.

3D sonic Information card for Campbell 21X datalogger — **M J Savage, Department of Agronomy, University of Natal** — **Page 1**

Program:3dsonic4.dld
20 October 1996
Program for Applied Technologies 3D sonic and use with 21X datalogger
Routine use of SAT-211 3D wind system
The format of the data via the digital port of the card cage is important. The format is: 7 bit ASCII word, even parity bit, 1 stop bit, full duplex and 9600 baud. The card cage to computer cable must be used to set this format prior to datalogger connection.

Card cage and sensor
WARNING: NEVER SWITCH ON THE POWER UNTIL ALL CABLES HAVE BEEN CONNECTED
1. The aluminium card cage has connectors for the probe (do not disconnect), DC voltage (12V) and a digital signal connector.
2. Usually, the probe should be directly coupled to the aluminium card cage. If not, the end of the probe wire must be connected to the probe via pushing wire through the square tube. Align the red dot at the end of the probe wire the red dot at the end of the 3D sensor. Push the probe wire end into the sensor end.
3. Once the sensor wire has been connected to the card cage, the power may be applied. The current drain is excessive (greater than 1A).
4. Check that the sensor cables are connected. Switch the card cage power switch on. Three red lights will come on and go off. The red light will go on and stay on. If the red lights stay on, there is a problem.
5. Assuming that three batteries are used, each with a capacity of 50 Ah (-conservative), then the battery life is 3 x 50 Ah/1A = 150 h = 6 days.

Digital to analogue converter
1. Connect the digital wire from the card cage to the D-A converter (black box) - the serial in port.
2. Connect the D-A power port to power supply.
3. Connect the analogue out cable to the datalogger.
4. Switch the D-A box on (pull switch out and up). The red lights should go on and then off with the busy light then flashing. If the voltage supply to the D-A converter decreases below 11.5 V, the ERROR red light will come on and stay on.

Noise
(E-mail from Herb Zimmerman, 20 June 1996)
Sudden increases in wind speed, particularly the v component could be due to noise in the system rather than with a temperature problem. Spikes previously noticed did not happen on any kind of peak or low point in the temperature, or at a regular temperature point.
There are two types of noise that can cause this problem: there may be some external noise being picked up by the probe or cable, or there may be some transmitter noise creeping into the receive window. The transmitter noise is the more likely choice, if there really is a temperature dependence. The frequency of the transducers drifts with temperature so the band-pass adjustment is somewhat dependent on temperature. This effect seems to be much worse in the 100 mm (200 kHz) application. This is one of the reasons why the alternative 150 mm "Vx" type probe was developed. It can use the 100 kHz transducers.
The other possibility of noise is the external type. The probe and probe cable do act as an antenna to external radiation of all types. This can be a perplexing problem if there is a transmitter near by that only gets used, or turned on, at certain times of the day or even on a random basis.
If it is suspected that the problem is due to temperature changes, there is one thing that one could try. There are some capacitors we use on the counter board, and in some applications we have found these to be unstable over temperature. As a final possibility, Applied Technologies can supply some temperature stable parts. The temperature stable parts are much bigger then the regular parts and will have to be soldered in place of the old parts, but it can be done.
With the 100 mm probe, the best solution is for you to become proficient with the Tx/Rx board setup procedure (Section 6 in the manual) using an oscilloscope. This is the best solution to the noise problems described above.
Careful adjustment of the Tx/Rx boards can make a big difference in whether or not there will be noise in the output. Once one is familiar with these adjustments and the effect of these adjustments have on the instrument, it becomes quite easy to keep the instrument operating properly.

Eddy correlation program using Applied Technologies 3D sonic anemometer for sensible and momentum flux densities.
This program is the fastest possible using fast single-ended measurements.

Single ended measurements
For single ended measurements, as in this program,
u, v: 5 V = 20 m/s or 1 mV = 0.004 m/s;
w: 5 V = 5 m/s or 1 mV = 0.001 m/s;
T: 5 V = 50 °C or 1 mV = 0.01 °C.

Differential ended measurements
For differential ended measurements, not used in this program since the voltage measurements take longer:
u, v: 10 V = 20 m/s or 1 mV = 0.002 m/s;
w: 10 V = 5 m/s or 1 mV = 0.0005 m/s;
T: 0 V = 50 °C or 1 mV = 0.005 °C.

Total execution time is approximately 164.5 ms

Input locations
loc 1 u; 2 v; 3 w; 4 T; 5 U; 6 w; 7 theta; loc 8 SDw; 9 SDT; 10 CVwT; 11 SDU; 12 SDw; 13 Uw

Output order
col 1 STN; 2 day; 3 time; 4 u; 5 v; 6 w; 7 T; 8 U;
col 9 THETA (sample); 10 SDw; 11 SDT; 12 wT;
col 13 SDU; 14 Uw

25 pin male datalogger inserted into SA-4wires
u+: brown; u-: pink; light green: ground;
v+: orange; v-: violet; red: ground;
w+: white; w-: yellow; grey: ground;
T+: dark green; T-: black; dark blue: ground

For single ended voltage measurements, brown is connected to 1H, orange to 1L, ;white to 2H and dark green to 1L. All other wires are connected to ground.

```
;{21X}
*Table 1 Program
  01: 0.2      Execution Interval (seconds)

1: Volts (SE) (P1)
  1: 4        Reps
  2: 15       5000 mV Fast Range
  3: 1        In Chan
  4: 1        Loc [ u     ]
  5: 0.004    Mult
  6: 0.0      Offset                          ;114.8 ms

2: Z=X*F (P37)
  1: 3        X Loc [ w     ]
  2: 0.25     F
  3: 3        Z Loc [ w     ]                 ;0.9 ms

3: Z=X*F (P37)
  1: 4        X Loc [ T     ]
  2: 2.5      F
  3: 4        Z Loc [ T     ]                 ;0.9 ms

4: Z=X*Y (P36)
  1: 1        X Loc [ u     ]
  2: 1        Y Loc [ u     ]
  3: 14       Z Loc [ TMP   ]                 ;1.2 ms

5: Z=X*Y (P36)
  1: 2        X Loc [ v     ]
  2: 2        Y Loc [ v     ]
  3: 5        Z Loc [ U     ]

6: Z=X+Y (P33)
  1: 5        X Loc [ U     ]
  2: 14       Y Loc [ TMP   ]
  3: 5        Z Loc [ U     ]

7: Z=X (P31)
  1: 3        X Loc [ w     ]
  2: 6        Z Loc [ w1    ]

8: Z=SQRT(X) (P39)
  1: 5        X Loc [ U     ]
  2: 5        Z Loc [ U     ]                 ;12.0 ms

9: Z=ARCTAN(X/Y) (P66)
  1: 2        X Loc [ v     ]
  2: 1        Y Loc [ u     ]
  3: 7        Z Loc [ THETA ]                 ; 6.7 ms

10: If time is (P92)
  1: 0        Minutes into a
  2: 20       Minute Interval
  3: 10       Set Output Flag High

11: Real Time (P77)
  1: 110      Day,Hour/Minute

12: Resolution (P78)
  1: 1        high resolution

13: CV/CR (OSX-0) (P62)
  1: 2        No. of Input Locations
  2: 0        No. of Means
  3: 0        No. of Variances
  4: 2        No. of Std. Dev.
  5: 1        No. of Covariance
  6: 0        No. of Correlations
  7: 6000     Samples per Average
  8: 3        First Sample Loc [ w     ]
  9: 8        Loc [ SDw     ]                 ;5 ms

14: CV/CR (OSX-0) (P62)
  1: 2        No. of Input Locations
  2: 0        No. of Means
  3: 0        No. of Variances
  4: 2        No. of Std. Dev.
  5: 1        No. of Covariance
  6: 0        No. of Correlations
  7: 6000     Samples per Average
  8: 5        First Sample Loc [ U     ]
  9: 11       Loc [ SDU     ]                 ;5 ms

15: Average (P71)
  1: 5        Reps
  2: 1        Loc [ u     ]                   ;2.8 ms

16: Sample (P70)
  1: 5        Reps
  2: 7        Loc [ THETA   ]

17: Sample (P70)
  1: 1        Reps
  2: 13       Loc [ CVUw    ]

18: Serial Out (P96)
  1: 30       SM192/SM716/CSMI

*Table 2 Program
  01: 0.0      Execution Interval (seconds)
*Table 3 Subroutines
End Program
-Input Locations-
1 u          5 4 3
2 v          25 5 3
3 w          9 5 3
4 T          21 3 4
5 U          17 8 4
6 w1         1 1 1
7 THETA      1 5 2
8 SDw        1 2 1
9 SDT        1 2 0
10 CVwT      4 2 1
11 SDU       8 2 2
12 SDw       8 1 1
13 CVUw      16 2 1
14 TMP       0 3 1
```

TO use a SM as the PRIMARY DATA STORAGE DEVICE.
1 Use a P96 instruction anywhere in the datalogger program, but preferably the first Table 1 instruction (-easy to find).
P96 can be used to set the type of storage device:
30 SM 192/716
2 Leave the SM connected, and data will be downloaded every time output storage occurs.
OR: use A MANUAL dump to SM.
*9 30 A 1 A A A
where *9 is the manual dump command.
30 A specifies SM
1 A is the start of the dump location
A for the end of dump location (latest data output)
3 or any number A type any number to execute.

Up to 8 programs may be stored on the SM.
Example 1:
*D 71A 1SA
to store datalogger program from logger to SM in storage area 8 (boot-up area).
Example 2.
*D 71A 2SA
to load SM program in area 8 to logger.
*D mode is used with option 71 and
1z to STORE program from logger to SM
2z to LOAD program from SM to logger
3z to clear program from SM
where z is program 1 to 8.
eg. *D 71A 24 A to load program 4 in SM to logger.

What to do if the 21X power fails
1. Make a note in diary that power failed. Try and establish the cause of power dip and note this in diary as well. 2. Power up the datalogger; 3. Set the date and time by pressing *5 A 96 A 278 A 0927 A *0 to set the year at 1996, the day of year 278 (corresponding to 5 October) and a time of day of 09h27); 4. Down-

load the datalogger program using a personal computer; 5. Alternatively, type in needle program Table 1 shown on the card.

File name convention

For raw data: ddmmnyee.prn where dd is day of month, mm month of year, n for needle anemometer data, y is 6 for 1996, 7 for 1997, etc., ee for Cedara, PM for PMB. Date used is date data was captured from datalogger or storage module. 11036nee.prn represents 11 March 1996 for Cedara.

Day of year conversion

Nonleap year 31 Jan: 31; 28 Feb: 59; 31 Mar: 90; 30 Apr: 120; 31 May: 151; 30 June: 181; 31 July: 212; 31 Aug: 243; 30 Sep: 273; 31 Oct: 304; 30 Nov: 334
Leap year 31 Jan: 31; 29 Feb: 60; 31 Mar: 91; 30 Apr: 121; 31 May: 152; 30 June: 182; 31 July: 213; 31 Aug: 244; 30 Sep: 274; 31 Oct: 305; 30 Nov: 335

Use of storage modules

Data

The SM192 and the SM716 are identical except for their storage capacity which is 192 896 bytes (six 32k RAM chips), and 716672 bytes (16 extra chips) respectively. Up to eight datalogger programs may be stored on the SM.
To manually dump all data in a data logger to a storage module, use the necessary 9-pin connectors and type the following at the data logger:
*9 30 A (for SM192/716 storage modules - 31 for a filemark)
1 A (start of dump); A (end of dump); 3 A (to start dumping).
To dump only the new data logger data, the pointer corresponding to the start of dumping has to have been previously recorded. If this pointer is say 45456, then typing *9 30 A 45457 A 3 A will transfer only the new data.
To routinely dump data to a SM permanently connected to a datalogger, ensure that there is a 196 command with a 30 option (for the SM192/716 SMs).

Programs

Use the *D mode with option 71 (for store/load/clear program from storage module):
1z to STORE program from logger to SM
2z to LOAD program from SM to logger
3z to clear program from SM
where z is a any number from 1 to 8 representing program #1 to #8. So, for example, *DA 71A 24 will transfer program 4 in SM to logger; *DA 71A 17 will transfer program 7 in logger to SM; *DA 71A 38 will clear program 8 of the SM.
Pre-17 July 1994
Order of dld programs in the storage modules: 1. 3l240594.dld (3D lower); 2. 3u240594.dld (3D upper); 3. tsurf.dld (IRT's); 4. b1r2505.dld (Bowen ratio, system on the left - newer HR system); 5. b2r2405.dld (Bowen ratio, system on the right - old Cath Peak system); 6. 210gpe.dld (AMET 210 group project on the met site data collection). All of these files, in this order were placed on the largest storage module on 14 June 1994. This storage module was connected to the second Bowen ratio system - this should be checked.

Program: 3DNED.DLD or 3DNEDCAL.DLD
1 to 9 April 1996
Program for collection of horizontal wind speed data for checking needle anemometer data.
Program is very similar to above program
Flag Usage:
Input Channel Usage:
Excitation Channel Usage:
Continuous Analog Output Usage:
Control Port Usage:
Pulse Input Channel Usage:
Output Array Definitions:

```
* 1 Table 1 Programs
01: 15 s Execution Interval

01: P78 Resolution
01: 1 High Resolution

02: P1 Volt (SE)
01: 4 Reps
02: 5 5000 mV slow Range
03: 1 IN Chan
04: 1 Loc :
05: .001 Mult
06: 0 Offset

03: P37 Z = X*F
01: 3 X Loc
02: .25 F
03: 3 Z Loc :

04: P31 Z = X
01: 3 X Loc
02: 6 Z Loc :

05: P37 Z = X*F
01: 4 X Loc
02: 2.5 F
03: 4 Z Loc :

06: P36 Z = X*Y
01: 1 X Loc
02: 1 Y Loc
03: 5 Z Loc :

07: P36 Z = X*Y
01: 2 X Loc
02: 2 Y Loc
03: 20 Z Loc :

08: P33 Z = X + Y
01: 5 X Loc
02: 20 Y Loc
03: 5 Z Loc :

09: P39 Z = SQRT(X)
01: 5 X Loc
02: 5 Z Loc :

10: P66 Z = ARCTAN(X/Y)
01: 2 X Loc
02: 1 Y Loc
03: 7 Z Loc :

11: P92 If time is
01: 0 minutes into a
02: 6 minute interval
03: 10 Set high Flag 0 (output)

12: P77 Real Time
01: 1110 Year,Day,Hour-Minute

13: P71 Average
01: 5 Reps
02: 1 Loc

14: P62 CV/CR (OSX-0)
01: 2 No. of Input Values
02: 0 No. of Means
03: 0 No. of Variances
04: 0 No. of Std. Dev.
05: 1 No. of Covariances
06: 0 No. of Correlations
07: 24 Samples per Average
08: 3 First Sample Loc
09: 8 Loc :

15: P62 CV/CR (OSX-0)
01: 2 No. of Input Values
02: 0 No. of Means
03: 0 No. of Variances
04: 0 No. of Std. Dev.
05: 1 No. of Covariances
06: 0 No. of Correlations
07: 24 Samples per Average
08: 5 First Sample Loc
09: 9 Loc :

16: P70 Sample
01: 3 Reps
02: 7 Loc

17: P82 Standard Deviation
01: 1 Rep
02: 5 Sample Loc

18: P End Table 1


* 2 Table 2 Programs
01: 0 Sec. Execution Interval

01: P End Table 2

* 3 Table 3 Subroutines

01: P End Table 3


* 4 Mode 4 Output Options
01: 0 (Tape OFF) (Printer OFF)
02: 0 Printer 300 Baud


* A Mode 10 Memory Allocation
01: 28 Input Locations
02: 64 Intermediate Locations

1: 3: 3: Z Loc : [w]
1: 5: 4: Z Loc : [T]
1: 6: 5: Z Loc : [U]
1: 8: 5: Z Loc : [U]
1: 9: 5: Z Loc : [U]
1: 4: 6: Z Loc : [w]
1: 10: 7: Z Loc : [direction O]
1: 14: 8: Loc : [wT]
1: 15: 9: Loc : [wT]


What to do if the 21X power fails

1. Make a note in diary that power failed. Try and establish the cause of power dip and note this in diary as well; 2. Power up the datalogger; 3. Set the date and time by pressing *5 A 96 A 278 A 0927 A *0 to set the year at 1996, the day of year 278 (corresponding to 5 October) and a time of day of 09h27); 4. Download the datalogger program using a personal computer; 5. Alternatively, type in needle program Table 1 shown on the card.

File name convention

For raw data: ddmmnyee.prn where dd is day of month, mm month of year, n for needle anemometer data, y is 6 for 1996, 7 for 1997, etc., ee for Cedara, PM for PMB. Date used is date data was captured from datalogger or storage module. 11036nee.prn represents 11 March 1996 for Cedara.

Day of year conversion

Nonleap year 31 Jan: 31; 28 Feb: 59; 31 Mar: 90; 30 Apr: 120; 31 May: 151; 30 June: 181; 31 July: 212; 31 Aug: 243; 30 Sep: 273; 31 Oct: 304; 30 Nov: 334
Leap year 31 Jan: 31; 29 Feb: 60; 31 Mar: 91; 30 Apr: 121; 31 May: 152; 30 June: 182; 31 July: 213; 31 Aug: 244; 30 Sep: 274; 31 Oct: 305; 30 Nov: 335

Use of storage modules

Data

The SM192 and the SM716 are identical except for their storage capacity which is 192 896 bytes (six 32k RAM chips), and 716672 bytes (16 extra chips) respectively. Up to eight datalogger programs may be stored on the SM.
To manually dump all data in a data logger to a storage module, use the necessary 9-pin connectors and type the following at the data logger:
*9 30 A (for SM192/716 storage modules - 31 for a filemark)
1 A (start of dump); A (end of dump); 3 A (to start dumping).
To dump only the new data logger data, the pointer corresponding to the start of dumping has to have been previously recorded. If this pointer is say 45456, then typing *9 30 A 45457 A 3 A will transfer only the new data.
To routinely dump data to a SM permanently connected to a datalogger, ensure that there is a 196 command with a 30 option (for the SM192/716 SMs).

Programs

Use the *D mode with option 71 (for store/load/clear program from storage module):
1z to STORE program from logger to SM
2z to LOAD program from SM to logger
3z to clear program from SM
where z is a any number from 1 to 8 representing program #1 to #8. So, for example, *DA 71A 24 will transfer program 4 in SM to logger; *DA 71A 17 will transfer program 7 in logger to SM; *DA 71A 38 will clear program 8 of the SM.
Pre-17 July 1994
Order of dld programs in the storage modules: 1. 3l240594.dll (3D lower); 2. 3u240594.dld (3D upper); 3. tsurf.dld (IRT's); 4. b1r2505.dld (Bowen ratio, system on the left - newer HR system); 5. b2r2405.dld (Bowen ratio, system on the right - old Cath Peak system); 6. 210gpe.dld (AMET 210 group project on the met site data collection). All of these files, in this order were placed on the largest storage module on 14 June 1994. This storage module was connected to the second Bowen ratio system - this should be checked.

Cable 3 Pin connections (5 m) for cable connecting serial to analogue converter (SA-4) (25 pin female) to datalogger

25 pin male datalogger
inserted into SA-4 wires
v. 16 brown
v. 4 pink
3 light green ground
v. 18 orange
v. 7 violet
6 red ground
v. 21 white
v. 10 yellow
```

9 grey ground
T_v25 dark green sonic temperature
T_v13 black
12 dark blue ground

The sonic temperature T_V is calculated from $T_v = c_s^2 M/R$ where c = speed of sound waves in an ideal gas, M is the molecular mass of air (kg mol^{-1}), R = 9.3143 J mol^{-1} K^{-1} and *** = c_p/c_v.
$c_s = d_s/4\,(1/t_1 + 1/t_2) + v^2$
v^2 = crosswind component
d = sound path
$t_{1,2}$ = transit times in upward and downward vertical directions
$\tau = \rho \overline{u'w'} = \rho u_*^2$
$F_h = \rho c_p \overline{w'T'}$

Cable 4: Cable to directly connect 9-pin serial in (male) of SA-4 (serial to analogue converter) to the digital strip connector housed inside the card cage.

Strip connector to the digital connector9-pin serial female inserted into SA-4 serial to analogue convertor

Card cage 5 pin connector
1 ground
2 serial out
3 serial in
4 ground
5 external trigger

Cable 5: Under the front panel of the card cage are wires connecting the external digital port to an internal strip connector. The wiring is as follows:

4
1

5

3
2
Internal stripDigital port
connectorpin numbers

Problems:
1. Need to directly couple the card cage digital connector to a computer.
Solutions: use a initial interface cable
Digital connector9 pin female inserted
(5 pin female)into IBM-PC
inserted intoCOM1 port
card cage

Ground 1green5
Serial out red2

Serial in 3white3

2. The SA-4 is not water proof
3. Only one connector for connecting to the digital connector port of the card cage.
4. Transistors on the transmit/receive boards may be damaged if the card cage unit is powered with no sensor connected to the probe connector of the card cage unit.

Final interface cable14/10/1994
Digital connector (5-pin female inserted into card cage

9-pin female inserted into COM1 port of IBM PC

1pink1
2red2
3orange3(1, 4, 6 common
4green47, 8 common)
5white5for handshaking and Xon/Xoff
6

This interface cable allowed use of Qbasic 4 for data transfer28/10/95
(a) Card cage to PC
Card cage digital connector9-pin serial to COM15-pin 9-pin
1green515
2red222
3orange331
4greenN/C4
5pinkN/C6
1

(b) Card cage to SA4
As above but connect green - pin 4 wire (previously not connected) SA4 to pin 5 of 9-pin connector

Refs
Moore '86 Est heat storage
Freq resp correct (for EC systems). Boundary-Layer Meteorology 37:17-35
McCraden '93 Turbulent exchange of momentum
Grace et al (Global)

Data out from the digital port of the card cage
PLUG Sonic into digital port before switching on the card cage unit
Used LICOR210 (on HALICOR 210)
1. md c:\LICOR 210
2. HALICOR210*.*c\LICOR210\v
3. Type c:\LICOR210\COMM enter
Enter
4. Press F1 and then type COM1: 9600, 7, 1, E
Enter
5. The data will then flash past at a rate of a line every 0.1 s in the following format
u 0.2 6.5 v-00.54 w-01.06 T 20.43
6. To capture the data to a file, press
F6
d:\sonic02.prn Enter
The data will then be stored in d:\sonic02.prn
20 h 28 Jan on 1
20 h 29 Jan on 2
20 h 30 Jan on 3
20 h 31 Jan off
20 h 32 Stopped data collection

Slash command execution using LICOR210
Slash command execution: at the card cage set the thumb wheel to 07 and set the "test" switch to the test position. The CED above the test switch will light up.
1. Type c:\licor210\comm Enter, Enter
2. Press
F1 and then type
COM1: 9600, 7, 1, E
Enter, Enter
3. The following will be displayed at the screen
UNREC CMD
CMD
4. Press the CAPS Lock key to execute commands such as /OT (sets data output mode to terse)
or
/OV (sets data output mode to verbose)

Problem
I used /OH to set the baud rate. The LICOR 210 program went crazy and nothing could apparently be done to change it back to 9600 (/OL).
XTALK was used to try and change the baud rate back to 9600. This did not work either. Eventually, I used good old kermit
1. c\kermit\kermit
2. set speed 19200 enter (to set baud at 19200)
3. set parity even Enter (to set parity even)
4. show comm enter (to show communications)
5. con enter (to connect). Set the card cage thumb wheel at 07 and set the "TEST" switched to the TEST position
6. the screen displays CMD
7. press CAPS lock and type /OL enter to alter the baud rate back to 9600).
8. Press CTRL] (simultaneously)
9. Type QUIT Enter to exit KERMIT.

Verbose data output mode:
U
Us**.** Vs**.** Ws**.** Ts**.**
where U, V, W and T are capital letters, s indicates sign, space indicates blanks and * indicates a numeric and . the decimal point. A negative sign is indicated by - and a positive by a blank. The first line of data may be incomplete. This also applies to the last line.

Terse data output mode:
s****s****s****s****
where s is the sign (- for negative and blank for positive). Notice that the numbers have been multiplied by 100 as there is no decimal point.

In terse mode, if each number occupies 4 bytes, then each data line will occupy about 16 bytes or more
10 x 4 x 4 = 160 bytes/s = 9600 bytes/mn = 576000 bytes/h = 13.824 Mbyte/24 h.

PND tasks
1. accuracy of levelling 0.1°, need a bubble level
2. need a 12 gauge earthing wire attached to a copper rod (-see Appendix B, page 3 of Operator's Manual for Three-Axis Sonic anemometer).

Problem with Kermit
I could not get KERMIT to give a time/date stamp to the data. I therefore decided to use QBASIC 4.

Use of QBASIC 4 for serial data transfer
For data transfer, pins 1, 4, 6 of the 9-pin female COM1 connector common as well as pins 7, 8 common.
CLS
Open "JUNK1.PRN" for append AS #2
Open "COM1:9600, e, 7, 1,." FOR INPUT AS #1
Do WHILE timer/3600 0
Line input #1, LineS
Write #2, MIDS(lineS, 2, 22)
Loop
Close #2

Comments on the use of qbasic
1. Pins 1, 4, 6 of the 9-pin female COM1 connector must be made common as well as pins 7, 8 for the OPEN "COM1: 9600, e, 7, 1, "FOR INPUT AS #1 command to succeed (-to disable XON/OFF and handshaking)
2. BGlank delineated data uses less data bytes than comma delineated data.
3. Useful commands:
(a) TIMER - returns the elapsed time(in seconds) since mid-night. SO TIMER/3600 will give the number of hours since midnight.
(b) LINE #1, LINES
Reads a line from filenumber 1 and places it in the string LINES
(c) OPEN "JUNK1.PRN" for APPEND as #2. Initializes the file JUNK1.PRN for appending information.
(d) WRITW #2, MIDS(Lines 1, 15). will write data to sequential file 2 according to the format MIDS(Lines 1, 15)
(e) MIDS(Lines 1, 15) will return a length specified substring from a given string expression beginning at position 1 and returning a total of number of characters of 15.
(f) String concatenation: SS = aS + bS + cS
(g) Do While Timer/3600 17 + 36/60, , Loop will execute the loop while the nmber of hours after midnight is less than 17.6 h.
(h) NAME "JUNK1.PRN" as "JUNK2.PRN".
(i) Kill "JUNK1.PRN"
will delete file JUNK1.PRN.
(j) GOTO BEGIN
will branch to the lable BEGIN:

Appendix 3.3a Schematic representation of wiring of the CR7X datalogger and the batteries for the performance of the BREB, surface temperature, Penman-Monteith and ThetaProbe techniques.

CR7X INPUT	CONNECTION	COLOR
ANALOG-CARD1		
1 H	R NET +	RED
1 L	R NET -	BLACK
AG		
2 H	COOLED MIRROR PRT	GREEN
2 L	COOLED MIRROR PRT	WHITE
AG	COOLED MIRROR PRT	BLACK/CLEAR
3 H	SOIL TEMP. TC - CHROMEL	PURPLE
3 L	SOIL TEMP. TC - CONSTANTAN	RED
AG		
4 H	UPPER AIR 0.003 TC-CHROMEL	PURPLE
4 L	LOWER AIR 0.003 TC-CHROMEL	PURPLE
AG	AIR TEMP. TCs	RED
5 H	SOIL HEAT FLUX PLATE #1	CLEAR WITH NOD
5 L	SOIL HEAT FLUX PLATE #2	CLEAR WITH NOD
AG	SOIL HEAT FLUX PLATE	CLEAR WITHOUT NOD
6 H	SOLAR RADIATION	
6 L		
AG	SOLAR RADIATION	
7 H		
7 L		
AG		
8 H		
8 L		
AG		
9 H	THETAPROBE #1	YELLOW
9 L	THETAPROBE #1	GREEN
AG	THETAPROBE #1	WHITE
10 H	THETAPROBE #2	YELLOW
10 L	THETAPROBE #2	GREEN
AG	THETAPROBE #3	WHITE
11 H	THETAPROBE #3	YELLOW
11 L	THETAPROBE #3	GREEN
AG	THETAPROBE #3	WHITE
12 H	THETAPROBE #4	YELLOW
12 L	THETAPROBE #4	GREEN
AG	THETAPROBE #4	WHITE
13 H	THETAPROBE #5	YELLOW
13 L	THETAPROBE #5	GREEN
AG	THETAPROBE #5	WHITE
14 H		

	CONNECTIONS	COLOR
ANALOG-CARD2		
1 H		
1 L		
AG		
2 H		
2 L	IRT#1	PINK
AG	IRT#1/2	WHITE
3 H	IRT#2	PINK
3 L	IRT#3	PINK
AG	IRT#3/4	WHITE
4 H	IRT#4	PINK
4 L		
AG		
5 H	SOIL TEMP (θ)#1 -COP/CONSTANT	BLUE
5 L	SOIL TEMP (θ)#1 -COP/CONSTANT	BLUE
AG	GROUNDS	WHITE
6 H	SOIL TEMP (θ)#1 -COP/CONSTANT	BLUE
6 L	SOIL TEMP (θ)#1 -COP/CONSTANT	BLUE
AG	GROUNDS	WHITE
7 H		
7 L		
AG		
8 H	WIND SPEED (SN 218)	GREEN
8 L	WIND SPEED (SN 225)	BLACK
AG	GROUNDS	WHITE & YELLOW
9 H	WIND SPEED (SN240)	BLUE
9 L	GROUND	RED
AG		
10 H	T107#1	RED?
10 L	RH207#1	COLOR
AG		
11 H	T107#2	
11 L	RH207#2	
AG		
12 H		
12 L		
AG		
13 H		
13 L		
AG		
14 H	CONNECTION	COLOR

AG				AG		
BATTERY #2 FOR SENSORS	CONNECTION	COLOR		**EXCIT-CARD1**		
STRIP CONNECTOR						
12	THETAPROBE#1	RED		1 E	COOLED MIRROR EXCITATION	RED
-12	THETAPROBE#1	BLUE		AG	COOLED MIRROR EXCITATION	BROWN
12	THETAPROBE#2	RED		2 E	T107/RH207#1	
-12	THETAPROBE#2	BLUE		AG		
12	THETAPROBE#3	RED		3 E	T107/RH207#2	
-12	THETAPROBE#3	BLUE		AG		
12	THETAPROBE#4	RED		4 E		
-12	THETAPROBE#4	BLUE		AG		
12	THETAPROBE#5	RED		5 E		
-12	THETAPROBE#5	BLUE		AG		
12	IRT#1	RED		6 E		
-12	IRT#1	BLACK		AG		
12	IRT#2	RED		7 E		
-12	IRT#2	BLACK		AG		
12	IRT#3	RED		8 E		
-12	IRT#3	BLACK				
12	IRT#4	RED		**BATTERY FOR LOGGER**		
-12	IRT#4	BLACK		12	CR7X	RED
				-12	CR7X	BLACK
				-12	-12 BATTERY SENSORS	BLACK
				-12	LIGHTNING ROAD	
PORT-CARD 1	CONNECTIONS	COLOR		**PULSE-CARD 1**	CONNECTIONS	
1 PT	FOR LOWER AIR INTAKE	GREEN		1 PS	RAINGAUGE	RED
2 PT	FOR UPPER AIR INTAKE	WHITE		AG	RAINGAUGE	BLACK
3 PT	PUMP & MIRROR POWER ON	BLACK		2 PS		
4 PT	PUMP & MIRROR POWER OFF	RED		AG		
AG	GROUND WIRE	BROWN		3 PS		
5 PT				AG		
6 PT				4 PS		
7 PT				AG		
8 PT						

Appendix 3.3b Schematic representation of wiring to the 21X Datalogger, batteries, aluminium card cage and D-A convertor of the eddy correlation technique.

21X DATALOGGER	CONNECTION	COLOR
ANALOG	25 PIN GREY (SMALLER) CABLE FROM THE D-A CONVERTOR	
1 H	u WIND VECTOR	BROWN
1 L	v WIND VECTOR	ORANGE
AG	GROUNDS	PINK, LIGHT GREEN, VIOLET, RED
2 H	w WIND VECTOR	WHITE
2 L	TEMPERATURE	DARK GREEN
AG	GROUNDS	YELLOW, GREY, BLUE, DARK BLUE
3 H		
3 L		
AG		
4 H		
4 L		
AG		
5 H		
5 L		
AG		
6 H		
6 L		
AG		
7 H		
7 L		
AG		
8 H		
8 L		
AG		

EXCITATION		
1 E		
2 E		
AG		
3 E		
4 E		

D-A CONVERTOR	CONNECTION	
2 PINS	BATTERY	RED AND BLACK WIRES
25 PINS	DATALOGGER	GREY (SMALLER) CABLE
8 PINS SERIAL IN	AL. CARD CAGE	(5 PINS) WHITE CABLE

EXCIT	CNNECTION	COLOR
1 E		RED
AG		BROWN
2 E		
AG		
3 E		
AG		
4 E		
AG		

CONTROL PORT		
1 PT		
2 PT		
3 PT		
4 PT		
AG		

BATTERY #1 FOR LOGGER		
+12	21X DATALOGGER	RED
-12	21X DATALOGGER	BLACK
+12		BLACK
-12		

BATTERY FOR SENSORS		
12	ALUMINIUM CARD CAGE	RED
-12	ALUMINIUM CARD CAGE	BLACK
12	D-A CONVERTOR	RED
-12	D-A CONVERTOR	BLACK

ALUMINIUM CARD CAGE	CONNECTIONS	CABLE SPECIFICATION
PROBE	PROBE	18 PINS GREY LARGE CABLE
DIGITAL	D-A CONVERTOR BOX	5 PINS WHITE CABLE
DC	BATTERY	2 PINS WITH RED AND BLACK

Appendix 3.4 The prompts sheet for CR7 (a) and 21X (b) dataloggers for quick programming and monitoring.

CR7 INSTRUCTION AND PARAMETER SUMMARY

INPUT/OUTPUT INSTRUCTIONS

PARAMETERS

DESCRIPTION	01:	02:	03:	04:	05:	06:	07:	08:	09:	10:	11:	12:
1 VOLT (SE)	REPS	RANGE†	IN CARD	IN CHAN	LOC	MULT.	OFFSET					
2 VOLT (DIFF)	REPS	RANGE†	IN CARD	IN CHAN	LOC	MULT.	OFFSET					
3 PULSE	REPS	IN CARD	IN CHAN	CONFIG.†	LOC	MULT.	OFFSET					
4 EX-DEL-SE	REPS	RANGE†	IN CARD	IN CHAN	EX CARD	EX CHAN	MEAS/EX	DEL 0.01s	EXCIT mV	LOC	MULT.	OFFSET
5 AC HALF BR	REPS	RANGE†	IN CARD	IN CHAN	EX CARD	EX CHAN	MEAS/EX	EXCIT mV	LOC	MULT.	OFFSET	
6 FULL BR	REPS	RANGE†	IN CARD	IN CHAN	EX CARD	EX CHAN	MEAS/EX	EXCIT mV	LOC	MULT.	OFFSET	
7 3W HALF BR	REPS	RANGE†	IN CARD	IN CHAN	EX CARD	EX CHAN	MEAS/EX	EXCIT mV	LOC	MULT.	OFFSET	
8 FULL BR MEX	REPS	EX RANGE†	BR RANGE†	IN CARD	IN CHAN	EX CARD	EX CHAN	MEAS/EX	EXCIT mV	LOC	MULT.	OFFSET
10 BATT. VOLT	LOC											
11 TEMP (107)	REPS	IN CARD	IN CHAN	EX CARD	EX CHAN	LOC	MULT.	OFFSET				
12 RH (207)	REPS	IN CARD	IN CHAN	EX CARD	EX CHAN	MEAS TEMP	T LOC	RH LOC	MULT.	OFFSET		
13 TEMP-TC SE	REPS	RANGE†	IN CARD	IN CHAN	TC TYPE†	REF LOC	LOC	MULT.	OFFSET			
14 TEMP-TC DIFF	REPS	RANGE†	IN CARD	IN CHAN	TC TYPE†	REF LOC	LOC	MULT.	OFFSET			
16 TEMP-RTD	REPS	R/R0 LOC	LOC	MULT.	OFFSET							
17 TEMP-PANEL	IN CARD	LOC										
18 TIME	OPTION†	MOD BY	LOC									
19 SIGNATURE	LOC											
20 PORT SET	OPTION†	EX CARD	PORT NO									
21 ANALOG OUT	EX CARD	CAO CHAN	mV LOC									
22 EXCIT-DEL	EX CARD	EX CHAN	DEL W/EX	DEL AFTER	EXCIT mV (del units 0.01s)							
23 IO MODULE	MODULE NO.											
26 TIMER	LOC (to reset and run timer, use the inst. with LOC = 0)											
29 SDM-CD16	REPS	DEVICE (?)	ADDR	EX CARD	LOC							

† Option Codes

INST. DESCRIPTION
1-14 RANGE codes:
Slow (16.6ms integ. time)
Fast (250 µs integ. time)
[illegible]

1	11	±	1500	µV
2	12	±	5000	µV
3	13	±	15	mV
4	14	±	50	mV
5	15	±	150	mV
6	16	±	500	mV
7	17	±	1500	mV
8	18	±	5000	mV

INST. DESCRIPTION
3 CONFIGuration codes:
To record all counts,
00 High freq.
01 Low level AC
02 Switch Closure
To discard counts from excessive intervals:
10 High freq.
11 Low level AC
12 Switch Closure
To discard counts, output frequency (Hz):
20 High freq.
21 Low level AC
22 Switch closure

INST. DESCRIPTION
13, 14 TC TYPE Thermocouple Type codes:
1 T (copper-constantan)
2 E (chromel-constantan)
3 K (chromel-alumel)
4 J (iron-constantan)
5 [illegible]
6 [illegible]
7 [illegible]
1x Output temp difference
2x Skip every other channel (Inst. 13 only)
To increment REF LOC with each rep, enter the REF LOC as [illegible]

INST. DESCRIPTION
18 OPTION codes:
0 0.1 seconds into minute (max 600)
1 minutes into day (max 1440)
2 hours into year (max 8784)
20 OPTION codes:
0 Set low
1 Set high
1x Set according to flag x
2x Set opposite of flag x
30 Set active card

PROCESSING INSTRUCTIONS

PARAMETERS *

DESCRIPTION	01:	02:	03:	04:	05:	06:	07:	08:	09:
30 Z=F	F	Z							
31 Z=X	X	Z							
32 Z=Z+1	Z								
33 Z=X+Y	X	Y	Z						
34 Z=X+F	X	F	Z						
35 Z=X-Y	X	Y	Z						
36 Z=X*Y	X	Y	Z						
37 Z=X*F	X	F	Z						
38 Z=X/Y	X	Y	Z						
39 Z=SQRT(X)	X	Z							
40 Z=LN(X)	X	Z							
41 Z=EXP(X)	X	Z							
42 Z=1/X	X	Z							
43 Z=ABS(X)	X	Z							
44 Z=FRAC(X)	X	Z							
45 Z=INT(X)	X	Z							
46 Z=X MOD F	X	F	Z						
47 Z=X^Y	X	Y	Z						
48 Z=SIN(X)	X	Z							
49 SPA. MAX	SWATH	1ST LOC	MAX†						
50 SPA. MIN	SWATH	1ST LOC	MIN†						
51 SPA. AVG	SWATH	1ST LOC	AVG						
53 A*X+B	START LOC	A1	B1	A2	B2	A3	B3	A4	B4
54 BLOCK MOVE	NO VALS	S LOC	STEP	D LOC	STEP				
55 POLYNOMIAL	REPS	X	F(X)	C0	C1	C2	C3	C4	C5
56 SAT. VP	TEMP	VP							
57 WB/DBT-VP	PRESSURE	DB TEMP	WB TEMP	VP					
58 LP FILTER	REPS	X	F(X)	W					
59 RA(1-X)	REPS	X	MULT.						
61 INDIR. MOVE	SOURCE	DESTN.							
62 COV/COR	NO VALS.	NO MEANS	NO VAR†	NO SD	NO COV	NO COR	SAMP AVG	X	F(X)
66 Z=ARCTAN(X/Y)	X	Y	Z						

† Option Codes

INST. DESCRIPTION
49-52 MAX MIN codes:
[illegible]

* F is fixed data (constant); X, Y, and Z are Input Locations.

OUTPUT PROCESSING INSTRUCTIONS

PARAMETERS

DESCRIPTION	01:	02:	03:	04:	05:	06:	07:
69 WIND VECTOR	REPS	SAMP/SUB INT	SEN OUT †	WS/E	WD/N		
70 SAMPLE	REPS	LOC					
71 AVERAGE	REPS	LOC					
72 TOTALIZE	REPS	LOC					
73 MAXIMIZE	REPS	TIME†	LOC				
74 MINIMIZE	REPS	TIME†	LOC				
75 HISTOGRAM	REPS	BINS	FORM†	BSEL LOC	WV LOC†	LO LIM	HI LIM
77 REAL TIME	OPTION†						
78 RESOLUTION	OPTION†						
79 SMPL ON MM	REPS	LOC					
80 STORE AREA	AREA†	LOC ID					
82 STD DEV	REPS	LOC					

† Option Codes

INST. DESCRIPTION
69 SENsor/OUTput type codes:
x0 Avg WS, θ1, σ(θ1)
x1 Avg WS, θ1
x2 Avg WS, resultant U, θu, σ(θu)
x = 0 Polar (speed & direction)
x = 1 Orthogonal (East & North)
73, 74 TIME of max or min options:
00 Maximum value only
01 With Seconds
10 With hours-minutes
11 With hours-minutes, Seconds

INST. DESCRIPTION
75 FORM codes:
0 Closed form (data beyond limits is included)
1 Closed form (data beyond limits is excluded)
WV LOCation:
0 frequency distribution

INST. DESCRIPTION
77 OPTION codes:
1xxx Seconds
x1xx Hour-Minute
xx1x Hour-Minute, 2400 at midnight
xxx1 Day
x1xx Day, Previous day at midnight
1xxx Year
10 = no output, e.g.,
110 = Day, hour-minute)

INST. DESCRIPTION
78 OPTION codes:
0 Low resolution
1 High resolution
80 AREA codes:
1 Final Storage
2 Input Storage

PROGRAM CONTROL INSTRUCTIONS

PARAMETERS *

DESCRIPTION	01:	02:	03:	04:	05:	06:	07:	08:	09:	–	10 + NO.RF.	–
83 IF CASE < F	F	COMMAND										
85 LABEL SUBR.	SUBR. NO. (1-9)											
86 DO	COMMAND†											
87 LOOP	DELAY	COUNT										
88 IF X ⇔ Y	X	COMP.†	Y	COMMAND†								
89 IF X ⇔ F	X	COMP.†	F	COMMAND†								
90 LOOP INDEX	STEP											
91 IF FLAG	FLAG†	COMMAND†										
92 IF TIME	Time INT	INT (min)	COMMAND†									
93 BEGIN CASE	CASE LOC											
94 ELSE												
95 END												
96 SERIAL OUT	OPTION†											
97 INIT. TELE.	OPTION†	FLAG	LM (hrs)	F.DEL (sec)	NO.TRYS	S.DEL (min)	TRY LOC	ID	NO.RF	RF STA.	NO. DIGIT	PHONE NO.
98 SEND CHAR.	BAUD/CHAR											

† Option Codes

INST. DESCRIPTION
83-93 COMMAND codes:
0 Go to end of Pgm. Table
1-9, 79-99 Call Subroutine 1-9, 79-99
10-19 Set flag 0-9
20-29 Reset flag 0-9
30 Then Do
31 Exit Loop if true
32 Exit Loop if false
41-48 Set Port high
51-58 Set Port low
61-68 Toggle Port
71-78 Pulse Port

INST. DESCRIPTION
88, 89 COMParison codes:
1 X = Y   X = F
2 X ≠ Y   X ≠ F
3 X ≥ Y   X ≥ F
4 X < Y   X < F
91 FLAG codes:
1x Do if flag x is set
2x Do if flag x is reset
96 OPTION codes, 2 digits:
30 Tape
1x Printer, ASCII
2x Printer, binary
x Baud rate code
50 SM192/716
51 Transmit to SM192/716

INST. DESCRIPTION
97 OPTION codes, 2 digits:
0x RF modem
1x Direct
2x DC112
x Baud rate code

FLAG DESCRIPTIONS:
0 Output flag
1-8 User flags
9 Intermed. proc. disable flag

BAUD RATE CODES:
0 300
1 1200
2 9600
3 76,800

* F is fixed data (constant); X, Y, and Z are Input Locations.

ERROR CODES

1 - I/O Module does not respond
3 - Program Table full
4 - Intermediate Storage full
6 - I/O Module Address not between 1 and 4
8 - CR7 was reset by watch dog timer
9 - Input Storage not allocated
11 - Attempt to allocate unavailable storage
20 - Subroutine encountered before necessary END
21 - END without IF, LOOP, or SUBROUTINE
22 - Missing END; None instant SUBROUTINE
24 - ELSE in SUBROUTINE without IF
25 - ELSE without IF
26 - EXIT LOOP without LOOP
30 - IFs and or LOOPS nested too deep
31 - SUBROUTINES nested too deep
40 - Table 2 Execution interval too short or instruction does not exist
97 - Time out in *0 Mode
98 - Uncorrectable tape read errors
99 - Wrong file type

DAY OF YEAR CALENDAR

	1	2	3	4	5	6	7	8	9	10	11	12	13	14	15	16	17	18	19	20	21	22	23	24	25	26	27	28	29	30	31
JAN	1	2	3	4	5	6	7	8	9	10	11	12	13	14	15	16	17	18	19	20	21	22	23	24	25	26	27	28	29	30	31
FEB	32	33	34	35	36	37	38	39	40	41	42	43	44	45	46	47	48	49	50	51	52	53	54	55	56	57	58	59	60		
MAR	60	61	62	63	64	65	66	67	68	69	70	71	72	73	74	75	76	77	78	79	80	81	82	83	84	85	86	87	88	89	90
APR	91	92	93	94	95	96	97	98	99	100	101	102	103	104	105	106	107	108	109	110	111	112	113	114	115	116	117	118	119	120	
MAY	121	122	123	124	125	126	127	128	129	130	131	132	133	134	135	136	137	138	139	140	141	142	143	144	145	146	147	148	149	150	151
JUN	152	153	154	155	156	157	158	159	160	161	162	163	164	165	166	167	168	169	170	171	172	173	174	175	176	177	178	179	180	181	
JUL	182	183	184	185	186	187	188	189	190	191	192	193	194	195	196	197	198	199	200	201	202	203	204	205	206	207	208	209	210	211	212
AUG	213	214	215	216	217	218	219	220	221	222	223	224	225	226	227	228	229	230	231	232	233	234	235	236	237	238	239	240	241	242	243
SEP	244	245	246	247	248	249	250	251	252	253	254	255	256	257	258	259	260	261	262	263	264	265	266	267	268	269	270	271	272	273	
OCT	274	275	276	277	278	279	280	281	282	283	284	285	286	287	288	289	290	291	292	293	294	295	296	297	298	299	300	301	302	303	304
NOV	305	306	307	308	309	310	311	312	313	314	315	316	317	318	319	320	321	322	323	324	325	326	327	328	329	330	331	332	333	334	
DEC	335	336	337	338	339	340	341	342	343	344	345	346	347	348	349	350	351	352	353	354	355	356	357	358	359	360	361	362	363	364	365

Add 1 to red values during leap years.

CAMPBELL SCIENTIFIC, INC.

P.O. Box 551
Logan, UT 84321
USA
Phone (801) 753-2342
TLX 453058
FAX 801-752-3268

Campbell Scientific Canada Corp.
9525 43rd Avenue
Edmonton, Alberta T6E 5X7
CANADA
Phone (403) 461-5158
TLX 037-2956 (EDM)
FAX 403-450-2531

Campbell Scientific Ltd.
14-20 Field Street
Shepshed, Leics. LE12 9AL
ENGLAND
Phone (44) 509 601141
FAX (44) 509 601091

Printed October 1991

CR7 PROMPT SHEET
(0S7-0.1 PROMs)

*MODES

To enter each Mode, key in a * ("star"), followed by the desired mode number. The KEY DEFINITION SUMMARY lists commands that are used to interrogate and program the CR7. Please refer to the CR7 Manual for detailed information and examples.

KEY DEFINITION SUMMARY

0-9 Enter numeric data, instruction number, or parameter

A Advance through a program table or data storage, or enter the displayed number

B Back up through a program table or data storage

C Change the sign of a floating point number, or index an input location

D Enter a decimal point

Clear digit just keyed; display storage location number

*0 Compile program, LOG data and indicate Active Table(s)

*1, *2 Display or Enter Program Instructions or Parameters in Table 1 or 2

01:xx Instruction location to advance to
01.x.xxxx Execution Interval:
Valid entries

are multiples of	for Range of
0.0125 s. ...	0.0125 to 1 s. (Table 1 only)
0.1 s. ...	1 to 6553 s.

01.Pxx Program Instruction (see following pages for Instruction and Parameter listings)

*Commands Specific to *1 and *2 Modes:*
#A Advance to next instruction
#B Back up to previous instruction
#D Delete entire instruction

*3 Display or Change Subroutine Program Table

Same as for *1 and *2, except that *3 does not have an Execution Interval

*4 Enable Final Storage Output to Peripheral Device (do not use if Instruction 96 is in program)

01: A B Output Enable Code
A Tape
0 = disabled; 1 = enabled
B Printer
0 = disabled; 1 = enabled

02:0y Baud Rate Code (printer)
0 300 baud
1 1200 baud
2 9600 baud
3 76800 baud

*5 Display or Change Datalogger Time

HH:MM:SS (displays current datalogger time)
05:xx Year
05:xxxx Day of Year (calendar on back)
05:HHMM Hours Minutes

*6 Display or Change Input Storage Data Value/Flags. Compile Program without resetting Input Storage, Flags, or Ports

06:xxxx Input Storage Location to advance to

*Commands Specific to *6 Mode while viewing an Input Location:*
Display Input Location Number or enter location to jump to
C Enter or Change value in Input Location
D Display flags 1-8, toggle flag with keys 1-8
0 Display ports 8-1, toggle with keys 1-8. Active port card is set with Instruction 20

*7 Display Final Storage Data

07:xxxx DSP location or enter location to advance to

*Commands Specific to *7 Mode:*
Display Final Storage location number; enter location to jump to, or C to display data
#A Advance to start of next array
#B Back up to start of array

*8 Manual Data Dump to Tape

01:xxxx TPTR location/start of dump
02:xxxx DSP location/end of dump
03:xx Enter any number to start dump
(# Aborts dump)

*9 Manual Dump to Printer or Storage Module

09:xx Enter Output Code
1y Printable ASCII
2y Final Storage Format } y=Baud Rate (see *4)
30 SM192/716 Storage Module
31 Filemark to SM192/716
01:xxxx PPTR location/start of dump
02:xxxx DSP location/end of dump
03:xx Enter any number to start dump

*A Display or Change Memory Allocation

01:xxxx Input Storage locations
02:xxxx Intermediate Storage location
03:xxxx Final Storage location
04:xxxx Remaining program memory (Bytes)

*B Display Signatures

01.xxxx Program signature
02:xxxx First PROM signature
03:xxxx Second PROM signature
04:xxxx Third PROM signature
05:xxx Memory Test
06:xx No. of E08 Errors
07:xx No. off Overrun Errors
08:xxx.x Version number
09:xxxx Revision number
11:00 Enter I/O Module No.
01:xxxx I/O RAM Signature
01:xxxx I/O PROM Signature

*C Display/Change Security

12:0000 ((if enabled) Enter password
01:xx
00 Temporarily disable security
01 Advance to window 2 to set new password
02:xxxx Set password, 0000 disables security if window 1 is set to 0

*D Store/Load Program

13:xx Enter command
(Commands 1 and 2 require baud rate code. See *4 mode)
1 - Print program (ASCII)
2 - Load program (ASCII)
71 - Store/Load/Clear program from Storage Module
Storage Module Command Codes
1z Store program z in Storage Module
2z Load program z from Storage Module
3z Clear program z from Storage Module
(z=1-8)

NOTE: x represents a digit from 0 to 9 unless otherwise defined.

CAMPBELL SCIENTIFIC, INC.

21X INSTRUCTION AND PARAMETER SUMMARY

INPUT/OUTPUT INSTRUCTIONS

INST. DESCRIPTION	01:	02:	03:	04:	05:	06:	07:	08:	09:
1 VOLT (SE)	REPS	RANGE†	IN CHAN	LOC	MULT	OFFSET			
2 VOLT (DIFF)	REPS	RANGE†	IN CHAN	LOC	MULT	OFFSET			
3 PULSE	REPS	IN CHAN	CONFIG†	LOC	MULT	OFFSET			
4 EXCIT-DEL-SE	REPS	RANGE†	IN CHAN	EXCIT CHAN†	DELAY 0.01s	EXCIT mV	LOC	MULT	OFFSET
5 AC HALF BR.	REPS	RANGE†	IN CHAN	EXCIT CHAN†	EXCIT mV	LOC	MULT	OFFSET	
6 FULL BR.	REPS	RANGE†	IN CHAN	EXCIT CHAN†	EXCIT mV	LOC	MULT	OFFSET	
7 3W HALF BR.	REPS	RANGE†	IN CHAN	EXCIT CHAN†	EXCIT mV	LOC	MULT	OFFSET	
8 EXCIT-DEL-DIFF	REPS	RANGE†	IN CHAN	EXCIT CHAN†	DELAY 0.01s	EXCIT mV	LOC	MULT	OFFSET
9 FULL BR. w MEAS. EXCIT	REPS	EXCIT RANGE†	BR. RANGE†	IN CHAN	EXCIT CHAN†	EXCIT mV	LOC	MULT	OFFSET
10 BATT VOLT	LOC								
11 TEMP (107)	REPS	IN CHAN	EXCIT CHAN†	LOC	MULT	OFFSET			
12 RH (207)	REPS	RH CHAN	EXCIT CHAN†	TEMP LOC	RH LOC	MULT	OFFSET		
13 TEMP-TC (SE)	REPS	RANGE†	IN CHAN	TC TYPE†	REF. LOC	LOC	MULT	OFFSET	
14 TEMP-TC (DIFF)	REPS	RANGE†	IN CHAN	TC TYPE†	REF. LOC	LOC	MULT	OFFSET	
16 TEMP-RTD	REPS	R/R0 LOC	LOC	MULT	OFFSET				
17 TEMP-PANEL	LOC								
18 TIME	OPTION†	MOD-BY	LOC						
19 SIGNATURE	LOC								
20 PORT SET	OPTION†	PORT NO.							
21 ANALOG OUT	CAO CHAN	mV LOC							
22 EXCIT-DEL	EXCIT CHAN	DEL w/ exc.	DEL after ex.	EXCIT mV	(delay units 0.01s)				
†23 see below									
26 TIMER	LOC (0 resets timer)								
‡131 SDM-INT8	ADDR	C:8765	C:4321	F:8765	F:4321	OUT.OPT.†	LOC	MULT	OFFSET
‡107 SDM-SW8A	REPS	ADDR	FUNCTION†	CHAN	LOC	MULT	OFFSET		
‡103 SDM-A04	REPS	ADDR	LOC						
‡104 SDM-CD16	REPS	ADDR	LOC						

INST. DESCRIPTION	01:	02:	03:	04:	05:	06:	07:	08:	09:	10:	11:	12:
†23 BURST MODE	NO. CHAN	RANGE†	IN CHAN	OPTION†	SCAN(ms)	SCANS (10³)	TR. OFF.	TR. LIM. mV	EXCIT mV	LOC	MULT	OFFSET

† Option Codes

INST. DESCRIPTION

1-14 RANGE codes:

Slow (16.67 ms integ. time)	Fast (250 μs integ. time)	Full scale range
1	11	± 5 mV
2	12	± 15 mV
3	13	± 50 mV
4	14	± 500 mV
5	15	± 5000 mV

3 CONFIGuration codes:
To record all counts:
- 0 High frequency
- 1 Low level AC
- 2 Switch Closure
- 3 High frequency, 16 bit
- 4 Low level AC, 16 bit

To discard counts from excessive intervals:
- 1x (x= 0-4 from above)

Discard counts, output frequency (Hz):
- 2x (x= 0-4 from above)

4-12 EXCIT CHANnel codes:
- 0x Excite all reps w/ EXCIT CHAN x
- 1x Increment EXCIT CHAN w/ each rep

13,14 TC TYPE = Thermocouple Type codes:
- 1 T (copper-constantan)
- 2 E (chromel-constantan)
- 3 K (chromel-alumel)
- 4 J (iron-constantan)

For common mode error checking (DIFF only):
- 9x (x= 1-4 from above)

18 OPTION codes:
- 0 0.1 seconds into minute (max 600)
- 1 minutes into day (max 1440)
- 2 hours into year (max 8784)

20 OPTION codes:
- 00 Set low
- 01 Set high
- 1x Set according to flag x
- 2x Set opposite flag x

23 RANGE codes:
(250 μs integ. time)

	Full scale range
12	± 15 mV
13	± 50 mV
14	± 500 mV
15	± 5000 mV

23 OPTION code, 4 digits: ABCD

A Trigger
- 0 — Trigger on 1st analog channel used
- 1 — Digital trigger on S.E. channel 1H
- 2 — Same as 0, but sets Control #1 high on trigger, low when finished

B Trigger option
- 0 — Trigger immediately
- 1 — Trigger if above limit (high)
- 2 — Trigger if below limit (low)
- 3 — Trigger on rising edge
- 4 — Trigger on falling edge

C Destination
- 0 — Input Storage
- 1 — Serial port, 9600 baud
- 2 — Serial port, 76,800 baud

D Measurement
- 0 — Differential measurement
- 1 — Single-ended measurement

101 C:8765, C:4321 Each digit Configures respective channel:
- 0 High level, rising edge
- 1 High level, falling edge
- 2 Low level, rising edge
- 3 Low level, falling edge

101 F:8765, F:4321 Each digit sets Function for respective channel:
- 0 No value returned
- 1 Period, ms
- 2 Frequency, kHz
- 3 Time since previous channel, ms
- 4 Time since channel 1, ms
- 5 Counts on 2 since 1, interpolated
- 6 Low resolution frequency, kHz
- 7 Counts
- 8 Integral counts on 2 since 1

101 OUTput OPTions:
- 0 Average over execution interval
- 0– Continuous averaging
- xxxx Specify avg. interval in ms
- -xxxx– Capture all events until xxxx edges of channel 1
- 9999– Test Memory

102 FUNCTION:
- 0 Channel state
- 1 Duty cycle
- 2 Counts
- 3 Memory test

* STANDARD IN OSX-0.1 † STANDARD IN OSX-1.1 ‡ STANDARD IN OSX-2.1

PROCESSING INSTRUCTIONS

INST. DESC.	01:	02:	03:	INST. DESC.	01:	02:	03:	INST. DESC.	01:	02:	03:
30 Z=F	F	Z		38 Z=X/Y	X	Y	Z	45 Z=INT(X)	X	Z	
31 Z=X	X	Z		39 Z=SQRT(X)	X	Z		46 Z=X MOD F	X	F	Z
32 Z=Z+1	Z			40 Z=LN(X)	X	Z		47 Z=X^Y	X	Y	Z
33 Z=X+Y	X	Y	Z	41 Z=EXP(X)	X	Z		48 Z=SIN(X)	X	Z	
34 Z=X+F	X	F	Z	42 Z=1/X	X	Z		49 SPA. MAX	SWATH	1ST LOC	MAX†
35 Z=X-Y	X	Y	Z	43 Z=ABS(X)	X	Z		50 SPA. MIN	SWATH	1ST LOC	MIN†
36 Z=X*Y	X	Y	Z	44 Z=FRAC(X)	X	Z		51 SPA. AVG	SWATH	1ST LOC	AVG
37 Z=X*F	X	F	Z								

INST. DESCRIPTION	01:	02:	03:	04:	05:	06:	07:	08:	09:
53 A*X+B	STRT. LOC	A1	B1	A2	B2	A3	B3	A4	B4
54 BLOCK MOVE	NO. VALS	S LOC	STEP	D LOC	STEP				
55 POLYNOMIAL	REPS	X	F(X)	C0	C1	C2	C3	C4	C5
56 SAT. VP	TEMP	VP							
57 WB/DB T to VP	PRESSURE	DB TEMP	WB TEMP	VP					
58 LP FILTER	REPS	X	F(X)	WGHT F					
59 X/(1-X)	REPS	X	MULT						
†60 FFT	LOG2(SMPL)	OPTIONS†	LOG2(BINAVG)	IN LOC	MULT				
†61 INDIR. MOVE	SOURCE	DESTIN							
‡62 COV/CORR	NO. VALS	NO. MEANS	NO. VARS.	NO. S. DEVS.	NO. COVARS.	NO. CORRS.	NO. SAMPLES	S. LOC	D LOC
‡66 Z=ARCTAN(X/Y)	X	Y	Z						

† Option Codes

INST. DESCRIPTION

49-51 MAX, MIN:
- 0xxx Store swath max or min at location xxx
- 1xxx Max or min at location xxx and location of max or min at xxx+1

60 OPTION codes:
- 0x Power Spectra
- 1x Real and Imaginary
- 2x Magnitude and Phase
- x=0 No Taper
- x=1 Taper

OUTPUT PROCESSING INSTRUCTIONS

INST. DESC.	01:	02:	03:	04:	05:
69 WIND VECTOR	REPS	SAMP/SUB INT	S/D OUT.†	WS/E	WD/N
70 SAMPLE	REPS	LOC			
71 AVERAGE	REPS	LOC			
72 TOTALIZE	REPS	LOC			
73 MAXIMIZE	REPS	TIME†	LOC		
74 MINIMIZE	REPS	TIME†	LOC		

INST. DESC.	01:	02:	03:	04:	05:	06:	07:
75 HISTOGRAM	REPS	BINS	FORM†	B.SEL. LOC	WV LOC†	LOW LIM.	HIGH LIM.
77 REAL TIME	OPTION†						
78 RESOLUTION	OPTION†						
79 SMPL ON M.M.	REPS	LOC (must follow Inst. 73 or 74)					
80 STORE AREA	AREA†	LOC/ID					
81 see below							
82 STD. DEV.	REPS	LOC					

INST. DESC.	01:	02:	03:	04:	05:	06:	07:	08:	09:	10:
†81 RAINFLOW HISTOGRAM	REPS	S. LOC	SWATH	MEAN BINS	AMP. BINS	LOW LIM.	HIGH LIM.	MIN AMP.	OPTION†	D. LOC

† Option Codes

INST. DESCRIPTION

69 S/D OUTput type codes:
- x0 Avg WS, θ1, σ(θ1)
- x1 Avg WS, θ1
- x2 Avg WS, resultant U, θu, σ(θu)
- x = 0 Polar (speed & direction)
- x = 1 Orthogonal (East & North)

73,74 TIME of max or min:
- 00 Max/min value only
- 01 With Seconds
- 10 With Hour-Minute
- 11 With Hour-Minute, Seconds

75 FORM codes:
- 0 Open form (data beyond limits is included)
- 1 Closed form (data beyond limits is excluded)

WV LOCation:
- 0 frequency distribution

77 OPTION codes:
- xxx1 Seconds
- xx1x Hour-Minute
- xx2x Hour-Minute, 2400 at midnight
- x1xx Day
- x2xx Day, Previous day at midnight
- 1xxx Year
- (0 = no output, e.g., 110 = Day, Hour-Minute)

78 OPTION codes:
- 0 Low resolution
- 1 High resolution

80 AREA codes:
- 1 Final Storage
- 3 Input Storage

81 OPTION codes, 2 Digits:
- 00 - Closed form/Fraction output
- 01 - Closed form/Counts output
- 10 - Open form/Fraction output
- 11 - Open form/Counts output

PROGRAM CONTROL INSTRUCTIONS

INST. DESC.	01:	02:	03:	04:
83 IF CASE < F	F	COMMAND†		
85 LABEL SUBR.	SUBR† (1-8, 79-99)			
86 DO	COMMAND†			
87 LOOP	DELAY	COUNT		
88 IF X <=> Y	X	COMP†	Y	COMMAND†
89 IF X <=> F	X	COMP†	F	COMMAND†
90 LOOP INDEX	STEP			
91 IF FLAG	OPTION†	COMMAND†		
92 IF TIME	Time INT	INT (min)	COMMAND†	
93 BEGIN CASE	CASE LLOC			
94 ELSE				
95 END				
96 SERIAL OUT†	OPTION†			
97 see below				
‡98 SEND CHAR.	BAUD/CHAR†			

INST. DESC.	01:	02:	03:	04:	05:	06:	07:	08:	09:			
‡97 INIT. TELE.	OPTION†	FLAG	LAI(SEC)	F.DEL(SEC)	NO.TRYS	S.DEL(MIN)	FAILURE LOC	ID	NO. of IV STA(X)	STA ID	NO.DIGITS	PHONE NO.

† Option Codes

INST. DESCRIPTION

83-93 COMMAND codes:
- 0 Go to end of Program Table
- 1-8, 79-99 Call Subroutine
- 10-19 Set flag 0-9 high
- 20-29 Set flag 0-9 low
- 30 Then Do
- 31 Exit Loop if true
- 32 Exit Loop if false
- 41-46 Set Port 1-6 high
- 51-56 Set Port 1-6 low
- 61-66 Toggle Port 1-6
- 71-76 Pulse Port 1-6

88,89 COMParison codes:
- 1 X = Y X = F
- 2 X ≠ Y X ≠ F
- 3 X ≥ Y X ≥ F
- 4 X < Y X < F

91 OPTION codes:
- 1x Do if flag x is high
- 2x Do if flag x is low

96 SERIAL OUT
Cannot output to both printer and Storage Module.

96 OPTION codes:
- 00 Tape
- 1y Printer, ASCII
- 2y Printer, Binary
- 30 SM192/716
- 31 Prompt to SM192/716

97 OPTION codes:
- 0y RF modem
- 1y DIRECT
- 2y DC112

98 BAUD/CHARacter Value
- yxxx xxx = ASCII Value (0-127)

(y = Baud Rate Code)

FLAG DESCRIPTIONS:
- 0 Output Flag
- 1-8 User Flags
- 9 Intermed. proc. disable flag

BAUD RATE CODES (y):
- 0 300 baud
- 1 1200 baud
- 2 9600 baud
- 3 76,800 baud

* F represents a real number; X,Y and Z represent Input Locations

ERROR CODES

3 – Program Table full
4 – Intermediate Storage full
8 – 21X was reset by watch dog timer
9 – Insufficient Input Storage
11 – Attempt to allocate unavailable storage
20 – Subroutine encountered before necessary END
21 – END without IF, LOOP, or SUBROUTINE
22 – Missing END, nonexistent SUBROUTINE
24 – ELSE in SUBROUTINE without IF
25 – ELSE without IF
26 – EXIT LOOP without LOOP
30 – IFs and/or LOOPS nested too deep
331 – SUBROUTINES nested too deep
440 – Table 2 Execution Interval too short or Instruction does not exist
670 – Inadequate Input Storage for Burst/FFT
671 – Burst Mode Scan Rate too short

**D Mode Errors

997 – Time out on tape read
998 – Uncorrectable errors on tape read
999 – Wrong file type, program error, or program not received

DAY OF YEAR CALENDAR

	1st	2	3	4	5	6	7	8	9	10	11	12	13	14	15	16	17	18th	19	20	21	22	23	24	25	26	27	28	29	30	31
JAN	1*	2	3	4	5	6	7	8	9	10	11	12	13	14	15	16	17	18th	19	20	21	22	23	24	25	26	27	28	29	30	31
FEB	32nd	33	34	35	36	37	38	39	40	41	42	43	44	45	46	47	48	49th	50	51	52	53	54	55	56	57	58	59	60		
MAR	60	61	62	63	64	65	66	67	68	69	70	71	72	73	74	75	76	77th	78	79	80	81	82	83	84	85	86	87	88	89	90
APR	91	92	93	94	95	96	97	98	99	100	101	102	103	104	105	106	107	107th	109	110	111	112	113	114	115	116	117	118	119	120	
MAY	121st	122	123	124	125	126	127	128	129	130	131	132	133	134	135	136	137	138th	139	140	141	142	143	144	145	146	147	148	149	150	151
JUN	152nd	153	154	155	156	157	158	159	160	161	162	163	164	165	166	167	168	169th	170	171	172	173	174	175	176	177	178	179	180	181	
JUL	182nd	183	184	185	186	187	188	189	190	191	192	193	194	195	196	197	198	199th	200	201	202	203	204	205	206	207	208	209	210	211	212
AUG	213th	214	215	216	217	218	219	220	221	222	223	224	225	226	227	228	229	230th	231	232	233	234	235	236	237	238	239	240	241	242	243
SEP	244th	245	246	247	248	249	250	251	252	253	254	255	256	257	258	259	260	261st	262	263	264	265	266	267	268	269	270	271	272	273	
OCT	274th	275	276	277	278	279	280	281	282	283	284	285	286	287	288	289	290	291st	292	293	294	295	296	297	298	299	300	301	302	303	304
NOV	305th	306	307	308	309	310	311	312	313	314	315	316	317	318	319	320	321	322nd	323	324	325	326	327	328	329	330	331	332	333	334	
DEC	335th	336	337	338	339	340	341	342	343	344	345	346	347	348	349	350	351	352nd	353	354	355	356	357	358	359	360	361	362	363	364	365

Add 1 to red values during leap years

CAMPBELL SCIENTIFIC, INC.

P.O. Box 551
Logan, UT 84321
Phone (801) 753-2342
TLX #53058
FAX 801-752-3268

9525 41st Avenue
Edmonton, Alberta T6E 5X7
CANADA
Phone (403) 461-5158
TLX 037-2964 (ETCM)
FAX 403-450-2551

14-20 Field Street
Shepshed, Leics. LE12 9AL
ENGLAND
Phone 011445096011 41
TLX 9401838393 (CAMP G)
FAX 011445096010 91

Printed July 1990

21X PROMPT SHEET

*MODES

To enter each Mode, key in a * ("star"), followed by the desired mode number. The KEY DEFINITION SUMMARY lists commands that are used to interrogate and program the 21X. Please refer to the 21X Manual for detailed information and examples.

KEY DEFINITION SUMMARY

0-9 Enter numeric data, instruction number, or parameter
A Advance through a program table or data storage, or enter the displayed number
B Back up through a program table or data storage
C Change the sign of a floating point number, or index an input location
D Enter a decimal point
Clear digit just keyed; display storage location number

*0 Compile program, LOG data and indicate Active Table(s)

*1, *2 Display or Enter Program Instructions or Parameters in Table 1 or 2

01:xx Instruction location to advance to
01:x.xxxx Execution Interval:

Valid entries are multiples of	for Range of
0.0125 s. . . .	0.0125 to 1 s. (Table 1 only)
0.1 s. . . .	1 to 6553 s.

01:Pxx Program Instruction (see following pages for Instruction and Parameter listings)

*Commands Specific to *1 and *2 Modes:*
#A Advance to next instruction
#B Back up to previous instruction
#D Delete entire instruction

*3 Display or Change Subroutine Program Table

Same as for *1 and *2, except that *3 does not have an Execution Interval

*4 Enable Final Storage Output to Peripheral Device (do not use if Instruction 96 is in program)

01: A B Output Enable Code
A Tape
0 = disabled; 1 = enabled
B Printer
0 = disabled; 1 = enabled

02:0y Baud Rate Code (printer)
0 300 baud
1 1200 baud
2 9600 baud
3 76800 baud

*5 Display or Change Datalogger Time

HH:MM:SS (displays current datalogger time)
05:xx Year
05:xxxx Day of Year (calendar or back)
05:HHMM Hours Minutes

*6 Display or Change Input Storage Data Values/Flags. Compile Program without resetting Input Storage, Flags, or Ports

06:xxxx Input Storage Location to advance to

*Commands Specific to *6 Mode while viewing an Input Location:*
Display Input Location Number or enter location to jump to
C Enter or Change value in Input Location
D Display flags 1-8, toggle flag with keys 1-8
0 Display ports 6-1, toggle with keys 1-6

*7 Display Final Storage Data

07:xxxx DSP location or enter location to advance to

*Commands Specific to *7 Mode:*
Display Final Storage location number; enter location to jump to, or C to display data
#A Advance to start of next array
#B Back up to start of array

*8 Manual Data Dump to Tape

01:xxxx TPTR location/start of dump
02:xxxx DSP location/end of dump
03:xx Enter any number to start dump (# Aborts dump)

*9 Manual Dump to Printer or Storage Module

09:xx Enter Output Code
1y Printable ASCII
2y Final Storage Format
(y=Baud Rate (see *4))
30 SM192/716 Storage Module
31 Filemark to SM192/716
01:xxxx PPTR location/start of dump
02:xxxx DSP location/end of dump
03:xx Enter any number to start dump

*A Display or Change Memory Allocation

01:xxxx Input Storage locations
02:xxxx Intermediate Storage locations
03:xxxx Final Storage locations
04:xxxx Remaining program memory (bytes)

*B Display Signatures

01:xxxx Program signature
02:xxxx First PROM signature
03:xxxx Second PROM signature
04:xxxx Third PROM signature
05:xxxx Memory Test
06:xx No. of EQ8 Errors
07:xx No. of Overrun Errors
08:xxxx.x Version number
09:xxxx Revision number

*C Display/Change Security (OS X-0.1 only)

12:0000 (if enabled) Enter password
01:xx
00 Temporarily disable security
01 Advance to window 2 to set new password
02:xxxx Set password, 0000 disables security if window 1 is set to 0

*D Store/Load Program

13:xx Enter Command (Commands 1 and 2 require baud rate code. See *4 mode)
1 – Print program (ASCII)
2 – Load program (ASCII)
71– Store/Load/Clear program from Storage Module

Storage Module Command Codes
1z Store program z in Storage Module
2z Load program z from Storage Module
3z Clear program z from Storage Module
(z=1-8)

NOTE: x represents a digit from 0 to 9 unless otherwise defined

CAMPBELL SCIENTIFIC, INC.

Appendix 3.5a Calculation procedure for estimating the particle size distribution (Gee and Bauder, 1986)

$$\%coSi + fiSi + clay = 265\ g_{coSi + fiSi + clay}(1 + w) \quad 1$$
$$\%fiSi + clay = 265\ g_{fiSi + clay}(1 + w) \quad 2$$
$$\%caly = 265\ g_{clay}(1 + w) \quad 3$$
$$\%coSi = 1 + 2 \quad 4$$
$$\%fiSi = 2 - 3 \quad 5$$
$$\%coSa = 5\ g_{coSa}(1 + w) \quad 6$$
$$\%meSa = 5\ g_{meSa}(1 + w) \quad 7$$
$$\%fiSa = 5\ g_{fiSa}(1 + w) \quad 8$$
$$\%VfiSa = 5\ g_{vfiSa}(1 + w) \quad 9$$

where (coSa) is the coarse sand (g), (meSa) is the medium sand (g), (fiSa) is the fine sand, (vfiSa) is the very fine sand (g), (coSi) is the coarse silt (g), (fiSi) is the fine silt and w is the soil water content of the air-dry soil.

Appendix 3.5b Calculation procedure for estimating the percentage organic matter using Walkley, A (1947) (taken from 320 Soil Science Course, Un. Natal, Pietermaritzburg).

Column 1	Column 2	Column 3	Column 4	Column 5	Column 6	Column 7	
Depths	Volume Titre	V. Not react	V. React	org carb	org mat	Depth-avg	
mm	ml	ml	ml	%	%	%	
0 to 55a	14.9	7.45	2.55	2.07	3.57		
0 to 55b	15.7	7.85	2.15	1.75	3.01		
55 to 120a	15.3	7.65	2.35	1.91	3.29	3.29	
55 to 120b	15.2	7.60	2.40	1.95	3.36		
120 to 200a	16.3	8.15	1.85	1.50	2.59	3.33	
120 to 200b	15.2	7.60	2.40	1.95	3.36		
200 to 280a	15.9	7.95	2.05	1.67	2.87	2.98	
200 to 280b	16	8.00	2.00	1.63	2.80		
280 to 360a	16.3	8.15	1.85	1.50	2.59	2.84	
280 to 360b	14.9	7.45	2.55	2.07	3.57		
						3.08	
Calculations		(C2*C12)/C13	c14-c3	(c4*(12/4)*1.33*100/(C11*1000)	c5*1.724		

	Column9	Column 10	Column 11	Column 12	Column 13	Column 14	Column 15
	Air-dry Sample	Grav. SWC	Ov.-dry samp	C. Fas Bla.	C. K2Cr2O7	V. K2Cr2O7	V. Fas Bla.
	g	g/g	g	N	N	ml	
	0.50	0.0185	0.49075	0.5	1	10	20
Calculations				(C13*C14)/C15			

Appendix 3.6 The splits program used for joining data from table 1 and table 2 recorded using the CR7 datalogger.

Nome/s of input FILE(s): c:\gastao\data\talavall\02116t01.dat,c:\gastao\data\talavall\02116t01.dat,
c:\gastao\data\talavall\02116t01.dat,c:\gastao\data\talavall\02116t01.dat
Name of output FILE(s) to generate: c:\gastao\split\talavall\02116tal.prn
START reading in: 2:3
START reading in: 2:3
START reading in: 2:3
START reading in: 2:3
STOP reading in:
STOP reading in:
STOP reading in:
STOP reading in:
SELECT element (s) # in: 1[110]
SELECT element (s) # in 1[237]
SELECT element (s) # in 1[237]
SELECT element (s) # in 1[237]
COPY from: 2,3+(int(4/100.))/24.+(4/100.-int(4/100.))/14.4,4,(2.*6+7)/2.,7,9,11
COPY from: 5,(6+7)/2.,8,9,15..19,22,23
COPY from: 24..33
COPY from: 34..41,42..58
HEADING for report: TALA VALLEY SPLIT DATA
VARIABLES names: YEAR
DAY
TIME
AVGT
AVGdT
VP LO
VP HI
AVG RN
AVG FX
Tsoil
dTs
thet03
thet08.
thet16
thet24
thet32
IRT1
IRT2
IRT3
IRT4
T1071
RH1
es1
e1
T1072
RH2
es2
s2
Is
Ts08
Ts16
Ts24
Ts32
U
theta
Rain
BW1
BW2
BW3
BW4
BW5
BW6
BW7
BW8
BW9
BW10
BW11
BW12